ADVANCES IN SMART HEALTHCARE TECHNOLOGIES

NANOSENSORS AS ROBUST NON-INVASIVE DIAGNOSTIC TOOLS FOR REMOTE HEALTH MONITORING

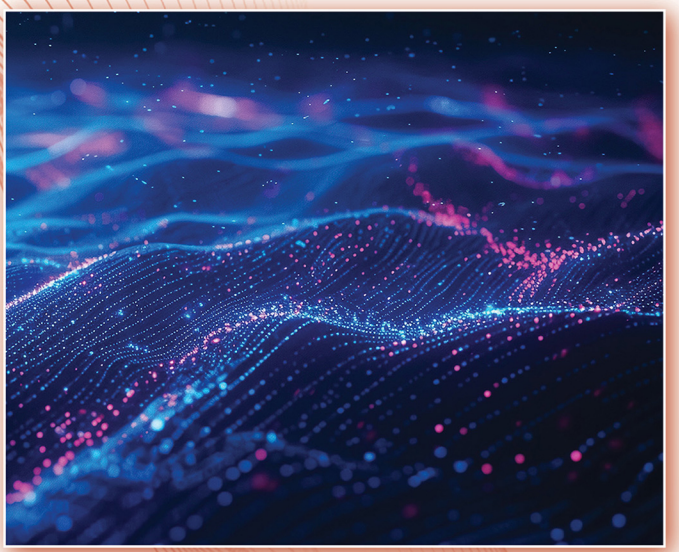

EDITED BY
PRIYANKA DWIVEDI, CHINMAY CHAKRABORTY, GWANGGIL JEON, AND YAN ZHANG

CRC Press
Taylor & Francis Group

Nanosensors as Robust Non-Invasive Diagnostic Tools for Remote Health Monitoring

This book addresses advancement in nanomaterials to design and develop non-invasive healthcare sensors including a combination of hybrid nanocomposites to design non-invasive devices for diagnosing human diseases. The cost-effectiveness is addressed with the methodologies to increase the scalability of the fabrication process. It aims to provide a complete end-to-end solution for smart non-invasive diagnosis developed indigenously and is a cost-effective complete guide to implement a deployable healthcare solution in real-time scenarios.

Key Features:

- Focuses on the design and development of healthcare sensor devices.
- Reviews different AI techniques using sensors for healthcare.
- Focuses on the application of nanomaterials in different biosensing applications.
- Explores non-invasive and painless diagnosis with remote healthcare.
- Discusses remote healthcare with IoMT integration and smart app communication.

This book is aimed at graduate students and researchers in biomedical engineering, medical devices, machine learning/pattern recognition, and nanotechnology.

Advances in Smart Healthcare Technologies

Nanosensors as Robust Non-Invasive Diagnostic Tools for Remote Health Monitoring
Edited by: Priyanka Dwivedi, Chinmay Chakraborty, Gwanggil Jeon, and Yan Zhang

Nanosensors as Robust Non-Invasive Diagnostic Tools for Remote Health Monitoring

Edited by Priyanka Dwivedi, Chinmay Chakraborty, Gwanggil Jeon, and Yan Zhang

CRC Press
Taylor & Francis Group
Boca Raton London New York

CRC Press is an imprint of the
Taylor & Francis Group, an **informa** business

Designed cover image: Shutterstock

First edition published 2025
by CRC Press
2385 NW Executive Center Drive, Suite 320, Boca Raton FL 33431

and by CRC Press
4 Park Square, Milton Park, Abingdon, Oxon, OX14 4RN

CRC Press is an imprint of Taylor & Francis Group, LLC

© 2025 selection and editorial matter, Priyanka Dwivedi, Chinmay Chakraborty, Gwanggil Jeon, and Yan Zhang; individual chapters, the contributors

Reasonable efforts have been made to publish reliable data and information, but the author and publisher cannot assume responsibility for the validity of all materials or the consequences of their use. The authors and publishers have attempted to trace the copyright holders of all material reproduced in this publication and apologize to copyright holders if permission to publish in this form has not been obtained. If any copyright material has not been acknowledged please write and let us know so we may rectify in any future reprint.

Except as permitted under U.S. Copyright Law, no part of this book may be reprinted, reproduced, transmitted, or utilized in any form by any electronic, mechanical, or other means, now known or hereafter invented, including photocopying, microfilming, and recording, or in any information storage or retrieval system, without written permission from the publishers.

For permission to photocopy or use material electronically from this work, access www.copyright.com or contact the Copyright Clearance Center, Inc. (CCC), 222 Rosewood Drive, Danvers, MA 01923, 978-750-8400. For works that are not available on CCC please contact mpkbooks permissions@tandf.co.uk

Trademark notice: Product or corporate names may be trademarks or registered trademarks and are used only for identification and explanation without intent to infringe.

ISBN: 978-1-032-62300-9 (hbk)
ISBN: 978-1-032-99173-3 (pbk)
ISBN: 978-1-003-60272-9 (ebk)

DOI: 10.1201/9781003602729

Typeset in Times
by codeMantra

Contents

Preface vii
About the Editors xi
Contributors xiii

Chapter 1 Machine Learning-Based Intelligent Smart Embedded Sensors for Automatic Detection and Classification of Neuromuscular Disorders Using EMG Signals 1

Abdelouahad Achmamad, Mohamed Elfezazi, Abdellah Chehri, Rachid Saadane, Gwanggil Jeon and Atman Jbari

Chapter 2 Connectivity Attributes for Remote Insulin Therapy 24

Richa Mishra and Tarun Kanti Bhattacharyya

Chapter 3 Deep Learning-Driven Human Activity Recognition for Remote Health Applications in Internet of Things-Enabled Smart Cities 41

Namita Sethi, Sujit Bebortta, Subhranshu Sekhar Tripathy and Subhendu Kumar Pani

Chapter 4 Gas Sensors as a Non-Invasive Diagnostic Device for Smart Life Applications 77

P Divyashree and Monoj Kumar Singha

Chapter 5 Revolutionizing Personalized Healthcare: The Role of Nanosensors in NonInvasive Monitoring 95

P. Nedumal Pugazhenthi, K. Vijayakumar, S. Selvaperumal and G. Prabhakar

Chapter 6 Robust Non-Invasive Support System for Blood Cell Image Classification Using Generative Adversarial Networks 108

Mohammad Shabaz, Mukesh Soni and Mohammed Wasim Bhatt

Chapter 7 Impact of Channel Thickness on the MoS_2 FET Performance Metrics and Their Application in Biosensing 127

Sharmila B, Agraj Khare, Monoj Kumar Singha and Priyanka Dwivedi

Chapter 8 Nanodiagnostics for Precision Breast Cancer Classification in Remote Health—A Comprehensive Study Employing Various Machine Learning Models 138

Kanik Makhija, Swayam Mahindroo, Mehul Batra and Dr. Safina Shokeen

Index 157

Preface

This book mainly covers the use of nanosensors, artificial intelligence (AI), and advanced technology for the non-invasive detection of diseases in smart healthcare applications. Recent technologies such as nanosensors, novel electronic devices, machine learning, deep learning, and the Internet of Things (IoT) have emerged to a large extent. The incorporation of these advanced technologies in the healthcare sector will transform traditional diagnostics to the next level. This facilitates the efficient and cost-effective detection of diseases with remote health monitoring. The quality of life during diagnosis and treatment can be significantly upgraded with the transformation of nanosensors into non-invasive diagnostic tools for the smart healthcare sector. The embedded sensor networks combined with IoT connectivity will provide proactive patient care while remotely monitoring the health condition of the patient. Intelligent analytics to interpret the disease is possible by the use of AI algorithms. The person-specific treatment plans can be scheduled, as each patient is unique and requires specialized healthcare solutions. The Internet of Health Things is an integration of wearable sensors, AI, and IoT to continuously monitor health parameters. In this way, the smart healthcare solution can be adapted into daily lives to provide early information about health conditions. To improve the performance of AI results in healthcare, the sensor data collected from the patient need to be more reliable. This is possible if sensor is more efficient. The advancements and innovations in the metal oxide semiconductor, nanostructures, and sensor design parameters are crucial for miniaturization and better sensing performance. Thus, the efficient smart healthcare solution can be deployed for real-time use with the advancements in technology.

This book focuses on the innovations from sensor design, data analytics, AI model development, and IoT integration to provide an effective smart healthcare solution. The gold standard technological sectors are explored toward achieving personalized, remote, and smart healthcare assistance.

Book Organization

The book consists of eight chapters on the field of nanosensors and AI for non-invasive disease detection. A summary of each chapter is presented below.

Chapter 1: Machine Learning-Based Intelligent Smart Embedded Sensors for Automatic Detection and Classification of Neuromuscular Disorders Using EMG Signals

This chapter focuses on the development of a novel computer-aided health monitoring system for diagnosing neuromuscular disorders (NMDs). Additionally, it used embedded sensor networks to facilitate proactive patient care and remote health monitoring. This method combines the discrete wavelet transform with two supervised machine learning algorithms: the multiclass support vector machine and the k-nearest neighbors classifiers. The proposed embedded system can serve as a portable diagnostic device for the automatic detection of NMDs.

Chapter 2: Connectivity Attributes for Remote Insulin Therapy

In this chapter, various attributes of a connected drug delivery system using insulin therapy are presented. The chapter then looks into the common sensors and

actuators being employed in insulin delivery devices. A layout of AI algorithm steps is presented which may be used for basic understanding to provide more precise and personalized insulin dosing recommendations for individuals with diabetes. The regulatory compliances required to launch connected insulin delivery devices on the global platform are discussed.

Chapter 3: Deep Learning-Driven Human Activity Recognition for Remote Health Applications in Internet of Things-Enabled Smart Cities

This chapter aims to develop a human activity recognition system to process patient data by integrating wearable and ambient sensors with edge computing techniques. Security is still an issue with IoT integration in healthcare and smart cities, despite the benefits. To protect patients' essential surveillance data, it is imperative to implement strong cyber-security safeguards. Internet of Health Things (IoHT) use also extends outside of healthcare environments, with smartwatches and other smart gadgets including smartphones, health-monitoring functions, heart rate, oxygen saturation, and activity tracking. This enables users to carefully observe their body's actions, demonstrating how IoHT is becoming an essential component of people's daily lives in the present era.

Chapter 4: Gas Sensors as a Non-Invasive Diagnostic Device for Smart Life Applications

This chapter focuses on understanding the non-invasive data collection techniques using gas sensors for smart applications. The applications where gas sensors are deployed include sustainable healthcare, environment monitoring for pollution control, smart home, automated industry, and sustainable management of agriculture yield. To make an intelligent decision, having precise data is the primary requirement and sensors should provide accurate responses. Therefore, the design and development of a good sensor is crucial for any process to take place in a smart application. The research is heading toward advancements in technology like metal oxide semiconductors, nanocomposites, and light-induced gas sensing mechanisms to improve the sensing capability.

Chapter 5: Revolutionizing Personalized Healthcare: The Role of Nanosensors in Non-Invasive Monitoring

This chapter is used to examine how non-invasive nanosensors are revolutionizing the field of personal healthcare. With their incredibly small size and amazing sensitivity, nanosensors have the potential to completely change how we monitor various aspects of our health. This chapter explores the wide range of nanosensors available, their uses in ongoing health monitoring, and how they might advance personalized therapy. The significant influence of nanosensors on the future of healthcare is highlighted by case studies and future prospects.

Chapter 6: Robust Non-Invasive Support System for Blood Cell Image Classification Using Generative Adversarial Networks

This chapter proposes a multi-scale conditional generative adversarial network employing a multi-scale discriminator that generates numerous realistic leukocyte images. This approach can be used for classification and to mitigate the issue of low detection accuracy attributed to limited leukocyte samples and imprecise features of the cell pictures. Experiments revealed that incorporating a multi-scale discriminator and gradient similarity enhances the generated cell image quality. Also, cell

classification and detection accuracy improved from 90.3% to 94.7% when compared to the case of actual data training.

Chapter 7: Impact of Channel Thickness on the MoS_2 FET Performance Metrics and Their Application in Biosensing

This chapter demonstrates the characteristics and electrical trends of assorted thicknesses of monolayer MoS_2. The trends are obtained via precise COMSOL Multiphysics simulations for the back-gated MoS_2-based FET devices, where the thickness of the MoS_2 active layer is varied. This contribution elucidates the advantages and shortcomings of each variant with respect to electrical trends and the change in material characteristics with the bulk effect. Characterization of each variant is presented, explaining ranges where their application would be optimum.

Chapter 8: Nanodiagnostics for Precision Breast Cancer Classification in Remote Health—A Comprehensive Study Employing Various Machine Learning Models

This chapter presents the application of machine learning techniques to improve classification accuracy and address the ongoing global health challenge of breast cancer. Acknowledging the global urgency for enhanced breast cancer screening, the study endeavors to improve diagnostic precision via machine learning. The emphasis on random forest highlights its exceptional ability to classify instances of breast cancer. This study helps professionals and scholars choose the best model for a more accurate diagnosis of breast cancer. Pointing out random forest's superiority is a request to investigate how it may be included in routine diagnostic processes to improve patient outcomes, in addition to serving as a benchmark. In general, this work advances the field of healthcare diagnostics and supports continued attempts to address the complexity of breast cancer.

At last, we would like to extend our sincere thanks to authors from industry, academia, and policy expertise to complete this work for aspiring researchers in this domain. I am confident that this book would play a key role in providing readers with a comprehensive view of intelligent secured health informatics and developments around it and can be used as a learning resource for various examinations that deal with cutting-edge technologies.

Priyanka Dwivedi, Chinmay Chakraborty,
Gwanggil Jeon, and Yan Zhang

Taylor & Francis
Taylor & Francis Group
http://taylorandfrancis.com

About the Editors

Dr. Priyanka Dwivedi is an Assistant Professor at the Department of Electronics and Communication Engineering, Indian Institute of Information Technology, Sri City, Chittoor, India. Her current research projects focus on micro/nanodevices, flexible electronics, neuromorphic computing, and BioMEMS for environmental and health issues. She completed her Ph.D. from the Indian Institute of Technology Delhi followed by postdoc from the USA. She has published patents, peer-reviewed journals, and conferences in the area of microsensors and MEMS technology.

Dr. Chinmay Chakraborty is an Assistant Professor in the Department of Electronics and Communication Engineering, BIT Mesra, India. He has received Young Research Excellence Award, Global Peer Review Award, Young Faculty Award, and Outstanding Researcher Award.

Dr. Gwanggil Jeon is a Professor at Incheon National University, Incheon, South Korea. He was a general chair of IEEE SITIS 2023 and served as a workshop chair in numerous conferences. He is an Associate Editor of *IEEE Transactions on Circuits and Systems for Video Technology*, Elsevier's *Sustainable Cities and Society*, *IEEE Access*, *Springer Real-Time Image Processing*, *Journal of System Architecture*, and Wiley's *Expert Systems*. He was a recipient of the IEEE Chester Sall Award in 2007, ACM's Distinguished Speaker in 2022, the ETRI Journal Paper Award in 2008, and the Industry-Academic Merit Award by the Ministry of SMEs and Startups of Korea Minister in 2020.

Dr. Yan Zhang is a Professor at Xi'an Shiyou University, Xi'an, China. His major research interests include signal and information processing, modeling, and simulation of environmental cognition and machine learning. He is the reviewer of many journals, including the topmost journal *IEEE Access* and *Multimedia Tools and Applications*.

Taylor & Francis
Taylor & Francis Group
http://taylorandfrancis.com

Contributors

Abdelouahad Achmamad
National Graduate School of Arts and Crafts
ENSAM
Morocco

Mehul Batra
Vivekananda Institute of Professional Studies
Technical Campus

Sujit Bebortta
Department of Computer Science
Ravenshaw University
Cuttack 753003, India

Mohammed Wasim Bhatt
Department of CSE, University Centre for Research & Development
Chandigarh University
Mohali, Punjab 140413, India

Dr. Tarun Kanti Bhattacharyya
Department of Electronics and Electrical Communication Engineering
Indian Institute of Technology Kharagpur
Kharagpur 721302, India

Abdellah Chehri
Department of Mathematics and Computer Science
Royal Military College of Canada
Kingston

P Divyashree
Department of Electronics and Communication Engineering
Indian Institute of Information Technology (IIIT), Sri City
Andhra Pradesh, India

Priyanka Dwivedi
Indian Institute of Information Technology (IIIT), Sri City
Chittoor, India

Mohamed Elfezazi
National Graduate School of Arts and Crafts
ENSAM
Morocco

Atman Jbari
Mohammed V University
Rabat, Morocco

Gwanggil Jeon
Department of Embedded Systems Engineering
Incheon National University
Incheon, South Korea

Agraj Khare
University of Southern California
USA

Swayam Mahindroo
Vivekananda Institute of Professional Studies
Technical Campus

Kanik Makhija
Vivekananda Institute of Professional Studies
Technical Campus

Dr. Richa Mishra
Department of Electronics and Communication Engineering
Birla Institute of Technology, Mesra
Ranchi, India

Subhendu Kumar Pani
Krupajal Engineering College
Biju Patnaik University of Technology (BPUT), Kausalya Ganga
Bhubaneswar 751002, Odisha, India

Dr. G. Prabhakar
Department of Electronics and Communication Engineering
Thiagarajar College of Engineering
Madurai

Dr. P. Nedumal Pugazhenthi,
Department of Biomedical Engineering
Dr. N.G.P. Institute of Technology
Coimbatore

Rachid Saadane
Hassania School of Public Works
Casablanca
Morocco

Dr. S. Selvaperumal
Department of Electrical and Electronics Engineering
Mohamed Sathak Engineering College
Kilakkarai

Namita Sethi
Department of Computer Science
Ravenshaw University
Cuttack 753003, India

Mohammad Shabaz
Model Institute of Engineering and Technology
Jammu, J&K
India

Sharmila B
Indian Institute of Information Technology (IIIT), Sri City
Chittoor
India

Dr. Safina Shokeen
Vivekananda Institute of Professional Studies
Technical Campus

Monoj Kumar Singha
University of Allahabad
India

Mukesh Soni
Dr. D. Y. Patil Vidyapeeth, Pune
Dr. D. Y. Patil School of Science & Technology
Tathawade, Pune, India

Subhranshu Sekhar Tripathy
School of Computer Engineering
KIIT Deemed to be University
Bhubaneswar 751024, India

Dr. K. Vijayakumar
Department of Electrical and Electronics Engineering
Dr. Mahalingam College of Engineering and Technology
Pollachi

1 Machine Learning-Based Intelligent Smart Embedded Sensors for Automatic Detection and Classification of Neuromuscular Disorders Using EMG Signals

Abdelouahad Achmamad, Mohamed Elfezazi, Abdellah Chehri, Rachid Saadane, Gwanggil Jeon and Atman Jbari

1.1 INTRODUCTION

Neuromuscular disorders (NMDs) encompass conditions that affect skeletal muscle, neuromuscular junctions, and nerves [1–2]. According to a research report, the world-wide prevalence of lifetime NMDs is per population, which is similar to Parkinson's disease [3]. In addition, amyotrophic lateral sclerosis (ALS) and myopathy represent the most prevalent NMDs affecting both genders of all ages [4].

Common characteristics of ALS and myopathy are respiratory failure, muscle weakness, and wasting [5–6]. These symptoms are caused by unexpected damage to neuromuscular junctions and abnormal functioning or atrophy of muscle fibers [7–8]. As a result, ALS and myopathy can bring tremendous pain to patients and even death. Therefore, a practical and early diagnosis of these disorders is paramount to alleviate the sufferer's pain.

Classification and feature extraction have played an essential role in automated systems for the detection of NMDs. This is possible because of the development of machine learning and advanced signal processing-based methods. In this regard, multiple electromyography (EMG) classification algorithms have been proposed [9–13]. They concern two main classification problems: binary and multiclass problems.

DOI: 10.1201/9781003602729-1

In 2019, Chatterjee et al. proposed employing the modified window Stockwell transform to classify ALS and myopathy EMG signals [14]. Their method outperformed all the comparison methods. The result indicated that the best-performing classifiers were k-nearest neighbors (k-NN) and support vector machine (SVM), with the highest classification accuracy of 98.58% and 98.33%, respectively.

Recently, discrete wavelet transforms (DWT) and its variant version, known as tunable Q-factor wavelet transform (TQWT), have been used successfully in the multiclass problem of EMG signals.

For example, Gokgoz and Subasi adopted a framework to find an effective machine learning algorithm for classifying EMG signals [15]. Before feature extraction, EMG signals were preprocessed with multiscale principal component analysis for EMG denoising. Subsequently, the authors put forward a Daubechies wavelet to break down EMG signals into multilevel DWT decomposition (six-level). Then, the obtained frequency sub-bands were compressed by calculating four statistical features to make a powerful feature vector.

The classification of EMG signals using only computer simulations (e.g., MATLAB or Python) is no novelty, but being able to perform the classification on an embedded system in real time would potentially save the lives of the patients with NMDs.

The aforementioned research has shown promising results in solving both classification problems. However, to the best of our knowledge, there has been no attempt to date to conceive an embedded EMG classification.

Therefore, this chapter focuses on multiclass EMG signals classification and its implementation on an embedded CompactRIO-9035 real-time controller. The original contributions and novelties of this paper are as follows:

- Developing a new framework that can process and classify EMG signals.
- Determining the suitable features that can discriminate among the three categories of EMG signals.
- Improving the classification performance of EMG signals based on the DWT method.
- Implementing DWT algorithm, multiclass SVM, and k-NN classifiers on the real-time processor.
- Proposing a new embedded system for real-time processing and classification of EMG signals.

The rest of the chapter is organized as follows: in Section 1.2, the details of the dataset and the theoretical background are explained. Section 1.3 reviews the implementation scenario and results. In Section 1.4, the implementation scenario and results are provided. Section 1.5 compares the performance of the proposed solution. The conclusions and perspectives are given in the final section.

1.2 MATERIALS AND THEORETICAL BACKGROUND

1.2.1 Dataset Description

In this study, EMG signals were procured from a publicly available dataset as described by Nikolic [16]. The dataset consists of ten normal subjects aged 21–37

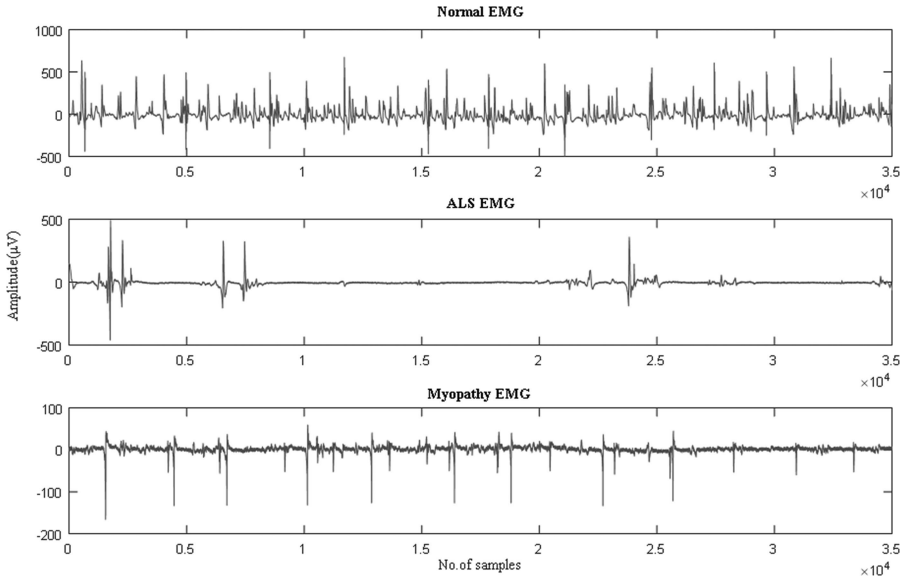

FIGURE 1.1 Sample EMG signals belonging to normal, ALS, and myopathy classes.

years, six males and four females. Six out of ten were in excellent physical condition (except one patient). Moreover, the EMG signals were digitized at a sampling frequency rate of 23437.5 Hz. An analog-to-digital converter of the 16-bit resolution was used and subsequently pass-band filtered at 2 Hz and 10 kHz by an EMG amplifier filter. Typical EMG signals (one from each EMG class) are depicted in Figure 1.1.

1.2.2 EMG Signal Decomposition Based on Discrete Wavelet Transform

DWT, called multiresolution analysis or multiscale approximation, is a well-known technique. DWT allows time-scale representation. In terms of implementation, DWT provides lower complexity and computational cost advantages than continuous wavelet transform. Moreover, it has the inherent property of increasing temporal and frequency resolution for low- and high-frequency components, thereby making it an appropriate tool for analyzing biomedical signals [17]. For instance, DWT was widely employed in the processing of the nonstationary EMG signal for feature extraction [18], data compression [19], and denoising [20].

In practice, DWT can be implemented using two filter banks iteratively, as outlined by the Mallat algorithm. The main concept behind this algorithm is to primarily pass the input signal through a series of low-pass filter LoD_k and a series of high-pass filter HiD_k followed by a downsampling process of factor two 2↓, or so-called dyadic decimation:

$$\mathrm{HiD}_k = (-1)^k \,\mathrm{LoD}_{L_w-1-k} \tag{1}$$

where $k = 1, 2, \ldots, L_w$ and L_w is the length of the filter (an even number).

The pyramidal Mallat algorithm involves decomposing the input signal into a coarse of details and approximation coefficients. The downsampled outputs of the first high-pass filter provide the detail coefficients cD_1. The output of low-pass filters provides the approximation coefficients cA_1. The first approximation cA_1 can be further decomposed, and this process can be iterated as described in Algorithm 1.

Each iteration increases the frequency resolution of low- and high-frequency components by two, as well as decreases the number of samples of sub-band signals until the maximum J_{Max} is reached, which is essentially limited by the length N of $\text{EMG}(n)$. Depending on the simulation results from this study, the optimum level of decomposition was set at $J = 7$, as there was no significant improvement in classification performance after $J \geq 7$.

Considering seven-level DWT decomposition, eight sub-band signals were obtained as given in Eq. 2. Herein, Symlet wavelet of order 11 (sym_{11}) was considered during DWT decomposition, even though other types of mother wavelets also yielded satisfactory results.

$$C = \{sB_1,\ sB_2,\ldots,\ sB_7,\ sB_8\} \tag{2}$$

where the sub-band signals from sB_1 to sB_7 are signals having detail coefficients and sB_8 is the sub-band signal having approximation coefficients. The number of samples in each of these sub-band signals depends upon the scaling parameter.

Algorithm 1: Discrete Wavelet Transform

Input: $\boldsymbol{cA_0(n) = EMG(n)}$, $\boldsymbol{n = 1,2,\ldots N}$

$$\boldsymbol{LoD_k = (Lod_0,\ldots\ LoD_{k-1}),\ k = 0,1,\ldots L_w - 1}$$

$$\boldsymbol{f_s \leftarrow \textbf{sampling rate}}$$

Output: approximation and detail coefficients

Step1: Calculate maximum level of decomposition

$$\boldsymbol{J_{\text{Max}} = \textbf{fix}\left[\log_2\left(\frac{N}{(L_w - 1)}\right)\right]} \tag{3}$$

Step 2: Choose an appropriate level of decomposition $\boldsymbol{J \leq J_{\text{Max}}}$;

Begin

for $j = 1$ to J

Step 3: Decompose the EMG signal into a low- and high-pass frequency part.

$$\boldsymbol{d_j : \left[\frac{f_s}{2^{j+1}}, \frac{f_s}{2^j}\right],\ a_j : \left[0, \frac{f_s}{2^{j+1}}\right]} \tag{4}$$

for $n = 1$ to $\boldsymbol{N / 2^j}$

Step 4: Get approximation coefficients

$$cA_j(n) = \sum_{k=0}^{L_w-1} cA_{j-1}(2n-k) \times LoD_k \tag{5}$$

Step 5: Get detail coefficients

$$cD_j(n) = \sum_{k=0}^{L_w-1} cA_{j-1}(2n-k) \times (-1)^k \, LoD_{L_w-1-k} \tag{6}$$

end for

end for

end

Return $(cA_1, \ldots, cA_J, cD_1, \ldots, cD_J)$

1.3 HARDWARE IMPLEMENTATION BASED ON COMPACTRIO-9035 CONTROLLER

Throughout this section, we will introduce how the proposed system works and describe in detail how the mathematical equations reviewed have been implemented on CompactRIO-9035 real-time controller. Finally, we will present the hardware implementation results of the adopted system.

1.3.1 System Architecture

The algorithms were validated in MATLAB using Statistics, Machine Learning, and Wavelet Toolbox to allow quick functional verification. Once the algorithms were tested on the personel computer, a dedicated hardware platform was developed to test our automated system's performance for NMD detection in real time. Figure 1.2 shows the schematic diagram of the CompactRIO-9035-based hardware implemented for this application.

NI-ELVIS II+ board was used as a function generator (FGEN) to generate the test signal (New EMG signal) derived from the testing set of EMG signals. The resulting analog output signal in AO_0 is fed to the analog input module (NI-9215) to acquire the test signal from AI_0. The acquisition data are controlled using an integrated embedded processing unit with a field programmable gate array (FPGA).

A virtual instrument (VI) designed in FPGA implements direct memory access (DMA) with an injection of a first-in, first-out (FIFO) buffer to queue the acquired data and to control the sampling frequency of 5 kHz (Figure 1.3). In addition, this VI is responsible for setting DMA-FIFO properties and the sampling delay (ticks). The configuration settings used in the FPGA target VI are shown in Table 1.1.

Each data element available is sent from the FPGA target buffer to the real-time target buffer via the Peripheral Component Interconnect (PCI) bus. It should be noted that when the real-time side buffer fills up, the DMA-FIFO engine stops streaming data, and the FPGA-side FIFO alerts the overflow error as a time-out condition (please refer to reference [21] for further details regarding the transfer process).

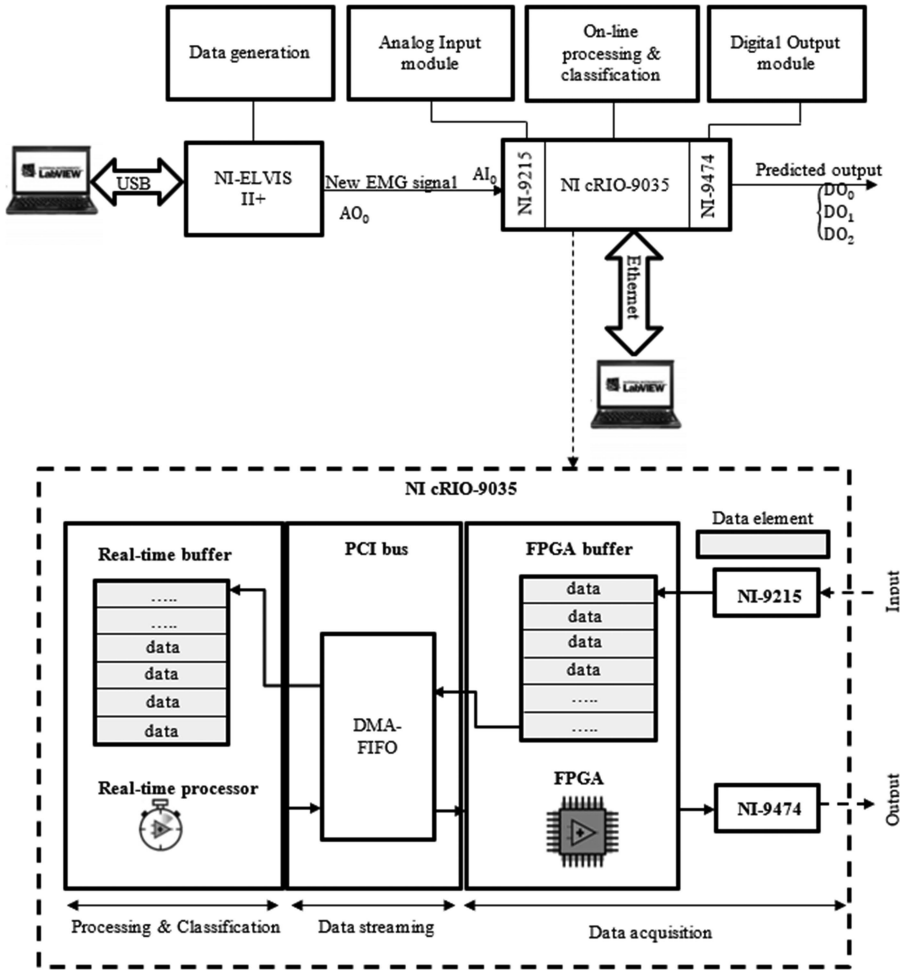

FIGURE 1.2 Schematic diagram of the NI-compactRIO-9035-based hardware and DMA-FIFO engine mechanism in cRIO technology.

DMA-FIFO has been retained among the transfer methods because it offers certain unique benefits such as:

- Efficient separation of processing tasks between the FPGA and real-time processor.
- Automatic synchronization for data transfer between the real-time processor and the FPGA.
- Allows a fast data transfer with a low system utilization.

Figure 1.4 shows the block diagram designed to continuously read the acquired data from the real-time side buffer by calling the read method. The procedure is as follows: (1) open reference to an FPGA VI or bit file; (2) add the invoke method node;

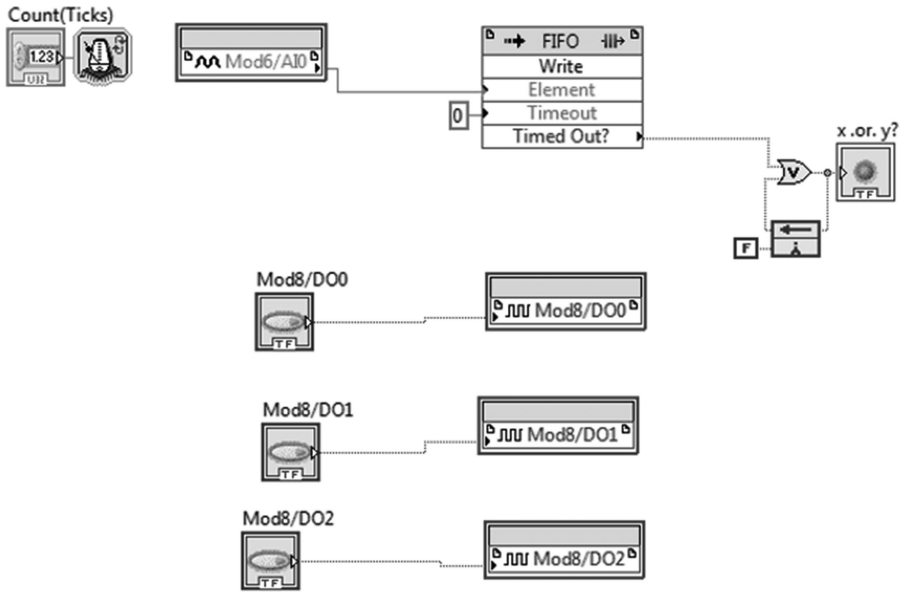

FIGURE 1.3 Block diagram of FPGA (data acquisition using LabVIEW).

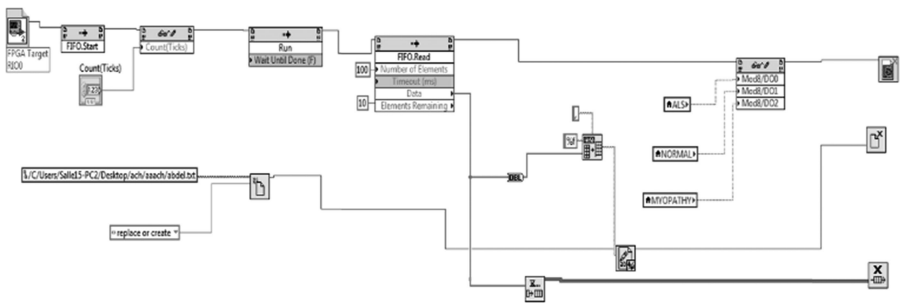

FIGURE 1.4 Block diagram of real-time host VI (data reading using LabVIEW).

TABLE 1.1
FPGA configuration parameters

Attribute	Specification
Count (ticks)	8,000
Name	FIFO
Integer word length	5 bits
FIFO's depths	1,024
Data type	Fixed point
Word length	26 bits
Type	Target to host DMA

and (3) select the FIFO read. To prevent overflow errors, the user must check whether the FPGA and real-time side buffer sizes are correctly set before reading data.

Furthermore, online processing and classification were made on a real-time processor by taking advantage of LabVIEW real-time module. Once the LabVIEW application has been built, deploying host VI over Ethernet may become necessary to run on the real-time processor.

The prototype includes a digital output module (NI-9474) to operate the device stand-alone. The NI-9474 returns the results to the Boolean indicators DO0, DO1, and DO2, corresponding to ALS, standard, and myopathy. Meanwhile, there is also the possibility to display the classification results through LabVIEW software's user-friendly interface, which is an essential point for systems that work with supervision and analysis. Moreover, it is a straightforward way to detect and classify NMDs automatically.

1.3.2 Hardware Description

As depicted in Figure 1.5, a national instrument (NI) CompactRIO-9035 real-time controller and related devices have been exploited for real-time implementation of the automated system for NMD detection. The practical implementation of the proposed scheme includes software and hardware design.

For many reasons, LabVIEW software was the obvious answer when choosing what development environment to use to develop our application. First is the fact that it offers the performance of a powerful programming language.

The hardware consists of an NI-CompactRIO (cRIO) chassis, NI-9215 input module, NI-9474 output module, NI-ELVIS II+ board, Universal Serial Bus (USB) cable, Ethernet cable, and host computers. The principal hardware components are illustrated in Figure 1.5.

cRIO system incorporates a real-time operating system with an embedded floating-point processor. cRIO is designed for multipurpose uses such as stand-alone

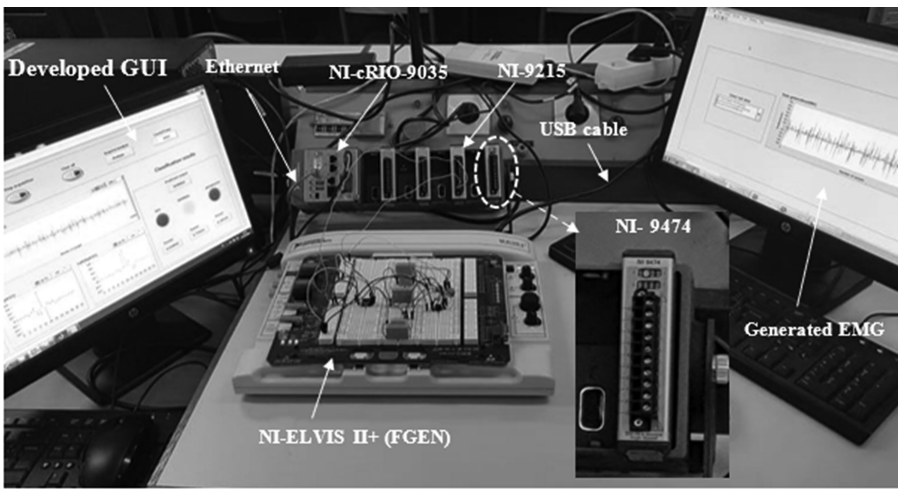

FIGURE 1.5 Experimental setup for software and hardware implementation.

operations, real-time processing needs, data acquisition, and deterministic control applications.

It has an outstanding FPGA performance with its clock of 40 MHz, interchangeable analog and digital input/output modules with hardware flexibility, and connects additional I/O over Ethernet technology (EtherCAT communication protocol). Each module in cRIO is directly connected to the FPGA. The FPGA is physically interfaced to the real-time processor via a PCI bus, as shown in Figure 1.6.

1.3.3 Embedded Hardware Design

Some striking features of NI-CompactRIO-9035 and its two I/O modules are listed in Table 1.2. Therefore, cRIO is more suitable for laboratories where versatility is beneficial. For this reason and its availability in our laboratory, NI-CompactRIO-9035 was chosen as the controller for system development.

FIGURE 1.6 Hardware instrumentation: (1) NI-CompactRIO chassis, (2) NI-9215 input module, (3) NI-9474 output module, and (4) NI-ELVIS II+ board.

TABLE 1.2
Hardware feature summary

Hardware name	Attribute	Specification
NI-cRIO-9035 [22]	CPU	Intel Atom E3825
	CPU frequency	1.33 GHz
	Number of cores	2
	RAM	4 GB
	Slot count	8-Slot
NI-9215 [23]	Simultaneous	Yes
	Module type	Voltage input
	Sample rate	100 kS/s/ch
	Resolution	16-Bit
	Channels	4 Differential
NI-9474 [24]	Module type	Sourcing output
	Channels	8 (DO_0,ㅇ ,DO_7)
	Update rate	1 μs

The NI-ELVIS II+ is a multifunctional data acquisition (DAQ) device that consolidates 12 widely-used instruments, including an oscilloscope, Bode frequency analyzer, digital multimeter, function generator (FGEN), among others.

This board instrument is implemented in NI-LabVIEW, which offers an intuitive command set for observing and analyzing experimental data. The platform is connected to the computer's USB port and supplied at 220 V/50 Hz electric network. It also offers eight differential or 16 single-ended channels, each capable of up to 1.25 MS/s (mega-samples per second) at a resolution of 16 bits in the ADC (analog-to-digital converter).

1.3.4 SVM-Based Classification

The suggested automated system for NMD detection was finally implemented successfully on a CompactRIO-9035 real-time controller after obtaining satisfactory simulation test results.

Figure 1.7 shows its simplified design for three-class Radial Basis Function (RBF) -SVM classification according to the pairwise approach. Three classes (ALS, normal, and myopathy) imply $M(M-1)/2|_{M=3}$ binary learners with $\mathrm{CM} \in \{-1,0,1\}^{3\times 3}$.

The first learner plays ALS vs. normal, the second learner plays ALS vs. myopathy, and the third learner usually plays vs. myopathy. The proposed LabVIEW real-time design consists of four major sub-VIs: three learner blocks and one voting

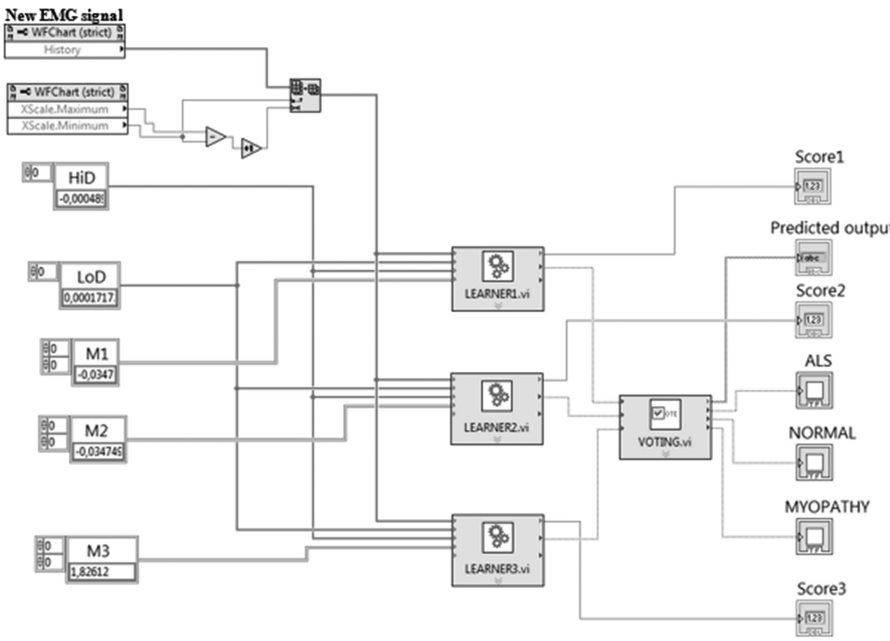

FIGURE 1.7 LabVIEW real-time design for implementation of three-class RBF-SVM.

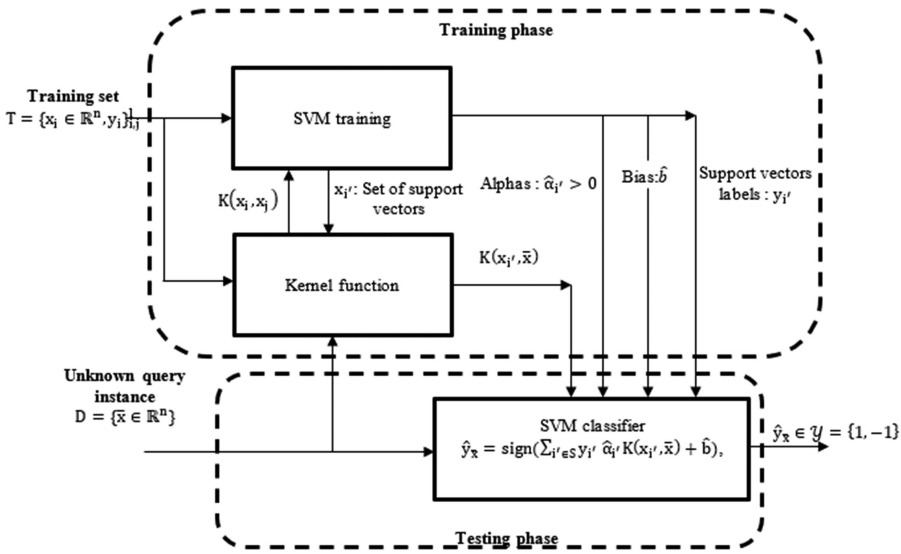

FIGURE 1.8 General architecture of the binary SVM learner and offline training.

bloc. Each learner block receives in its inputs the new EMG signal, the coefficients of the mother wavelet-based filters, and the corresponding trained binary SVM model.

As shown in Figure 1.8, the user's binary SVM models provided during the offline training phase are directly uploaded onto real-time host VI for online use. It enables a prediction to be made for a given new EMG signal. This completes the three-class-based SVM classification.

This paper has implemented a CompactRIO-9035 real-time controller. Compared to standard EMG processing, such as denoising, decomposition, and compression, EMG classification causes much higher computational complexity and storage requirements. Retraining is often unnecessary, and the algorithm's training phase can be realized offline. Therefore, reducing power consumption and hardware overhead are fundamental aspects of the EMG classification processor.

The "fitcecoc" MATLAB function constructs a multiclass SVM model using the One-vs-One (OVO) strategy during the training phase. This approach seeks to establish a decision boundary for each individual SVM binary learner, facilitating effective multiclass classification.

Figure 1.9 represents the default scheme regarding the binary SVM learner. The output (sign) provides the classification decision, being one of $\{-1, +1\}$, that is, the final score is compared to '0'; if it is greater than '0', $\underline{x}$ belongs to (class: +1). Otherwise, $\underline{x}$ belongs to (class: −1).

As shown in Figure 1.8, the global design of the binary SVM learner is composed mainly of two modules. The first one corresponds to EMG processing, including DWT-based decomposition, feature extraction, and Z-score normalization.

The second one corresponds to the SVM classification that implements the decision boundary. Having a new EMG signal (Input1) as input, the binary SVM classifier

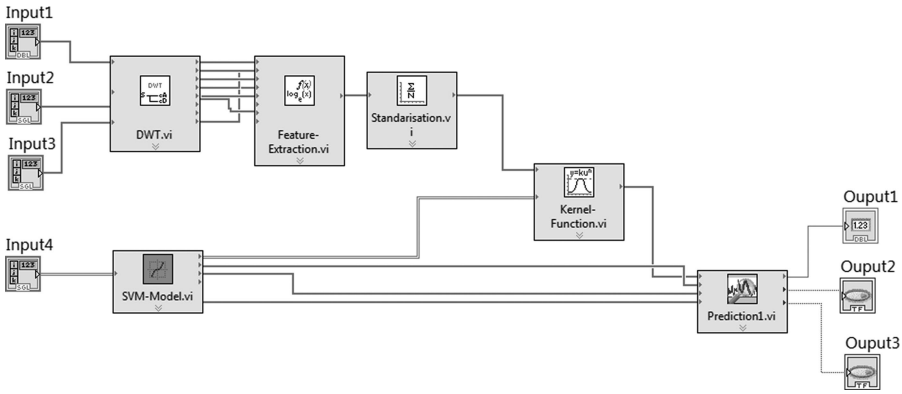

FIGURE 1.9 LabVIEW real-time-based design of binary SVM learner 1.

provides a class label (Output2 or Output3) and a score (Output1) that depends on the distance between the unknown query instance to classify and the boundary that the SVM created between the two classes. The implementation details of the following two modules are presented: (1) EMG processing module and (2) SVM classification module.

1.3.5 EMG Processing Module

DWT sub-VI was designed for the decomposition of EMG signal up to the seventh level. The seven-wavelet analysis levels were implemented on CompactRIO-9035 real-time controller.

Figure 1.10 depicts the architectural design of the DWT-based decomposition block. Using the basis of convolution as defined in Eqs. (5) and (6), the hardware implementation of the two primary filters has been completed. First, the EMG signal is multiplied by Symlet wavelet coefficients.

Table 1.3 enumerates the two filter coefficients using the "wfilters" MATLAB function. Downsampling follows the outputs of each filter block. Thus, the detail coefficients cD1 and the approximation coefficients cA1 are obtained for the first decomposition level.

The obtained cA1 becomes the input of the low- and high-pass filter blocks of the upcoming decomposition level. The process repeats exactly the same calculation at each stage of the seven decomposition levels. As output, we find the calculated sub-band signals for the EMG signal.

Then, we have implemented the proposed DWT features as shown in Figure 1.11. Next, the feature extraction sub-VI input is forwarded into the standardization sub-VI to reach the last step of the EMG processing module.

This block allows obtaining a standardized feature vector, making it insensitive to the scales on which they are measured. Finally, the obtained standardized feature vector is ready for classification.

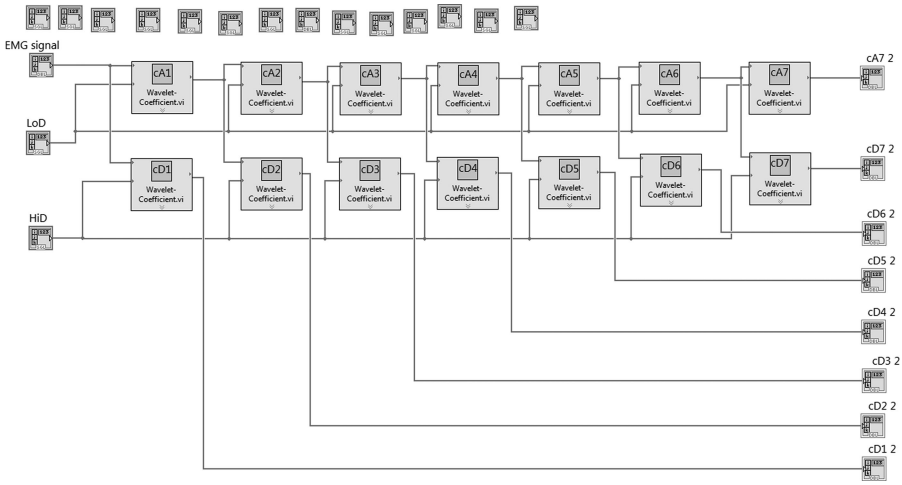

FIGURE 1.10 LabVIEW real-time design for computing detail and approximation coefficients.

1.3.6 SVM Classification Module

The classification process involves giving a standardized feature vector $\underline{x_j} = \left[\underline{x_1}\ \underline{x_2} \ldots \underline{x_{N_f}}\right]$ to the trained binary SVM model, where $\underline{x}$ has not been seen by the classifier previously.

The prediction block implements, which can be divided into Eqs. (7)–(13) for simplifying the LabVIEW real-time design, aim to reduce the computational complexity. We started by implementing the decision boundary by following these steps:

- **Step 1:** define the matrix $x_{I,j}$

$$x_{i,j} = \left[x_{1,1}\ x_{1,2}\ x_{2,1}\ \ldots\ x_{2,2}\ \ldots\ x_{N_{sv},1}\ x_{N_{sv},2}\ \vdots\ \vdots\ \ddots\ \vdots\ x_{1,N_f}\ x_{2,N_f}\ \ldots\ x_{N_{sv},N_f}\right] \in R^{N_f \times N_{sv}} \tag{7}$$

  where $i = 1,\ldots, N_f$; N_f denotes the number of features/dimensional space; $j = 1, \ldots, N_{sv}$; N_{sv} is the number of support vectors. The parameters of three trained binary SVM models with different sizes are given in Table 1.4. The multiclass SVM model exhibits over 98% accuracy, sensitivity, and specificity.

- **Step 2:** define a new vector w_j

$$w_j = \left[\left(\hat{\alpha}y\right)_1 \left(\hat{\alpha}y\right)_2 \vdots \left(\hat{\alpha}y\right)_{N_{sv}}\right] \tag{8}$$

TABLE 1.3
Coefficients of filters based on Sym_{11} mother wavelet

Filter taps	Analysis filters	
	Low pass (LiD_k)	High pass (HiD_k)
0	0.000171721950699348	–0.000489263610261923
1	–0.000038795655736158	0.000110535097642721
2	–0.001734366267297869	0.006389603666454892
3	0.000588352735396991	–0.002003471900109388
4	0.006512495674771450	–0.043000190681552280
5	–0.009857934828789794	0.035266759564466550
6	–0.024080841595864003	0.144602343705315600
7	0.037037415978859400	–0.204654794495800600
8	0.069976799610734140	–0.237689090049248970
9	–0.022832651022562687	0.730343549088395700
10	0.097198394458909470	–0.572022978010087100
11	0.572022978010087100	0.097198394458909470
12	0.730343549088395700	0.022832651022562687
13	0.237689090049248970	0.069976799610734140
14	–0.204654794495800600	–0.037037415978859400
15	–0.144602343705315600	–0.024080841595864003
16	0.035266759564466550	0.009857934828789794
17	0.043000190681552280	0.006512495674771450
18	–0.002003471900109388	–0.000588352735396991
19	–0.006389603666454892	–0.001734366267297869
20	0.000110535097642721	0.000038795655736158
21	0.000489263610261923	0.000171721950699348

- **Step 3:** calculate the RBF kernel function

$$I_{i,j} = \exp\left(-\gamma \| x_{i,j} - \underline{x_i}^T \|^2\right) \tag{9}$$

RBF kernel has been implemented on LabVIEW, as shown in Figure 1.12, where there are mainly three operations:

1. Calculation of the squared Euclidean distance between the support vector matrix (Input1: $x_{i,j}$) and the standardized feature vector (Input2: $\underline{x_i}$)

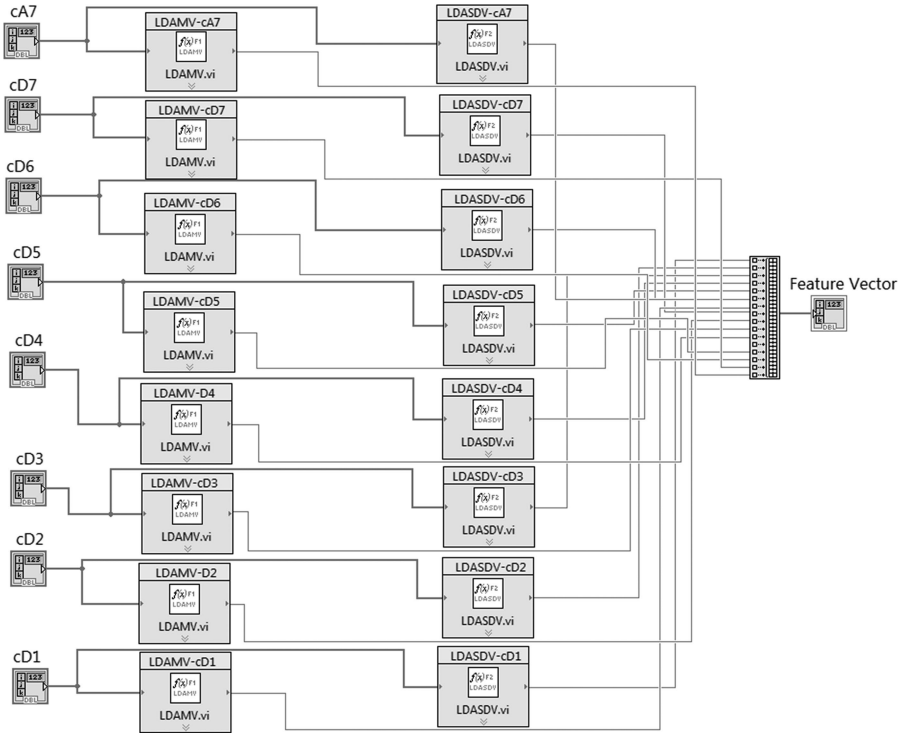

FIGURE 1.11 LabVIEW real-time design for computing LDAMV and LDASDV features.

TABLE 1.4
Multiclass SVM model parameters

Parameter	Binary SVM learners		
	Learner 1	Learner 2	Learner 3
N_{sv}	642	671	578
N_f	16	16	16

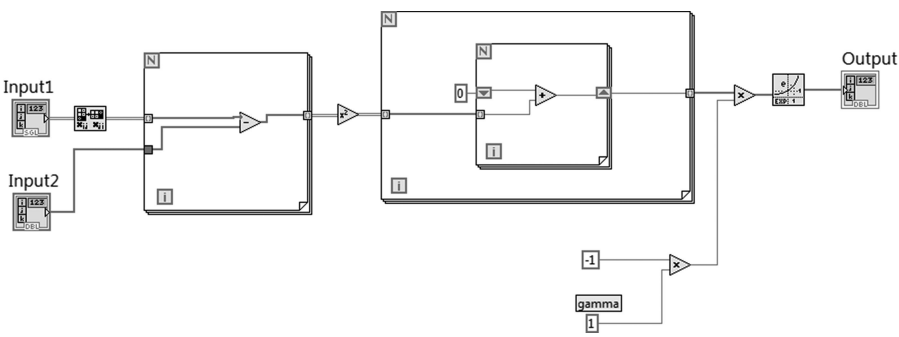

FIGURE 1.12 RBF kernel implemented on LabVIEW.

2. Multiplication between the dot products $\left\| x_{i,j} - \underline{x_i}^T \right\|^2$ and the parameter γ
3. Exponential function.

Then, the RBF kernel can be written in vector form (Output) as follows:

$$K_j = \left[\sum I_{i,1} \sum I_{i,2} \ \ldots \ \sum I_{i,N_{sv}} \right]^T \tag{10}$$

- **Step 4:** calculate the dot product a

$$a = \left(\sum_{j=1}^{N_{sv}} w_j \times K_j \right) \tag{11}$$

- **Step 5:** add the final value a to the bias term $\hat{b}$

$$\text{Score} = a + \hat{b} \tag{12}$$

- **Step 6:** assign a class label to the calculated score

$$\hat{y}_{\underline{x}} = \text{sign}(\text{Score}) = \{+1, \text{ Score} > 0 \ -1, \text{ Score} < 0 \tag{13}$$

1.3.7 k-NN-Based Classification

Figure 1.13 shows the block diagram of the multiclass k-NN implementation used for real-time automatic detection of NMDs. Its first module concerns EMG processing, which is precisely identical to the process described in point (a) of the previous subsection. Next, however, the classification module takes up the complete steps of Algorithm 4. Then, the training samples and their corresponding class labels are uploaded onto LabVIEW real-time host VI.

The Euclidean distance sub-VI combines the first three steps of the k-NN algorithm. First, it is responsible for finding the Euclidean distance between the given test sample and training samples, followed by sorting them to pick out the $k = 3$ smallest distance. At the final step, the k-NN voting sub-VI assigns the class label of the testing sample based on the majority voting.

1.4 IMPLEMENTATION RESULTS AND REAL-TIME EVALUATION

For increased user convenience, control functionalities were implemented using LabVIEW. Figure 1.14 illustrates the LabVIEW-based graphic user interface (GUI), that is, the front panel of the developed LabVIEW real-time application.

Thanks to this GUI, the user can easily access the results and controls, enabling a quick understanding of the facility's process. After successful deployment on a real-time processor, the user could validate the implemented automated system's feasibility and validity for NMDs detection.

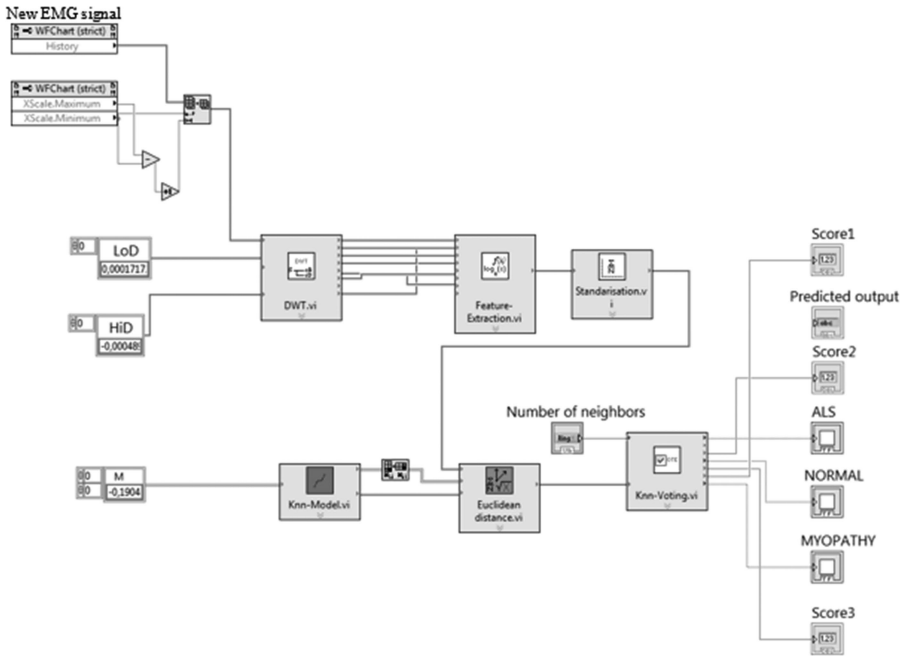

FIGURE 1.13 LabVIEW real-time design for implementation of multiclass k-NN with $k = 3$.

For more flexibility, the user has the privilege to start and stop the real-time acquisition data at any instant by clicking on the "start/stop acquisition" button. In addition, configuration parameters related to data acquisition, processing, and classification modules are available to the user. The application contains "acquire" mode and "analyze" mode.

The user may clear the waveform chart while the application is in 'acquire' mode and can restart the acquisition. At the end of the first mode, storing the acquired EMG signal to file for historical review and later investigation is also possible. In addition, the application is scalable and expandable since the developer can add other signal processing and machine learning algorithms.

When the user turns to the second mode, the classification function identifies the class label of the acquired EMG signal.

The real-time EMG signal and classification results are displayed on the GUI of the application. For example, when the EMG signal is that of an ALS case, the predicted output indicator shows "ALS" along with LED lighting up [Figure 1.14(a) and (b)]. Alternately, the class identification results are sent to the NI-9474 digital output module and LED DO_0 lights up.

In a similar manner, when the typical case is detected, LED DO_1 lights up, whereas LED DO_2 lights up for the myopathy case. Furthermore, whenever a new EMG signal is being tested, the class labels and the scores (score 1–score 3) returned by the SVM and k-NN classifiers based on the prototype are relatively consistent with those obtained using MATLAB's "SVMpredict" and "KNNpredict"

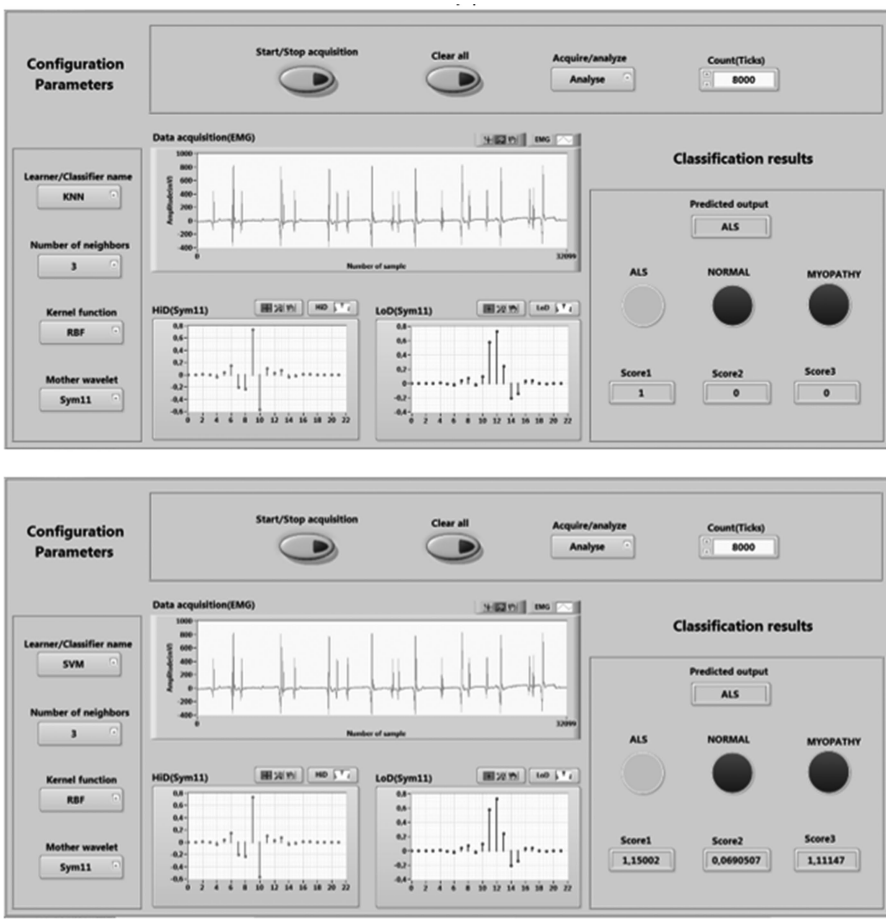

FIGURE 1.14 LabVIEW-based GUI: (a) SVM classification and (b) k-NN classification.

functions running on the PC. Consequently, this will replace the computer-aided diagnosis (CAD) tool of NMDs entirely with an embedded platform based on CompactRIO-9035 real-time controller.

1.5 DISCUSSION

The primary purpose of this study was to efficiently perform an automated classification framework to detect NMDs using clinical EMG signals. Our big challenge was extracting relevant features from the raw EMG signals enough to analyze and characterize them and then enhance the classification performance. As shown in Table 1.5, the proposed methodology highlights the use of the DWT method, resulting in a helpful time–frequency analysis of the nonstationary EMG signals. The obtained multiclass model achieved an accuracy of 98.43% when using RBF-SVM and 98.78% when using k-NN with tenfold CV.

TABLE 1.5

Descriptive comparison between different studies for NMDS classification and their achieved accuracy

Abbreviations: N = normal, A = ALS, M = myopathy, FS = feature selection, FESVM = evolutionary support vector machine, RF = random forest, LDA = linear discriminant analysis, MLPNN = multiple-layer perceptron neural network.

Reference		Feature extraction method	Classifier	Assess group		Evaluation			
N°	Year			N° Classes	N° Signals	Nf	FS	Acc (%)	CV
[28]	2013	DWT	ESVM	(N, A, M)	–	17	No	97	10-fold
[25]	2014	MUSIC	SVM	(N, A, M)	(200, 200, 200)	–	–	92.55	10-fold
[15]	2015	DWT	RF	(N, A, M)	(1200,1200, 1200)	27	No	96.6	10-fold
[26]	2016	TF, EEMD	LDA	(N, A, M)	(50, 50,150)	5	Yes	98	3-fold
[27]	2018	VMD	ELM	(N, A, M)	(107, 133, 89)	7	Yes	97.75	10-fold
[29]	2018	FE, DWT	ANN	(N, A, M)	(40, 40, 40)	10	Yes	98.0	10-fold
[30]	2019	DWT	MLPNN	(N, A, M)	(60, 60, 60)	–	–	86.5	–
[13]	2020	TQWT	ELM	(N, A, M)	(107, 133, 89)	6	Yes	98.54	10-fold
Proposed techniques (2023)		DWT	k-NN	(N, A, M)	(660, 660, 660)	16	No	98.78	10-fold
		DWT	SVM	(N, A, M)	(660, 660, 660)	16	No	98.43	10-fold

The analysis revealed that the proposed DWT-based features (LDASDV and LDAMV) combined with data standardization had demonstrated high discriminant information for EMG signal classification. Also, the 75:25 hold-out CV strategy was used to validate our developed embedded system (accuracy = 98.99%, 99.19%) obtained using RBF-SVM and k-NN classifier, respectively.

Table 9 presents a straightforward comparison of the simulation results of our method to other state-of-the-art methods available in the literature handling the multiclass classification problem. Only methods evaluated in the same dataset are included for a significant comparison.

As can be seen, the adopted method performs much better than other well-known NMDs detection methods such as multiple single classification (MUSIC) feature extraction method [25], time feature (TF), ensemble empirical mode decomposition (EEMD) [26], variation mode decomposition (VMD) [27], and TQWT [13]. However, its performance is roughly comparable to DWT-based features [15], [28–30].

The secondary purpose of this research was to conceive an embedded system to address the limitations of software implementation. So far, there has been a remarkable research process aimed at developing approaches in EMG signal classification. In this chapter, such a CompactRIO-9035 solution based on SVM or k-NN has proved itself valuable in the real-time diagnosis of NMDs in a clinical environment where the presence of healthcare professionals is in deficit.

1.6 CONCLUSION

Throughout this work, it has been found that the inherent nature of the proposed automated system for NMD detection, based on a combination of the DWT method and SVM or k-NN algorithm, is suitable for real-time operation on an embedded platform. Therefore, we have carried out two different implementation approaches of the adopted method in this vein. The first one was on a MATLAB-based CAD to test and verify the algorithms' theoretical background. The second one was on an embedded platform based on a CompactRIO-9035 real-time controller.

We investigated the use of two different supervised machine learning classifiers to early detect and classify NMDs using the public EMG signals database of the University of Copenhagen (UC database). The training model was built offline, and only the testing phase was implemented on an embedded platform. We found that when data standardization was applied, the RBF-SVM and k-NN with $k = 3$ classifier was the best, with a high classification accuracy of more than 98%.

Using LabVIEW software, an embedded system based on the CompactRIO-9035 real-time controller was selected to implement the DWT, multiclass SVM, and k-NN algorithms. The hardware implementation of the algorithms exploits the main benefit of CompactRIO, that is, its high speed and deterministic operations.

This work will contribute to our ongoing research on the application of electronics [31], signal processing [32,33], and artificial intelligence [34,35] in the field of medicine, specifically in the context of Medicine 4.0. For future research, we suggest expanding the database of EMG signals to validate the results obtained from different proposed methodologies. Furthermore, the proposed approach will undergo real-time evaluation to accurately classify various other disorders. It is particularly

recommended for diagnosing conditions such as myasthenia gravis, Parkinson's disease, muscle soreness, and neurological disorders.

REFERENCES

1. Meng, Haiying. Neuromuscular disorders. In Meng, Haiying (ed) *Self-Assessment Questions for Clinical Molecular Genetics*, 2019, pp. 543–567. https://doi.org/10.1016/B978-0-12-809967-4.00010-7.
2. Essers JMN, Murgia A, Peters AA, Janssen MMHP, Meijer K.. Recommendations for studies on dynamic arm support devices in people with neuromuscular disorders: A scoping review with expert-based discussion. *Disability and Rehabilitation: Assistive Technology*, 2020, vol. 2, pp. 1–14.
3. Deenen, Johanna C.W., Corinne G.C. Horlings, Jan J.G.M. Verschuuren, André L.M. Verbeek, and Baziel G.M. van Engelen. The epidemiology of neuromuscular disorders: A comprehensive overview of the literature. *Journal of Neuromuscular Diseases*, vol. 2, no. 1, 2015, pp. 73–85. https://doi.org/10.3233/JND-140045.
4. Meyer, Alain, Nicolas Meyer, Mickael Schaeffer, Jacques-Eric Gottenberg, Bernard Geny, and Jean Sibilia. Incidence and prevalence of inflammatory myopathies: A systematic review. *Rheumatology*, vol. 54, no. 1, 2015, pp. 50–63. https://doi.org/10.1093/rheumatology/keu289.
5. Singh, Anushikha, Malay Kishore Dutta, and Carlos M. Travieso. Analysis of EMG signals for automated diagnosis of myopathy. *4th IEEE Uttar Pradesh Section International Conference on Electrical, Computer and Electronics*, 2017, pp. 628–631.
6. Zhang, Xu, Paul E. Barkhaus, William Zev Rymer, and Ping Zhou. Machine learning for supporting diagnosis of amyotrophic lateral sclerosis using surface electromyogram. *IEEE Transactions on Neural Systems and Rehabilitation Engineering*, vol. 22, no. 1, 2014, pp. 96–103.
7. Abdelali, B., A. Achmamad, and A. Jbari. Classification and diagnosis of myopathy EMG signals using the continuous wavelet transform. *Scientific Meeting on Electrical-Electronics & Biomedical Engineering and Computer Science*, 2019, pp. 1–4.
8. Ko, Kyung Dae, Tarek El-Ghazawi, Dongkyu Kim, and Hiroki Morizono. Predicting the severity of motor neuron disease progression using electronic health record data with a cloud computing Big Data approach. *Conference on Computational Intelligence in Bioinformatics and Computational Biology*, 2014, pp. 1–6.
9. Kamali, Tahereh, Reza Boostani, and Hossein Parsaei. A multi-classifier approach to MUAP classification for diagnosis of neuromuscular disorders. *IEEE Transactions on Neural Systems and Rehabilitation Engineering*, vol. 22, no. 1, 2014, pp. 191–200.
10. Subasi, Abdulhamit. Diagnosis of neuromuscular disorders using DT-CWT and rotation forest ensemble classifier. *IEEE Transactions on Instrumentation and Measurement*, vol. 69, no. 5, 2019, 1940–1947.
11. Doulah, A.B.M. Sayeed Ud, Shaikh Anowarul Fattah, W-P. Zhu, and M. Omair Ahmad. Wavelet domain feature extraction scheme based on dominant motor unit action potential of EMG signal for neuromuscular disease classification. *IEEE Transactions on Biomedical Circuits and Systems*, vol. 8, no. 2, 2014, pp. 155–164.
12. Abdelali, B., A. Achmamad, and A. Jbari. Myopathy detection and classification based on the continuous wavelet transform. *Journal of Communications Software and Systems*, vol. 15, no. 4, 2019, pp. 336–342. https://doi.org/10.24138/jcomss.v15i4.796.
13. Verma, Agya Ram, and Bhumika Gupta. Detecting neuromuscular disorders using EMG signals based on TQWT features. *Augmented Human Research*, vol. 5, no. 1, 2020, pp. 1–9.

14. S. Chatterjee, K. Samanta, N. R. Choudhury and R. Bose et al. Detection of myopathy and ALS electromyograms employing modified window Stockwell transform. *IEEE Sensors Letters*, vol. 3, no. 7, 2019, pp. 1–4. https://doi.org/10.1109/LSENS.2019.2921072.
15. Gokgoz, E., and S. Abdulhamit. Comparison of decision tree algorithms for EMG signal classification using DWT. *Biomedical Signal Processing and Control*, vol. 18, 2015, pp. 138–144.
16. Nikolic, M. Detailed analysis of clinical electromyography signals EMG decomposition, findings and firing pattern analysis in controls and patients with myopathy and amytrophic lateral sclerosis. PhD Thesis, Faculty of Health Science, University of Copenhagen, 2001.
17. Chakraborty, Jayeeta, and Anup Nandy. Discrete wavelet transform based data representation in deep neural network for gait abnormality detection. *Biomedical Signal Processing and Control*, vol. 62, 2020, pp. 102076. https://doi.org/10.1016/j.bspc.2020.102076.
18. Abdulhamit, S., et al. Automated EMG signal classification for diagnosis of neuromuscular disorders using DWT and bagging. *Procedia Computer Science*, vol. 140, 2018, pp. 230–237.
19. Berger, P.A., F.A.O. Nascimento, J.C. Carmo, A.F. Rocha, and Icaro dos Santos. Algorithm for compression of EMG signals. In *Proceedings of the 25th Annual International Conference of the IEEE Engineering in Medicine and Biology Society*, vol. 2, 2003, pp. 1299–1302.
20. Joseph, R.K., G. Titus, and M.S. Sudhakar. Effective EMG denoising using a hybrid model based on WAT and GARCH. *Biomedical Signal Processing and Control*, vol. 45, 2018, pp. 305–312.
21. National Instruments. FPGA Module User Manual. https://www.ni.com/documentation/fr/labview-comms/5.0/fpga-targets/data-transfer-using-fifos/ [accessed October 2023].
22. National Instruments. NI cRIO-9035 Manual. https://www.ni.com/fr-fr/support/model.crio-9035.html [accessed October 2023].
23. National Instruments. Ni 9215 Manual. https://www.ni.com/fr-fr/support/model.ni-9215.html [accessed October 2023].
24. National Instruments. Ni 9474 8 Manual. https://www.ni.com/fr-fr/support/model.ni-9474.html [accessed October 2023].
25. Gokgoz, Ercan, and Abdulhamit Subasi. Effect of multiscale PCA de-noising on EMG signal classification for diagnosis of neuromuscular disorders. *Journal of Medical Systems*, vol. 38, no. 4, 2014, pp. 1–10. https://doi.org/10.1007/s10916-014-0031-3.
26. Naik, Ganesh R., S. Easter Selvan, and Hung T. Nguyen. Single-channel EMG classification with ensemble-empirical-mode-decomposition-based ICA for diagnosing neuromuscular disorders. *IEEE Transactions on Neural Systems and Rehabilitation Engineering*, vol. 24, no. 7, 2016, pp. 734–743.
27. Nagineni, Sukumar, Sachin Taran, and Varun Bajaj. Features based on variational mode decomposition for identification of neuromuscular disorder using EMG signals. *Health Information Science and Systems* vol. 6, no. 1, 2018, pp. 1–10. https://doi.org/10.1007/s13755-018-0050-4.
28. Abdulhamit, S. A decision support system for diagnosis of neuromuscular disorders using DWT and evolutionary support vector machines. *Signal, Image and Video Processing*, vol. 9, no. 2, 2018, pp. 399–408. https://doi.org/10.1007/s11760-013-0480-z.
29. Vallejo, Marcela, Carlos J. Gallego, Leonardo Duque-Muñoz, and Edilson Delgado-Trejos. Neuromuscular disease detection by neural networks and fuzzy entropy on time-frequency analysis of electromyography signals. *Expert Systems*, vol. 35, no. 4, 2018, pp. 1–10.

30. Jose, Shobha, S. George, and P.S. Roopchand. DWT-based electromyogram signal classification using maximum likelihood-estimated features for neurodiagnostic applications. *Signal, Image and Video Processing*, vol. 14, no. 3, 2020, pp. 601–608. https://doi.org/10.1007/s11760-019-01590-6.
31. Chehri, A., H. Mouftah, and G. Jeon. A smart network architecture for e-health applications. In: Tsihrintzis, G.A., Damiani, E., Virvou, M., Howlett, R.J. and Jain, L.C. (eds) *Intelligent Interactive Multimedia Systems and Services. Smart Innovation, Systems and Technologies*, vol. 6. Springer, Berlin, Heidelberg, 2010. https://doi.org/10.1007/978-3-642-14619-0_16
32. Chehri, A., and H.T. Hussein. Survivable and scalable wireless solution for E-health and emergency applications. *Proceedings of the 1st International Workshop on Engineering Interactive Computing Systems for Medicine and Health Care EICS4MED* 2011, pp. 25–29, 2011.
33. Chehri, A., and Mouftah, H.T. Internet of things - Integrated IR-UWB technology for healthcare applications. *Concurrency Computation Practice Experience*, vol. 32, 2020, p. e5454. https://doi.org/10.1002/cpe.5454
34. Ahmed, I., G. Jeon, and A. Chehri. An IoT-enabled smart health care system for screening of COVID-19 with multi layers features fusion and selection. *Computing,* vol. 105, 2023, pp. 743–760. https://doi.org/10.1007/s00607-021-00992-0
35. Ahmed, I., A. Chehri, and G. Jeon. Artificial intelligence and blockchain enabled smart healthcare system for monitoring and detection of COVID-19 in biomedical images. *IEEE/ACM Transactions on Computational Biology and Bioinformatics*. vol. 21, no. 4, pp. 814-822, July–Aug. 2024, https://doi.org/10.1109/TCBB.2023.3294333.

2 Connectivity Attributes for Remote Insulin Therapy

Richa Mishra and Tarun Kanti Bhattacharyya

2.1 INTRODUCTION

Diabetes has become a significant health concern in India, and its prevalence has been steadily increasing over the years. In 2019, the International Diabetes Federation estimated that India had approximately 77 million adults aged 20–79 years with diabetes. The COVID-19 pandemic saw the confinement of people in their homes for months together to observe social distancing to contain the pandemic. It was during these times that a strong need was felt for patients with diabetes to be periodically remain connected with their doctors for advice and medical treatment plan. Remote drug delivery devices, such as automated medication dispensers or medication delivery services, allow patients to receive essential medications at home, thereby reducing their exposure to healthcare settings where the risk of transmission of infection may be higher. The remotely controlled devices provide reminders that the patients received their medications on time, thereby improving medication adherence and overall health outcomes. These devices can help manage diabetes ensuring a consistent supply of medications and monitoring patient compliance and virtual consultation with healthcare providers. Some of the remotely controlled devices are equipped with sensors and data collection capabilities which allow better health management. These devices offer convenience, thereby reducing the need for travel and providing control over medication management [1].

Diabetes management through insulin therapy is a crucial aspect of diabetes treatment particularly for type 1 and 2 diabetes through various forms of insulin treatment including rapid-, short-, intermediate-, long-, and ultralong-acting insulin. Insulin doses are individualized based on factors such as blood sugar levels, carbohydrate intake, physical activity, and overall health.

2.2 NEED FOR CONNECTIVITY

The following are some of the reasons why constant connection between home-confined patients with diabetes and medical professionals was sought.

a. Remote Monitoring: Patients with diabetes often require regular monitoring of their blood sugar levels, medication adherence, and overall health. Connectivity

 DOI: 10.1201/9781003602729-2

allows doctors to remotely track their patients' conditions, thereby reducing the need for in-person visits which can be risky during the pandemic.

b. Adaptation of Treatment Plans: A pandemic like the COVID-19 may impact diabetes management, and the situation may require adjustments to treatment plans. Connectivity allows doctors to assess their patients' conditions and make necessary modifications to their medication, diet, and lifestyle recommendations.
c. Preventing Hospitalization: By staying connected, doctors can intervene early to help patients with diabetes maintain optimal blood sugar levels and reduce the risk of diabetes-related emergencies.
d. Data Sharing: Connectivity allows patients with diabetes to share real-time data, such as blood sugar readings, with their healthcare providers. These data can be used for more informed decision-making and personalized care.

It is needless to say that such a situation required drug delivery devices which ensure safe and efficient distribution of medication to patients, thereby reducing the need for in-person visit to hospitals.

Some of the methods by which insulin delivery is addressed are given below. Figure 2.1 shows the key features of common insulin delivery devices.

a. Insulin Pens: Insulin pens have become increasingly popular because of their ease of use and portability. They are available both in reusable and disposable forms. They allow precise dosing, thereby reducing the need for vials and syringes.

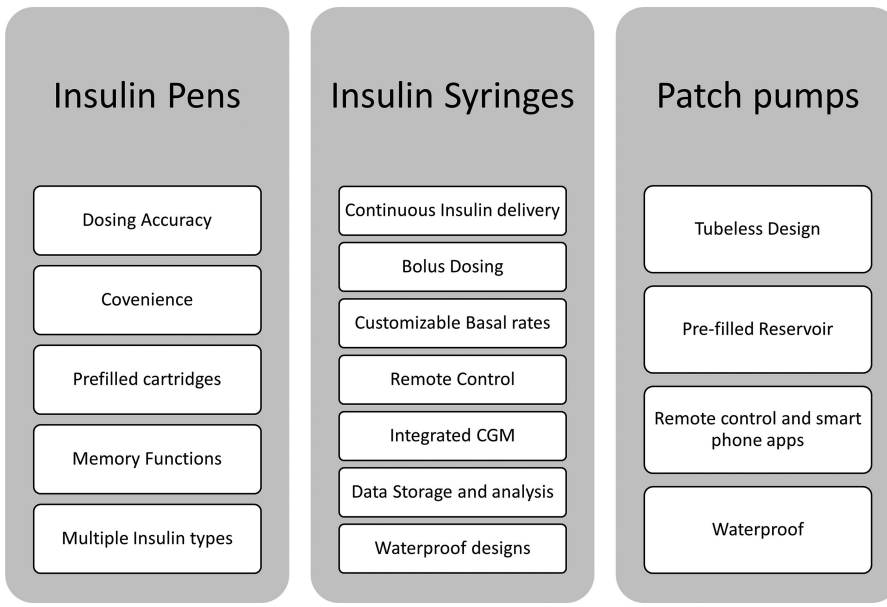

FIGURE 2.1 Chart showing various key features of common insulin delivery devices.

b. Insulin Pumps: Insulin pumps are wearable devices that continuously deliver insulin through a tiny tube (cannula) inserted under the skin. Modern insulin pumps are integrated with advanced features such as automated insulin delivery algorithms (closed loop systems) that adjust insulin doses in real time based on blood glucose levels.
c. Patch Insulin Delivery: Patch pumps are a type of insulin pump that attaches directly to the skin. They deliver insulin without tubing.

Some of the notable commercial smart insulin delivery devices currently available in the market are shown in Figure 2.2.

The connectivity features in insulin delivery devices particularly insulin pumps have become increasingly prevalent in recent years and have revolutionized diabetes management for many individuals. Figure 2.3 shows the key connectivity features in insulin delivery devices.

Insulin pumps with connectivity allow for seamless data transfer between the pump and other devices such as smartphones, continuous glucose monitors (CGMs), or insulin management applications [2–4]. This enables the following features:

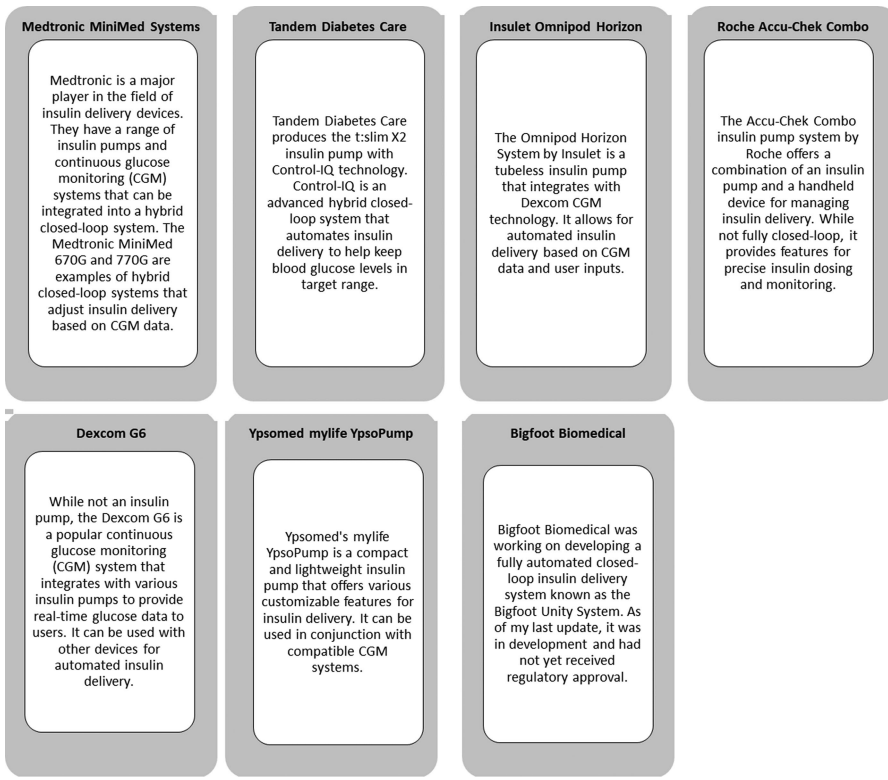
Medtronic MiniMed Systems
Medtronic is a major player in the field of insulin delivery devices. They have a range of insulin pumps and continuous glucose monitoring (CGM) systems that can be integrated into a hybrid closed-loop system. The Medtronic MiniMed 670G and 770G are examples of hybrid closed-loop systems that adjust insulin delivery based on CGM data.
Tandem Diabetes Care
Tandem Diabetes Care produces the t:slim X2 insulin pump with Control-IQ technology. Control-IQ is an advanced hybrid closed-loop system that automates insulin delivery to help keep blood glucose levels in target range.
Insulet Omnipod Horizon
The Omnipod Horizon System by Insulet is a tubeless insulin pump that integrates with Dexcom CGM technology. It allows for automated insulin delivery based on CGM data and user inputs.
Roche Accu-Chek Combo
The Accu-Chek Combo insulin pump system by Roche offers a combination of an insulin pump and a handheld device for managing insulin delivery. While not fully closed-loop, it provides features for precise insulin dosing and monitoring.
Dexcom G6
While not an insulin pump, the Dexcom G6 is a popular continuous glucose monitoring (CGM) system that integrates with various insulin pumps to provide real-time glucose data to users. It can be used with other devices for automated insulin delivery.
Ypsomed mylife YpsoPump
Ypsomed's mylife YpsoPump is a compact and lightweight insulin pump that offers various customizable features for insulin delivery. It can be used in conjunction with compatible CGM systems.
Bigfoot Biomedical
Bigfoot Biomedical was working on developing a fully automated closed-loop insulin delivery system known as the Bigfoot Unity System. As of my last update, it was in development and had not yet received regulatory approval.

FIGURE 2.2 Key features of commercially available insulin delivery devices.

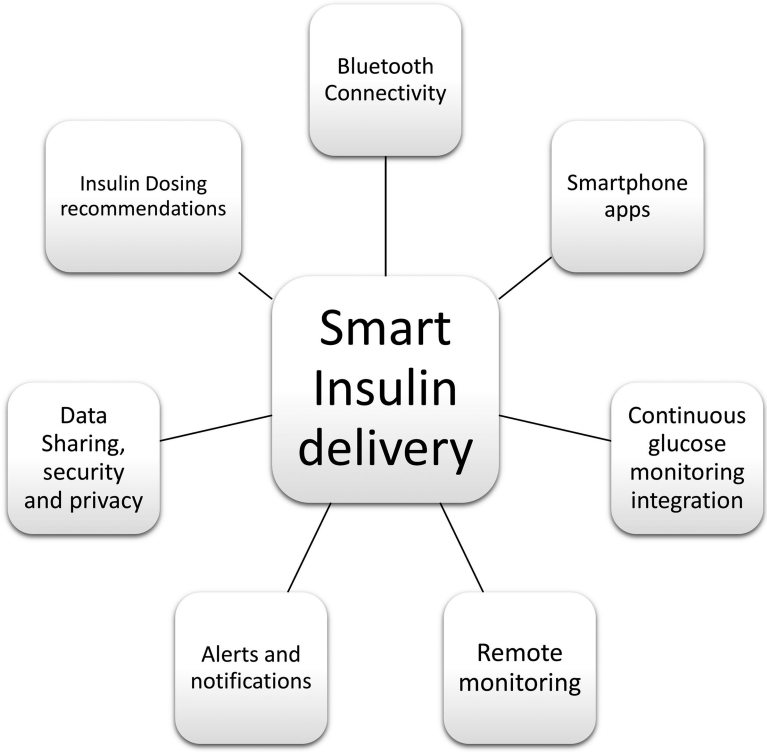

FIGURE 2.3 Connectivity features of insulin delivery devices.

a. Real-time monitoring of blood glucose levels and easy access to pump settings, making it more convenient for users for their diabetes management.
b. The caregivers or healthcare professionals can remotely monitor a user's blood glucose levels and pump data, thereby providing valuable insights and support.
c. One of the features in connected insulin delivery devices are the bolus calculators. These bolus calculators consider factors like current blood sugar levels, carbohydrate intake, and insulin sensitivity to recommend appropriate insulin doses. The calculations simplify the process of determining insulin requirements, thereby reducing the likelihood or errors and supporting better glycemic control.
d. The connectivity feature in insulin delivery devices allows for integration between insulin pumps and CGMs, creating a closed-loop system known as artificial pancreas or hybrid closed-loop system. This integration enables automatic adjustments to insulin delivery based on real-time CGM readings.
e. With connectivity, insulin pumps can receive firmware updates wirelessly allowing for enhancement of the pumps' functionality and addition of new features over time. Encryption protocols and secure data transmission may also be provided to the connected insulin pumps.

2.3 IOT-BASED INSULIN DELIVERY SYSTEMS

Internet of Things (IoT)-based insulin delivery systems leverage the power of IoT technology to enhance insulin therapy management for individuals with diabetes. This platform may enable communication with a node (laptop or smart phone) for data collection, device monitoring, and patient status [5,6]. For this the following components are required.

a. Sensor: A sensor to collect data and an actuator to effect the change, thereby minimizing human intervention.
b. Microcontroller or Processor with Preinstalled Program: These are the brains of the insulin devices, responsible for executing commands, managing data, and controlling the devices' operations. Modern microcontrollers are equipped with sufficient processing power to handle complex connectivity tasks.
c. Power Source: A battery power source needed to run the device—Insulin devices need a reliable power source to operate, and most are battery-powered. Some devices use rechargeable batteries, while others use replaceable ones. Power management hardware ensures efficient use of energy.
d. Wireless Technologies to Serve as Communication Module: To establish connectivity, insulin devices typically incorporate wireless communication modules. Common options include the following:

    - Bluetooth: Bluetooth modules allow for wireless communication with smartphones, tablets, and other compatible devices. They are often used for remote control and data syncing.
    - Wi-Fi: Some insulin devices can connect to Wi-Fi networks, thereby enabling seamless data transmission and remote monitoring. Wi-Fi connectivity may be useful in home settings or healthcare facilities.
    - Cellular: Insulin devices equipped with cellular modules can transmit data to remote servers or healthcare providers without relying on local Wi-Fi or Bluetooth connections. This is particularly valuable for real-time remote monitoring and telehealth.
    - Near-Field Communication (NFC): NFC technology allows for short-range wireless communication between devices. It is commonly used for pairing the insulin device with a smartphone or other compatible devices.

e. Memory and Storage: To store data, insulin devices include memory chips or storage components. This allows for the retention of historical insulin delivery data, glucose readings, and device settings.
f. Security Components: To ensure data privacy and security, IoT insulin devices incorporate security features such as encryption and authentication protocols.
g. Cloud Services Integration: IoT insulin devices connect to cloud platforms to securely store and transmit data, thereby enabling remote monitoring and access by healthcare providers and users.

h. Software and Firmware: IoT devices rely on software and firmware to manage device operations, data processing, and connectivity protocols.

The general workflow of IoT-based insulin delivery device is shown in Figure 2.4.

2.4 SENSORS IN CONNECTED INSULIN DEVICES

Present-day IoT insulin delivery devices often incorporate various sensors to monitor and manage diabetes more effectively [2,7,8].

Some of the sensors commonly integrated into IoT insulin devices are given below:

a. Continuous Glucose Monitoring Sensors: CGM sensors are essential components of IoT insulin devices. They are typically inserted under the skin and continuously measure blood glucose levels in the interstitial fluid. The data collected by CGM sensors can be transmitted wirelessly to a connected device or cloud platform.
b. Insulin Pumps: These pumps often include built-in sensors to monitor the device's status and insulin delivery. These sensors can detect issues such as occlusions (blockages in the infusion set) or low-insulin reservoir levels. Notifications and alerts can be generated when problems are detected.
c. Temperature Sensors: These are integrated into insulin devices to ensure that insulin remains within the recommended temperature range. Extreme temperatures may degrade insulin efficacy. These sensors also monitor the storage conditions.
d. Accelerometers and Motion Sensors: Some IoT insulin devices include accelerometers and motion sensors to detect physical activity and movement. This information is required to adjust insulin delivery based on activity levels and improve glucose control during exercise or periods of increased activity.
e. Pressure Sensors: These may be used in insulin pumps to monitor the pressure within the insulin reservoir and ensure consistent and accurate insulin delivery.
f. Battery Life and Power Indication: IoT insulin devices often include sensors to monitor battery life and power consumption. Users can receive notifications when the battery is low ensuring that the device remains operational.
g. Sensors Related to Wireless Communication (e.g., Bluetooth, Wi-Fi): These sensors are essential for transmitting data between the insulin device and a smartphone app or cloud platform. These sensors help maintain a reliable connection for data transfer.
h. Touch Sensors or Capacitive Sensors: These sensors are integrated into devices, thereby allowing users to interact with the devices through touch controls or buttons.
i. Alarm and Alert Sensors: These sensors are used to trigger alarms and alerts for various conditions, such as low blood glucose levels, insulin delivery errors, or device malfunctions.

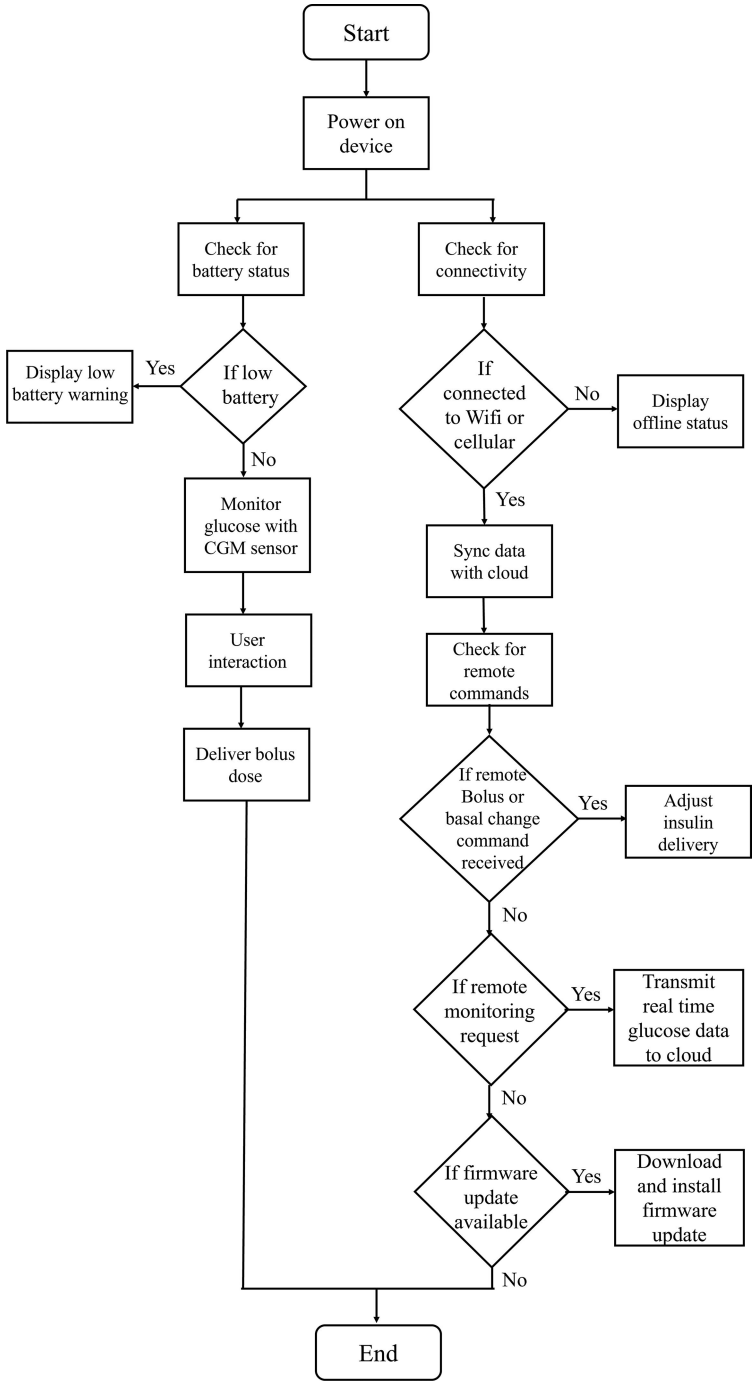

FIGURE 2.4 General workflow of IoT-based insulin delivery.

j. Environmental Sensors: These sensors measure factors like humidity or air pressure, which can impact insulin storage and stability.
k. Data Security: While not traditional sensors, IoT insulin devices prioritize data security. Encryption and security measures are implemented to protect patient data and ensure that they remain confidential and tamper resistant.

2.5 ACTUATORS USED IN INSULIN DELIVERY DEVICES

Insulin delivery devices, such as insulin pumps and insulin pens, rely on various types of actuators to dispense insulin [9,10].

Some common actuators used in insulin delivery devices are given below:

1. Motor-Driven Piston Actuators: These actuators use a small electric motor to drive a piston that pushes insulin out of a cartridge or reservoir and into a fine needle or cannula for subcutaneous injection. Motor-driven actuators offer precise control over the insulin flow rate and can be programmed to deliver specific doses at set intervals.
2. Solenoid Actuators: Solenoids are electromagnetic devices that can push or pull a plunger to dispense insulin. They are often used in disposable insulin pens and some insulin pumps. Solenoid actuators are compact and provide consistent insulin delivery.
3. Piezoelectric Actuators: Piezoelectric materials change shape when an electric voltage is applied, thereby making them suitable for micro-dispensing insulin in insulin pumps. These actuators are known for their precision and rapid response, thereby allowing for fine-tuned dosing.
4. Mechanical Button Actuators: In some insulin pens, a mechanical button on the pen's exterior is used as the actuator. Pressing the button triggers a mechanical mechanism inside the pen to deliver a specific insulin dose.
5. Infusion Pump Mechanisms: Insulin infusion pumps use a variety of mechanisms to deliver insulin continuously or in programmed doses. Some use rotary peristaltic pumps, which squeeze a flexible reservoir to push insulin through a tube and into the body. Others may use syringe-based mechanisms.
6. Pressure-Based Actuators: Some insulin delivery devices utilize pressure-based actuators to control insulin flow. These actuators rely on pressure differentials to move insulin from the reservoir to the injection site.
7. Microfluidic Systems: Microfluidic systems are used for extremely precise control of insulin flow. These systems may use micropumps and valves, offering the ability to adjust insulin delivery in real time based on sensor readings.
8. Smartphone-Controlled Actuators: Modern insulin delivery devices often come with Bluetooth or other wireless connectivity, thereby allowing users to control their insulin delivery through smartphone apps. The actuators in such devices can be remotely controlled, thereby providing convenience and ease of use.

2.6 NANOTECHNOLOGY IN INSULIN DELIVERY

Nanotechnology has been instrumental in advancing various fields, including medical applications such as the development of insulin sensors. Insulin sensors play a crucial role in monitoring and managing diabetes, a condition characterized by impaired insulin production or utilization, leading to elevated blood glucose levels. Figure 2.5 shows the pictorial representation of the role of nanotechnology in insulin delivery.

Nanomaterials, such as nanoparticles and nanocomposites, can enhance the sensitivity and selectivity of insulin sensors. For instance, nanomaterials such as carbon nanotubes, graphene, and metal nanoparticles have unique electrical, optical, and catalytic properties that can be exploited to improve the detection of insulin or glucose levels. Nanomaterials can be engineered to be biocompatible, meaning they are well-tolerated by biological systems. This is particularly important for implantable or wearable insulin sensors, as they need to interact with biological tissues without

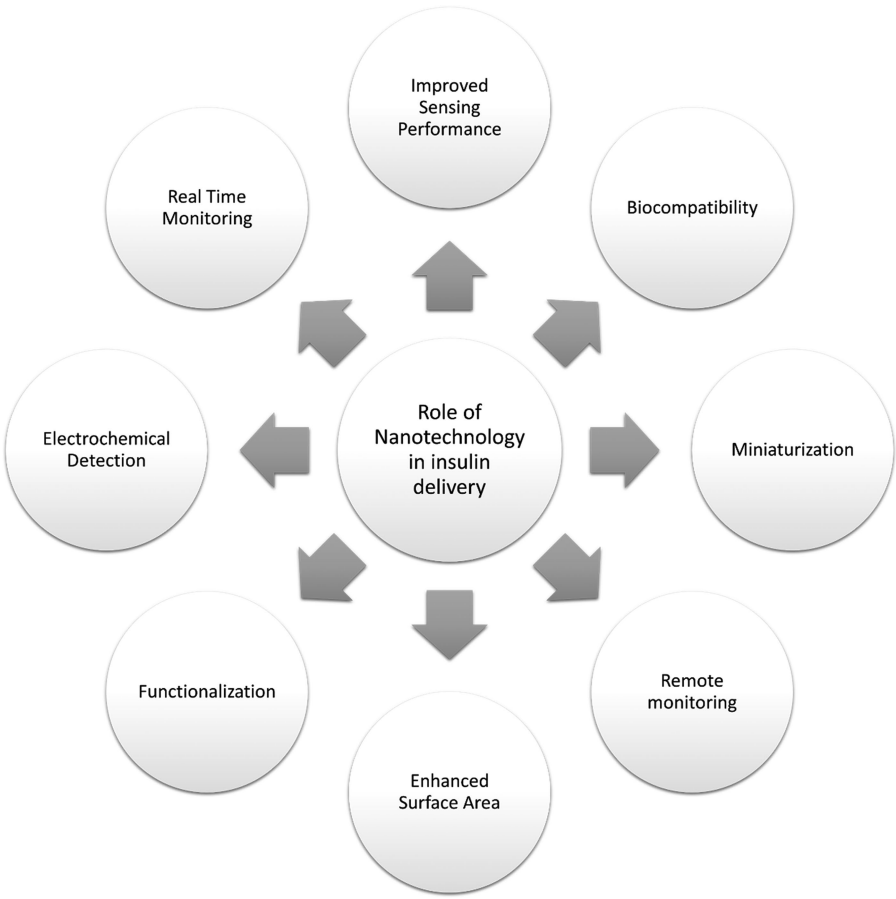

FIGURE 2.5 Role of nanotechnology in insulin delivery.

causing adverse reactions. Nanostructured materials can be designed to minimize immune responses and improve the overall biocompatibility of the sensor.

Nanotechnology allows for the miniaturization of devices, thereby enabling the creation of small and portable insulin sensors. This is especially advantageous for developing wearable or implantable sensors that can continuously monitor blood glucose levels in real time, thereby providing more accurate and timely information for diabetes management.

Nanomaterials have a high surface area-to-volume ratio, which can be advantageous for increasing the active surface area of the sensor. This increased surface area allows for more efficient binding of insulin or glucose molecules, leading to improved sensor sensitivity. Nanoparticles can be functionalized with specific molecules or receptors that selectively bind to insulin or glucose. This functionalization enhances the specificity of the sensor, thereby reducing interference from other substances present in the biological environment.

Nanomaterials are often used in electrochemical sensors for insulin detection. For example, nanomaterial-modified electrodes can facilitate electron transfer reactions, resulting in measurable electrical signals that correlate with insulin concentrations. Nanotechnology enables the development of sensors capable of real-time monitoring. This is particularly valuable for individuals with diabetes, as it allows for prompt adjustments to insulin administration based on dynamic changes in blood glucose levels [11–14].

2.7 FIRMWARES

Insulin delivery devices often rely on firmware to control their operation and user interfaces. Firmware is the software embedded in the device's hardware that governs how the device functions. Firmware plays a critical role in the overall functionality, safety, and user experience of insulin delivery devices. Manufacturers continuously update and improve firmware to enhance device performance, add new features, and address any identified issues to ensure the best possible care for individuals living with diabetes [15–21]. Figure 2.6 shows the representation of insulin delivery device firmwares.

2.8 MACHINE LEARNING-BASED ALGORITHMS FOR INSULIN DELIVERY

Machine learning-based algorithms for insulin delivery have shown promise in optimizing insulin dosing and improving glucose management for individuals with diabetes. Machine learning-based algorithms can analyze individualized data, including blood glucose levels, insulin sensitivity, carbohydrate intake, and activity levels, to create personalized insulin dosage recommendations [22]. These algorithms can adapt and learn from historical data to optimize insulin dosing based on specific needs, leading to better glycemic control. They can adapt to changes in an individual's physiology and lifestyle factors over time. As new data are collected, the algorithms continuously update their models to reflect the evolving insulin requirements.

Insulin delivery Device Firmwares				
Control and Dosing Algorithms Firmware contains control algorithms that determine how insulin is delivered based on user input and sensor data. These algorithms calculate insulin doses, adjust basal rates, and handle bolus dosing to help maintain target blood glucose levels.	**Safety Features** Safety is paramount in insulin delivery devices. Firmware includes features such as safeguards against insulin overdose, alerts for low insulin levels, occlusion detection, and mechanisms to prevent accidental button presses.	**User Interface** The firmware provides the user interface on the device's display screen or through a companion app. It allows users to set basal rates, enter mealtime boluses, review history, and interact with the device.	**Wireless Connectivity** Many modern insulin pumps and pens have Bluetooth or other wireless capabilities. Firmware manages the wireless connectivity, allowing the device to communicate with other devices, such as smartphones, continuous glucose monitors (CGMs), and data-sharing platforms.	**Data Logging and Storage** Firmware records and stores data related to insulin delivery, including timestamped insulin doses, basal rates, and bolus history. This information is crucial for both users and healthcare providers for diabetes management.
Remote Updates Some insulin pumps are designed to receive firmware updates remotely. This allows manufacturers to improve device functionality, fix bugs, and enhance security without requiring users to replace their hardware.	**User Profiles** Firmware may support multiple user profiles, allowing individuals with diabetes to configure the device according to their unique needs and preferences. This can include different basal rate schedules and insulin sensitivity factors.	**Security and Encryption**: Security features are essential to protect patient data and ensure the device's integrity. Firmware may include encryption algorithms and authentication mechanisms to safeguard sensitive information.	**Integration with Continuous Glucose Monitors (CGMs)** For closed-loop insulin delivery systems (artificial pancreas), firmware integrates with CGMs to receive real-time glucose data and adjust insulin delivery accordingly to maintain glucose within target ranges.	**Customization and Alerts** Firmware allows users to customize alarms, alerts, and notifications based on their preferences and needs. These alerts can include low reservoir warnings, battery status, or connectivity issues.

FIGURE 2.6 Chart showing various features of firmware installed in the contemporary insulin delivery devices.

Machine learning-based algorithms can integrate data from various sources, such as CGMs, insulin pumps, meal tracking apps, and physical activity monitors. By fusing these data streams, algorithms can provide a comprehensive view of an individual's glucose dynamics and insulin needs, facilitating more accurate insulin dosing recommendations. The algorithms are utilized in closed-loop insulin delivery systems, also known as artificial pancreas systems. Machine learning-based algorithms also analyze historical data to identify patterns and trends in blood glucose levels, insulin requirements, and other factors influencing diabetes management. They also optimize insulin therapy by considering various factors simultaneously, such as meal timing, exercise, stress levels, and insulin absorption rates. By incorporating these complex variables, algorithms can recommend insulin dosage adjustments. They can

continuously learn and improve over time as more data become available. With continuous feedback and refinement, these algorithms can enhance their accuracy and precision, thereby leading to increasingly effective insulin dosing recommendations.

It's important to note that machine learning-based algorithms for insulin delivery are still being developed and validated in clinical trials. While they hold great promise, their real-world implementation requires careful consideration, rigorous testing, and regulatory approvals to ensure safety, efficacy, and adherence to medical standards [23–24].

It's crucial for individuals with diabetes and healthcare professionals to collaborate closely when utilizing machine learning-based algorithms for insulin delivery. Healthcare providers can provide guidance on the appropriate use of these algorithms and ensure proper integration into an individual's diabetes management plan [25].

2.9 ARTIFICIAL INTELLIGENCE IN INSULIN DELIVERY

Artificial intelligence (AI)-based insulin dosing optimization is an approach to diabetes management that leverages AI algorithms to provide more precise and personalized insulin dosing recommendations for individuals with diabetes [26,27]. This technology aims to improve blood glucose levels, reduce the risk of hypoglycemia (low blood sugar), and enhance the overall quality of life for people with diabetes. Here's how it works (Figure 2.7):

The benefits of AI-based insulin dosing optimization show themselves in the form of improved glucose levels, as it makes more precise and personalized insulin dosing recommendations. AI algorithms can help minimize the risk of hypoglycemia by proactively adjusting insulin doses. AI provides valuable insights into glucose patterns, trends, and the impact of various lifestyle factors on blood sugar levels [28,29]. While AI-based insulin dosing optimization holds great promise, it is crucial for these systems to undergo rigorous testing, gain regulatory approval, and be used under the guidance of healthcare professionals.

2.10 REGULATORY COMPLIANCES

Connected insulin delivery devices, which are also known as "smart" or "digital" insulin pumps, have the potential to improve the management of diabetes but also raise several regulatory issues and challenges. These issues can vary by country, but some common regulatory concerns associated with connected insulin delivery devices are addressed in this section. Figure 2.8 shows details of various regulatory compliances for developing connected insulin delivery devices.

Before these devices can be marketed and sold, they typically need to gain regulatory approval from the relevant health authorities, such as the U.S. Food and Drug Administration in the United States. The approval process can be lengthy and expensive, and it involves demonstrating the safety and efficacy of the device. Moreover, connected insulin pumps are vulnerable to cybersecurity threats, including hacking and data breaches. Regulators may require manufacturers to implement robust cybersecurity measures to protect patient data and ensure the safe operation of the device. Collecting and transmitting health data from these devices raises privacy

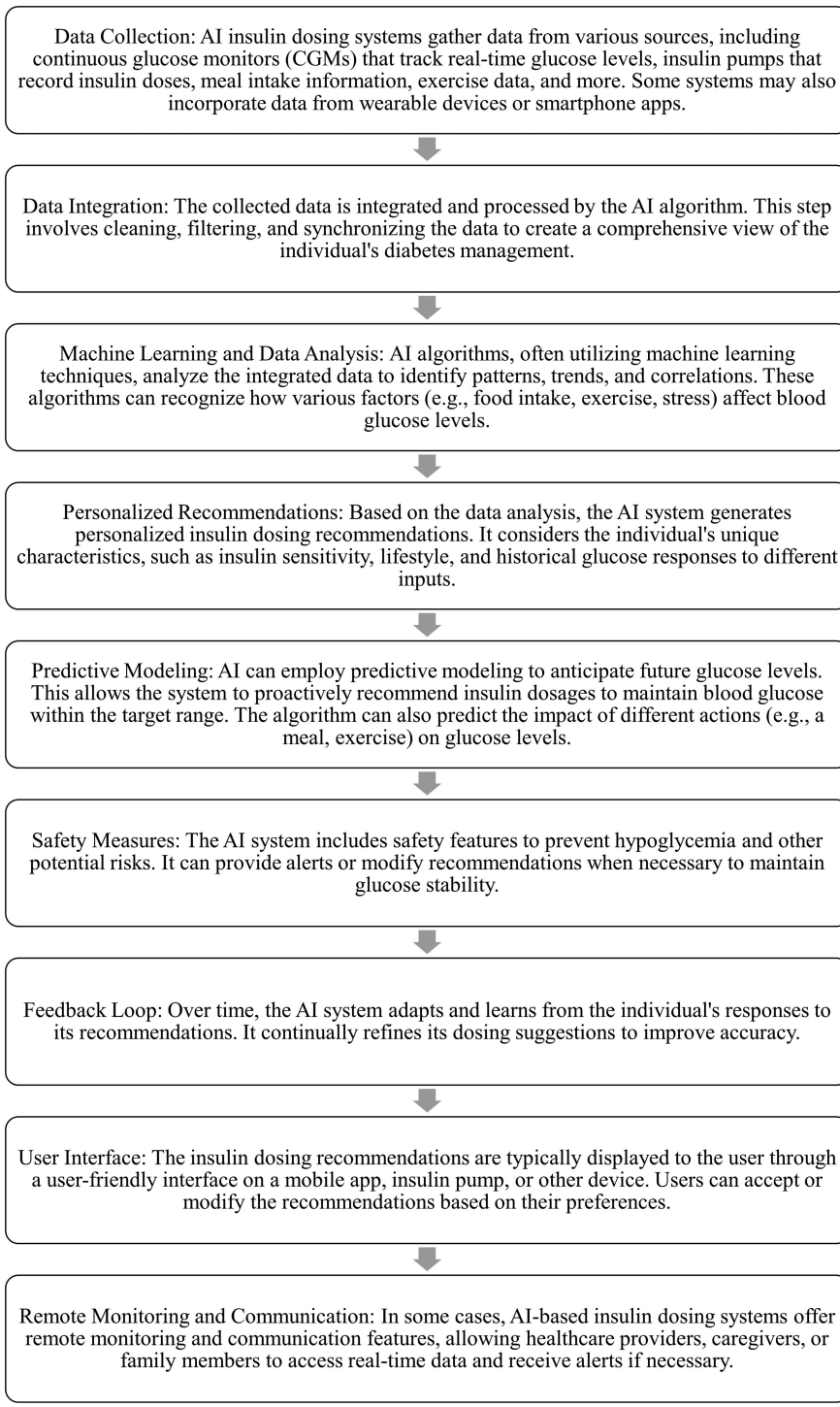
Data Collection: AI insulin dosing systems gather data from various sources, including continuous glucose monitors (CGMs) that track real-time glucose levels, insulin pumps that record insulin doses, meal intake information, exercise data, and more. Some systems may also incorporate data from wearable devices or smartphone apps.
Data Integration: The collected data is integrated and processed by the AI algorithm. This step involves cleaning, filtering, and synchronizing the data to create a comprehensive view of the individual's diabetes management.
Machine Learning and Data Analysis: AI algorithms, often utilizing machine learning techniques, analyze the integrated data to identify patterns, trends, and correlations. These algorithms can recognize how various factors (e.g., food intake, exercise, stress) affect blood glucose levels.
Personalized Recommendations: Based on the data analysis, the AI system generates personalized insulin dosing recommendations. It considers the individual's unique characteristics, such as insulin sensitivity, lifestyle, and historical glucose responses to different inputs.
Predictive Modeling: AI can employ predictive modeling to anticipate future glucose levels. This allows the system to proactively recommend insulin dosages to maintain blood glucose within the target range. The algorithm can also predict the impact of different actions (e.g., a meal, exercise) on glucose levels.
Safety Measures: The AI system includes safety features to prevent hypoglycemia and other potential risks. It can provide alerts or modify recommendations when necessary to maintain glucose stability.
Feedback Loop: Over time, the AI system adapts and learns from the individual's responses to its recommendations. It continually refines its dosing suggestions to improve accuracy.
User Interface: The insulin dosing recommendations are typically displayed to the user through a user-friendly interface on a mobile app, insulin pump, or other device. Users can accept or modify the recommendations based on their preferences.
Remote Monitoring and Communication: In some cases, AI-based insulin dosing systems offer remote monitoring and communication features, allowing healthcare providers, caregivers, or family members to access real-time data and receive alerts if necessary.

FIGURE 2.7 Different steps of artificial intelligence-enabled insulin delivery.

FIGURE 2.8 Various regulatory compliances required to be taken into account while developing connected insulin delivery devices.

concerns. Manufacturers must comply with data protection regulations, such as the Health Insurance Portability and Accountability Act in the United States, and the General Data Protection Regulation in the European Union. Ensuring that connected insulin delivery devices can seamlessly integrate with other diabetes management tools and electronic health records is important for patient care. Regulatory bodies may set standards or guidelines for interoperability to improve the user experience and overall care quality. The complexity of these devices may require specialized training for healthcare providers and patients. Regulators may require manufacturers to develop training materials and provide ongoing support to users to ensure safe and effective use. Manufacturers must establish systems for reporting and investigating adverse events related to their devices. This is essential for monitoring and addressing safety concerns. Manufacturers must provide clinical evidence of the device's safety and effectiveness. This evidence typically comes from clinical trials and real-world studies.

Regulatory requirements for connected insulin delivery devices are subject to change and may vary by jurisdiction. Manufacturers and developers must work closely with regulatory agencies, stay informed about evolving standards, and prioritize patient safety and data security in the development and deployment of these devices [30,31].

2.11 CONCLUSION

Smart connected insulin delivery devices are insulin delivery systems that are equipped with advanced technology and connectivity features to enhance diabetes management and provide users with greater control and convenience. These devices often integrate with smartphone apps, CGM systems, and other tools to provide real-time data, remote monitoring, and personalized insulin dosing. To create an IoT-based insulin delivery device, we need a combination of hardware components that can collect, process,

and transmit data. It's important to note that developing an IoT-based insulin delivery device requires expertise in electronics, medical regulations, and software development. The use of AI and machine learning-based algorithms will likely increase in future. Manufacturers and developers must work closely with regulatory agencies, stay informed about evolving standards, and prioritize patient safety and data security in the development and deployment of connected insulin devices.

REFERENCES

1. Bhavani, T., Vamsee, Krishna P., Chinmay, C., & Priyanka, D. (2022). Stress Classification and Vital Signs Forecasting for IoT-Health Monitoring. *IEEE/ACM Transactions on Computational Biology and Bioinformatics*, 10.1109/TCBB.2022.3196151
2. Vargas, E., Aiello, E., Pinsker, J., Teymourian, H., Tehrani, F., Church, M., Laffel, L., Doyle, F., Patti, M., Dassau, E., & Wang, J. (2022). Development of a Novel Insulin Sensor for Clinical Decision-Making. *Journal of Diabetes Science and Technology*, 17, 1029–1037. https://doi.org/10.1177/19322968211071132.
3. Boizel, R., Pinget, M., Lachgar, K., Parkin, C., Grulet, H., Guillon-Metz, F., & Weissmann, J. (2014). Clinical Evaluation of the Use of a Multifunctional Remotely Controlled Insulin Pump. *Journal of Diabetes Science and Technology*, 8, 1145–1150. https://doi.org/10.1177/1932296814545670.
4. Gu, W., Liu, Y., Chen, Y., Deng, W., Ran, X., Chen, L., Zhu, D., Yang, J., Shin, J., Lee, S., Cordero, T., & Mu, Y. (2017). Multicentre Randomized Controlled Trial with Sensor-Augmented Pump vs Multiple Daily Injections in Hospitalized Patients with Type 2 Diabetes in China: Time to Reach Target Glucose. *Diabetes & Metabolism*, 43(4), 359–363. https://doi.org/10.1016/j.diabet.2016.12.009.
5. Valsalan, P., Hasan, N.U., Farooq, U., Zghaibeh, M., & Baig, I. (2022 December 21). IoT Based Expert System for Diabetes Diagnosis and Insulin Dosage Calculation. *Healthcare* (*Basel*), 11(1), 12. https://doi.org/10.3390/healthcare11010012. PMID: 36611472; PMCID: PMC9819254.
6. Gopalakrishnan, K., Balakrishnan, A., Govardhanan, K., & Selvarasu, S. (2022 December 28). Propositional Inference for IoT based Dosage Calibration System Using Private Patient-Specific Prescription against Fatal Dosages. *Sensors (Basel)*, 23(1), 336. https://doi.org/10.3390/s23010336. PMID: 36616934; PMCID: PMC9824616.
7. Basatneh, R., Najafi, B., & Armstrong, D. (2018). Health Sensors, Smart Home Devices, and the Internet of Medical Things: An Opportunity for Dramatic Improvement in Care for the Lower Extremity Complications of Diabetes. *Journal of Diabetes Science and Technology*, 12, 577–586. https://doi.org/10.1177/1932296818768618.
8. Nguyen, Q., Caro, A., Raoux, M., Quotb, A., Floderer, J., Bornat, Y., Renaud, S., & Lang, J. (2013). A Novel Bioelectronic Glucose Sensor to Process Distinct Electrical Activities of Pancreatic Beta-Cells. 2013 35th Annual International Conference of the IEEE Engineering in Medicine and Biology Society (EMBC), 172–175. https://doi.org/10.1109/EMBC.2013.6609465.
9. Kroon, L. (2009). Overview of Insulin Delivery Pen Devices. *Journal of the American Pharmacists Association: JAPhA*, 49(5), e118–131. https://doi.org/10.1331/JAPhA.2009.08125.
10. Ward, W., Castle, J., Jacobs, P., & Cargill, R. (2014). Can Glucose Be Monitored Accurately at the Site of Subcutaneous Insulin Delivery? *Journal of Diabetes Science and Technology*, 8, 568–574. https://doi.org/10.1177/1932296814522805.
11. Mansoor, S., Kondiah, P., Choonara, Y., & Pillay, V. (2019). Polymer-Based Nanoparticle Strategies for Insulin Delivery. *Polymers*, 11(9), 1380. https://doi.org/10.3390/polym11091380.

12. Ramírez, A., Corro, G., Zehe, A., & Thomas, A. (2018). Nanotechnological Approach to the Treatment of Diabetes. *American Journal of Medical Sciences and Medicine*, 6(2), 19–26.https://doi.org/10.12691/ajmsm-6-2-1.
13. Veiseh, O., Tang, B., Whitehead, K., Anderson, D., & Langer, R. (2014). Managing Diabetes with Nanomedicine: Challenges and Opportunities. *Nature Reviews Drug Discovery*, 14, 45–57. https://doi.org/10.1038/nrd4477.
14. Krol, S., Ellis-Behnke, R., & Marchetti, P. (2012). Nanomedicine for Treatment of Diabetes in an Aging Population: State-of-the-Art and Future Developments. *Maturitas*, 73(1), 61–67. https://doi.org/10.1016/j.maturitas.2011.12.004.
15. Chu, M., Chen, J., Gordijo, C., Chiang, S., Ivovic, A., Koulajian, K., Giacca, A., Wu, X., & Sun, Y. (2012). In Vitro and in Vivo Testing of Glucose-Responsive Insulin-Delivery Microdevices in Diabetic Rats. *Lab on a Chip*, 12(14), 2533–2639. https://doi.org/10.1039/c2lc40139h
16. Braune, K., Lal, R.A., Petruželková, L., Scheiner, G., Winterdijk, P., Schmidt, S., Raimond, L., Hood, K.K., Riddell, M.C., Skinner, T.C., Raile, K., Hussain, S. (2022 January). OPEN International Healthcare Professional Network and OPEN Legal Advisory Group. Open-Source Automated Insulin Delivery: International Consensus Statement and Practical Guidance for Health-Care Professionals. *Lancet Diabetes Endocrinology*, 10(1), 58–74.
17. https://novoengineering.com/portfolio/insulin-pump-controller-embedded/ accessed on 05.10.2023.
18. Ward, W., Castle, J., Jacobs, P., & Cargill, R. (2014). Can Glucose Be Monitored Accurately at the Site of Subcutaneous Insulin Delivery? *Journal of Diabetes Science and Technology*, 8, 568–574. https://doi.org/10.1177/1932296814522805.
19. Wang, Y., Xie, H., Jiang, X., & Liu, B. (2014). Intelligent Closed-Loop Insulin Delivery Systems for ICU Patients. *IEEE Journal of Biomedical and Health Informatics*, 18, 290–299. https://doi.org/10.1109/JBHI.2013.2269699.
20. Doorn, W., Foreman, Y., Schaper, N., Savelberg, H., Koster, A., Kallen, C., Wesselius, A., Schram, M., Henry, R., Dagnelie, P., Galan, B., Bekers, O., Stehouwer, C., Meex, S., & Brouwers, M. (2021). Machine Learning-Based Glucose Prediction with Use of Continuous Glucose and Physical Activity Monitoring Data: The Maastricht Study. *PLoS ONE*, 16(6), e0253125. https://doi.org/10.1371/journal.pone.0253125.
21. Thyde, D., Mohebbi, A., Bengtsson, H., Jensen, M., & Mørup, M. (2020). Machine Learning-Based Adherence Detection of Type 2 Diabetes Patients on Once-Daily Basal Insulin Injections. *Journal of Diabetes Science and Technology*, 15, 98–108. https://doi.org/10.1177/1932296820912411.
22. Amit, K., Chinmay, C., & Wilson, J. (2021). Reinforcement Learning for Medical Information Processing over Heterogeneous Networks. *Springer Multimedia Tools and Applications*, 80, 1–22. https://doi.org/10.1007/s11042-021-10840-0
23. Thomas, A., & Heinemann, L. (2021). Algorithms for Automated Insulin Delivery: An Overview. *Journal of Diabetes Science and Technology*, 16, 1228–1238. https://doi.org/10.1177/19322968211008442.
24. Davidson, P., Steed, R., & Bode, B. (2005). Glucommander: A Computer-Directed Intravenous Insulin System Shown to be Safe, Simple, and Effective in 120,618 h of Operation. *Diabetes Care*, 28(10), 2418–2423. https://doi.org/10.2337/DIACARE.28.10.2418.
25. Contreras, I., & Vehí, J. (2018). Artificial Intelligence for Diabetes Management and Decision Support: *Journal of Medical Internet Research*, 20(5), 1–5. https://doi.org/10.2196/10775.
26. Priyanka, D., Achintya, K.S., Chinmay, C., Monoj, S., Vineet, R. (2021). Application of AI on Post Pandemic Situation and Lesson Learn for Future Prospects. *Journal of Experimental & Theoretical Artificial Intelligence*, 35(3), 1–24. https://doi.org/10.1080/0952813X.2021.1958063

27. Divyashree, P., & Dwivedi, P. (August 2023). AI Computing as Ubiquitous Healthcare Solution: Predict Parkinson's for Large Masses in Society. *IEEE Transactions on Computational Social Systems*, 10(4), 1752–1757. https://doi.org/10.1109/tcss.2022.3224046.
28. Curran, K., Nichols, E., Xie, E., & Harper, R. (2010). An Intensive Insulinotherapy Mobile Phone Application Built on Artificial Intelligence Techniques. *Journal of Diabetes Science and Technology*, 4, 209–220. https://doi.org/10.1177/193229681000400126.
29. Garza, K., Jedraszko, A., Weil, L., Naranjo, D., Barnard, K., Laffel, L., Hood, K., & Weissberg-Benchell, J. (2018). Automated Insulin Delivery Systems: Hopes and Expectations of Family Members. *Diabetes Technology & Therapeutics*, 20(3), 222–228. https://doi.org/10.1089/dia.2017.0301.
30. Heinemann, L., Khatami, H., Mckinnon, R., & Home, P. (2015). An Overview of Current Regulatory Requirements for Approval of Biosimilar Insulins. *Diabetes Technology & Therapeutics*, 17, 510–526. https://doi.org/10.1089/dia.2014.0362.
31. Kroon, L. (2009). Overview of Insulin Delivery Pen Devices. *Journal of the American Pharmacists Association: JAPhA*, 49(5), e118–131. https://doi.org/10.1331/JAPhA.2009.08125.

3 Deep Learning-Driven Human Activity Recognition for Remote Health Applications in Internet of Things-Enabled Smart Cities

Namita Sethi, Sujit Bebortta, Subhranshu Sekhar Tripathy and Subhendu Kumar Pani

3.1 INTRODUCTION

The Internet of Things (IoT) has evolved as a game-changing technology that connects diverse devices and allows for seamless data sharing and communication. The emergence of IoT applications has given rise to the Internet of Healthcare Things (IoHT) in the healthcare industry and has completely changed the way how healthcare services are provided and accessed. IoHT uses mobile applications, wearable sensors, and interconnected medical devices to monitor patient health, deliver remote care, and enhance overall healthcare results. We are using IoT as one type of network environment where every interconnected nodes has the ability to communicate with other nodes to share critical healthcare data in order to facilitate critical and immediate action making. Due to these factors, the utilization of IoT proves highly beneficial in emergency situations like some medical application. The IoT is an effective framework, as it helps to develop intelligent healthcare systems. To assist individuals, including students and those with disabilities who may struggle with independent living, it enables prompt connection of patients to healthcare services [1]. Consequently, the increasing deterioration of students' health motivates our focus on online health monitoring systems to prevent life-threatening diseases like cancer.

DOI: 10.1201/9781003602729-3

3.1.1 Background and Motivation

IoT is a groundbreaking idea which makes it possible for connecting different networks. IoT creates new chances to improve operations in a variety of industries, including manufacturing, agriculture, the economy, and healthcare services, by linking everything to the internet. The healthcare industry is one of these industries that is important and presents social and economic problems in every country. The public and private sectors are placing increasing demands on healthcare professionals, who are under pressure to adjust. This is crucial since there are more and more vulnerable people living alone or in remote places, such as elderly people, people with disabilities, and people suffering from chronic illnesses. As a result, remote patient monitoring is becoming more and more necessary and commonplace. In the past few years, healthcare monitoring has expanded dramatically as a result of cutting-edge technologies in the internet, IoT, and sensing devices fields. Many hospitals employ mobile applications to schedule appointments, check patients' records, and review results. However, medical wearable technology can be used to track physiological signs like blood pressure, blood sugar, ECG, and others. The monitored data may be saved in a dataset or sent to the information platform for real-time patient diagnosis.

The development of intelligent medical equipment provides further advantages, including lower costs, improved patient medical comprehension, and reduced workload for hospital staff. The goal of IoT infrastructure is to enable automated information gathering and processing so that e-services for the older people living in their homes may be constructed on top of it [2]. IoT is primarily supported technically by ongoing development of software for wireless sensor/actuator networks and by the production of affordable, energy-efficient hardware for device connection. Due to factors such as an ageing population, an increase in chronic diseases, and a shortage of healthcare resources, the global healthcare system is under increasing pressure. By enabling remote monitoring and proactive healthcare interventions, human activity recognition (HAR) in IoHT offers a chance to lessen some of these difficulties. It is driven by the need to investigate HAR's potential in IoHT to improve patient outcomes, enhance healthcare delivery, and ease the burden on healthcare systems.

Every person has different daily routines and healthcare requirements. Personalized healthcare strategies can be created by utilizing HAR in IoHT and adapting interventions based on individual activity profiles and health conditions. The goal of this research is to harness the potential of HAR in IoHT to enable more individualized and accurate healthcare, which will increase patient satisfaction and treatment outcomes. Access to healthcare is a major issue in many places, especially in rural or underdeveloped areas. By providing remote monitoring, virtual consultations, and prompt actions, HAR in IoHT can solve this major issue [3]. The potential of HAR in IoHT to increase health equality and decrease healthcare disparities while extending healthcare access to underserved groups is the driving force for this concept which needs to be implemented. Because of developments in sensor technology, machine learning (ML) algorithms, and data analytics, the field of HAR in IoHT is continually changing. By examining the most recent approaches, detecting gaps, and suggesting new directions and solutions, this research aims to contribute to the ongoing technological advancement. This paper intends to contribute to the establishment

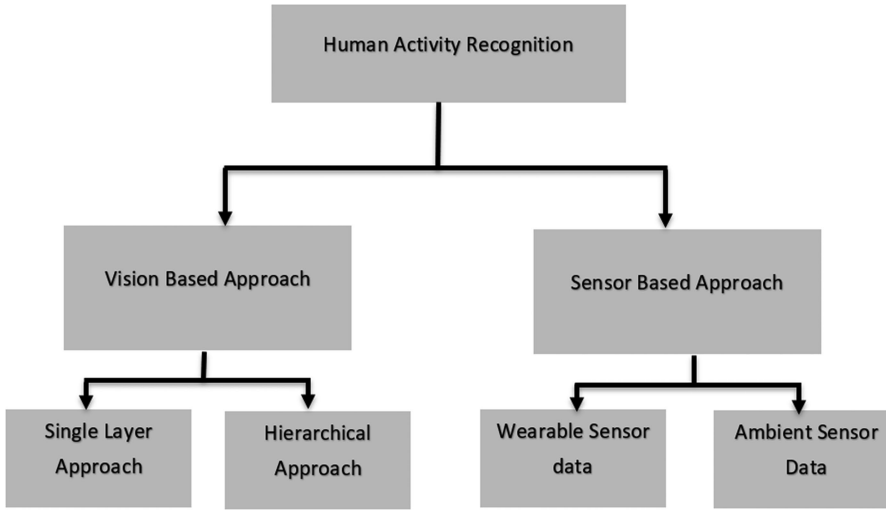

FIGURE 3.1 Classification of the HAR.

of reliable and effective healthcare systems by encouraging innovation in HAR for IoHT. IoHT integration in healthcare brings up significant ethical and privacy issues. HAR systems gather sensitive information about people's activities and health status; hence, strong privacy protection methods and ethical standards are required. The goal of this study is to examine the ethical effect of HAR in IoHT, offer answers to privacy issues, and make sure that technology is used in healthcare responsibly. Figure 3.1 shows the classification of HAR.

3.1.2 Overview of Internet of Healthcare Things

The IoT is a revolutionary paradigm that is being used by the IoHT to revolutionize the management, monitoring, and delivery of healthcare. To build a connected ecosystem within the healthcare industry, smart devices, sensors, data analytics, and communication technologies must be integrated.

The essential elements and traits of IoHT are:

a **Interconnected Devices:** It discusses the many categories of interconnected devices utilized in IoHT, including wearable sensors, medical equipment, smart implants, mobile, wearable technology, healthcare systems, and communication technologies. It will place a strong emphasis on the IoHT's seamless connectivity and integration. It highlights their part in gathering current health-related data. The key components and infrastructure of IoHT include sensors, data storage and processing systems, connectivity protocols, and security mechanisms [4]. It explains how these components work together to create a robust and interconnected healthcare ecosystem. The key elements of IoHT, such as medical devices (such as wearable sensors and smart implants), communication networks (such as wireless, cellular,

and cloud infrastructure), data analytics platforms, and healthcare applications, will be covered in this paper.

b **Data Analytics:** It examines the value of data analytics in IoHT and how it makes it possible for healthcare practitioners to make sense of the gathered data. It encompasses methods for data analysis and pattern identification like ML and deep learning (DL). To promote smooth integration and effective data sharing among various healthcare devices and systems, IoHT also examines the importance of standardization and interoperability in IoHT. It places particular emphasis on the necessity of compatible technologies and data exchange standards. It also describes how IoHT makes it possible to collect, analyze, and make decisions about data in real time to enhance patient outcomes and streamline healthcare procedures.

c **Communication Technologies:** This section examines the IoHT's communication infrastructure, including networking protocols and wireless technologies like Wi-Fi, Bluetooth, and Zigbee. It talks about their part in transferring data across healthcare systems securely and effectively. Communication technologies are essential in the IoHT ecosystem for enabling seamless data transfer between interconnected devices, systems, and healthcare stakeholders. These technologies make it possible to share health-related data quickly while maintaining confidentiality, security, and dependability. The following are some crucial elements using communication technology in IoHT. IoHT relies on various wireless technologies to establish connectivity between devices. Medical equipment, smart sensors, and data hubs are frequently connected in healthcare facilities via Wi-Fi, which enables high-speed wireless communication. Large amounts of data, including real-time patient monitoring information and medical picture data, can be transmitted through it. Wearable technology and mobile health applications can benefit from Bluetooth's short-range wireless communication capabilities [4]. It allows for the seamless movement of data between nearby devices, making it possible to continuously check health and collect data.

d **Healthcare Monitoring and Management**: It emphasizes the uses and advantages of IoHT in illness management, healthcare monitoring, and preventive care. It goes over how IoHT makes it possible for real-time health tracking, remote patient monitoring, and individualized healthcare interventions. Important facets of IoHT healthcare monitoring and management IoHT technologies make it possible to continuously monitor a person's health measurements, giving vital information about how they are doing. Real-time tracking enables healthcare professionals to continuously monitor patients' development, adherence to treatment programs, and early indications of difficulties. This monitoring can be especially helpful for patients with chronic conditions or those receiving postoperative care. Healthcare practitioners can quickly intervene or modify treatment strategies by analyzing the gathered data. IoHT is essential in advancing preventive healthcare practices [5]. IoHT systems can offer early warnings or alarms for potential health concerns by continually monitoring and analyzing people's health data.

e **Challenges and Considerations**: These address issues including data privacy and security, interoperability, and regulatory compliance that come up while adopting IoHT in the healthcare industry. The ethical issues around data collecting, consent, and patient autonomy are also discussed. For IoHT to be successfully deployed, there are a number of issues and problems that must be taken into account. To ensure data privacy and security, IoHT entails the gathering and transmission of sensitive health-related data. This entails preventing unauthorized access to patient information, guarding against data breaches, and adhering to privacy laws like Health Insurance Portability and Accountability Act or General Data Protection Regulation. IoHT data collection for personal health presents moral questions about patient autonomy, informed permission, and data ownership. In the IoHT ecosystem, it is crucial to respect patient privacy, uphold transparency, and gain explicit authorization for data use and sharing. It is essential to incorporate ethical principles and rules into the development and application of IoHT [6-8]. To guarantee patient safety, data security, and ethical practices, healthcare institutions must adhere to a number of laws and standards. IoHT solutions must abide by these laws, which can differ between different regions or nations. For the implementation of IoHT, adherence to regulatory regulations and rules, such as acquiring the appropriate certifications and approvals, is crucial.

3.1.3 Importance of Human Activity Recognition in IoHT

An essential component of the IoHT ecosystem is HAR. HAR makes a variety of applications possible by automatically identifying and categorizing human activity. These applications help to improve patient care, healthcare administration, and general well-being. The following points will help you understand the significance of HAR in IoHT:

→ HAR in IoHT enables continuous and real-time monitoring of people's activities, offering insightful data on their daily activities, mobility patterns, and general well-being. The ability to assess patients' health state, spot irregularities or behavioral changes, and take appropriate action quickly depends on this information for healthcare professionals.

→ Healthcare professionals can analyze patients' well-being remotely thanks to HAR's ability to monitor their activities continuously and in real time. HAR systems can spot anomalies or breaks from routine patterns by precisely identifying actions like walking, sitting, sleeping, or completing particular exercises. By doing so, possible health problems can be proactively identified, falls can be predicted, and patient safety is increased.

→ Recognizing human activity is essential for controlling chronic illnesses and assisting with the rehabilitation process. IoHT systems can help in the construction of individualized treatment programs, monitoring progress, and giving patients timely interventions or reminders for medication

adherence, exercise routines, and other therapeutic activities by precisely tracking and classifying activities.

→ Falls are a major worry, especially for the senior population. IoHT-integrated HAR systems can detect falls or aberrant activity patterns and send out instant notifications to carers or emergency services. By acting quickly, negative effects from falls, such as injuries and postponed medical care, may be reduced.

→ The IoHT enables the creation of intelligent environments that adjust to people's needs and preferences by recognizing human behavior. IoHT systems can automate a variety of operations, such as altering lighting, temperature, and appliance usage, to improve comfort, energy efficiency, and general quality of life by comprehending the activities that users carry out within their living spaces.

→ The older people can benefit greatly from HAR's promotion of independent living. HAR systems can track activities of daily living (ADLs) including cooking, bathing, or dressing with wearable sensors and ambient devices. Careers or family members can be informed of emergencies or when assistance is needed by spotting anomalies or changes in activity patterns. Seniors can keep their independence with the use of HAR-based solutions, which also secure their safety and provide carers and loved ones peace of mind.

→ IoHT's human activity identification technology helps deliver personalized healthcare by identifying each patient's unique activity patterns and customizing therapies. IoHT systems can offer personalized recommendations, reminders, and treatments that are tailored to a person's unique requirements and preferences by learning about their daily routines, eventually enhancing the efficacy and efficiency of healthcare services.

→ By examining a person's everyday activities and delivering individualized solutions, HAR in IoHT promotes personalized healthcare. It can assist medical personnel in learning more about patients' dietary preferences, exercise regimens, sleeping habits, and mobility levels. To enhance overall health outcomes, such information can be used to create individualized treatment plans, optimize pharmaceutical regimens, and offer focused lifestyle advice. The IoHT creates a large amount of data from HAR that can be used for population-level analysis, clinical research, and public health campaigns. Information about population health trends, disease prevalence, and the influence of lifestyle factors on health outcomes can be found in aggregated and anonymized activity data. The creation of preventive measures, the allocation of healthcare resources, and policymaking can all benefit from this data-driven approach. IoHT's aggregated data from HAR can offer useful information for population health management, policy development, and healthcare research. The identification of trends, risk factors, and predictive models for different health issues can be accomplished by extensive analysis of activity patterns, allowing for proactive interventions, resource allocation, and evidence-based decision-making [9-13].

In Figure 3.2 we can clearly see two different layers in a health monitoring framework using IoT: IoT layers and health monitoring layers.

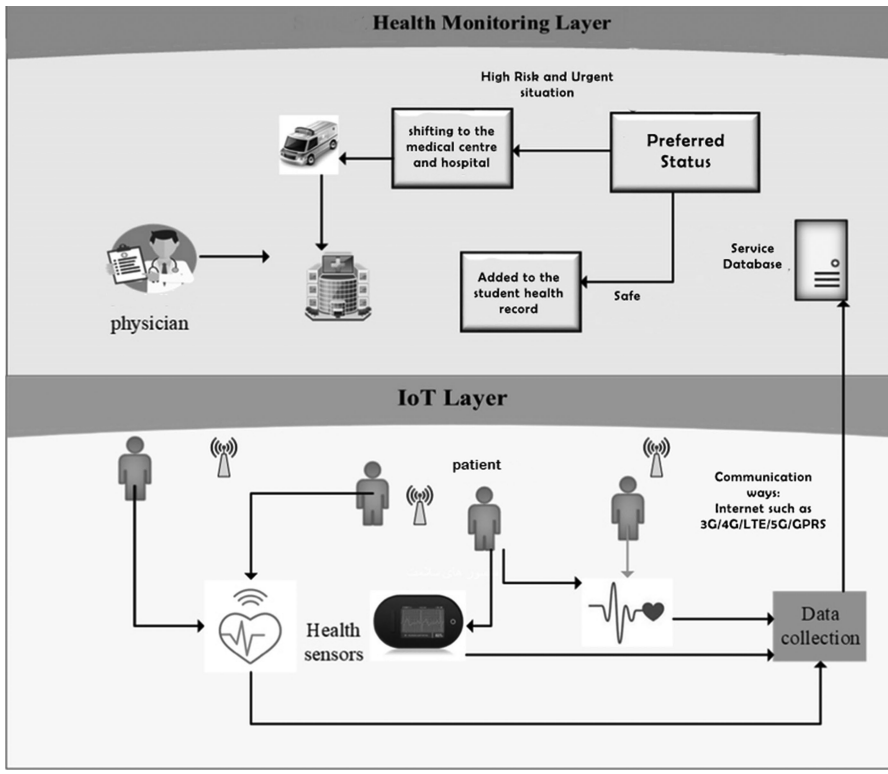

FIGURE 3.2 Health monitoring framework using IoT.

In IoT layer, the data will be collected from different patient's wearable devices, and it will be closely monitored. The monitored data include a patient's heart rate, oxygen level, and so on, and if the sensor found any unusual drastic change in the monitoring such as drop of heart rate or oxygen level, then it will give a warning to the patient or SOS warning to saved and preferred hospital given by the patient. In health monitoring layer, the data that were transferred to hospital in case of emergency will be marked as critical by the hospital and will try to reach the patient, and by ambulance the patient will be shifted to hospital and a doctor will check and make sure whether everything is fine with patient health condition. The data will be stored in cloud computing systems on a server, and later, checkup will be conducted based on the patient's health history. This will overhead in-terms of re-evaluating the physiological parameters like heart rate and oxygen level in the hospital which will save lot of time.

3.1.4 Related Work

Due to its potential use in a number of industries, including healthcare, sports, robots, and smart environments, HAR has attracted a lot of attention recently. Based on sensor data gathered from wearable, smartphones, or other sensing technologies, HAR

includes automatically recognizing and categorizing human behaviors. The important techniques, difficulties, and developments in the area are highlighted in this section's survey of the literature that has already been written about HAR. Describe the subject of HAR and its importance in a number of industries, including sports, healthcare, and wellness monitoring. Draw attention to the increased demand for HAR brought on by the development of wearable technology, sensor technologies, and the IoT. Declare that the goal of literature review is to give a thorough overview of the HAR's methods, research, and achievements.

Ganesan et al. utilized robust frameworks that are aimed at guessing/predicting cardiac disease at the general population using UCL repository dataset [14]. Work involved building a powerful model, which are cloud-based and IoT-based models, to monitor, forecast, and diagnose heart disease. Furthermore, patient data were categorized using classification algorithms to detect the presence of heart diseases. At first, with the help of a dataset of heart illness the algorithm underwent a training phase where it was taught to recognize heart-related illness. Subsequently, the trained classifier was capable of accurately evaluating incoming patient information to determine the presence of heart related illness. For the experiment purpose, different types of classifiers including J48, logistic regression, multilayer perception (MLP), and support vector machine (SVM) were tested on the benchmark dataset. These simulation outcomes provided compelling evidence that "J48 classifier" outperformed other classifiers across multiple factors, such as recall, accurateness, correctness, F-scores, and k-value. Notably, these comprehensive experimental findings clearly indicated that J48 classifier is the most perfect algorithm for this IoT-based healthcare prediction model for heart-related illness, exhibiting a precision value of 91.50, the highest recall value, with a 82.68 maximum k-value.

Kumar et al. [15] developed a "BDSDT" within an IoT-enabled healthcare system. All IoT devices underwent registration and verification (using zero knowledge proof) before being integrated into the electronic-Proof of Work (ePoW) consensus mechanism that enables the blockchain network to operate seamlessly through a smart contract-based system. Subsequently, the integration of the BDSDT with an Ethereum smart contract effectively tackled data security concerns, and the utilization of the Inter Planetary File System enabled off-chain storage, thus overcoming data storage cost challenges. Additionally, an advanced DL architecture was used for HS network intrusion detection, leveraging authenticated data. This approach combined the Deep Sparse Auto Encoder with the Bidirectional Long Short-Term Memory, which results in efficient intrusion detection systems. Experimental evaluations are conducted on CICIDS-2017 and TON-IOT which are actually two public data sources, and it reveals that compared to other alternative methods these two perform better, demonstrating nearly 99% accuracy across both the datasets, in both of the blockchain- and non-blockchain-based scenarios.

They illustrate that Intrusion Detection System (IDS) has obtained 87.31% precision, 99.04% of Author Response:accuracy, and the F1-score obtained is 83.20% and 82.89% of detection rate. so it means that it demonstrated meaningful results and performed well in comparison to other peer intrusion detection methodologies.

Kaur et al. [16] described a healthcare system that combines IoT and a random forest classifier. It utilizes IoT infrastructure and cloud computing for real-time health

monitoring. To evaluate its effectiveness, the proposed work is tested using diverse datasets related to diseases such as thyroid, heart-related illness, diabetes, and liver problems. The system leverages historical and empirical data stored in the cloud to generate recommendations. The authors' approach aims to uncover hidden patterns and facilitate reliable decision-making by searching for information in databases. This study focuses on predicting conditions like heart disease, breast cancer, diabetes, single photon emission computed tomography (SPECT) of heart thyroid, dermatology, and liver disorders, and surgical data using various ML techniques, including k-nearest neighbors (k-NN), MLP, decision tree (DT), random forest (RF), and SVM. The RF algorithm achieves an impressive accuracy of 97.26% on the Dermatology dataset and generally produces accurate results across all considered datasets. By incorporating a larger dataset and training the system with different ML methods, it is expected to improve its accuracy. Furthermore, the authors suggest that this research can help other problems such as Earth monitoring and weather reports in the near future. Since IoT devices rely on existing technologies to collect and transmit data, data security becomes a significant concern in IoT-based frameworks.

Souri et al. [17] introduced a student health monitoring system that utilizes smart student care technology and IoT technology to evaluate vital signs and detect changes in students' biological and behavioral patterns. The proposed system follows a three-tiered approach, incorporating the conceptual model and modular design of the suggested system. These stages encompass the identification of relevant data based on biological and behavioral indicators, data collection using biomedical sensors and intelligent IoT devices, and data preprocessing. To evaluate the model, various categorization techniques were used, including SVM, DT, RF, and MLP classifiers. The classification algorithms showcased remarkable performance in terms of precision, recall, accuracy, and F-score, as evidenced by the experimental results. SVM emerged as the top-performing model, achieving accuracy of 99.1%, precision of 97.2%, recall of 99.5%, and F-score 93.2% in disease prediction within our specific scenario. The notable accuracy advantage of SVM over other classifiers positions it as a valuable tool for real-time monitoring of children's health. In the upcoming stages, the primary objective of this research is to present a data processing system centered around edge computing to bring computation and data storage in close proximity to the patient's location. This approach would enhance the response time of emergency services and optimize bandwidth usage throughout the system. By developing such a system, it is anticipated that the healthcare provided to children can be further improved, thereby leveraging the potential for faster response times compared to the current suggested system.

The main focus of the study by Zhou et al. [18] revolves around utilizing DL techniques and weakly labeled sensor data to improve HAR within IoHT scenarios. To achieve more accurate HAR, the researchers devised a semi-supervised DL framework comprising two crucial function modules: an auto-labeling module and a long short-term memory (LSTM)-based classification module. The auto-labeling strategy leverages a Deep Q-Network and a novel distance-based reward rule to address the problem of improperly labeled motion data in everyday life samples. This approach enhances learning effectiveness within IoT environments. Additionally, an LSTM-based nervous network is constructed to extract contextual high-level features

from sequential motion data, thereby facilitating the identification of fine-grained patterns. Furthermore, a multi-sensor based data fusion mechanism integrates on-body sensor data, context sensor data, and personal profile data seamlessly. The study uses two sensor datasets collected from smartphones and on-body wearable devices. Comparative valuation outcomes highlight the success and utility of the given strategy when compared to three baseline techniques. Real-world trials and evaluations further demonstrate the efficacy of the approach. Future research endeavors will prioritize the development of more effective DL methods to identify significant patterns in sparsely labeled data. To enhance algorithm accuracy and effectiveness, extensive evaluations will be conducted across various scenarios.

Sharma et al. [19] introduced a framework called DeTrAs: DL-based Internet of Health, aiming to assist patients with Alzheimer's disease. DeTrAs operates through three main stages. To begin with, an Alzheimer Estimate system is put forward, using sensory movement data and a recurrent neural network (RNN). Subsequently, a two-component ensemble approach is devised for monitoring abnormalities in patients with Alzheimer's disease. The first component uses convolutional neural networks (CNNs) for emotion detection, while the second component uses time-stamp windows for a natural language processing (NLP) scheme. Additionally, an IoT-based support system for Alzheimer patients is described. Comparative evaluation of DeTrAs against existing ML algorithms demonstrates an improvement in accuracy of approximately 10%–20%. During phase 2, individuals identified via video and audio feeds undergo additional evaluation to determine the severity of abnormalities, thereby aiming to offer supportive healthcare services in the last stage. The assessment of DeTrAs incorporates various metrics, including accuracy, precision, recall, true-positive rate, false-positive rate, F-score, and the correct classification of incidents, utilizing diverse datasets for assessment purposes.

Manocha et al. [20] introduced an e-healthcare framework aimed at identifying abnormalities related to an individual's health, behavior, physical posture, and environment. Within this study, a fog module is incorporated into a health monitoring system to enhance decision-making speed and data processing efficiency. By utilizing the fog layer, abnormalities in data instances can be anticipated and events can be classified as either normal or abnormal, thereby leading to a decrease in the volume of data transmitted to the cloud for subsequent analysis. This integration of computing significantly improves the performance of the monitoring solution. Additionally, the seriousness of the health conditions is calculated on the cloud/web to determine the criticality of events and enhance the framework's usability in the healthcare sector. To preserve sensitivity in the healthcare domain, an event-based two-phased triggering mechanism is introduced, thereby leveraging the benefits of IoT and fog technologies. The fog layer uses a weighted K-mean clustering technique as the first stage of data processing, thereby enabling the detection of anomalies and enhancing manageability within the healthcare domain. Additionally, the cloud layer introduces a hybrid approach known as WKMC-ANN for early health severity prediction, supported by a multi-stage decision-making system that optimizes resource allocation. This framework is evaluated by continuously monitoring 15 individuals between 32 and 45 years of age for 30 days in an indoor setting, thereby demonstrating its effectiveness in determining irregularities with an accurateness of 94.51%,

compassion of 93.75%, particularness of 91.32%, precision of 91.58%, and f-measure of 92.78%. These results highlight the framework's capability in identifying health discrepancies across both cloud and fog layers. Future research aims to integrate sensor technology with framework, micro-controller technologies, and simulation in actual cloud environments.

In the study by Gupta et al. [21], COVID-19 (coronavirus) is predicted using ML (ABC and SVM) for IoT data systems. On a San Francisco COVID-19 dataset, this method applied two techniques of machine learning: the Artificial Bee Colony method and the SVMC. Using a confusion matrix, the system's performance was assessed. For ABC-LSVM, it achieved an accuracy of 95%, sensitivity of 95%, specificity of 95%, precision of 95%, F1-score with 96%, Matthews correlation coefficient of 89%, and similarly for ABC-Q-SVM, it achieved an accuracy of 97%, sensitivity of 95%, and we got 100% result for both precision and specificity along with F1-score of 97% and finally 93.1% Matthews correlation coefficient. Consequently, the utilization of ABC feature extraction methods for dimensionality reduction in the system enhances the output of SVM classification, presenting a comparative advantage in extracting relevant information from IoT systems before classification.

This research significantly enhances the prognosis and diagnosis of COVID-19, holding great potential for success. ML techniques, including model dimensionality reduction and classification algorithms, were used in the proposed solution. The ABC model for SVM classifiers incorporates the dimensionality reduction model into its function collection. The performance analysis and evaluation conducted for this study demonstrates that Q-SVM performs better than the L-SVM classification algorithm. The arrangement of COVID-19 data was investigated and improved through this analysis. Researchers have suggested numerous reviews utilizing presentation measures, and results demonstrated that the dimensionality reduction model might help in increasing classification output. Through gene characteristics, the stored data in IoT can aid in the monitoring/observation and assessment of COVID-19-related illnesses.

It will be crucial to look into if recently proposed studies would create feature extraction models and algorithms. This study confirms the necessity for artificial intelligence, ML, and IoT technologies to combat COVID-19 outbreak through modern work including extra reliable data and also performing research on classifiers like k-NN. Combination of telemedicine's benefits into an IoT strategy could enable software access to patient health records and support the e-communication networks among doctors and patients. Upgrading the system as one, this is best for long-term medical uses as opposed to only our current situation.

The recommended method for early case detection has the potential to reduce the danger of infectious illness and also the fatality rate. These strategies will also make it possible to track recovered instances and manage importance more effectively. The authors may decide to apply DL methods in the future to implement and identify the COVID-19 sickness. In the IoT system, the use of visual saliency to detect is used by the authors. To improve the outcome, compound rank-k projection can be used for the examination of the study and additionally we can also add the reliable feature to IoT systems. In the future, self-supervised learning may also be used.

Shaikh et al. [22] suggested that Event Process Healthcare (EPH) method introduces novel algorithms based on cloud-based DL, the amalgamation of ML techniques, an intelligent cloud infrastructure, and DL principles which forms the bedrock for catering to patients and revolutionizing the healthcare industry. These algorithms are one of the key foundations for serving patients and the healthcare sector. One of the key benefits of the suggested method is the guarantee it offers for the reliability of health data, addressing the regular issues of data loss or corruption when storing medical records. By handling all manipulations and storage on a distant server end instead of the local machine, the method utilizes machine probability level to initiate the simulation, yielding results with a remarkable 98% accuracy range. This simulation significantly enhances healthcare parameters and is utilized to obtain empirical results.

Moreover, the EPH method has demonstrated increased accuracy, reduced costs and enhanced health outcomes. Real-time data transmitted across multiple wireless networks can pose challenges for analysis and decoding in IoT applications. To tackle this issue, the EPH utilizes a data stream monitoring technique to gather pertinent data from network outcomes, thereby facilitating prompt decision-making. The suggested approach outlines a reliable event-based IoT framework that incorporates event, context, and service layers to analyze healthcare applications.

The findings presented in this work support the efficacy of our approach. Furthermore, future developments would be to focus on enhancing the right way of using the developed program in an actual-world scenario.

Islam et al. [23] developed a system to evaluate the present healthcare and patient relations systems developed for anticipating cardiac-related illness. We first reviewed the corpus of prior research, following which we got conceptual structure for systems that were created using the necessities acquired. The system's many components were developed and finished based on the conceptual framework. Finally, the success, usability, and competence of that designed system were taken into consideration when developing the evaluation research technique. We put forth a solution that consists of wearable gadgets and a mobile app that informs users of their cardiovascular disease (CVD) risk levels in the future. A system that can categorize its users into three levels of risk which is critical or high, medium or moderate and less or low risk of having a CVD with the assistance of the IoT and ML techniques. The UCI Repository dataset was utilized to estimate the levels of risk for the users using a stacking classifier, which incorporates the best-performing ML techniques.

The study's objective is to offer a full system with reliable wearing devices and a good user interface for users so that end-users can easily monitor real-time data to predict the level of risk for CVD. This study investigated the calculation of CVD by testing a total of 11 alternative models of ML algorithms. It makes use of the hardware in a useful way to gather actual or real-time data at end-user level. Our prediction method was created using two assembling classifier models within an F1-value of 91% in Level 2 and 80.4% in Level 3. The developed stacking classifier gives a 91% precision and 91% of recall score for two-zone classification and 79.3% and 81.6% for the three-zone classification.

Finally, using real-time data from 40 participants, the estimate of this system was carried out to ascertain its efficacy, effectiveness, and usabilities. These participant data are used to evaluate the system's capacity for accurate prediction, and the findings revealed a F1-score of 89.3 for the two-zone classification and 87.7% for the three-zone classification. The system's prediction quality and status have been assessed for efficiency. The findings shows that, on average, the task takes 19.325 clicks and 80.21 seconds to complete. A good outcome for usabilities is considered as the System Usability Scale score of 75.8125, which is used as the indicator to quantify usability.

3.2 PROPOSED FRAMEWORK

A thorough framework is needed to execute HAR in the context of IoHT. This framework is made up of numerous important parts that work together to make HAR accurate and effective. Data collection, preprocessing, feature extraction, activity classification, and result interpretation are just a few of the processes that the suggested framework should cover. A suggested framework for HAR in IoHT is provided below:

3.2.1 Data Collection

IoHT is based on a system of interconnected sensors that can gather different kinds of information about human activity. These sensors can be included in medical equipment or wearable devices like smartwatches and fitness bands [24]. Examples include ambient sensors, heart rate monitors, gyroscopes, and accelerometers such as motion detectors and webcams. A sensor network is created and implemented to gather information about human activity. Real-time data from these sensors are gathered and securely sent to a central data repository or a cloud-based platform for additional processing.

3.2.2 Data Preprocessing

Fusion of data from many sensors to obtain a comprehensive picture of the activity is being carried out.

3.2.3 Data Cleaning

Using methods like filtering, smoothing, and denoising clean up noise, outliers, and artifacts from the sensor data that have been acquired.

Segmentation: For further analysis, divide the continuous sensor data into informative activity segments.

Normalization of sensor data takes into account variations in user characteristics, calibration, and sensor positioning. Feature extraction is the process of identifying pertinent features from preprocessed sensor data that can be used to infer important information about human activity [25,26,27,28]. This could involve numerical measurements, geographical features, time-domain features, or frequency-domain features.

3.3 METHODOLOGIES FOR HUMAN ACTIVITY RECOGNITION

For HAR, there are some strategies and approaches available depending on the particular requirements and characteristics of the activity. Here are a few often employed HAR methodologies:

- Sensor-based approaches
- Deep learning approaches
- Machine learning approaches
- Vision-based approaches

3.3.1 Sensor-Based Approaches

A sensor-based technique relies on information gathered from a variety of sensors, including wearable technology and gyroscopes, depth cameras, magnetometers, and accelerometers. In these methods, the sensor data are often preprocessed before important features; to extract pertinent data from sensor data, feature extraction techniques can be used. These techniques include features such as numerical features, time domain, frequency domain, and wavelet-based [29]. The accuracy and robustness of HAR models can also be increased by using sensor fusion techniques, which incorporate data from various sensors. Activity detection algorithms take as input unprocessed signals from sensors or unprocessed sensor data. The activities are then differentiated using ML or DL algorithms based on the retrieved attributes.

3.3.2 Deep Learning Approaches

Because DL approaches can automatically learn hierarchical representations from unprocessed sensor data, they have become more prominent in HAR. DL architectures for HAR that are frequently used include CNNs and RNNs. While RNNs are proficient at simulating temporal connections in sequential activity data, CNNs are superior at extracting spatial patterns from sensor data. DL techniques frequently need a lot of labeled data for training and a lot of processing power. CNNs are used to extract spatial patterns from sensor data; they are especially useful for recognizing activity based on images and videos. Using RNNs or its derivatives, such as LSTM or gated recurrent unit, to describe temporal dependencies in sequential sensor data is appropriate for time-series-based activity detection [30]. Applying transformer-based models for HAR tasks can extract long-range dependencies and contextual information from sensor data. These models were initially created for NLP.

CNNs, RNNs, and other DL techniques in particular have achieved notable success in HAR. While RNNs are good at modeling temporal relationships in sequential data, CNNs are better at capturing spatial patterns and hierarchical characteristics. DL models may automatically learn features from unprocessed sensor or visual data, but they frequently need a lot of labeled data for training.

3.3.2.1 Convolutional Neural Networks

The performances of CNNs in HAR tasks have been demonstrated. Because they can extract spatial patterns and hierarchical features from unprocessed signals or raw sensor data, CNNs are especially well-suited for HAR. HAR has been successfully accomplished using CNNs. CNNs are perfect for HAR tasks involving sensor data or preprocessed sensor signals because they excel at processing visual data. In tasks requiring the identification of HAR, CNNs have demonstrated outstanding performance, especially when working with sensor data or image-based inputs. CNNs are excellent at extracting spatial and temporal information from unprocessed data, which makes them suitable for jobs requiring activity recognition. A summary of CNNs' potential for HAR is given below:

Data Representation: Over time, sensor data, such as gyroscope or accelerometer readings, can be gathered to represent human actions. Time-series sequences are frequently used to obtain these data. Steps like normalization, filtering, or feature extraction may be used before putting the data into a CNN. These actions are meant to improve the input data's relevance and quality.

Raw pictures or time-series sensor data are only a couple of the numerous types of input data that CNNs can use. The sensor data are portrayed as a CNN-friendly input format. It is frequently organized as 2D or 3D matrices, where the dimensions represent time steps, sensor channels, and sometimes more geographic data. For the purposes of training and assessing the model, the data are divided into training, validation, and testing sets.

Preprocessing methods like sliding windows or feature extraction methods can be used to transform time-series sensor data into a format that the CNN can use. Techniques like scaling, normalization, and augmentation can be applied to raw photos.

Architecture Design: Multiple convolutional layers are often followed by pooling layers and fully linked layers in the architecture of a CNN for HAR. By using filters or kernels on the incoming data, the convolutional layers are in charge of learning spatial patterns. The feature maps' spatial dimensions are reduced by the pooling layers' downsampling. The final network layers, which are fully connected, use the previously learnt elements and generate the final activity predictions.

Convolutional layers, pooling layers, and fully connected layers are typically present in CNN architectures for HAR. Applying a collection of trainable filters to the input data, convolutional layers extract pertinent features by convolving over the input. To reduce dimensionality and retrieve the most important characteristics, pooling layers downsample the feature maps. The categorization is carried out by fully connected layers at the network's edge using the extracted features [31].

The initial convolutional layer or layers, which apply filters to the input data in CNNs, are often one or more. These filters pick up regional dependencies and spatial patterns.

Training: Each sample in the labeled data used to train the CNN is assigned a particular activity label. The network learns to optimize its weights and biases during training to reduce the discrepancy between predicted and actual activity labels.

Through backpropagation and gradient descent during training, the network learns to optimize its internal parameters (weights and biases), thereby minimizing a predetermined loss function.

To obtain the best performance, hyperparameters including learning rate, batch size, and number of layers are tweaked.

Evaluation and Testing: After training, the CNN model's performance is evaluated using the validation set to measure its ability to recognize activities. Metrics such as accuracy, precision, recall, and F1-score are calculated to assess the model's performance. Subsequently, the model is tested using the independent testing set to determine its robustness and generalizability.

Utilizing evaluation parameters such as accuracy, precision, recall, and F1-score, the CNN model's performance is evaluated. These metrics gauge how well the model can categorize various activities.

3.3.2.2 Convolution Neural Network

We will discuss the concept of grouped convolution in this part and describe the heterogeneous convolution architecture that has been suggested for our healthcare activity recognition problem.

The segmentation of sensor time series is particularly important for the subsequent processes of healthcare activity recognition. The sliding window technique is perfectly suited for real-time HAR- applications, then the sensor time series can be divided into consecutive fixed lengths samples, allowing for an overlap rate. It is simple to construct and requires no preprocessing [32]. The heterogeneous sensor results are then normalized by subtracting the mean and dividing by the standard deviation into zero mean and unit variance.

Without losing simplification, a typical convolutional layer is made up of some group of the filters using the formula $\theta = [\theta_1, \theta_2, \ldots, \theta_N]$, where $\theta_i = i$th filter.

The sensor input $X = [x_1, x_2,\ldots, x_N]$ can be turned into an output $z = [z_1, z_2,\ldots, z_N]$ by using ordinary convolution, where N = number of filters.

The output feature map at channel i can be expressed notationally as follows without the filter size and bias terms:

$$z_i = \theta_i * X = \sum_{j=1}^{N} \theta_i^j * x_j \tag{1}$$

where * represents convolutional operation.

Every output F-map can then be calculated using the total of all the channels.

We can get the final output z by repeating Eq. (1) N times. Actually, the fixed kernel size largely determines the accessible field within a given CNN layer. Although the tiny filter is computationally effective, long-range contextual information is difficult to collect, which may result in fewer discriminative feature maps.

To overcome the aforementioned issue, we use heterogeneous convolution by leveraging the idea of grouped convolution, thereby boosting the performance of HAR and mitigating the problem at hand.

For $N = \hat{N}$, we first partition a group of filter sets θ into four equal sections, e.g., θ_1, θ_2, θ_3, θ_4, given that the filter sets have the shape (N, N, T, S), In this scenario, T represents the filter's height while S represents its width. The channel C is halved in this case. Unlike clustered convolution, each (N/2, N/2, T, and S) section serves a unique purpose. The input X is divided into X_1 and X_2, both with the shape (N/2, T, and S), utilizing the aforementioned four filters. These two parts are then delivered to a specific branch, which may collect contextual data at various scales.

These are actually two different scale spaces: a downsampling small-scale space that can be easily acquired using β operation and an original scale space that has the same resolution as the original sensor input. We describe the heterogeneous convolution in detail as follows:

Due to the fact that we only downsample sensor time series, the β size and stride in small-scale space for the former are both (r, 1), which may be written as follows:

$$\rho_1 = \beta_r(X1) \tag{2}$$

The feature transformation applied to β_r is based on θ_1:

$$X_1^{'} = U\left(k_1\left(\rho_1\right)\right) = U\left(\rho_1 * f_1\right) \tag{3}$$

where U(.) is the bilinear interpolation operator used to restore the resolution of small-scale space feature maps. The operation can still be expressed as follows in the original scale:

$$X_2' = k_2\left(X_1\right) = X_1 * f_2 \tag{4}$$

As a result of the pooling procedure, f_1's receptive field is magnified by a factor of r compared to f_2's, where r represents a hyperparameter of the pooling method.

As a result, in the original space the featured transformation can be guided by the small-scale space. We calibrate the weights for guiding using the X_1 residuals, which may be advantageous because:

$$Y_1' = X_1' \cdot \sigma U\left(X_1'\right) f_3 \tag{5}$$

where

'.' = element wise operator; and

σU = Sigmoid activation.

This branch's output Y_1' can be expressed as:

$$Y_1 = k_3\left(Y_1'\right) = Y_1' * f_3 \tag{6}$$

Equations (2)–(6), respectively, present the first branch's process.

This procedure is the second branch and can be described for the latter as follows:

$$Y_2 = k_4\left(X_2\right) = X_2 * f_4 \tag{7}$$

It uses standard convolution to protect the sensor time series' original contextual information. To achieve the ultimate desired output Y, we concatenate on both the intermediate outputs, Y_1 and Y_2.

3.3.3 Machine Learning Approaches

For HAR, a variety of ML techniques can be used. A key stage in these techniques is frequently feature engineering, which entails picking or manipulating pertinent characteristics from the sensor data. In HAR, ML techniques are crucial. In these methods, models are trained on labeled data to identify patterns and forecast the activities. Because they can learn from data and generalize to new examples, ML techniques are frequently used for HAR. ML techniques use labeled training data to train classifiers or models that recognize actions. Many algorithms have been utilized in HAR tasks to improve model performance; these methods necessitate feature extraction, choice, and hyperparameter optimization.

3.3.3.1 Artificial Neural Networks

HAR challenges have made extensive use of artificial neural networks (ANNs), which have been shown to be effective at handling challenging nonlinear data. By utilizing their capacity to learn and extract pertinent information from input data, ANNs, more specifically feed forward neural networks, can be used for activity recognition [33].

The structure and operation of biological neural networks serve as the basis for the class of ML models known as ANNs.

Here are the key steps involved in using ANNs for HAR:

Data Preparation: The gathering and preprocessing of the raw data is the initial phase. The information is often composed of sensor readings from wearable technology or other sources, such as gyroscope or accelerometer data. To improve the quality and usefulness of the data, preprocessing techniques like normalization, noise removal, and feature extraction may be used.

Data Representation: The actions are then represented using the retrieved features in a way that is appropriate for ANNs. The features can be arranged as input vectors, where each vector represents a particular occurrence of an activity or period of time. The ANN model is trained and assessed using the input vectors.

The input features for the ANN are represented by the preprocessed sensor data. Depending on the ANN architecture and data representation that is selected, the input data may take the form of feature vectors or time-series sequences.

Input-feature vectors are a common way to organize data, where each feature stands for a distinct facet of the activity under consideration.

Model Architecture: An input layer, one or more hidden layers, and an output layer are only a few of the layers that make up the ANN's design. The complexity of the HAR task and the make-up of the input features determine the number of nodes (neurons) in each layer and the connectivity between them. The performance of the model is also influenced by the choice of activation functions for the neurons, such as sigmoid or ReLU.

Experimentation and hyperparameter tuning can be used to examine the total number of hidden layers and some of the nodes in each layer. Complex patterns in HAR data can be effectively captured using deep ANNs with several hidden layers.

The preprocessed sensor data or extracted features are delivered to the input layer. For various activity classes, the output layer produces forecasts or probabilities.

Training: The ANN gains the ability to spot trends and connections between input features and activity labels during the training phase. The weights and biases of the neurons are frequently modified using backpropagation and gradient descent techniques to maximize the network's capacity for accurate activity classification. During training, the network is shown labeled training examples, prediction errors are calculated, and iterative model parameter updates are made. Presenting the training data to the network, computing prediction errors, and iteratively changing the model parameters to minimize the mistakes are all steps in the training process.

Evaluation and Testing: After training, validation and testing datasets are used to assess the ANN's performance. Evaluation measures that measure the model's aptitude for accurately classifying activities include speed, correctness, recollected, and F1-score. With the generalization capacity of trained ANN, the test dataset was evaluated [34,35,36], which is separate from the training data. Testing the network with unknown data allows for the evaluation of its robustness and generalization ability.

3.3.3.2 Artificial Neural Network

To effectively address the nonlinear international classification for standards (ICS) data presented in this paper, we use the ANN model, which is a commonly employed technique for effectively managing intricate nonlinear data. Several works have also documented the effectiveness of this model in time-series analysis. The input layer, hidden layer, and output layer are the three layers that this model takes into account. As a result, if we assume that O_τ represents the ANN's output, then we can model it as follows:

$$O_\tau = \varepsilon_z + \sum_{j=1}^{n} w_{jk} \left(\ln \ln \left(j \right) \right) \tag{8}$$

where w_{jk} signifies the weight between the nodes of the hidden layer and output layer, with $j = 1, 2, \ldots, l$ and $k = 1, 2, \ldots s$ representing the nodes of the hidden layer and output layer, respectively, and ε_z represents the bias corresponding to the resulting layer.

In this instance, the activation function is represented by $p(\ln(j))$.

$$\ln \ln \left(j \right) = \varepsilon_j + \sum_{p=1}^{m} \pi_i w_{pj} \tag{9}$$

where α_p stands for the value assigned to node pth in the input layer, where $p = 1, 2, \ldots s$.

To process the result of Eq. (9), which may be expressed as follows, we use the sigmoid function as the activation function.

$$\text{Sigmoid}(\pi) = \frac{1}{1+\exp(\pi)} \tag{10}$$

Now, by substituting the values in Eqs. (9) and (10) in Eq. (8), we get

$$O_\tau = \varepsilon_z + \sum_{j=1}^{n} \omega_{jk}\, p\left(\varepsilon_j + \sum_{i=1}^{m} \pi_i \omega_{pj}\right) \tag{11}$$

3.3.3.3 Performance Evaluation

The evaluation procedure will use popular metrics like accuracy, precision, recall, and F-measure. The confusion matrix affects four criteria.

So let us understand in a simple way what is a confusion matrix:

Now let us understand the basic terms used in confusion matrix:

- True Positive (TP): The overall counts with both values are positive.
- True Negative (TN): The overall counts with both values are negative.
- False Positive (FP): The total counts indicate a YES forecast but an actual NO result; it is also called Type 1 error.
- False Negative (FN): It is the total counts that were predicted to be NO when they were actually YES; it is also called Type 2 error.

In essence, it is a longer variation of the confusion matrix. The four models and its performance can be better understood and analyzed using the following metrics other than the confusion matrix:

a) Accuracy
b) Error rate
c) Precision
d) Recall
e) F1-score

Accuracy:

The accurateness is determined by dividing the total number of accurate predictions by the dataset's total number of observations. The best accuracy score is 1, while the poorest is 0.

1 – ERR can also be used to calculate it.

Formula for accuracy calculation = (TP + TN)/*N*

where *N* = total.

3.3.3.4 Rate of Error

It is defined as the ratio between the number of all inaccurate predictions with the overall number of the dataset. The best error rate is 0, while the poorest is 1.

Formula for error rate calculation = (FP + FN)/*N*

3.3.3.5 Recall

It ensures the proportion of correctly expected positive to actual positive.

Formula for recall calculation = TP/TP + FN

Precision: It determines whether an expected positive was accurate.

Formula for precision calculation = TP/TP + FP

F1-score: It is the recall and precision average, weighted. The F1-score will become 1 if the recall and precision are both 1.

Formula for F1-score calculation = (2 × precision × recall) / (precision + recall)

Specificity: It calculates the amount of time, actual and expected numbers are equal.

Formula for specificity calculation = TP/(TN + FP)

False positive rate = It determines the frequency with which actual negative equals to expected positive.

Formula for false positive rate calculation = FP/(FP + TN)

3.4 EVALUATION AND VALIDATION

To evaluate the effectiveness and dependability of HAR systems, evaluation and validation are essential procedures. They aid in ensuring that the suggested models or frameworks appropriately categorize actions and have good generalizability to unobserved data. Here are some typical methods for HAR evaluation and validation:

3.4.1 Train-Test Split

A prominent method for assessing HAR models is the train-test split. A training set and a testing set are created by splitting the labeled dataset into these two groups. In most of the cases, 70%–80% are training accounts and 20%–30% for testing.

3.4.2 Cross-Validation

1. The dataset is split into *k* subsets or folds for cross-validation.
2. Each fold serves as the testing set while the other folds are utilized for training the model. The model is trained and evaluated *k* times.
3. After then, the performance metrics are averaged over the *k* iterations.
4. Cross-validation gives a more accurate assessment of model performance and aids in the identification of overfitting.

3.4.3 Evaluation Metrics

Choosing the right assessment metrics should be based on the HAR task's unique specifications.

Accuracy, precision, recall, F1-score, confusion matrix, and area under the receiver operating characteristic curve are examples of common measurements.

Accuracy: The percentage of actions that were correctly classified.

Precision: Predictive accuracy is the percentage of accurate positive forecasts among all positive predictions.

Recall: The percentage of accurate positive predictions among all real positives.

F1-score: A balanced indicator of model performance that is the harmonic mean of precision and recall.

Confusion Matrix: A table that lists true positives, true negatives, false positives, and false negatives for each activity type for comparison against the ground truth labels.

3.5 RESULTS AND DISCUSSIONS

3.5.1 Dataset Description

The HAR database was constructed by utilizing recordings of 30 study participants who were wearing a smartphone strapped to their waist with inertial sensors while engaging in ADL. The objective is to categorize the activities into one of the six accomplished actions.

3.5.2 Experiment Analysis

The trials involved a group of 30 volunteers, aged between 19 and 48 years, who utilized a Samsung Galaxy SII Smartphone while participating in six different activities (WALKING, WALKING_UPSTAIRS, WALKING_DOWNSTAIRS, SITTING, STANDING, and LAYING). We captured three-axial linear acceleration and three-axial angular velocity data at a constant rate of 50 Hz using the smartphone's built-in accelerometer and gyroscope. To enable manual labeling of the data, we recorded the experiments on video. Afterward, we randomly divided the resulting dataset into two sets, with 30% of the volunteers selected for test data and 70% for training data.

To prepare the data, we first implemented noise filters on the accelerometer and gyroscope sensor data. Subsequently, we used fixed-width sliding windows of 2.56 seconds with a 50% overlap, which yielded 128 readings per window [37,38,39,40]. Our objective was to differentiate between the gravitational force and body motion in the sensor acceleration data, so we utilized a Butterworth low-pass filter. Considering that the gravitational force mainly comprises low-frequency components, we used a filter with a cutoff frequency of 0.3 Hz. From each window, we derived a feature vector by computing variables in both the time and frequency domains.

3.5.3 Attribute Description

The taken dataset includes the below information for every records:

- Total acceleration and estimated body acceleration obtained from the triaxial accelerometer.
- Triaxial angular velocity measured by the gyroscope.
- A 561-feature vector containing variables from both the time and frequency domains.
- Activity label indicating the specific activity.
- Subject identifier representing the individual who conducted the experiment.

Figure 3.3 shows the architecture of HAR.

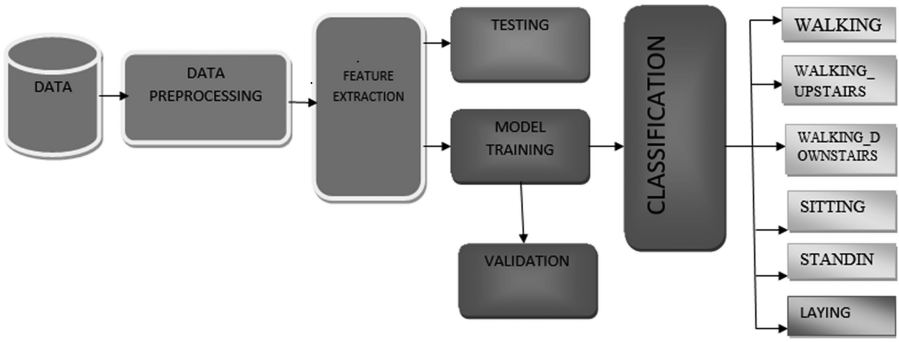

FIGURE 3.3 HAR architecture.

3.5.4 Exploratory Analysis

Exploratory analysis on a HAR dataset entails looking at multiple numbers to learn more about various actions like standing, sitting, lying down, walking, and walking upstairs and downstairs. The descriptions of the typical figures used in this analysis are as follows:

1. *Bar Plot:* The frequency or count of each activity in the dataset is shown as a bar plot. It displays various activities on the *x*-axis and a count or percentage for each activity on the *y*-axis. With the aid of bar plots, you can see how activities are distributed and get a general sense of the data balance and any potential class imbalances that might have an impact on activity recognition algorithms. Figure 3.4 presents the bar plot corresponding to different activities, namely, standing, sitting, laying, and walking (downstairs and upstairs) for different frequency of their occurrence.
2. *Box Plot:* A box plot, sometimes referred to as a whisker plot, summarizes the sensor reading distribution for each activity. The median, quartiles, and any probable outliers are all shown. A visual comparison of the central tendency, dispersion, and occurrence of extreme values for various activities is possible by comparing the box plots for those activities. This facilitates the discovery of activity-specific traits in the sensor data [41]. Figure 3.5 provides the box plot for different activities, namely, standing, sitting, laying, and walking (downstairs and upstairs) over *X*-, *Y*-, and *Z*-axes respectively. Figure 3.6 represents the box plot for different activities corresponding to varying wearable sensors, namely, accelerometers and gyroscope along the *X*-axis. Figure 3.7 illustrates the box plot for different activities corresponding to varying wearable sensors, namely, accelerometers and gyroscope along the *Y*-axis. Figure 3.8 depicts the box plot for different activities corresponding to varying wearable sensors, namely, accelerometers and gyroscope along the *Z*-axis.
3. *Scatter Plot:* The association between two sensor readings or attributes taken from the dataset is displayed in a scatter plot. With one sensor reading in the *x*-axis and the other in the *y*-axis, each point on the display represents a sample of data. It is feasible to spot any clustering or patterns that might

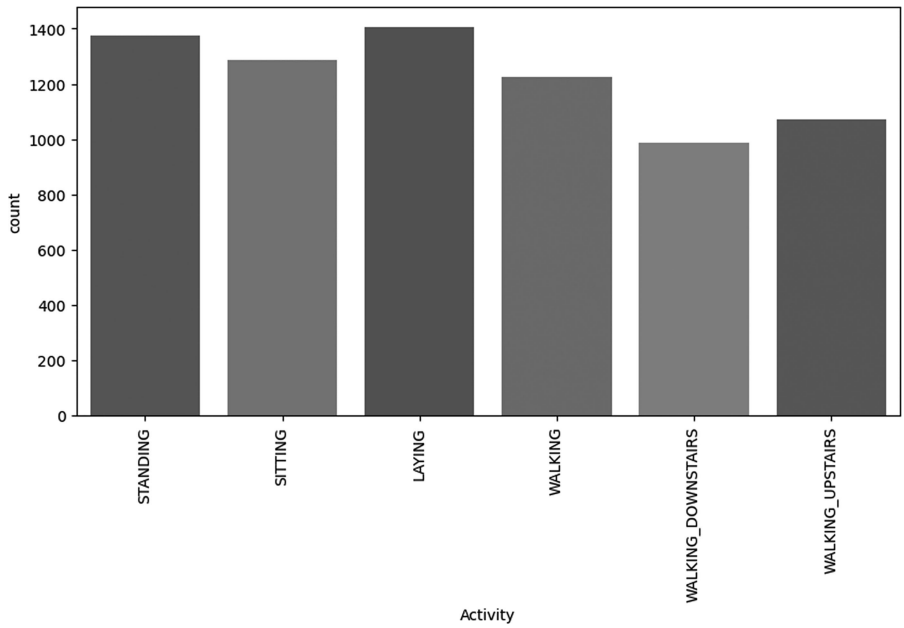

FIGURE 3.4 Bar plot for different activities to represent the frequency of each activity.

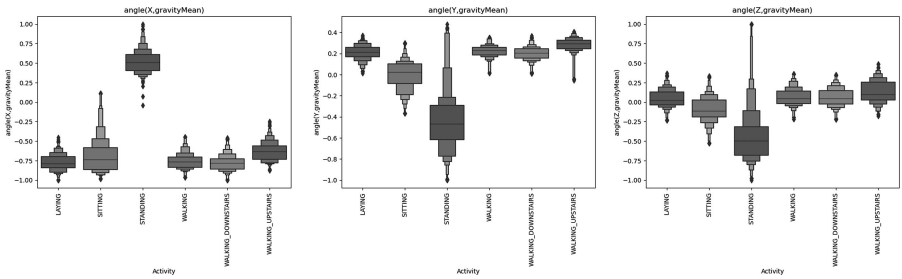

FIGURE 3.5 Box plot for different activities.

distinguish various activities by coloring the points according to the activity labels. The probable feature combinations that could support activity recognition can be found using scatter plots in Figure 3.9.

4. Figure 3.9(a) provides 3D scatter plot for all mean values corresponding to different wearable sensor data. Figure 3.9(b) gives 3D scatter plot for all minimum values corresponding to different wearable sensor data. Figure 3.9(c) provides 3D scatter plot for all maximum values corresponding to different wearable sensor data [42].

3.5.5 Analysis of Results

During result analysis on a HAR dataset to assess how well an ANN algorithm performs for various actions like standing, sitting, lying, walking, walking upstairs, and

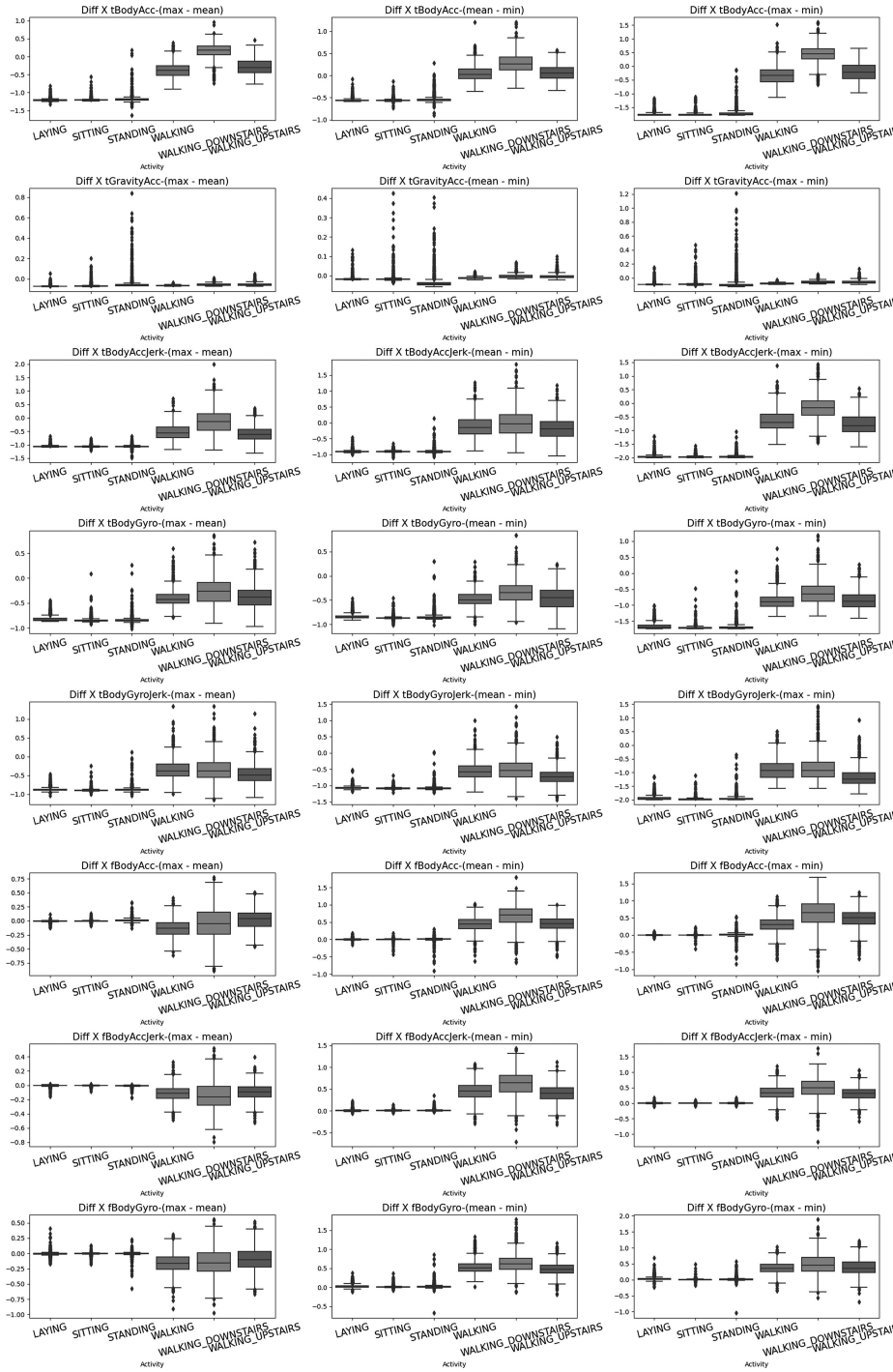
Diff X tBodyAcc-(max - mean)
Diff X tBodyAcc-(mean - min)
Diff X tBodyAcc-(max - min)
Diff X tGravityAcc-(max - mean)
Diff X tGravityAcc-(mean - min)
Diff X tGravityAcc-(max - min)
Diff X tBodyAccJerk-(max - mean)
Diff X tBodyAccJerk-(mean - min)
Diff X tBodyAccJerk-(max - min)
Diff X tBodyGyro-(max - mean)
Diff X tBodyGyro-(mean - min)
Diff X tBodyGyro-(max - min)
Diff X tBodyGyroJerk-(max - mean)
Diff X tBodyGyroJerk-(mean - min)
Diff X tBodyGyroJerk-(max - min)
Diff X fBodyAcc-(max - mean)
Diff X fBodyAcc-(mean - min)
Diff X fBodyAcc-(max - min)
Diff X fBodyAccJerk-(max - mean)
Diff X fBodyAccJerk-(mean - min)
Diff X fBodyAccJerk-(max - min)
Diff X fBodyGyro-(max - mean)
Diff X fBodyGyro-(mean - min)
Diff X fBodyGyro-(max - min)
LAYING
SITTING
STANDING
WALKING
WALKING_DOWNSTAIRS
WALKING_UPSTAIRS
Activity

FIGURE 3.6 Box plot for different activities corresponding to varying wearable sensors, namely, accelerometers and gyroscope along the *X*-axis.

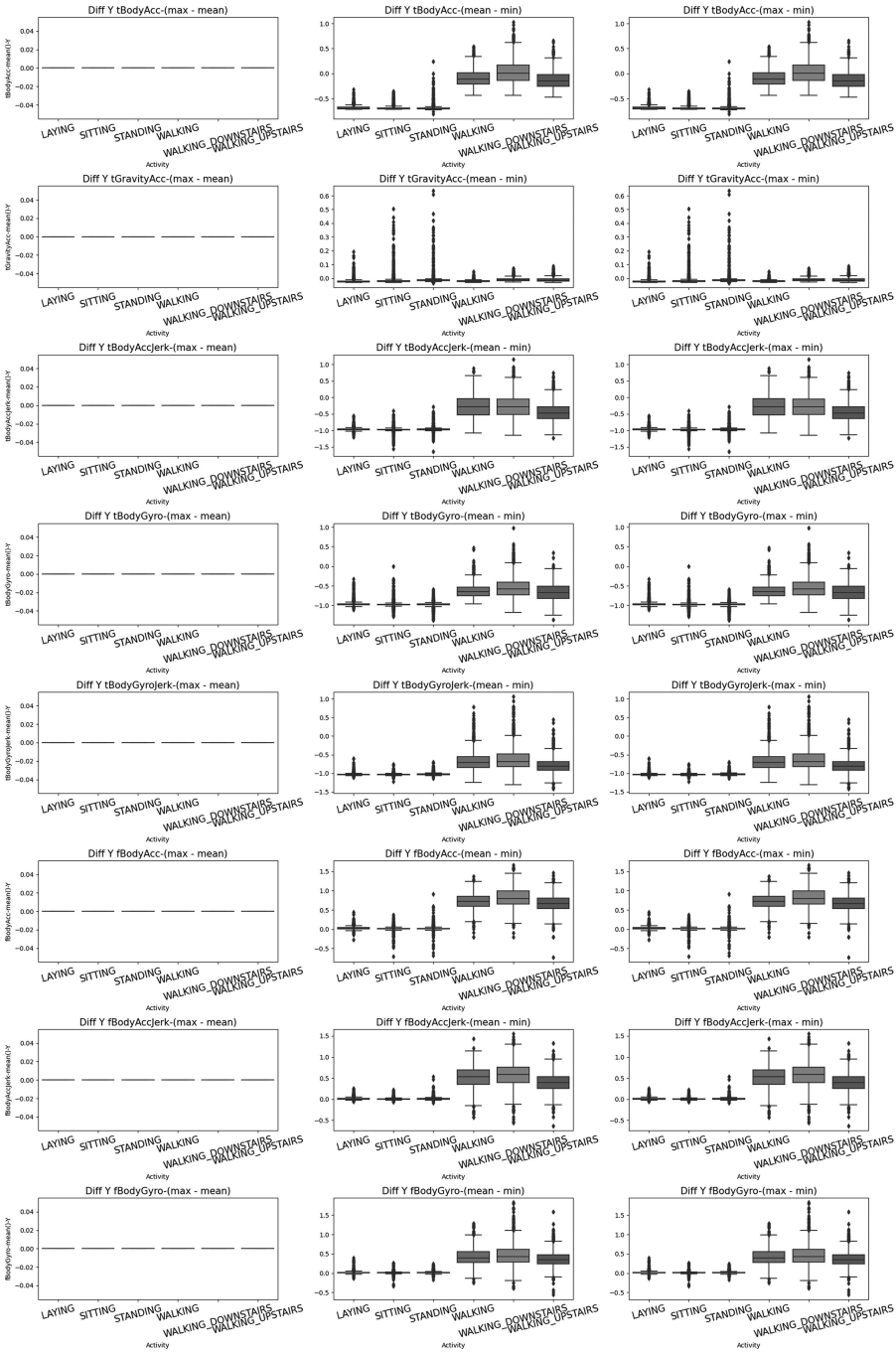
Diff Y tBodyAcc-(max - mean)
Diff Y tBodyAcc-(mean - min)
Diff Y tBodyAcc-(max - min)
Diff Y tGravityAcc-(max - mean)
Diff Y tGravityAcc-(mean - min)
Diff Y tGravityAcc-(max - min)
Diff Y tBodyAccJerk-(max - mean)
Diff Y tBodyAccJerk-(mean - min)
Diff Y tBodyAccJerk-(max - min)
Diff Y tBodyGyro-(max - mean)
Diff Y tBodyGyro-(mean - min)
Diff Y tBodyGyro-(max - min)
Diff Y tBodyGyroJerk-(max - mean)
Diff Y tBodyGyroJerk-(mean - min)
Diff Y tBodyGyroJerk-(max - min)
Diff Y fBodyAcc-(max - mean)
Diff Y fBodyAcc-(mean - min)
Diff Y fBodyAcc-(max - min)
Diff Y fBodyAccJerk-(max - mean)
Diff Y fBodyAccJerk-(mean - min)
Diff Y fBodyAccJerk-(max - min)
Diff Y fBodyGyro-(max - mean)
Diff Y fBodyGyro-(mean - min)
Diff Y fBodyGyro-(max - min)
LAYING
SITTING
STANDING
WALKING
WALKING_DOWNSTAIRS
WALKING_UPSTAIRS
Activity

FIGURE 3.7 Box plot for different activities corresponding to varying wearable sensors, namely, accelerometers and gyroscope along the *Y*-axis.

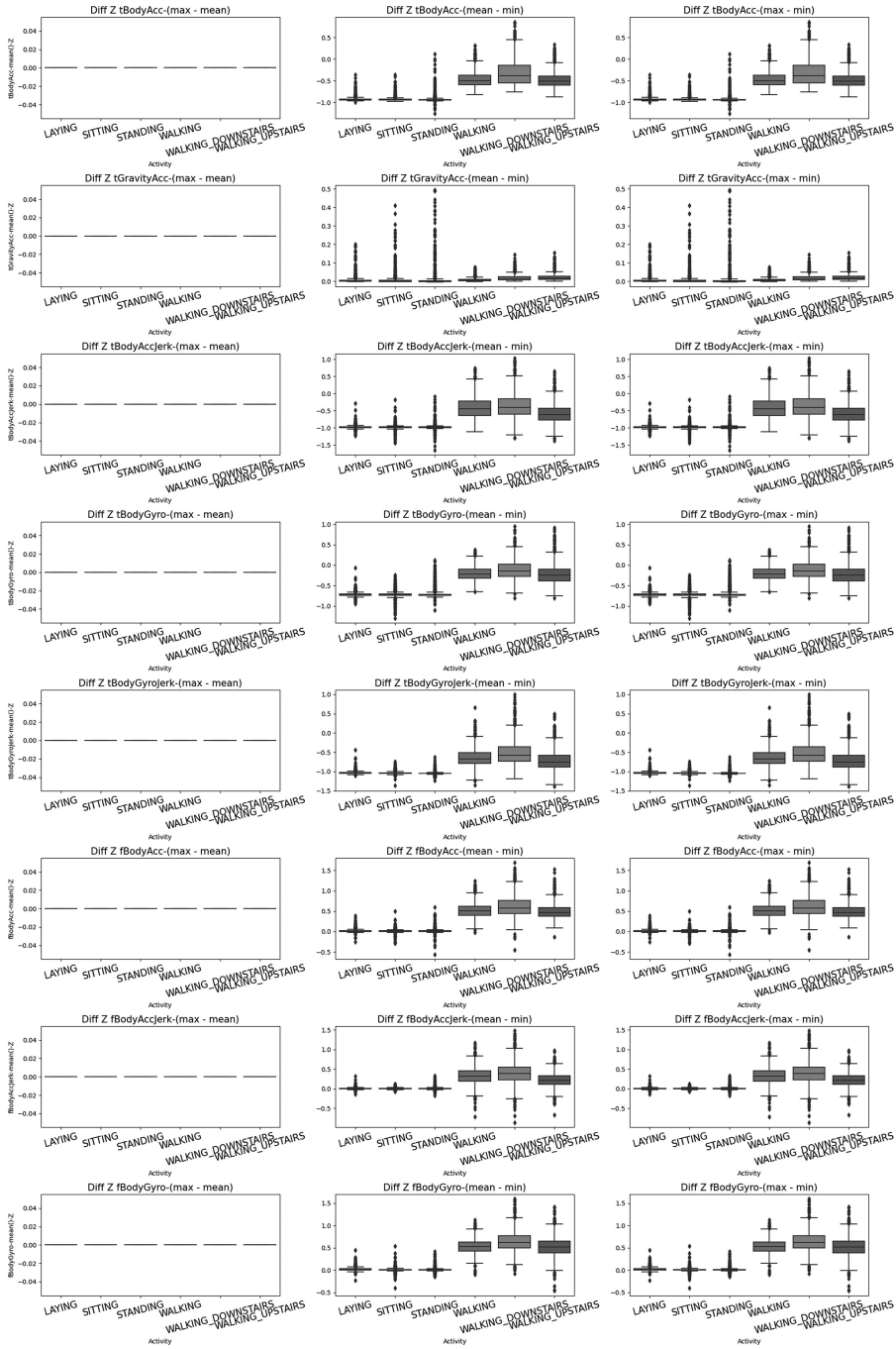
Diff Z tBodyAcc-(max - mean)
Diff Z tBodyAcc-(mean - min)
Diff Z tBodyAcc-(max - min)
Diff Z tGravityAcc-(max - mean)
Diff Z tGravityAcc-(mean - min)
Diff Z tGravityAcc-(max - min)
Diff Z tBodyAccJerk-(max - mean)
Diff Z tBodyAccJerk-(mean - min)
Diff Z tBodyAccJerk-(max - min)
Diff Z tBodyGyro-(max - mean)
Diff Z tBodyGyro-(mean - min)
Diff Z tBodyGyro-(max - min)
Diff Z tBodyGyroJerk-(max - mean)
Diff Z tBodyGyroJerk-(mean - min)
Diff Z tBodyGyroJerk-(max - min)
Diff Z fBodyAcc-(max - mean)
Diff Z fBodyAcc-(mean - min)
Diff Z fBodyAcc-(max - min)
Diff Z fBodyAccJerk-(max - mean)
Diff Z fBodyAccJerk-(mean - min)
Diff Z fBodyAccJerk-(max - min)
Diff Z fBodyGyro-(max - mean)
Diff Z fBodyGyro-(mean - min)
Diff Z fBodyGyro-(max - min)
LAYING
SITTING
STANDING
WALKING
WALKING_DOWNSTAIRS
WALKING_UPSTAIRS
Activity

FIGURE 3.8 Box plot for different activities corresponding to varying wearable sensors, namely, accelerometers and gyroscope along the *Z*-axis.

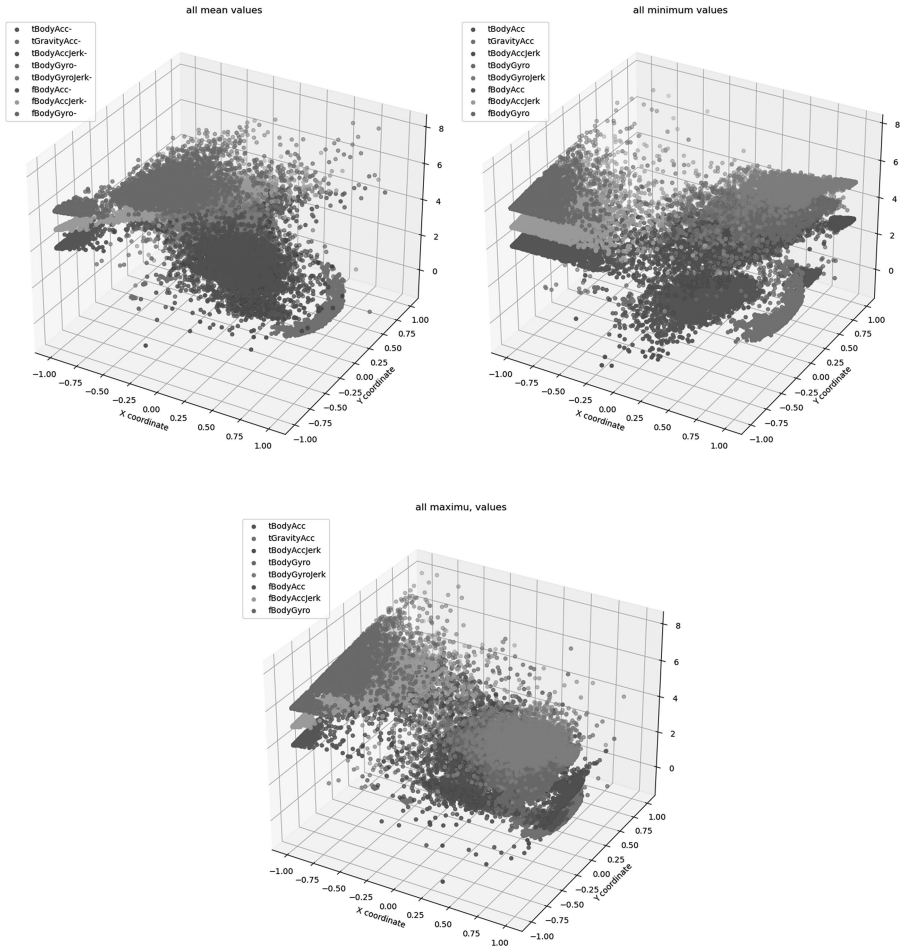

FIGURE 3.9 (a) 3D scatter plot for all mean values corresponding to different sensor data. (b) 3D scatter plot for all minimum values corresponding to different wearable sensor data. (c) 3D scatter plot for all maximum values corresponding to different wearable sensor data.

walking downstairs, we require several plots like training loss, validation loss, training accuracy, and validation accuracy curves. The descriptions of the typical figures used in this analysis are as follows:

A. *Training Loss Curve:* The training loss curve shows how the loss function changes over time and is commonly calculated using metrics like mean squared error or category cross-entropy. The training loss is plotted on the *y*-axis against the total number of training epochs or iterations on the *x*-axis.
B. *Validation Loss Curve:* The validation loss curve depicts the evolution of the loss function on the validation dataset throughout the training process, illustrating the relationship between the number of training iterations or epochs (*x*-axis) and the corresponding validation loss (*y*-axis) [43]. By showcasing the model's capacity to generalize to new data, this curve allows

us to identify potential instances of over- or underfitting. Ideally, we aim for a decreasing validation loss, indicating continuous improvement in the model's ability to generalize effectively.

C. *Training Accuracy Curve:* The training accuracy curve shows how the accuracy of the model on the training dataset has improved over the training iterations or epochs. It depicts the number of iterations or epochs on the *x*-axis and the training accuracy on the *y*-axis. The curve shows how well the model is doing when it comes to correctly classifying the activities during training. An increased training accuracy indicates that the model is improving its ability to categorize training data.

D. *Validation Accuracy Curve:* The model's accuracy on the validation dataset over the training iterations or epochs is shown by the validation accuracy curve. It depicts the number of iterations or epochs on the *x*-axis and the validation accuracy on the *y*-axis. The curve shows how well the model can generalize and categorize previously undiscovered data. Monitoring the validation accuracy enables the model's ideal balance between performance and generalization to be found.

Figure 3.10 provides the curves for training loss, validation loss, training accuracy, and validation accuracy for different epochs. The curve sheds light on how the ANN model's convergence and optimization processes worked. The model is improving its ability to fit the training set of data if the training loss is reducing over different epochs [44]. Figure 3.11 provides the confusion matrix for the algorithm.

Figure 3.12 is used to evaluate the performance of a CNN algorithm for various activities like standing, sitting, lying, walking, walking upstairs, and walking

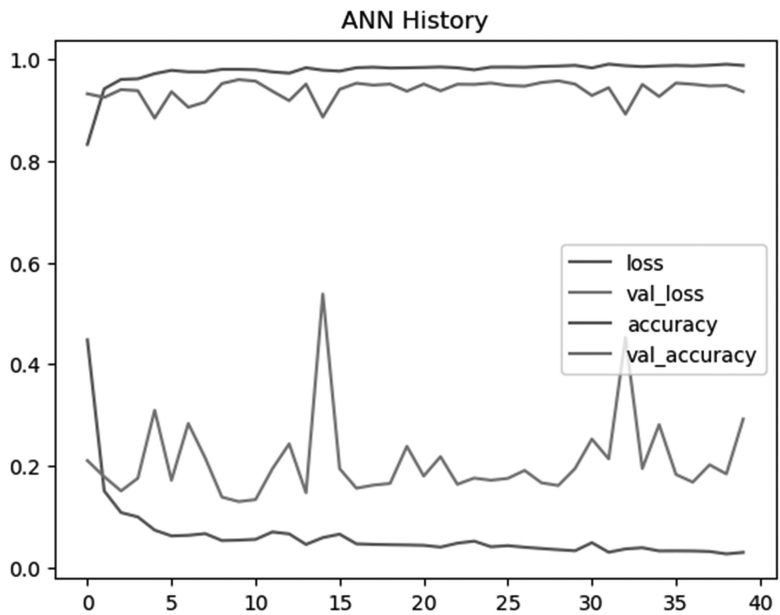

FIGURE 3.10 Representation of training loss, training accuracy, validation loss and validation accuracy for ANN algorithm.

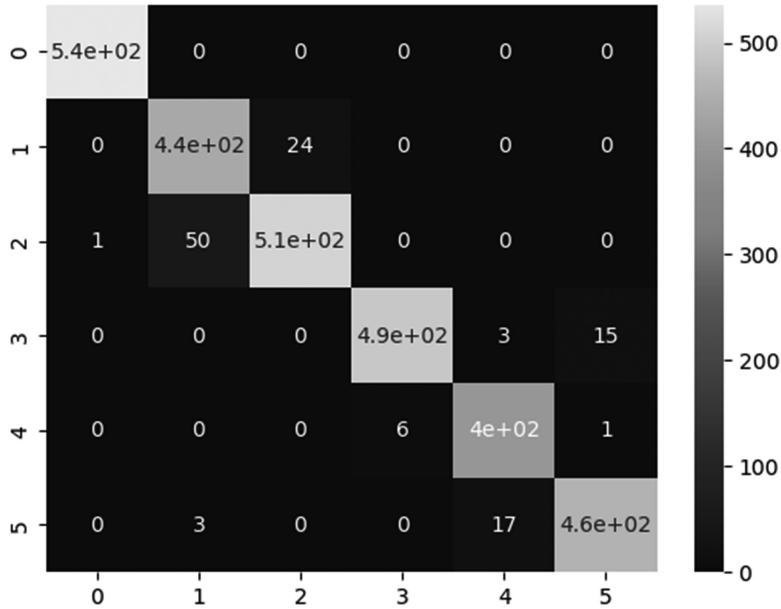

FIGURE 3.11 Confusion matrix for ANN algorithm.

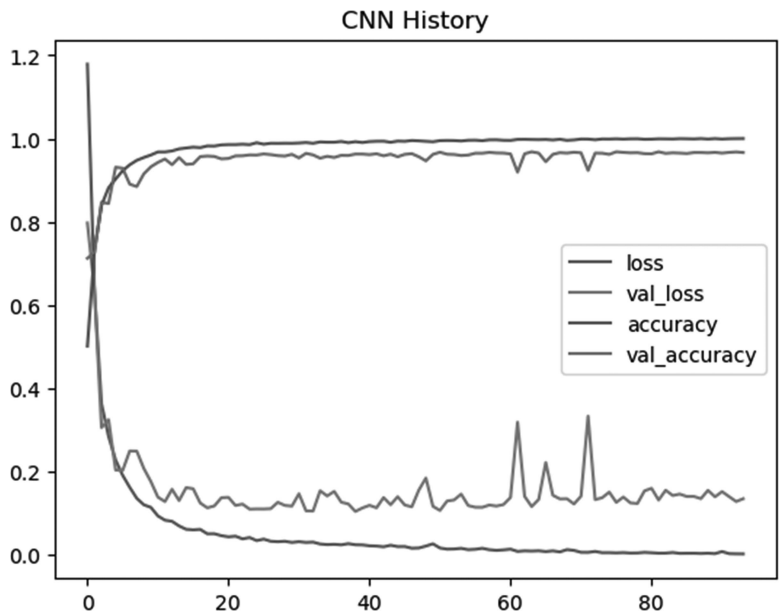

FIGURE 3.12 Representation of training loss, training accuracy, validation loss, and validation accuracy for CNN algorithm.

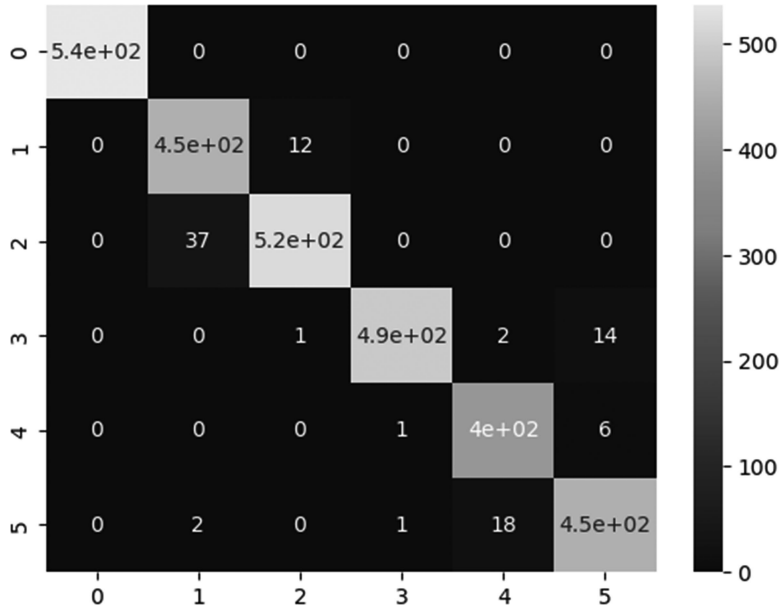

FIGURE 3.13 Confusion matrix for CNN algorithm.

downstairs during result analysis on a HAR dataset. In Figure 3.12, the representation of training loss, training accuracy, validation loss, and validation accuracy for CNN algorithm can be observed for different epochs. Figure 3.13 provides the plot of the confusion matrix for CNN algorithm.

3.6 CONCLUSIONS AND FUTURE WORK

The IoT and HAR integration has enormous potential to transform healthcare and enhance patient monitoring and management for the healthcare industry [45,46]. Accurate and real-time detection of human activities can be accomplished by integrating IoT devices and sensors with sophisticated ML and DL algorithms. With the use of this technology, medical professionals may remotely monitor patients, spot irregularities, and act quickly to enhance patient outcomes and deliver individualized care [47]. SVM, RF, k-NN, CNN, RNN, and hidden Markov models are just a few of the algorithms that have showed promise in effectively identifying and categorizing human activity. The success of various ML and DL algorithms serves as the testament to a significant advancement made in HAR for IoT in healthcare. An extensive framework for HAR in the IoHT has been examined and offered by the study given in this paper. Nonlinear IoT sensor data can be effectively handled by using ANN models, enabling precise recognition of human activities. The study has demonstrated how well an ANN model handles the nonlinear data provided by IoT devices.

In the paper that was just delivered, the application of HAR for IoT in healthcare was examined, and a thorough framework for activity recognition was suggested. The suggested framework demonstrated effectiveness in time-series analysis and handled complex nonlinear IoT data with ease using ANN and other ML approaches [48].

There are many opportunities for more study and development in the area of HAR in the IoHT, despite the fact that the suggested framework has produced encouraging results. The following are some potential directions for further work:

- Real-Time Activity Recognition: In healthcare situations, improving the framework to enable real-time activity recognition would enable prompt feedback and actions. Continuous monitoring and analysis of activities can be facilitated by exploring strategies like online learning or adaptive models. Work can be done to create real-time HAR systems that can instantly process and identify activities. As a result, patient safety and overall healthcare results would be improved through quick feedback and actions. Recognizing activity in real time is essential for prompt treatments and healthcare responses. Future research can concentrate on creating algorithms and systems that can identify activities in real time, reduce latency, and enable quick medical treatments. To enable instantaneous activity recognition and rapid intervention, this entails lowering latency in data processing and classification. This would entail streamlining the algorithms and architecture to effectively manage streaming sensor data, enabling quick detection and action in urgent situations.
- Personalized Interventions: A more all-encompassing approach to patient care would result from researching ways to incorporate the recognized activities with unique patient profiles, treatment plans, and electronic health data. Further research into tailored therapies based on identified behaviors can significantly improve patient care. Patient-specific information, like medical history, preferences, and contextual data, can be included to provide personalized therapies and improve patient outcomes. Additional study into customized treatments based on observed habits can vastly enhance patient care. It would be advantageous to incorporate individualized interventions based on the identified activities. To improve healthcare results, this could entail integrating the activity identification system with individualized treatment plans, flexible feedback systems, and patient-specific recommendations.
- Privacy and Security Considerations: Addressing privacy and security issues is essential because the IoHT involves the collection and transmission of sensitive patient data. To safeguard patient information and ensure data confidentiality, future work should concentrate on creating strong privacy-preserving systems, data encryption techniques, and secure communication protocols. It is crucial to address privacy and security concerns when IoT devices collect sensitive health data.
- Multimodal Sensor Fusion: The robustness and accuracy of the model can be increased by integrating data from a variety of sensors, including

wearables, cameras, and ambient sensors. Researching fusion methods, such as sensor-level fusion or feature-level fusion, can produce activity recognition models that are more thorough and trustworthy [49,50,51]. A deeper context for activity recognition can be obtained by investigating the fusion of data from several sensors, including wearables, ambient sensors, and video cameras. More thorough activity recognition may result from researching efficient fusion methods and creating models that use a variety of data sources [52-55].

- Integration with Electronic Health Records (EHR): A thorough understanding of a patient's health and activity patterns can be obtained by integrating HAR systems with EHR platforms. This integration can improve care coordination, help healthcare providers make better informed decisions, and reveal links between certain actions and certain health outcomes. Through this integration, healthcare personnel would be able to use the recognized activities in the context of patients' medical histories and current health issues, thereby facilitating a holistic approach to healthcare management.

REFERENCES

1. Nweke, Henry Friday, Ying Wah Teh, Ghulam Mujtaba, Mohammed Ali Al-garadi, "Data fusion and multiple classifier systems for human activity detection and health monitoring: Review and open research directions." *Information Fusion* 46 (2019): 147–170.
2. Mills, J., J. Hu, and G. Min, "Communication-efficient federated learning for wireless edge intelligence in IoT." *IEEE Internet of Things Journal* 7, no. 7 (2019): 5986–5994. https://doi.org/10.1109/JIOT.2019.2956615.
3. Wang, X., L. T. Yang, H. Liu, and M. J. Deen. "A big data-as-a-service framework: State-of-the-art and perspectives." *IEEE Transactions on Big Data* 4, no. 3 (1 September 2018): 325–340.
4. Yang, W., X. Liu, L. Zhang, and L. T. Yang, "Big data real-time processing based on storm." In *2013 12th IEEE International Conference on Trust, Security and Privacy in Computing and Communications*, Melbourne, VIC, 2013, pp. 1784–1787.
5. Lara, O. D., and M. A. Labrador. "A survey on human activity recognition using wearable sensors." *IEEE Commun. Surveys Tutorials* 15, no. 3 (3rd Quart., 2013): 1192–1209.
6. Zhang, Q., L. T. Yang, Z. Yan, Z. Chen, and P. Li. "An efficient deep learning model to predict cloud workload for industry informatics." *IEEE Transactions on Industrial Informatics* 14, no. 7 (July 2018): 3170–3178.
7. Turaga, P., R. Chellappa, V. S. Subrahmanian, and O. Udrea. "Machine recognition of human activities: A survey." *IEEE Transactions on Circuits and Systems for Video Technology* 18, no. 11 (2008): 1473–1488.
8. Daniela, M., M. Marco, N. Paolo, and UniMi B. SHAR. "A dataset for human activity recognition using acceleration data from smartphones." *Applied Sciences* 7, no. 10 (2017): 1101–1113.
9. Zhu, Q., Z. Chen, and C. S. Yeng. "A novel semi-supervised deep learning method for human activity recognition." *IEEE Transactions on Industrial Informatics* 15, no. 7 (2019): 3821–3830.

10. He, J., Q. Zhang, L. Wang, and L. Pei. "Weakly supervised human activity Recognition From wearable sensors by recurrent attention learning." *IEEE Sensors Journal* 19, no. 6 (15 March 2019): 2287–2297.
11. Bharti, P., D. De, S. Chellappan, and S. K. Das. "HuMAn: Complex activity recognition with multi-modal multi-positional body sensing." *IEEE Transactions on Mobile Computing* 18, no. 4 (1 April 2019): 857–870.
12. Qi, J., P. Yang, M. Hanneghan, S. Tang, and B. Zhou, "A hybrid hierarchical framework for gym physical activity recognition and measurement using wearable sensors." *IEEE Internet of Things Journal* 6, no. 2 (April 2019): 1384–1393.
13. Wang, F., W. Gong, and J. Liu, "On spatial diversity in WiFi-based human activity recognition: A deep learning-based approach." *IEEE Internet of Things Journal* 6, no. 2 (2019): 2035–2047.
14. Ganesan, M., and N. Sivakumar. "IoT based heart disease prediction and diagnosis model for healthcare using machine learning models." In *2019 IEEE International Conference on System, Computation, Automation and Networking (ICSCAN)*, pp. 1–5. IEEE, 2019.
15. Kumar, Prabhat, Randhir Kumar, Govind P. Gupta, Rakesh Tripathi, Alireza Jolfaei, and A. K. M. Najmul Islam. "A blockchain-orchestrated deep learning approach for secure data transmission in IoT-enabled healthcare system." *Journal of Parallel and Distributed Computing* 172 (2023): 69–83.
16. Kaur, Pavleen, Ravinder Kumar, and Munish Kumar. "A healthcare monitoring system using random forest and internet of things (IoT)." *Multimedia Tools and Applications* 78 (2019): 19905–19916.
17. Souri, Alireza, Marwan Yassin Ghafour, Aram Mahmood Ahmed, Fatemeh Safara, Ali Yamini, and Mahdi Hoseyninezhad. "A new machine learning-based healthcare monitoring model for student's condition diagnosis in Internet of Things environment." *Soft Computing* 24, no. 22 (2020): 17111–17121.
18. Zhou, Xiaokang, Wei Liang, I. Kevin, Kai Wang, Hao Wang, Laurence T. Yang, and Qun Jin. "Deep-learning-enhanced human activity recognition for Internet of healthcare things." *IEEE Internet of Things Journal* 7, no. 7 (2020): 6429–6438.
19. Sharma, Sumit, Rajan Kumar Dudeja, Gagangeet Singh Aujla, Rasmeet Singh Bali, and Neeraj Kumar. "DeTrAs: deep learning-based healthcare framework for IoT-based assistance of Alzheimer patients." *Neural Computing and Applications* (2020): 1–13.
20. Manocha, Ankush, Gulshan Kumar, Munish Bhatia, and Amit Sharma. "IoT-inspired machine learning-assisted sedentary behavior analysis in smart healthcare industry." *Journal of Ambient Intelligence and Humanized Computing* 14, no. 5 (2023): 5179–5192.
21. Arowolo, MichealOlaolu, Roseline OluwaseunOgundokun, Sanjay Misra, Blessing Dorothy Agboola, and Brij Gupta. "Machine learning-based IoT system for COVID-19 epidemics." *Computing* 105, no. 4 (2023): 831–847.
22. Shaikh, Naim, KishoriKasat, Rakesh Kumar Godi, V. Rama Krishna, Deepak Kumar Chauhan, and Jyoti Kharade. "Novel IoT framework for event processing in healthcare applications." *Measurement: Sensors* 27 (2023): 100733.
23. Islam, Muhammad Nazrul, Kazi Rafid Raiyan, Shutonu Mitra, MM Rushadul Mannan, TasfiaTasnim, AsimaOshinPutul, and Angshu Bikash Mandol. "Predictis: an IoT and machine learning-based system to predict risk level of cardio-vascular diseases." *BMC Health Services Research* 23, no. 1 (2023): 171.
24. Lu, W., F. Fan, J. Chu, P. Jing, and S. Yuting. "Wearable computing for internet of things: A discriminant approach for human activity recognition." *IEEE Internet of Things Journal* 6, no. 2 (2019): 2749–2759.

25. Wang, Y., and G. Mori. "Human action recognition by semilatent topic models." *IEEE Transactions on Pattern Analysis and Machine Intelligence* 31, no. 10 (2009): 1762–1774.
26. Chen, Z., J. Hu, G. Min, A. Zomaya, T. El-Ghazawi. "Towards accurate prediction for high-dimensional and highly-variable cloud workloads with deep learning." *IEEE Transactions on Parallel and Distributed Systems* 31, no. 4 (2019): 923–934. https://doi.org/10.1109/TPDS.2019.2953745.
27. Krishnan, N., D. Colbry, C. Juillard, and S. Panchanathan. "Real time human activity recognition using tri-axial accelerometers." In *Proceedings Sensors, Signals Information Processing Workshop*, 2008, pp. 3337–3340.
28. Gupta, P., and T. Dallas. "Feature selection and activity recognition system using a single tri-axial accelerometer." *IEEE Transation Biomedical Engineering* 61, no. 6 (June 2014): 1780–1786.
29. Ravi, N., N. Dandekar, P. Mysore, and M. L. Littman. "Activity recognition from accelerometer data." In *Proceedings 17th Conference Innovative Applications Artificial Intelligence*, 2005, pp. 1541–1546.
30. Lee, S. W., and K. Mase. "Activity and location recognition using wearable sensors," *IEEE Pervasive Computing* 1, no. 3 (2002): 24–32.
31. Mantyjarvi, J., J. Himberg, and T. Seppanen. "Recognizing human motion with multiple acceleration sensors." *Proceedings of the IEEE Internmational Conference* S*ystems, Man and Cybernetics 2* (2001); 747–752.
32. Chen, C., R. Jafari, and N. Kehtarnavaz. "A survey of depth and inertial sensor fusion for human action recognition." *Multimedia Tools Applications* 76 (2017): 4405–4425.
33. Bao, L., and S. Intille. "Activity recognition from user-annotated acceleration data." *Proceedings Pervasive* 3001 (2004): 1–17.
34. Kern, N., B. Schiele, H. Junker, P. Lukowicz, and G. Troster, "Wearable sensing to annotate meeting recordings." *Personal and Ubiquitous Computing* 7, no. 5 (2003): 263–274.
35. Lukowicz, P., J. A. Ward, H. Junker, and T. Starner. "Recognizing workshop activity using body worn microphones and accelerometers." In *Proceedings Pervasive Computing*, April 2004, pp. 18–23.
36. Patterson, D. J., L. Liao, D. Fox, and H. Kautz. "Inferring high-level behavior from low-level sensors." In *Proceediongs of the 5th Conference Ubiquitous Computing*, 2003, pp. 73–89.
37. Liao, L., D. J. Patterson, D. Fox, and H. Kautz. "Learning and inferring transporation routines." *Artificial Intelligence* 171, no. 5–6 (2007): 311–331.
38. Li, M., et al. "Multimodal physical activity recognition by fusing temporal and cepstral information." *IEEE Transactions Neural Systems and Reha-biliation Engineering* 18, no. 4 (2010): 369–380.
39. Xu, Y., J. Ren, G. Wang, C. Zhang, J. Yang, and Y. Zhang. "A blockchain-based nonrepudiation network computing service scheme for industrial IoT." *IEEE Transactions on Industrial Informatics* 15, no. 6 (2019): 3632–3641.
40. Xu, Y., J. Ren, Y. Zhang, C. Zhang, B. Shen, and Y. Zhang. "Blockchain empowered arbitrable data auditing scheme for network storage as a service." *IEEE Transactions on Services Computing* 13, no. 2 (2019): 289–300.https://doi.org/10.1109/TSC.2019.2953033
41. Chapelle, O., B. Schcolkopf, and A. Zien. *Semi-Supervised Learning*. Cambridge, MA: MIT Press, 2006.
42. Blum, A., and T. Mitchell. "Combining labeled and unlabeled data with co-training." In *Proceedings Annual Conference on Computional Learning Theory*, 1998, pp. 92–100.
43. Zhou, Z. H., and M. Li. "Semi-supervised learning by dis-agreement." *Knowledge and Information Systems* 24, no. 3 (2010): 415–439.

44. Stikic, M., D. Larlus, S. Ebert, and B. Schiele. "Weakly supervised recognition of daily life activities with wearable sensors." *IEEE Transactions and Pattern Analysis and Machine Intelligence* 33, no. 12 (December 2011): 2521–2537.
45. Divyashree, P., and P. Dwivedi. "AI computing as ubiquitous healthcare solution: Predict Parkinson's for large masses in society." *IEEE Transactions on Computational Social Systems* 10, no. 4, (2023): 1752–1757. doi: 10.1109/TCSS.2022.3224046.
46. Girish, M. V., A. Pallam, P. Divyashree, A. Khare, and P. Dwivedi. "Iot enabled smart healthcare assistance for early prediction of health abnormality." In *2021 IEEE International Symposium on Smart Electronic Systems (iSES) 2021* December 18, pp. 244–248. IEEE.
47. Bhavani, T., P. VamseeKrishna, C. Chakraborty, and P. Dwivedi. "Stress classification and vital signs forecasting for IoT-health monitoring." *IEEE/ACM Transactions on Computational Biology and Bioinformatics* 21, no. 4 (2024): 652–659. doi: 10.1109/TCBB.2022.3196151.
48. Miao, Y., M. Gowayyed, and F. Metze. "EESEN: End-to-end speech recognition using deep RNN models and WFST-based decoding." In *Proceedings Automatic Speech Recognition & Understanding*, 2016.
49. Sztyler, T., H. Stuckenschmidt, and W. Petrich. "Position-aware activity recognition with wearable devices." *Pervasive and Mobile Computing* 38 (2017): 281–295.
50. Tripathy, S. S., A. L. Imoize, M. Rath, N. Tripathy, S. Bebortta, C. C. Lee, … and S. Pani. K. "A novel edge-computing-based framework for an intelligent smart healthcare system in smart cities." *Sustainability* 15, no. 1 (2022): 735.
51. Bebortta, S., S. S. Tripathy, U. M. Modibbo, and I. Ali. "An optimal fog-cloud offloading framework for big data optimization in heterogeneous IoT networks." *Decision Analytics Journal* 8 (2023): 100295.
52. Bebortta, S., S. S. Tripathy, S. Basheer, and C. L. Chowdhary. "DeepMist: Towards deep learning assisted mist computing framework for managing healthcare big data." *IEEE Access* 11, (2023): 42485–42496.
53. Tripathy, S. S., M. Rath, N. Tripathy, D. S. Roy, J. S. A. Francis, and S. Bebortta. "An intelligent health care system in fog platform with optimized performance." *Sustainability* 15, no. 3 (2023): 1862.
54. Tripathy, S. S., S. Bebortta, and T. R. Gadekallu. "Sustainable fog-assisted intelligent monitoring framework for consumer electronics in Industry 5.0 applications." *IEEE Transactions on Consumer Electronics* 70, no. 1, (2024): 1501–1510. doi: 10.1109/TCE.2023.3332454.
55. Bebortta, S., S. S. Tripathy, S. Basheer, and C. L. Chowdhary. "FedEHR: A federated learning approach towards the prediction of heart diseases in IoT-based electronic health records." *Diagnostics* 13, no. 20 (10 October 2023): 3166.

4 Gas Sensors as a Non-Invasive Diagnostic Device for Smart Life Applications

P Divyashree and Monoj Kumar Singha

4.1 INTRODUCTION

A sensor is a device that detects and measures physical quantity from the environment and converts it to data that can be easily understood by humans or machines. The gas sensor will convert the concentration of the target analyte to standard electrical or optical signals [1]. For real-time and noninvasive monitoring, there is an immense need to use gas sensors. There is a huge market for the development of gas sensors and is expected to grow at the rate of 6.25% every year and exceed $1 billion [2]. Among many types of sensors, gas sensors are the ones that have a wide spectrum of applications as shown in Figure 4.1, where noninvasive disease detection in smart healthcare is possible with the use of appropriate gas sensors. Gas sensors will determine the anomaly and any physical changes that occur in the area where sensors are deployed. Smart gas sensor technology is an interdisciplinary field that involves material science, sensor signal capturing, communication, Internet of Things (IoT), data preprocessing, pattern recognition, and artificial intelligence (AI) techniques that will give integrated solutions to specific problems and cause disruption in traditional technology [3].

In the healthcare sector, there are innovations in wearable gas sensors for monitoring various biological parameters to make medical diagnoses noninvasive [4]. The choice of material was also crucial for getting the desired output response characteristics from the gas sensor. The appropriate selection of semiconductors, such as metal oxide (MO) nanostructures, helps in the design of miniaturized sensors with good sensitivity, selectivity, and stability [5–14]. The 2D nanomaterial graphene has very good electrical properties, and its variants such as reduced graphene oxide (rGO) have improved sensing because of more active sites with more functional groups and defects. Because of the special properties showcased when rGO is combined with MO is a good choice for sensing material design [15]. The nanocomposite-based sensor was used in biomedical applications. Miniaturized and wearable sensors designed from nanomaterials are placed on the surface of the patient to continuously monitor the biomedical parameters. This revolutionized the way the healthcare sector

DOI: 10.1201/9781003602729-4

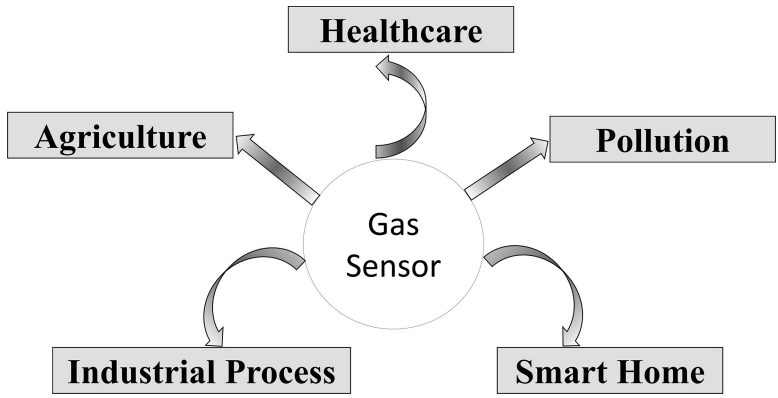

FIGURE 4.1 Scope of gas sensor in real-life applications.

functions. Noninvasive diagnosis using human breath and diagnosis with wearable sensors and treatment was provided remotely, as there was IoT-enabled connectivity for smart healthcare [16–22]. With the novel design of gas sensors in healthcare, sustainable healthcare and the overall wellness of patients can be monitored which improves the health condition and quality of life.

To have good health, environment and pollution control should be maintained with sustainability so that we can inhale pure gases that have no harmful effects on living beings. This means if we protect the environment, in return, it will protect our health. The environment is the basis for human survival; if we ignore the environment, then this can cause adverse effects on humans and other ecological creatures. To conserve the environment for the present generation and to save it for future generations, monitoring and controlling pollutants to a minimum quantity is possible with the use of appropriate gas sensors. The gas sensors will sense the presence and level of toxic gases; this will assist in taking necessary measures to detoxify. In this way, pollutants can be controlled and help in maintaining a pollution-free safe environment. NO_2 is one of the toxic pollutants that can be detected with an SnO_2/rGO-based gas sensor [23,24].

For smart life, the home we live in should be made intelligent with the installation of relevant gas sensors to continuously monitor the quality of air inside the home. The real-time indoor air quality was maintained with a Wi-Fi-based multisensor for smart home applications [25]. The fire detection can be done with the detection of CO, CO_2 gases, and smoke [26]. The heat, smoke, and chemical odors at home need to be monitored to avoid accidents and maintain clean air inside the home to make it a smart home. The industrial process has an effect on our environment, as the released gases have the potential to cause pollution. The environment will help in maintaining our health. To have a sustainable ecosystem every sector needs to be supervised with the required sensor network. In industrial processes, various harmful and explosive gases will be released. This causes pollution and degradation of air quality. Some of these gases may be toxic and explosive if present in larger quantities. In the case of odorless explosive gases, it is highly difficult to detect the presence of explosive gases by humans and to take preventive measures. Also, in some industrial processes, the feeding of gases is required in predefined quantities and specific flow

rates. Therefore, an appropriate gas sensor should be deployed that will detect the gases and assist in industrial process control. To even avoid fire accidents due to the presence of explosives, relevant sensors need to be employed. One such explosive gas is hydrogen (H_2). H_2 is produced in the petroleum industry; surface acoustic wave based sensor with TiO_2 sensing layer was proposed to detect H_2 gas [27]. The gas sensors in the automotive industry will mix the air and fuel in car engines such that there is complete combustion, thereby reducing pollution [28]. In addition to smart industrial control, intelligent decisions and cognitive actions are introduced with the era of the next-generation technology revolution of Industry 4.0. In Industry 4.0, multiple sensors have connectivity across different processes and communicate through IoT, where cognition was introduced with AI and cloud computing. The sensor data are processed, and the smart actions take place with cognitive automation.

Gas sensors also have an important role in agriculture. With agriculture, food items are produced, and these need to be maintained properly for distribution to all people nearby and faraway places. For sustainable management of agricultural yield, monitoring was done with the use of appropriate gas sensors. In the field of agriculture, the quality of the stored grain can be measured by the presence or absence of carbon dioxide. The contamination of food was found by analyzing odors it releases that have gases like CO_2 [29] and volatile organic compounds (VOCs) [30]. Fruit ripening is dependent on the release of ethylene gas. The amount of ethylene to control the ripening process was monitored with the help of an infrared-based selective ethylene gas sensor [31]. The different gas-sensing techniques in various applications are surveyed [32–34]. To improve the sensing capability, the method of altering morphology [35], and modifying material structures [36], by introducing UV radiation [37] and light source [38] was incorporated.

4.2 GAS SENSOR AND ITS SENSING MECHANISM

The gas sensor usually consists of the following components:

- Substrate: Material base over which the sensor will be fabricated.
- Micro-Heater: Micro-heater will provide an optimum temperature for the gas sensor to operate.
- Insulating Layer: Provides passivation and insulation between the micro-heater and other sensing layers to avoid short-circuits.
- Electrodes: Used for probing the device under test to perform electrical measurements and quantifying the change in electrical properties.
- Sensing layer: This is an active layer responsible for adsorbing target gas on its surface and translating chemical changes into electrical quantity to determine the target gas concentration.
- Gas Chamber: The sensor was placed inside the chamber to feed the target analytes.

An overview of the gas sensor is shown in Figure 4.2. The designed gas sensor should detect the particular analyte that is required for the desired application even if other cross-interfering gases are present. The sensor that detects the specific gas of interest

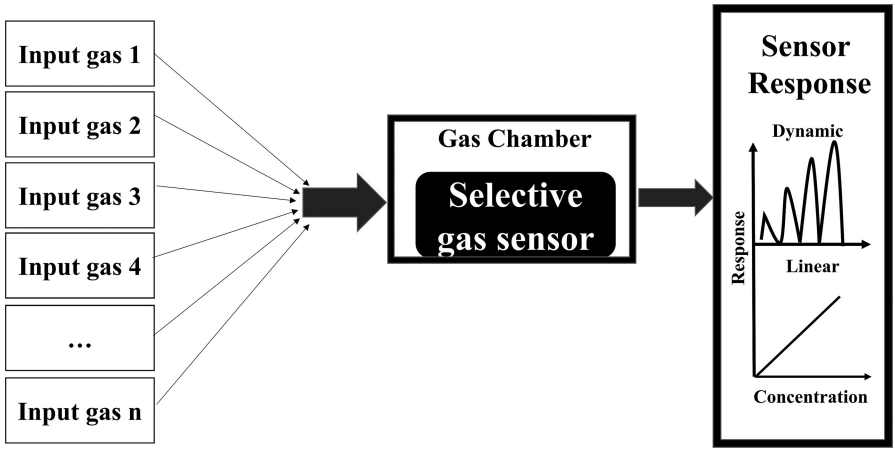

FIGURE 4.2 An overview of gas sensor.

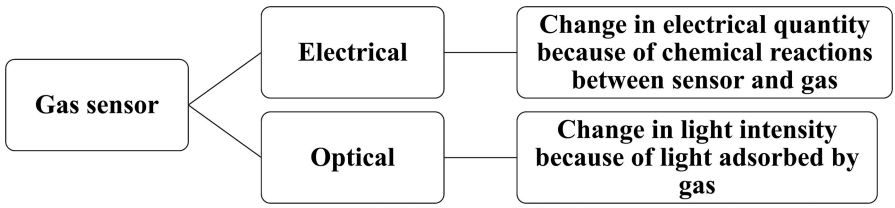
Gas sensor
Electrical
Optical
Change in electrical quantity because of chemical reactions between sensor and gas
Change in light intensity because of light adsorbed by gas

FIGURE 4.3 Sensing techniques in gas sensor.

is called a selective gas sensor. For that specific gas, response and recovery characteristics are computed. The dynamic response is the sensor output for switching the target gas on and off into the sensor for different concentrations. The response of the sensor was expected to be linear, that is, for a change in analyte concentration there is a corresponding change in output.

Gas sensors can be typically classified into two major techniques—electrical and optical sensors—as shown in Figure 4.3. The electrical gas sensor will determine the change in electrical characteristics like resistance or conductance. The change in electrical properties is due to chemical reactions taking place between the sensing surface and the target analyte. There is a loss or gain of electrons in surface reactions. The type of material used—p-type or n-type—will have an effect on the electrical properties after surface reactions. If the target gas is reducing gas and the sensor material is n-type, then the resistance of the sensor will decrease because of an increase in electrons. For the reducing target gas with a p-type sensor, the resistance will increase as the electrons and holes recombine and reduce the number of holes that are responsible for conductance. Similarly for oxidizing gas with n-type sensing material, resistance will increase, and for oxidizing target gas when interacting with a p-type sensor, resistance will decrease. Hence, these changes are used to find the concentration of the target gas. Another sensing measurement technique for

measuring the gas sensor response is the optical sensor. The adsorption of light by the gas is used as a measuring criterion for identifying gas concentrations. When the target gas is exposed to light, then gas molecules adsorb the light which decreases the intensity of light received at the detector. The decrease in light intensity corresponds to the target gas concentration. The two gas-sensing measurement techniques are illustrated in Figure 4.3.

The electrical method of gas sensing is illustrated in Figure 4.4(a). The electrical sensor consists of a substrate over which sensor layers are structured. The sensing layer on top of the gas sensor will attract the target gas molecules to get adsorbed. The surface interactions between the sensing layer and gas will impart changes in electrical properties that correspond to the target gas concentration. The optical method of gas sensing is shown in Figure 4(b). When the light source such as a laser is passed through the environment exposed to the gas of interest, the gas molecules will absorb light; hence, there will be a decrease in the intensity of light at the detector. This difference in light intensity at the source and detector is used to determine the gas concentration.

The important parameters for a gas sensor are as follows [5]:

- Sensitivity: The electrical change per unit analyte concentration.
- Selectivity: The response of the sensor toward a particular analyte of interest.
- Response Time: The time required to reach the final concentration value when there was a step concentration change from zero to the final value of the target gas.
- Recovery Time: The time required to reach the initial value of concentration when there is a step concentration change from the final value to zero of the target gas.
- Stability: The ability of a sensor to give reproducible results retaining the same sensitivity, selectivity, response and recovery time.
- Detection Limit: At a given temperature minimum concentration of analyte can be detected by the sensor.

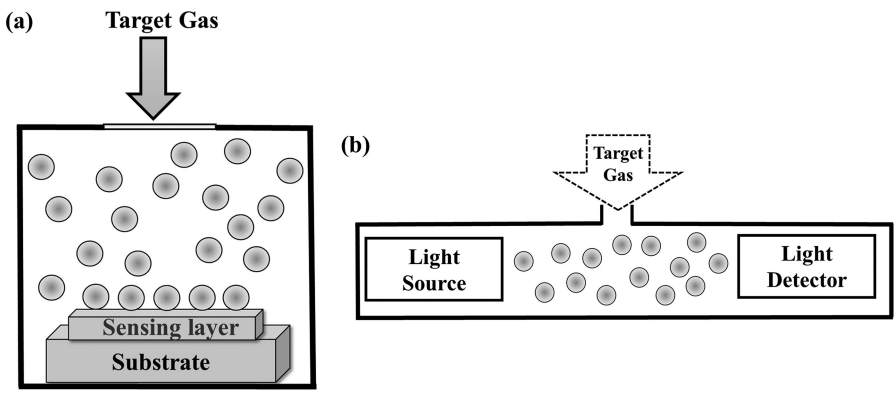

FIGURE 4.4 (a) Electrical method of gas sensing and (b) optical method of gas sensing.

- Dynamic Range: Concentration level between detection limit and maximum limiting.
- Linearity: The sensor response is a straight line illustrated as a linear response.
- Resolution: The lowest distinguishable change in concentration of analyte that can be detected by the sensor.
- Working Temperature: The temperature required for surface reactions to occur.
- Hysteresis: The maximum difference in output for increasing and decreasing analyte concentration.
- Life Cycle: The total time duration for which the sensor operates correctly.

The ideal sensor characteristics are it should have quick response and recovery times with lower detection limit, resolution, and hysteresis. The sensor should give stable results and a linear response with an increase in gas concentration. Also, the sensor must have a considerable lifespan so that it can be deployed in real-life applications. Therefore, designing gas sensors is an important step where there is a lot of innovation with advancements in technology. Intelligent decision-making is made with precise measurement of sensor quantity. The best sensor is the one that can measure the desired quantity precisely even at a low concentration and has high selectivity to detect target components in the presence of other components. To enhance the sensing performance, MO nanostructure-based sensors are being widely used [5]. In micro-level sensors, the sensor operates at the atomic level and hence gives the best sensing capability for even the minute presence of the target. The advancement in nanomaterials gave an exciting combination of different sensing materials for achieving high sensitivity and selectivity for target gas detection. The use of graphene-based nanostructures as a sensing material improves the sensing capability [15]. These are micro-level devices having precise sensing with the miniaturization of sensors. The sensor that gives the best performance can be deployed in smart systems.

The smart system is the collection of various systems interconnected to serve a required purpose. The schematic for the smart system is shown in Figure 4.5 which consists of sensors, IoT, cloud computing, AI, apps, and smartphones. The smart system consists of sensors to sense the desired quantity, and the sensed data can be used for further processes in the design of smart system. IoT is an important section where the sensed data are communicated to other devices in the smart system. The cloud is an online platform that can store data and perform computations with resources available in cloud infrastructure. The data has no significance if not properly analyzed and interpreted. AI is a technological advancement where the use of machine learning and deep learning techniques will give recommendations and decisive actions from sensor data analysis and computations. The sensor information and analytics need to be shared to the people and there is requirement of mobile applications to organize data and send reports to the end-users. A smartphone is an interface medium through which sensor data analysis and decisions are displayed in smart systems.

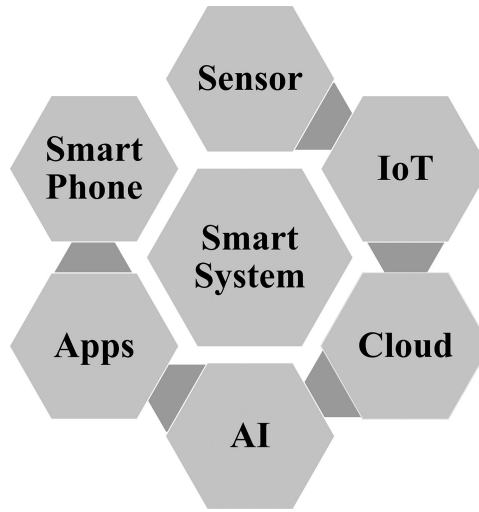

FIGURE 4.5 Schematic of smart systems.

4.3 SMART HEALTHCARE

In the medical field, the use of gas sensors with wearable devices brought a revolution in the diagnosis and treatment procedures of diseases. Noninvasive diagnosis was carried out with the use of specific sensors for biological parameter monitoring. The healthcare sector was automated with sensor technology and smart devices connected with IoT, AI, and cloud computing to give smart healthcare infrastructure.

4.3.1 Wearable Sensors in Medical Diagnosis

Nanomaterial-based wearable sensor devices can be worn or combined with textiles for real-time tracking of various physiological parameters. Nanomaterials like carbon nanotube, and graphene variants gave promising sensor performance. This sensor output can be used for healthcare, fitness analysis for daily activity, or sports performance. The wearable sensor hub mounted on a robotic structure or prosthetics can provide artificial movement from sensor response [16]. Nanotechnology is widely used to perform toxic gas detection in the application of biomedicine, energy, and environment [17]. Li et al. proposed wearable sensors to detect aldehyde for the diagnosis of asthma using an IoT-based system. Asthma is one of the most common chronic diseases affecting people of all ages. Nearly $3.2 billion is spent to treat asthma every year. Formaldehyde is the biomarker used for identifying asthma; fuel cell technology-based sensor was designed to detect aldehyde. The aldehyde sensor was embedded inside a wearable wristwatch and combined with Bluetooth-enabled smartphone and cloud services that will act as a personalized smartwatch continuously detecting aldehyde for diagnosing asthma [18].

4.3.2 Gas Sensors as Breath Analyzer

Noninvasive diagnosis in healthcare was made achievable with the help of breath analysis using gas sensor. Acetone is the biomarker used for detecting diabetes; measurement of acetone gas level in our breath leads to the detection of diabetes. To detect acetone, ZnO sensing layer was prepared by the coprecipitation method. The sensor was designed with platinum electrodes, silicon dioxide as an insulating layer, and ZnO as an active sensing surface. The sensor structure was built over a silicon substrate. Gas sensor works on the principle of transforming surface reactions to detectable signal when target gas is exposed to the active layer. The sensing film resistance varies for different concentrations of gas and temperature. The proposed design shows a good response for acetone concentration ranging from 1000 to 12.5 mol/m^3. The sensor has good sensitivity toward even low concentrations [19]. Simulation of COMSOL-based gas sensor was designed for detecting VOCs in human breath and validated with fabricated results. The proposed sensor converted human breath to digital measurable objects and was accessed through smartphones. Based on the concentration of the target VOC exposed to the sensor corresponding displacement can be observed in the piezoelectric material which can help in determining any respiratory disease and even different stages of lung cancer can be found [20].

There are numerous research heading toward the detection of diseases noninvasively. Ehrmann et al. proposed a novel MO micro gas sensor array to analyze odor quality in human breath. The odor of human breath is distinct; if there is any variation in breath odor, then corresponding health problems can be determined. Bad breath has social and medical complications. The malodor components are NH_3, H_2S, CH_3SH, $(CH_3)_3N$, indole, and putrescine. Bad breath odor signifies serious illness like diabetes, hepatic failure, a respiratory infection, gingivitis, and periodontal diseases. For detection of malodor in breath 40 monolithic sensor arrays were structured with 41 platinum stripes. There are four heaters at the back to provide the required temperature for adsorption of target gases. The sensor array comprised of MO segments on the silicon substrate. The first and last electrodes were used to measure surface temperature. Among this array of sensors, each sensor detected a specific target gas. The sensitivity and selectivity were achieved with temperature gradient and sensing layer thickness variation across the array. SnO_2 as an active layer gave a quick response and detected target gas within 1 minute. While WO_3 took several minutes to respond, this sensing layer exhibits less cross-interference with ethanol. Moreover, WO_3 can detect target gas with less cross-interference and also was not affected by relative humidity up to 70%–80%. Therefore, WO_3 was preferred for the detection of bad-odor gases [21].

An electronic nose (E-Nose) with a micro gas sensor array was designed and fabricated. For E-Nose, sensing was done with the sensor array, and recognition of gases was done with principal component analysis (PCA) and neural network. E-Nose was able to discriminate 4 gases which are CH_3SH, $(CH_3)_3N$, C_2H_5OH and CO when tested with 12 gas samples in the concentration of 0.1 to 100 ppm (or six flavors). The, six flavors include are carrot, green onion, women's perfume, men's perfume, 25% liquor (Korean soju), and 40% liquor (whisky). The E-Nose contained Teflon tubes, two solenoid switches to insert target gas and fresh air into the chamber, and

a pressure buffer to suppress pressure variations due to changes in flow rate. E-Nose system consists of a suction pump, interface card with central processing unit (CPU), analog-to-digital and digital-to-analog converter, and a personal computer. The sensor was tested with sensing layers WO_3 and ZnO. The detection of four gases was done using four different sensing layers. 1 wt.% palladium-doped WO_3 gave the best sensitivity for all gases in all concentrations. 6 wt.% Al_2O_3-doped ZnO gave a good response to CH_3SH and $(CH_3)_3N$. Pattern recognition was carried out using PCA and a neural network. The analyses of PCA data pattern reveal that 25% liquor has overlap with both 40% liquor and women's perfume. To have better recognition of gases without overlap a neural network was used. For detecting 12 gases, neural networks of 4 input units, 8 hidden units, and 12 output units were designed and iterated for 20,000 epochs that gave a recognition probability of 100%. For detecting six flavors, neural networks of 4 inputs, 6 hidden, and 6 output units iterated for 10,000 epochs gave an accuracy of 93% [22].

4.4 GAS SENSORS FOR POLLUTION MONITORING

The release of toxic gases causes pollution and degrades the quality of air. If this trend of harmful gases in the environment continues to grow, then it would become very difficult to lead a healthy life. Severe chronic health problems can arise if humans or animals inhale these pollutants. Hence, for effective control exact measurement of pollutants is critical. Therefore, research in the development of gas sensors to monitor and control pollution levels in the environment has tremendous importance. The major pollutants are NO_x gases, and the gas sensors to detect NO_2 to monitor pollution are given in further sections. NO_2 is a toxic gas produced by the incomplete combustion of vehicles and is a by-product in chemical processing industries. NO_2 is a poisonous gas to humans, animals, and plants. Inhalation of NO_2 even at minute levels will cause adverse ill effects and lead to mortality. Hence, the detection of NO_2 was very important to monitor the environment and take necessary precautions.

From the literature, it is found that WO_3 nanocrystals, ZnO nanowires, SnO_2 nanoribbons, and In_2O_3 nanoparticles require high operating temperatures. To reduce the operating temperature a heterojunction nanocomposite of SnO_2/rGO was utilized that operated at 50°C to detect NO_2. There was a reduction in power consumption as the operating temperature was reduced. The SnO_2/rGO sensor was designed with gold electrodes on the front and backside, RuO_2 as a heater, and Al_2O_3 as an insulating layer. The designed sensor gave a good response with high sensitivity, selectivity, and reproducibility. NO_2 gas was exposed to the sensor at 0.5–5 ppm. Variants of SNO_2/rGO concentrations were used for experiments. The variants were SnO_2-rGO-1, SnO_2-rGO-2, SnO_2-rGO-3, and SnO_2-rGO-4 with SnO_2 concentrations of 57.3%, 73.5%, 87.6%, and 92.1%, respectively. SnO_2/rGO-2 variant added with 0.24 g of $SnCl_4$ gave the best response of 3.31 for 5 ppm NO_2 and 1.5 for 0.5 ppm NO_2 [23]. NO_2 selective sensor was developed with sensing layer of SnO_2/rGO nanocomposite in COMSOL and cross-validated simulated results with fabricated sensor results. The sensor design was simulated as per dimension and material specifications that were given in [17,18]. NO_2 was passed into a cylindrical chamber in which the sensor was placed. NO_2 is a reducing gas that donates electrons when interacting with

the SnO_2/rGO sensing layer. NO_2 when exposed to the sensing surface the resistance of the layer decreases as more electrons are released by the target gas. There was a slight variation in simulation results and fabricated sensor results. This variation was due to differences in temperature distribution and concentration gradient in theory and practical implementation [24]. Pollution has a very important impact on our health. Toxic gases need to be monitored, and gas sensors help in determining the concentrations of these gases. Pollution causes severe chronic illness, even decreases lifespan and has adverse effects on health conditions. To safeguard our health, sensors for NO_2 detection [23,24] will help to know the level of these pollutants and further guide us in detoxifying them.

4.5 GAS SENSORS FOR SMART HOME

In a smart home, monitoring the indoor air quality for inhalation of clean air is very important to have a healthy life. Also, raising an alarm if any fire accident occurs and take precautionary measures plays an important role in a smart home system. To perform these actions, we need to establish gas sensors for intelligent smart homes. The air quality at home degrades mainly because of bacteria and fungi which can cause headaches, respiratory issues, and diarrhea. The growth of bacteria is dependent on temperature and humidity. Also, indoor air pollutants like formaldehyde, ethanol, and other VOCs are released by gas, tobacco smoke, decorative items, and other building objects. The continuous monitoring of VOCs, temperature, humidity, and dust particles will help to determine the air quality. Multiple sensors were connected with Arduino Yún, and sensed data were communicated to smartphones supporting HTML 5.0. The sensors detect temperature, humidity, VOCs, dust and sense PM2.5 (particulate matter with diameter 2.5 μm) and PM10 (diameter 10 μm). This system acts as a smart home application where indoor air quality is monitored 24/7 [25]. In addition to air quality monitoring, detection of fire and smoke in larger quantities should also be available in smart homes. Chen et al. proposed fire detection for CO/CO_2 and smoke. From the sensed concentration of CO/CO_2 and smoke, the algorithm was designed to raise an alarm when the level exceeds the maximum threshold that indicates fire. Implementation was done for cargo whereas the same system can be used in smart homes [26].

4.6 GAS SENSORS FOR INDUSTRIAL PROCESSES

Industries are the major source of releasing large chemical products in the form of solids, liquids, or gases. Solid and liquid by-products can be treated physically. Working on gaseous by-products, since these are not visible to the naked eyes, becomes difficult. Hence, proper gas sensors should be installed to check the levels of gases and take necessary actions and processes in industries. H_2 is widely used in oil refinement industries; presence of H_2 in more than the required quantity can cause fire accidents, as it is highly inflammable. Therefore, for industry monitoring of H_2 gas, a surface acoustic wave-based sensor was designed with $LiNbO_3$ piezoelectric material that was sandwiched between two aluminum interdigitated electrodes (IDEs). The sensor was tested with an active sensing surface of TiO_2 and ZnO with IDE heights varying

from 0.05 to 0.5 μm. The sensor was operated at a frequency of 44 MHz and was exposed to H_2 in the 0.1–100 ppm concentration range. Based on the electric field intensity applied and permeability of piezoelectric material, stress was created when exposed to H_2 gas. In correspondence to gas concentration, there was displacement and frequency variation in the piezoelectric material. The best response was obtained for IDE height of 0.05 μm and sensing material of TiO_2 that gave fast response and recovery times with zero hysteresis [27].

The research for increasing fuel efficiency while optimizing engine performance and decreasing pollution are important aspects of sustainable automation in the industry. If the air–fuel (A/F) ratio was provided at the stoichiometric ratio, complete combustion would take place which would decrease pollution but does not show improvement in efficiency. To increase performance, Velasco proposed a "Lambda sensor" with zirconium ceramic material. This sensor detected the nature of the A/F mixture, whether it was oxidizing or reducing and produced variation in voltage. When mixture composition varies around stoichiometric value, nearly 1 V variation was observed [28].

4.7 GAS SENSORS FOR AGRICULTURE

In agriculture sector, fruit/vegetable quality assessment is the highly demanded aspect for consumer market in present era. In the field of agriculture, crop health and freshness of stored food need to be monitored to get the maximum yield and profits. To protect the crop and control the ripening process of fruits till they reach the market, estimating spoiled food will be possible with the use of appropriate gas sensors. Various sensors for measuring CO_2 concentrations will give information on whether the food was spoiled in storage houses. The different techniques of sensing CO_2 with gas chromatography, mass spectrometer, infrared sensor, and fiber optic sensors called optodes were reviewed [29]. Fruit freshness was determined by the quartz crystal microbalance technique of gas sensing that detects VOCs of spoiled food [30]. An infrared-based silicon sensor was designed and fabricated to determine the concentration of ethylene which regulates the fruit ripening process [31].

4.8 TECHNIQUES FOR ENHANCING GAS SENSING

The traditional gas sensor usually operates at high temperatures, and sensing capability also needs to be improved. Higher temperature of the sensor consumes more power to generate heat and, also other peripherals associated with sensor devices when combined for a smart application may be damaged. There is an immense need to explore techniques for improving sensing capability at ambient temperatures to deploy in smart applications and to improve the detection performance at room temperatures. Studies have shown that with nanocomposite MO heterostructures, a significant reduction in operating temperature was observed. The morphological changes in the material contributed to the enhancement of gas sensor performance. The size and morphology of CuO_2 have a significant role in deciding the sensitivity of the sensor for ethanol detection [35]. To improve ethanol sensing, a ZnO/ZnS heterostructure-based hollow porous gas sensor was hydrothermally synthesized [36]. With

TABLE 4.1
State-of-the-art gas sensors for smart life applications

S/ No.	Sensing surface	Target analyte	Application	Range of detection
1	Fuel cell with platinum electrodes [15]	Aldehyde	Smart healthcare: Asthma detection	30 ppb–10 ppm
2	MO sensor with ZnO sensing [16]	Acetone	Smart healthcare: Diabetes	12.5–1000 mol/m^3
3	Microarray gas sensor [18]	NH_3, H_2S, CH_3SH, indole, Putrescine	Smart healthcare: Breath odor quality	0.2–200 ppm
4	Silicon-based micro gas [19]	CH_3SH, $(CH_3)_3N$, C_2H_5OH and CO and six flavors	E-nose	0.1–100 ppm
5	SnO_2-rGO [20,21]	NO_2	Smart healthcare: Pollution control	0.5–5 ppm
6	TiO_2 Surface acoustic wave [24]	H_2	Smart industry: Petroleum industry	0.1–100 ppm
7	Infrared based Silicon detector [28]	C_2H_4	Smart agriculture: Artificial fruit ripening	20–100 ppm
8	Cu_2O- Particle size and morphology-dependent gas sensing [32]	Ethanol	Smart healthcare: Pollution control	50–800 ppm
9	ZnO@ZnS heterostructures [33]	Ethanol	Smart home: Indore air quality	114.2–100 ppm
10	WO_3 nanowire [34]	C_2H_5OH and CH_4	Smart home: Indore air quality	15–75 ppm
11	N-hyper doped Silicon (N-Si) [35]	NO_2	Smart healthcare: Pollution control	5–2000 ppm

light-induced gas sensing, there was a considerable enhancement in sensing performance at ambient temperature. WO_3-based gas sensor's sensitivity and selectivity were increased with UV irradiation. The resistance fluctuation was enhanced when exposed to specific wavelengths of UV rays [37]. The NO_2 sensor with light having 940 nm wavelength and ~18 μW/cm^2 intensity exhibited improved performance with good response and sensitivity with detection over a wide range of concentrations [38]. Table 4.1 shows the details of the sensing surface, target gas, and applications with a range of detection for various gas sensors.

4.9 FUTURE DIRECTIONS AND RECOMMENDATIONS

In the next generation, gas sensor technology will have revolutionary improvements. Gas sensor design should have the highest sensitivity and selectivity in the detection of the target analyte. The lowest detection limit of gases will be very low, which means

even very little presence of the target analyte should be detected by the designed sensor. The desired characteristics of the gas sensor will be achieved with innovations in design aspects and the use of novel materials for the sensor. There are some challenges that high temperature was required for the gas sensor to operate; future perspective would be to design sensors that can be operated at room temperature. Research in the direction of improving sensing capability with the introduction of light was made. This light-induced sensing technology gave enhanced sensor performance at lower/ambient temperatures. Advanced research in the field of nanocomposite material and polymers will be helpful in the design and development of flexible and wearable sensors. Gas sensors are regarded as the core electronic component useful for real-life smart applications. Therefore, the understanding of state-of-the-art technologies and future perspectives to enhance their performance is important.

To innovate novel sensor design, a thorough understanding of state-of-the-art technologies is necessary, and this review will serve the purpose of introducing gas sensor fundamentals as a noninvasive diagnostic tool for smart applications in real life. The inclusion of IoT and intelligent data analytics can provide smart solutions [39]. The development of self-powered sensors with the use of advanced materials such as nanowires has significant importance for the deployment of IoT applications [40]. The future scope would be smart sensors where sensing and intelligent pattern recognition of various gases will be determined using advanced technologies such as AI algorithms.

Technology is making human life smarter owing to breakthroughs in wearable sensors, communication, AI, cloud computing, the Internet of Medical Things (IoMT), and so on. The communication between healthcare providers and patients is established through the IoMT network [41]. The IoMT design components comprise a sensor platform to extract biomedical data from patients, communication networks, storage modules, AI, and smart visualization. Thus, IoMT provides continuous multisensor vital parameter monitoring for the clinical decision support system. The interconnected medical things disseminate healthcare information without human intervention [42]. Through wearable sensors in IoMT architecture, remote home-based healthcare is possible. The self-care system information is made accessible to the patients and doctors to continuously monitor and take collaborative treatment actions. The future scope is to improve the sensing performance parameters for an efficient smart healthcare solution [43]. The data analytics of multisensor platforms is very important for the dissemination of smart systems. Information/data fusion is an efficient method to automatically/semiautomatically transform multisource heterogeneous sensor data into a meaningful representation providing effective assistance for human or automated decision-making. This can be performed in two scenarios: one is real-time mode and the other is offline mode (quick response is not expected). The use of data fusion techniques reduces the dimensions, optimizes the data traffic, lowers the bandwidth requirement, and consumes less power to extract useful information. Therefore, there is a considerable reduction in the communication overhead at the gateway (where sensor data fusion occurs) and reduces the computation cost [44]. Data fusion algorithms powered by sensing technologies and AI will detect a wide spectrum of biomarkers and diseases in real time for personalized healthcare [45]. Wearable systems with sensor fusion possess the capability for continuous monitoring of diseases with enhanced comfort and reduced invasion [46]. The unification of

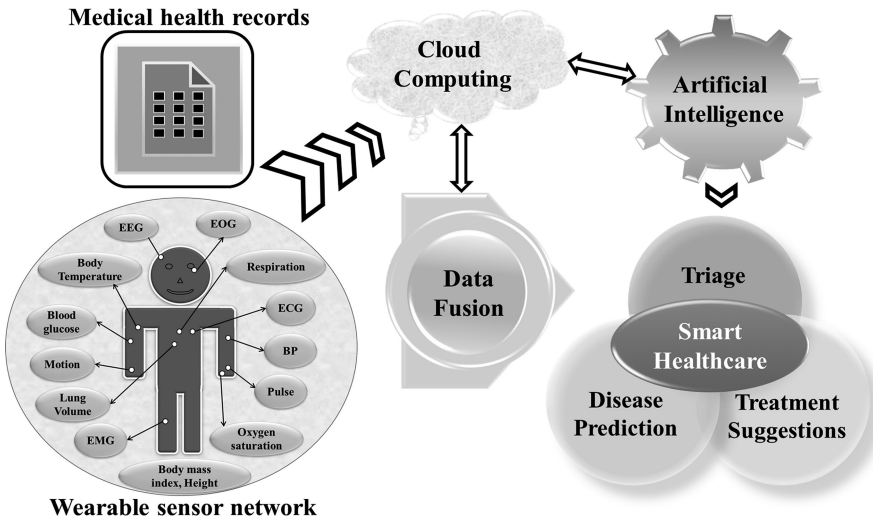

FIGURE 4.6 Data fusion-enabled smart healthcare system.

IoMT powered with AI and blockchain contributes to secured remote healthcare services. Henceforth, promoting home-based smart healthcare solutions that are reachable to any place at an affordable cost [47]. The involvement of data fusion with these technologies disseminates efficient and smart services. Thus, the quality of life is drastically improved with health and social care. Therefore, there is a transformation in the functioning of traditional clinical hospitals. Multimodal data fusion is widely used in the healthcare sector to detect diseases such as Alzheimer's [48], multimodal emotion recognition [49], hand movement classification [50], human motion tracking systems for sports wellness [51], and many more. Figure 4.6 illustrates the smart healthcare system using data fusion as one of the essential components. The wearable sensor network collects the biological signals from the patient at a remote location. This multisensor data can be transferred to the data fusion module which will combine into diverse data which will yield a meaningful representation. The cloud stores data and performs the computations for healthcare decision support systems using novel AI algorithms. This smart healthcare system is useful for early diagnosis, disease prediction, clinical decision support systems, treatment suggestions, and remote healthcare. It is expected that with the inclusion of the data fusion module in an IoMT system efficient smart healthcare solutions are discerned. Advanced analytics for health conditions estimation like triage, disease prediction, and treatment suggestions are the major outcomes of data fusion based IoMT technology.

Triage, that is, severity of disease can be estimated by using data fusion techniques in healthcare services. This helps in prioritizing the emergencies and taking appropriate actions for treatment. The severity of chronic disease is categorized into five packages: severe chronic disease, urgent level, sick level, cold state level requires minor treatment and normal level signifying stable condition [52]. Albahri et al. developed a novel distributed fault-tolerant health framework that improves triage and delegates timely services and treatment for patients with chronic heart disease [53].

4.10 CONCLUSION

Sensors are the major source for the collection of humongous data in various fields like smart healthcare, agriculture, industry, environment, and so on. Sensor data integrated with IoT, AI, and automation will provide smart systems. Data analysis is important if the data collected are of high accuracy. Therefore, the design of accurate sensors is crucial. From the intensive literature carried out in the gas sensors, there are numerous fields of smart life applications; it is concluded that optimizing the material composites and geometry structure of the sensor will provide high sensing performance. To the best of our knowledge from the literature carried out, the nanohybrid MO semiconductor-based sensors have better sensing at optimum temperature and detection of target gases at lower concentrations. Light-induced gas sensing has better sensing performance at ambient temperatures. The intelligent techniques to fuse the multisourced sensor data and integrate it with IoMT have tremendous potential for smart life applications.

REFERENCES

1. T. Singh, and U. Bonne. 2017. *Gas Sensors, Reference Module in Materials Science and Materials Engineering*, Elsevier, doi: 10.1016/b978-0-12–803581-8.00548-8.
2. S. Feng, F. Farha, Q. Li, Y. Wan, Y. Xu, T. Zhang, and H. Ning. 2019. Review on Smart Gas Sensing Technology, *Sensors*, vol. 19, no. 17, p. 3760, doi: 10.3390/s19173760.
3. J. B. A. Gomes, J. J. P. C. Rodrigues, R. A. L. Rabelo, N. Kumar, and S. Kozlov. 2019. IoT-Enabled Gas Sensors: Technologies, Applications, and Opportunities, *Journal of Sensor and Actuator Networks*, vol. 8, no. 4, p. 57, doi: 10.3390/jsan8040057.
4. A. Bag, and N. Lee. 2021. Recent Advancements in Development of Wearable Gas Sensors, *Advanced Materials Technologies*, vol. 6, no. 3, p. 2000883, doi: 10.1002/admt.202000883.
5. V. E. Bochenkov, and G. B. Sergeev. 2010. Sensitivity, Selectivity, and Stability of Gas-Sensitive Metal-Oxide Nanostructures, *Metal Oxide Nanostructures and their Applications*, vol. 3, pp. 31–52.
6. P. Dwivedi, S. Dhanekar, and S. Das. 2021. Near Room Temperature Sensing by In_2O_3 Decorated Silicon Nanowires for Sensitive Detection of Ethanol, *IEEE Sensors Journal*, vol. 21, no. 6, pp. 7275–7282, doi: 10.1109/jsen.2020.3046490.
7. B. Sharmila, P. Divyashree, and P. Dwivedi. 2023. MoS_2-based Optical Device as Artificial Synapse for Neuromorphic Computing, *IEEE Transactions on Electron Devices*, vol. 70, no. 3, pp. 1386–1392, doi: 10.1109/ted.2023.3239435.
8. B. Sharmila, and P. Dwivedi. 2022. Ultra-Sensitive, Highly Repeatable, Ultra-Fast MoO_3/P-Si Heterostructure based Photodetector, *IEEE Sensors Journal*, vol. 23, no.3, pp. 2047–2054, doi: 10.1109/JSEN.2022.3223102.
9. B. Sharmila, and P. Dwivedi. 2022. MoS_2/SiNWs Heterostructure Based Repeatable and Highly Responsive Photodetector, *Optical Materials*, vol. 133, p. 112918, doi: 10.1016/j.optmat.2022.112918.
10. B. Sharmila, P. Divyashree, S. Sharma, Priyanka Dwivedi, and S. Das. 2025. Scalable In_2S_3 based optical memristor devices as artificial synapse for logic realization and neuromorphic computing, *Materials Science in Semiconductor Processing,* vol. 185, p. 108985, doi: 10.1016/j.mssp.2024.108985.
11. P. Dwivedi, S Dhanekar, M. Agrawal, and S. Das. 2018. Interfacial Engineering in TiO_2/Nano-Si Heterostructure-based Device Prototype for E-Nose Application, *IEEE Transactions on Electron Devices*, vol. 65, no. 3, pp. 1127–1131, doi: 10.1109/ted. 2018.2797364.

12. S. B., M. K. Singha, and P. Dwivedi. 2023. Impact of Annealing on Structural and Optical Properties of ZnO Thin Films, *Microelectronics Journal*, vol. 135, p. 105759, doi: 10.1016/j.mejo.2023.105759.
13. P. Divyashree, H. Ali Quadri, P. Dwivedi, and S. Dhanekar. 2024. Demonstration of Intelligent Sensing by Nanosensors and Use of Classification and Regression Models for Electronic Nose Applications, *IEEE Sensors Journal*, vol. 24, no. 21, pp. 35423–35428, doi: 10.1109/JSEN.2024.3454381.
14. P. Dwivedi, J. Li, P. Divyashree, K. Crawford, and J. Thomas. 2023 Hybrid perovskite quantum dot-MWCNTs gas sensor for selective ethanol sensing. *MRS Communications,* vol. 13, no. 6, pp. 1156–1162, doi: 10.1557/s43579-023-00416-4.
15. S. Gupta Chatterjee, S. Chatterjee, A. K. Ray, and A. K. Chakraborty. 2015. Graphene–Metal Oxide Nanohybrids for Toxic Gas Sensor: A Review, *Sensors Actuators B Chemical*, vol. 221, pp. 1170–1181, doi: 10.1016/j.snb.2015.07.070.
16. S. Yao, P. Swetha, and Y. Zhu. 2018. Nanomaterial-Enabled Wearable Sensors for Healthcare, *Advanced Healthcare Materials*, vol. 7, no. 1, p. 1700889, doi: 10.1002/adhm.201700889.
17. C. Lin, W. Xu, Q. Yao, and X. Wang. 2019. Nanotechnology on Toxic Gas Detection and Treatment, Novel Nanomaterials for Biomedical, *Environmental and Energy Applications*, pp. 275–297, doi: 10.1016/B978-0-12–814497-8.00009-6.
18. B. Li, et al. 2019. Wearable IoT Aldehyde Sensor for Pediatric Asthma Research and Management, *Sensors Actuators B Chemical*, vol. 287, pp. 584–594, doi: 10.1016/j.snb.2019.02.077.
19. K. Arun, M. S. Lekshmi, and K. J. Suja. 2020. Design and Simulation of ZnO Based Acetone Gas Sensor Using COMSOL Multiphysics, 7th International Conference on Signal Processing and Integrated Networks, pp. 659–662, doi: 10.1109/SPIN48934.2020.9070835.
20. A. Nagamalli, and D. R. Alli. 2021. Multi Layered Bio Gas Sensor For External Breathe-A Comsol Multiphysics Based Analysis, *Solid State Technology*, vol. 63, no. 5, pp. 9058–9063.
21. P. Divyashree and Priyanka Dwivedi. 2023. AI Computing as Ubiquitous Healthcare Solution: Predict Parkinson's for Large Masses in Society, *IEEE Transactions on Computational Social Systems,* vol. 10, no. 4, pp. 1752–1757, doi: 10.1109/TCSS.2022.3224046.
22. P. Divyashree, S. B, and P. Dwivedi. 2025. MoS_2 photonic synaptic device development for non-invasive detection of Parkinson's disease, *Semiconductor Science and Technology,* vol. 40, no. 1, p. 015005, doi: 10.1088/1361-6641/ad93f7.
23. H. Zhang, J. Feng, T. Fei, S. Liu, and T. Zhang. 2014. SnO_2 Nanoparticles-Reduced Graphene Oxide Nanocomposites for NO_2 Sensing at Low Operating Temperature, *Sensors Actuators B Chemical*, vol. 190, pp. 472–478, doi: 10.1016/j.snb.2013.08.067.
24. F. Yaghouti Niyat, and M. H. Shahrokh Abadi. 2018. COMSOL-Based Modeling and Simulation of SnO_2/rGO Gas Sensor for Detection of NO_2, *Scientific Reports*, vol. 8, no. 1, p. 2149, doi: 10.103 8/s41598-018-20501-2.
25. Qianqian Yang, Guangyao Zhou, Wenhui Qin, Bin Zhang, and P. Y. Chiang. 2015. Air-kare: A Wi-Fi Based, Multi-Sensor, Real-Time Indoor Air Quality Monitor, *IEEE International Wireless Symposium*, pp. 1–4, doi: 10.1109/IEEE-IWS.2015.7164542.
26. S.-J. Chen, D. C. Hovde, K. A. Peterson, and A. W. Marshall. 2007. Fire Detection Using Smoke and Gas Sensors, *Fire Safety Journal*, vol. 42, no. 8, pp. 507–515, doi: 10.1016/j.firesaf.2007.01.006.
27. N. Harathi, and A. Sarkar. 2021. TiO_2 Based Surface Acoustic Wave Gas Sensor with Modified Electrode Dimensions for Enhanced H_2 Sensing Application*, International Journal Nanodimension*, vol. 12, no. 1, pp. 83–89.

28. G. Velasco, and J.-P. Schnell. 1983. Gas Sensors and Their Applications in the Automotive Industry, *Journal of Physical E*, vol. 16, no. 10, pp. 973–977, doi: 10.1088/0022–3735/16/10/006.
29. S. Neethirajan, D. S. Jayas, and S. Sadistap. 2009. Carbon Dioxide (CO_2) Sensors for the Agri-food Industry—A Review, *Food Bioprocess Technol*ogy, vol. 2, no. 2, pp. 115–121, doi: 10.1007/s 11947-008-0154-y.
30. K. Liu, and C. Zhang. 2021. Volatile Organic Compounds Gas Sensor Based on Quartz Crystal Microbalance for Fruit Freshness Detection: A Review, *Food Chemical*, vol. 334, p. 127615, doi: 10.1016/j.foodchem.2020.127615.
31. J. Kathirvelan, and R. Vijayaraghavan. 2017. An Infrared Based Sensor System for the Detection of Ethylene for the Discrimination of Fruit Ripening, *Infrared Physics & Technology*, vol. 85, pp. 403–409, doi: 10.1016/j.infrared.2017.07.022.
32. A. Dey. 2018. Semiconductor Metal Oxide Gas Sensors: A Review, *Materials Science and Engineering B*, vol. 229, pp. 206–217, doi: 10.1016/j.ms eb.2017.12.036.
33. G. W. Hunter et al. 2020. Editors' Choice-Critical Review-A Critical Review of Solid State Gas Sensors, *Journal of the Electrochemical Socety*, vol. 167, no. 3, p. 037570, doi: 10.1149/19 45–7111/ab729c.
34. X. Liu, S. Cheng, H. Liu, S. Hu, D. Zhang, and H. Ning. 2012. A Survey on Gas Sensing Technology, *Sensors*, vol. 12, no. 7, pp. 9635–9665, doi: 10.3390/s120709635.
35. X. Wan, J. Wang, L. Zhu, and J. Tang. 2014. Gas Sensing Properties of Cu_2O and Its Particle Size and Morphology-Dependent Gas-Detection Sensitivity, *Journal of Materials Chemistry A*, vol. 2, no. 33, pp. 13641–13647, doi: 10.1039/C4TA02659D.
36. Y. Li, S. Song, L.-B. Zhang, X.-X. Lian, L.-X. Shan, and Q.-J. Zhou. 2021. Fabrication of Hollow Porous ZnO@ZnS Heterostructures via Hydrothermal Method and Enhanced Gas-Sensing Performance for Ethanol, *Journal of Alloys Compounds*, vol. 855, p. 157430, doi: 10.1016/j.jallcom.2020.157430.
37. M. Trawka, J. Smulko, L. Hasse, C.-G. Granqvist, F. E. Annanouch, and R. Ionescu. 2016. Fluctuation Enhanced Gas Sensing with WO_3-Based Nanoparticle Gas Sensors Modulated by UV Light at Selected Wavelengths, *Sensors Actuators B Chemical*, vol. 234, pp. 453–461, doi: 10.1016/j.s nb.2016.05.032.
38. Y. Zhao et al. 2021. Light-Optimized Photovoltaic Self-Powered NO_2 Gas Sensing Based on Black Silicon, *Sensors Actuators B Chemical*, vol. 340, p. 129985, doi: 10.1016/j.snb.2021.129985.
39. T. Bhavani, P. VamseeKrishna, C. Chakraborty, and P. hy. 2022. Stress Classification and Vital Signs Forecasting for IoT-Health Monitoring, *IEEE/ACM Transactions on Computational Biology and Bioinformatics*, vol. 21, no. 4, pp. 652–659, doi: 10.1109/TCBB.2022.3196151.
40. S. Wei et al. 2022. A Self-Powered Portable Nanowire Array Gas Sensor for Dynamic NO_2 Monitoring at Room Temperature, *Advanced Materials*, vol. 35, no. 12, p. 2207199, doi: 10.1002/adma.202207199.
41. W. T. Al-Sit, N. A. Al-Dmour, T. M. Ghazal, and G. F. Issa. 2023. IoMT-Based Framework for Ambient Assisted Living Using a Convolutional Neural Network, *Computers, Materials and Continua*, vol. 74, no. 3, pp. 6867–6878, doi: 10.32604/cmc.2023.034952.
42. S. Vishnu, S. R. J. Ramson, and R. Jegan. 2020. Internet of Medical Things (IoMT) - An Overview, *in 2020 5th International Conference on Devices, Circuits and Systems (ICDCS)*, pp. 101–104, 2020, doi: 10.1109/ICDCS48716.2020.243558.
43. J. Srivastava, S. Routray, S. Ahmad, and M. M. Waris. 2022. Internet of Medical Things (IoMT)-Based Smart Healthcare System: Trends and Progress, *Computational Intelligence and Neuroscience*, vol. 2022, pp. 1–17, doi: 10.1155/2022/7218113.

44. W. Ding, X. Jing, Z. Yan, and L. T. Yang. 2019. A Survey on Data Fusion in Internet of Things: Towards Secure and Privacy-Preserving Fusion, *Information Fusion*, vol. 51, pp. 129–144, doi: 10.1016/j.inffus.2018.12.001.
45. H. Haick, and N. Tang. 2021. Artificial Intelligence in Medical Sensors for Clinical Decisions, *ACS Nano*, vol. 15, no. 3, pp. 3557–3567, doi: 10.1021/ac snano.1c00085.
46. J. I. Rodriguez-Labra, C. Kosik, D. Maddipatla, B. B. Narakathu, and M. Z. Atashbar. 2021. Development of a PPG Sensor Array as a Wearable Device for Monitoring Cardiovascular Metrics, *IEEE Sensors Journal*, vol. 21, no. 23, pp. 26320–26327, doi: 10.1109/JSE N.2021.3064219.
47. J. Srivastava, S. Routray, S. Ahmad, and M. M. Waris, 2022. Internet of Medical Things (IoMT)-Based Smart Healthcare System: Trends and Progress, *Computational Intelligence and Neuroscience*, vol. 2022, pp. 1–17, doi: 10.1155/2022/7218113.
48. S. El-Sappagh, J. M. Alonso, S. M. R. Islam, A. M. Sultan, and K. S. Kwak. 2021. A Multilayer Multimodal Detection and Prediction Model Based on Explainable Artificial Intelligence for Alzheimer's Disease, *Scientific Reports*, vol. 11, p. 2660, doi: 10.1038/s4159 8–021–82098-3.
49. Y. Huang, J. Yang, P. Liao, and J. Pan. 2017. Fusion of Facial Expressions and EEG for Multimodal Emotion Recognition, *Computational Intelligence and Neuroscience*, vol. 2017, pp. 1–8, 2017, doi: 10.1155/2017/2107451.
50. N. Rabin, M. Kahlon, S. Malayev, and A. Ratnovsky. 2020. Classification of Human Hand Movements Based on EMG Signals Using Nonlinear Dimensionality Reduction and Data Fusion Techniques, *Expert Systems with Applications*, vol. 149, p. 113281, 2020, doi: 10.1016/j.eswa.2020.113281.
51. M. P. Wilk, M. Walsh, and B. O'Flynn. 2021. Multimodal Sensor Fusion for Low-Power Wearable Human Motion Tracking Systems in Sports Applications, *IEEE Sensors Journal*, vol. 21, no. 4, pp. 5195–5212, doi: 10.1109/JSEN.2020.3030779.
52. O. S. Albahri, A. A. Zaidan, B. B. Zaidan, M. Hashim, A. S. Albahri, and M. A. Alsalem. 2018. Real-Time Remote Health-Monitoring Systems in a Medical Centre: A Review of the Provision of Healthcare Services-Based Body Sensor Information, Open Challenges and Methodological Aspects, *Journal of Medical Systems*, vol. 42, pp. 164, doi: 10.1007/s10916-018-1006-6.
53. A. S. Albahri et al., 2021. Development of IoT-Based Mhealth Framework for Various Cases of Heart Disease Patients, *Health Technology* (Berl.), vol. 11, no. 5, pp. 1013–1033, doi: 10.1007/s12553-021-00579-x.

5 Revolutionizing Personalized Healthcare

The Role of Nanosensors in NonInvasive Monitoring

P. Nedumal Pugazhenthi, K. Vijayakumar, S. Selvaperumal and G. Prabhakar

5.1 INTRODUCTION

The fusion of nanotechnology with customized medicine is causing a major revolution in the healthcare sector. Nanosensors, extraordinary tools, or materials created at the nanoscale enable this transition. We set off on a voyage into the world of noninvasive nanosensors and their crucial function in personal healthcare in this chapter.

5.2 THE IMPERATIVE FOR PERSONALIZED HEALTHCARE

A ray of hope for contemporary medicine has appeared in the form of personalized healthcare, which is characterized by treatments catered to specific patients. One-size-fits-all thinking has given way to precision medicine, in which treatments are specially created depending on a patient's genetic profile, way of life, and environmental circumstances. Precision medicine, as it is frequently called, is becoming more and more significant in contemporary medicine. This method acknowledges that each person is unique, and that each person's healthcare requirements should be catered to their particular traits, including genetics, environment, and lifestyle. Here, we discuss the significance of personalized healthcare with references to real studies and sources that highlight its importance. It allows for the development of treatment plans tailored to an individual's genetic makeup and medical history [1]. The authors in [2] emphasize preventive measures by identifying genetic predispositions to diseases, thereby enabling early intervention. Moreover, in [3], the authors facilitate the development of targeted therapies, thereby reducing side effects and improving treatment efficacy. Personalized medicine accelerates drug development by identifying specific patient populations that are most likely to benefit from new medications [4]. By preventing diseases and avoiding ineffective treatments, personalized healthcare can reduce healthcare costs in the long run [5]. In [6], the authors' personalized medicine places patients at the center of their care, thereby involving them in decision-making processes. The manuscript [7] states that advances in

DOI: 10.1201/9781003602729-5

genomics have enabled the rapid growth of personalized medicine, with the identification of disease-related genetic markers. As increasing treatment success rates in personalized approaches increase the likelihood of treatment success, therapies are chosen based on an individual's unique genetic and molecular profile [8]. In [9], the authors' ethical considerations in personalized healthcare, such as informed consent and data privacy, are crucial for maintaining patient trust. Personalized healthcare has the potential to advance public health by tailoring interventions to specific population groups as mentioned in [10]. Traditional healthcare monitoring methods often involve invasive procedures, sporadic blood tests, and manual data collection. Such approaches can be uncomfortable, inconvenient, and may miss critical insights into a patient's condition. Noninvasive monitoring, on the contrary, offers a less intrusive yet highly effective alternative. The authors of [11] have explained about the significance of Internet of Things-based wearable healthcare devices post-COVID-19 pandemic. The selective and highly sensitive performance of porous TiO_2 /nano-Si heterostructure for ethanol sensing and extremely sensitive and selective acetone sensor prototype which can be used as a platform for non-invasive diabetes detection is discussed in [12] and [13] respectively.

5.3 NANOSENSORS: AN EXEMPLAR SHIFT IN HEALTHCARE MONITORING

Nanosensors, which are components or materials distinguished by their small size, increased sensitivity, and extraordinary specificity, are at the core of this shift. By offering accuracy and sensitivity previously unattainable in healthcare monitoring, nanosensors defy expectations.

It is truly amazing how versatile nanosensors are in biomedical applications, providing a vast range of capacities and functionalities. They can be made to simultaneously monitor a number of biological factors, including pH values, glucose levels, and certain biomarkers. This multimodal sensing capability makes it possible to monitor biological systems completely and holistically. They are designed to target certain molecules or targets with a high degree of precision. Nanosensors can selectively attach to particular proteins, DNA sequences, or other biomolecules by changing the surface characteristics or functionalization of their surface. Real-time monitoring of dynamic biological processes is made possible by the quick reaction times of nanosensors. They are crucial for monitoring the course of diseases or the effectiveness of treatments because they can record changes in biological activity. Numerous nanoscale materials that are used in sensors can interact with biological systems without harming them or triggering immune reactions because they are biocompatible. They are suitable for in vivo applications due to this characteristic. For point-of-care diagnostics, portable and handheld nanosensor-based devices are being developed, allowing quick and affordable testing outside of conventional clinical settings. They can be used to visualize and examine biological structures and processes at the nanoscale using a variety of imaging techniques, including magnetic resonance imaging (MRI) and fluorescence microscopy. This supports research and early disease diagnosis. They can be placed inside the body in hard-to-reach places, delivering information without the need for intrusive operations. This is particularly helpful for ongoing monitoring in challenging locations.

They can track drug release and distribution inside the body and can be integrated into drug delivery systems. This feedback loop promotes treatment efficacy and permits precise drug administration. Nanosensors are not just used in medical settings. In addition, they are used in environmental monitoring to find infections, pollutants, and other toxins in soil, water, and air. Thus, they are useful resources for biologists and medical researchers. They make it easier to research biological functions, disease mechanisms, and the results of different treatments. Nanosensors' adaptability in biomedical settings expands their usefulness across a broad range of applications, from treatments to diagnostics and from fundamental research to clinical practice. Nanosensors are effective tools for furthering our understanding of biology and enhancing healthcare outcomes due to their versatility and multifunctionality.

5.3.1 The Nanoscale Advantage

Nanosensors have special qualities since they function at scales of nanometers (1–100 nm). Outstanding surface-to-volume ratios, the ability to interact with molecules at the molecular scale, and the ability to perform at the cellular or subcellular level are a few of these characteristics.

In biomedical applications, the nanoscale advantage of sensors is significant and provides a number of key advantages, including enhanced sensitivity, miniaturization, precision and specificity, real-time monitoring, biocompatibility, multiplexing, early disease detection, personalized medicine, drug delivery, and reduced sample size.

Nanoscale sensors are able to detect and react to very small changes in the environment, such as modest changes in molecular interactions or concentrations of biomolecules, since they have a larger surface area-to-volume ratio. They can be precisely tailored to target particular chemicals or biological indicators. In biomedical applications, this specificity is essential for precise diagnosis and focused treatments. Since nanosensors are so small, they can be used for in vivo monitoring and drug delivery systems inside the human body. Because of their small size, they can be treated without or with minimal invasiveness. Many of the nanoscale materials used in sensors are biocompatible, which means that there is little chance of toxicity or an immunological reaction and that they are well tolerated by biological systems. They may be made to simultaneously detect numerous analytes, allowing for thorough monitoring of intricate biological systems.

Nanosensors are useful tools for the early identification of diseases, such as cancer and infectious disorders, when therapy is frequently most effective due to their sensitivity. These sensors play a critical role in personalized medicine by providing data on an individual's unique biology and response to treatment. This allows for tailored therapeutic approaches. The rapid response time of nanosensors allows for real-time monitoring of biological processes, thereby providing immediate feedback for healthcare professionals and researchers. Nanosensors can be integrated into drug delivery systems to monitor drug release and ensure precise dosing, thereby improving the effectiveness and safety of treatments. Figure 5.1 shows the significance of noninvasive smart implants.

The greater feature of these sensors is they require smaller sample volumes, which is particularly beneficial when working with limited or precious biological samples. Overall, the nanoscale advantage of sensors in biomedical applications has

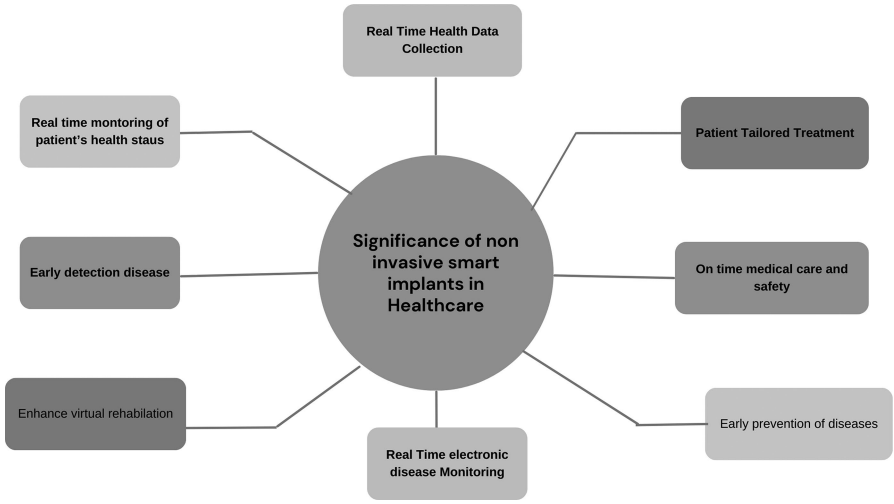
Real Time Health Data Collection
Real time montoring of patient's health staus
Patient Tailored Treatment
Significance of non invasive smart implants in Healthcare
Early detection disease
On time medical care and safety
Enhance virtual rehabilation
Early prevention of diseases
Real Time electronic disease Monitoring

FIGURE 5.1 Significance of noninvasive smart implants in healthcare.

the potential to revolutionize healthcare by enabling more accurate diagnostics, targeted therapies, and real-time monitoring, ultimately leading to improved patient outcomes and a deeper understanding of biological processes. They have versatility beyond measures, as they are not confined by limitations. They are designed to detect a myriad of health-related parameters, including blood glucose levels, specific biomarkers, ions, and vital signs. Since they can access continuous data streams, their real-time capabilities give patients and healthcare professionals quick access to information on health status.

5.4 TYPES OF NANOSENSORS IN NONINVASIVE MONITORING

Nanosensors come in many forms, including biological, chemical, and physical ones, each with its own specialties. The many kinds of nanosensors and their uses in noninvasive healthcare monitoring are examined in this section.

5.4.1 Biological Nanosensors

Biomolecules and biological nanosensors interact to provide highly sensitive detection of disease indicators. They offer potential for monitoring and early disease detection, opening the door to proactive healthcare. They are specialized tools or substances made to recognize and react to particular nanoscale biological molecules or occurrences. The interaction between these nanoscale sensors and biological molecules, which produces quantifiable signals or reactions, is central to the principles behind biological nanosensors.

To specifically recognize and attach to target biological molecules such as proteins, DNA, RNA, or tiny molecules like glucose, they are created to have molecules or structures on their surface. The biological nanosensor starts a transduction

pathway when it binds to the target molecule. The physical characteristics of the nanosensor, such as its fluorescence, electrical conductivity, or magnetic properties, may alter as a result of this mechanism. The biological nanosensor and the target molecule bind with a significant affinity and exhibit high specificity. This indicates that the sensor only detects the target molecule, ignoring other environmental chemicals. The target molecule's concentration or presence is proportional to the signal produced by the transduction process. When this signal is quantified and examined, the amount of the biological molecule in the sample is revealed. Amplification techniques are used by several biological nanosensors to increase their sensitivity. This may entail enzymatic signal amplification or the use of nanoparticles to magnify the signal.

They frequently have real-time monitoring capabilities for biological processes. Continuous observation is made possible by the sensor's ability to adapt its signal when the concentration of the target molecule changes over time. Because they are created at the nanoscale, biological nanosensors can interact with biological molecules on a molecular level. Their sensitivity is improved by this downsizing, which also lowers the quantity of sample needed for analysis. To ensure that biological systems, including living creatures, can be introduced to biological nanosensors without injury or immunological reactions, they are made from biocompatible materials. They can be customized to certain applications by changing their surface qualities or adding various recognition components. They are adaptable for a range of biomedical and research applications thanks to their customizability. Applications for biological nanosensors include disease diagnosis, drug development, environmental monitoring, and fundamental biological research. They make it possible to precisely identify and measure particular biomolecules, giving us important information about how biological processes work. The fundamentals of biological nanosensors focus around their high specificity and sensitivity in identifying and interacting with biological molecules, which eventually results in the development of quantifiable signals that carry significant biological information. These sensors are essential to expanding our knowledge of biology, enhancing healthcare, and developing diagnoses.

5.4.2 Chemical Nanosensors

Chemical nanosensors are made to recognize particular compounds, which makes them perfect for uses like drug monitoring and poison detection in the environment. Figure 5.2 displays a few products based on chemical sensors.

Chemical nanosensors are specialized tools or substances created to recognize and react to particular chemical molecules or compounds at the nanoscale. Chemical analytes that are the target of chemical nanosensors interact with these nanoscale sensors to produce detectable signals or reactions. Typically, they have specific molecules or surface features functionalized so that they can interact with the target chemical components. These functional groups can be designed to selectively attach to the analytes of interest and recognize them. The target chemical molecule and the functionalized nanosensor interact in a very particular manner that is marked by a high chemical affinity. This guarantees that the

FIGURE 5.2 A few wearable chemical sensors.

target molecule will be captured by the sensor with the least amount of interference from other molecules. The target chemical component undergoes binding or adsorption to the surface of the functionalized nanosensor when it comes into contact with the sensor. Changes in the sensor's mass, electrical conductivity, or optical features may result from this interaction. The target molecule's binding or adsorption activates transduction processes inside the nanosensor. These methods may entail modifications to surface plasmon resonance, fluorescence intensity, electrical conductivity (resistance), or other physical characteristics. A signal that is proportionate to the concentration or existence of the target chemical substance is produced by the transduction mechanism. The amount of the analyte in the sample can be determined by quantifying and measuring this signal. Chemical nanosensors have an extremely high sensitivity and can detect target analytes at very low concentrations. Their exceptionally high sensitivity is a result of their small size and high surface-to-volume ratio. These sensors have numerous uses, including environmental monitoring, industrial process control, chemical analysis, and medical diagnostics. They facilitate a variety of analytical activities by enabling accurate detection and quantification of particular chemical components.

Chemical nanosensors work on the basis of their capacity to selectively interact with target chemical analytes, thereby leading to quantifiable changes in the analytes'

characteristics that can be used for detection and quantification. These sensors are essential in a number of industries where precise and sensitive chemical analysis is needed.

5.4.3 Physical Nanosensors

Physical nanosensors can measure mechanical changes like pressure or strain and provide important information about physiological processes like breathing and heartbeat. Physical nanosensors are specialized tools or substances created to recognize and react to phenomena or physical changes at the nanoscale. These sensors function according to numerous physical interactions and principles. They rely on particular physical characteristics that adapt to the physical phenomenon they are trying to target. The method by which a physical change is transformed into a signal that can be measured is known as the transduction mechanism. Because of their nanoscale construction, they can interact with physical events at the most granular scales. Their little stature makes them more perceptive to even minute changes. Physical changes can be detected with great sensitivity by the nanosensors. They are useful tools for precise measurements due to their sensitivity, which enables them to detect minute fluctuations in physical properties. While functionalizing or designing physical nanosensors to react to particular sorts of physical changes or events can increase their specificity, physical nanosensors may primarily respond to a particular physical attribute. Various transduction modalities, such as piezoelectric, magnetoresistive, capacitive, optical, or electrical, are used by various physical nanosensors to function. Each mode uses a particular set of physical characteristics for sensing. Due to their distinctive physical characteristics and ability to be tuned for particular sensing applications, nanomaterials like nanoparticles, nanowires, or nanotubes are frequently used in physical nanosensors. To improve the ability to detect physical changes, certain physical nanosensors use signal amplification techniques, such as the use of nanoparticles or nanocomposites.

Electronics, aerospace, healthcare, materials science, structural health monitoring, and other industries all use physical nanosensors. They are utilized for duties like determining magnetic fields, assessing material stress, and keeping track of physiological parameters. In general, they work by identifying and reacting to particular nanoscale physical alterations or events. In a variety of applications, they provide accurate measurements and real-time monitoring of physical parameters by utilizing their small size, sensitivity, and unique transduction mechanisms.

5.5 APPLICATIONS AND CASE STUDIES

This section offers case studies and real-world applications that illustrate the revolutionary potential of noninvasive nanosensors in the field of personal healthcare. The successful use of glucose monitoring, biomarker identification, and continuous vital sign tracking is highlighted in case studies.

5.5.1 Case Studies

Case Study 1: Applications in Biomedicine: Early Cancer Detection

The effectiveness of cancer diagnosis and treatment is greatly improved by early detection of cancer biomarkers. The development of nanosensors has made it possible to detect these biomarkers with great sensitivity and specificity **[14].** Researchers created gold nanoparticle-based nanosensors in this case study that were functionalized with particular antibodies for cancer biomarkers. These nanosensors had the ability to bind to specific proteins, thereby changing the nanosensor's characteristics in a measured way. Even in complicated biological samples, the nanosensors were successful in detecting cancer indicators at incredibly low quantities. Early cancer detection with the help of this technology may result in more successful treatments and better patient outcomes.

Case Study 2: Monitoring the Environment: Water Quality

Since maintaining the quality of water supplies is crucial for preserving public health and the environment, this case study is thought to be significant. Real-time water quality monitoring made possible by nanosensors enables quick reaction to pollution events [15]. In this case study, scientists created nanosensors based on carbon nanotubes functionalized with molecules that respond to particular water contaminants, such as organic pollutants and heavy metals. Systems for monitoring water have been equipped with these nanosensors. Early detection of contaminants was made possible thanks to the constant, real-time data the nanosensors gave on water quality parameters. The potential for preventing pollution incidents and guaranteeing the security of water supplies exists with this proactive approach to monitoring.

Case Study 3: Electronics: Strain Sensing in Aerospace

For performance and safety, maintaining an aircraft's structural integrity is essential. Nanosensors can be incorporated into composite materials to track levels of stress and strain, which helps with the structural health monitoring process **[16].** In this case study, scientists integrated nanosensors made of carbon nanotubes into composite materials used in airplane building. The electrical characteristics of these nanosensors were engineered to adapt to mechanical stress. Real-time information on the degrees of strain in composite materials was provided by the embedded nanosensors. Continuous structural integrity monitoring allows maintenance crews to spot possible problems early, threby improving aircraft safety and lowering maintenance costs.

The aforementioned case studies highlight the different ways that nanosensors are being used in industries including healthcare, environmental monitoring, and aerospace to address pressing problems and enhance a variety of facets of our lives.

Case Study 4: Environmental Monitoring: Air Quality

Health effects from urban air pollution are significant. Real-time monitoring of airborne contaminants is made possible by nanosensors, thereby allowing for well-informed judgments and focused interventions. In this case study, scientists created nanosensors with the help of molecules that are sensitive to common urban pollutants including nitrogen dioxide (NO_2) and volatile organic compounds functionalized on graphene oxide nanomaterials **[17].** Urban areas were covered with these nanosensor installations. When pollutant concentrations changed, the nanosensors detected them and continuously provided data on air quality. Utilizing this knowledge will help manage and reduce urban pollution, thereby enhancing inhabitants' quality of life.

Case Study 5: Food Safety: Pathogen Detection

For the sake of the general welfare, food product safety must be ensured. Nanosensors can be used to quickly and highly sensitively identify pollutants and pathogens in food. In this case study, scientists created nanosensors using nanoparticles that were functionalized with DNA probes specific to Salmonella and *E. coli*, two frequent foodborne pathogens. Food samples were subjected to these nanosensors **[18]**. In contrast to conventional approaches, which may take hours or days, the nanosensors successfully identified the presence of pathogens in food samples in a matter of minutes. This skill of quick detection enables prompt responses to reduce the risk of foodborne illnesses and improve food safety.

These additional case studies highlight the adaptability and significance of nanosensors in tackling significant problems in environmental monitoring, food safety, and public health. They provide as an example of how nanosensors can quickly and accurately detect a variety of analytes, thereby enabling better judgment and more effective safety precautions.

5.6 FUTURE PROSPECTS AND CHALLENGES

The future of noninvasive nanosensors in personal healthcare is promising yet faces significant challenges. Ethical considerations, regulatory frameworks, and scalability issues are explored. Future prospects include wearable nanosensor devices, telehealth integration, and data-driven healthcare decision-making. The recent improvizations in nanosensors-based wearable devices are discussed in [19–21]. The few wearable devices using nanosensors are shown in Figure 5.3.

The future prospects of nanosensors in personal healthcare are promising, but they also come with several challenges. An overview of both the prospects and challenges is presented here.

5.6.1 Future Prospects

- Personalized Medicine: Nanosensors will play a pivotal role in the advancement of personalized medicine by providing real-time data on an individual's health status, thereby allowing for tailored treatments and interventions.

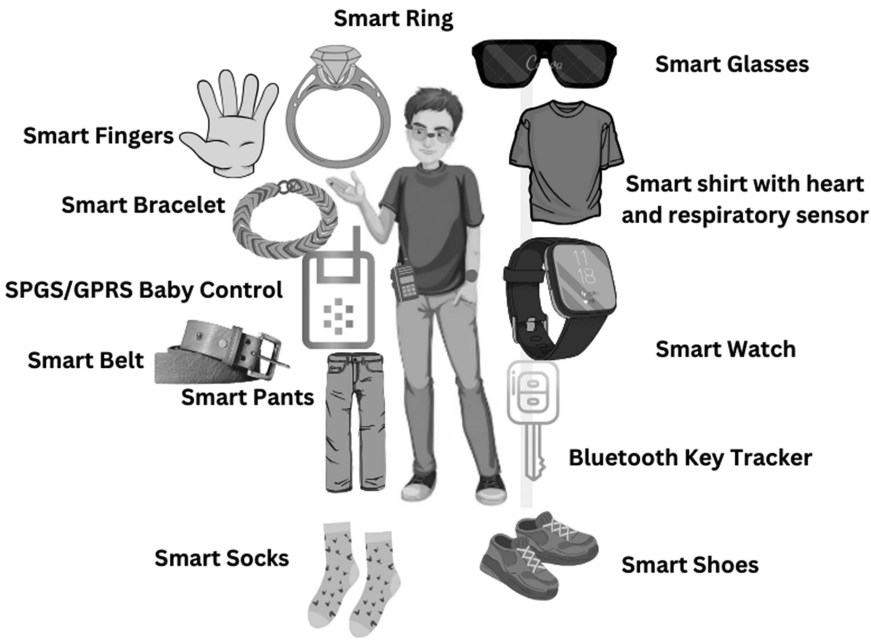

FIGURE 5.3 A few wearable devices using nanosensors.

- Continuous Monitoring: These sensors can enable continuous health monitoring, thereby providing a wealth of data that can be analyzed to detect early signs of diseases or changes in health parameters.
- Wearable Health Tech: Integration of nanosensors into wearable devices, such as smart watches or clothing, will make continuous monitoring seamless and convenient for users.
- Point-of-Care Diagnostics: Portable nanosensor-based devices for point-of-care diagnostics will become more accessible, thereby allowing for rapid testing and early disease detection outside of traditional healthcare settings.
- Drug Delivery Optimization: By integrating these sensors into drug delivery systems, it is possible to monitor medication release and effectiveness and increase the accuracy of treatments.
- Nanosensors in Telemedicine: Integration of nanosensors into telehealth platforms allows for remote patient monitoring and consultations, which is particularly useful in remote or underserved locations.
- Disease Prevention: Nanosensors can support preventative healthcare, lowering the burden of disease, by offering early warnings and insights into health trends.

5.6.2 Challenges

- Data Security and Privacy: The ongoing collection of private, sensitive health information poses serious questions regarding data security and privacy, thereby necessitating strong encryption and protection techniques.

- Regulatory Hurdles: The approval and regulation of nanosensor-based medical devices can be complex and time-consuming, requiring adherence to stringent safety and efficacy standards.
- Ethical Considerations: Ethical issues regarding informed consent, data ownership, and potential misuse of health data need careful consideration.
- Cost and Accessibility: Developing and implementing nanosensor technologies can be expensive, thereby limiting accessibility for certain populations.
- Interoperability: Ensuring that nanosensor data can be seamlessly integrated into electronic health records and healthcare systems is a technical challenge.
- Long-Term Safety: The long-term effects of nanosensors within the body need further study to ensure they do not pose unintended health risks.
- Data Overload: Continuous monitoring generates vast amounts of data, which must be efficiently managed, analyzed, and interpreted to provide meaningful insights without overwhelming healthcare professionals or patients.
- User Adoption: Acceptance and adoption of nanosensor-based technologies may vary among different demographics, thereby requiring educational efforts and user-friendly interfaces.

Nanosensors hold great promise in revolutionizing personal healthcare by providing real-time data and enabling personalized treatments, addressing challenges related to regulation, privacy, and data management is crucial for their successful integration into the healthcare ecosystem. Overcoming these challenges will pave the way for a future where nanosensors contribute significantly to improved health outcomes and patient well-being.

5.7 CONCLUSION

In conclusion, noninvasive nanosensors are poised to redefine the landscape of personal healthcare. Their remarkable properties and versatility empower individuals and healthcare providers with continuous, precise, and noninvasive health monitoring. As we continue to unlock the potential of nanosensors, we stand at the threshold of a new era in healthcare, one where personalization and prevention take center stage. The future of nanosensors in healthcare holds immense promise. These tiny yet powerful sensors have the potential to revolutionize personalized medicine, enable continuous monitoring, and enhance early disease detection. From wearable devices to implantable sensors, nanosensor technology is poised to provide invaluable insights into our health. However, alongside these prospects, significant challenges like data privacy, regulation, and cost must be addressed. As researchers work on advancing nanosensor capabilities and ethical frameworks, they pave the way for a future where these nanoscale marvels contribute substantially to improving healthcare outcomes and enhancing our understanding of the human body and its environment.

REFERENCES

1. Collins, F. S., &Varmus, H. A new initiative on precision medicine. *New England Journal of Medicine,* 2015; 372(9), 793–795.

2. Kullo, I. J., & Jouni, H. Disclosing genetic information in the electronic health record: A policy model. *Genetics in Medicine,* 2015; 17(11), 854–856.
3. Rebocho, A. P., & Marais, R. New insight puts CRAF in sight as a therapeutic target. *Cancer Discovery,* 2011; 1(2), 98–99.
4. Hamburg, M. A., & Collins, F. S. The path to personalized medicine. *New England Journal of Medicine,* 2010 July 22; 363(4), 301–304.
5. Ganesan, P., Jain, H., Bagal, B., Subramanian, P. G., George, B., Korula, A., Mehra, N., Kalaiyarasi, J. P., Bhurani, D., Agrawal, N., Ahmed, R., Kayal, S., Bhattacharyya, J., Yanamandra, U., Kumar, S., Philip, C. C., John, M. J., Nadaraj, A., Karunamurthy, O., Lakshmanan, J., Mathews, V., & Sengar, M. Outcomes in adolescent and young adult acute lymphoblastic leukaemia: a report from the Indian Acute Leukaemia Research Database (INwARD) of the Hematology Cancer Consortium (HCC). *British Journal of Haematology,* 2021 April; 193(1), e1–e4.
6. Bazzano, L. A., Durant, J., & Brantley, P. R. A modern history of informed consent and the role of key information. *Ochsner Journal,* 2021 Spring; 21(1), 81–85.
7. Manolio, T. A., & Collins, F. S. The HapMap and genome-wide association studies in diagnosis and therapy. *Annual Review of Medicine,* 2009; 60, 443–456.
8. Hofstatter, E. W., & Bale, A. E. The promise and pitfalls of genomics-driven cancer medicine. *Virtual Mentor,* 2013 August 1; 15(8), 681–686.
9. McGuire, A. L., & Beskow, L. M. Informed consent in genomics and genetic research. *Annual Review of Genomics Human Genetics,* 2010; 11, 361–381.
10. Khoury, M. J., Millikan, R., Little, J., & Gwinn, M. The emergence of epidemiology in the genomics age. *International Journal of Epidemiology,* 2004 October; 33(5), 936–944. https://doi.org/10.1093/ije/dyh278. Epub 2004 Aug 19. PMID: 15319400.
11. Dwivedi, P., & Singha, M. K. IoT based wearable healthcare system: Post COVID-19. In: Chakraborty, C., Roy, S., Sharma, S., & Tran, T. A. (Eds.), *The Impact of the COVID-19 Pandemic on Green Societies,* 2021; 305–321. Cham: Springer. https://doi.org/10.1007/978-3-030-66490-9_13.
12. Dwivedi, P., Dhanekar, S., Agrawal, M., & Das, S. Interfacial engineering in TiO2/Nano-Si heterostructure-based device prototype for E-nose application. *IEEE Transactions on Electron Devices*, 2018 March; 65(3), 1127–1131. https://doi.org/10.1109/ted.2018.2797364.
13. Dwivedi, P., Dhanekar, S., & Das, S. MoO3/nano–Si heterostructure based highly sensitive and acetone selective sensor prototype: A key to non-invasive detection of diabetes. *Nanotechnology,* 2018 May; 29(27), 275503. https://doi.org/10.1088/1361–6528/aabcef.
14. Nam, Jwa-Min, et al. Nanoparticle-based bio-bar codes for the ultrasensitive Detection of proteins. *Science,* 2003; 301, 1884–1886. https://doi.org/10.1126/science.1088755
15. Ally, N., & Gumbi, B. A Review on metal nanoparticles as nano-sensors for environmental detection of emerging contaminants. *Materials Today: Proceedings* 2023. https://doi.org/10.1016/j.matpr.2023.08.032.
16. Ehrmann, A., Nguyen, T. A., & Tri, P. N. (Eds.). *Nanosensors and Nanodevices for Smart Multifunctional Textiles.* 2020, Elsevier. https://doi.org/10.1016/C2019-0-02500-9
17. Mohamed, E. F., & Awad, G. Development of nano-sensor and biosensor as an air pollution detection technique for the foreseeable future. *Comprehensive Analytical Chemistry* 2022; 99, 163–188. https://doi.org/10.1016/bs.coac.2021.11.003
18. Li, Shuang, Zhang, Danhua, et al. Electrochemiluminescence on smartphone with silica nanopores membrane modified electrodes for nitroaromatic explosives detection. *Biosensors and Bioelectronics,* 2019; 129, 284–291. https://doi.org/10.1016/j.bios.2018.09.055

19. Gaobotse, Goabaone, Mbunge, Elliot, et al. Non-invasive smart implants in healthcare: Redefining healthcare services delivery through sensors and emerging digital health technologies. *Sensors International,* 2022; 3, 100156. https://doi.org/10.1016/j.sintl.2022.100156
20. Promphet, Nadtinan, Ummartyotin, Sarute, et al. MNon-invasive wearable chemical sensors in real-life applications. *Analytica Chimica Acta*, 2021; 1179, 338643. https://doi.org/10.1016/j.aca.2021.338643
21. Kazanskiy, N. L., Butt, M. A., & Khonina, S. N. Recent advances in wearable optical sensor automation powered by battery versus skin-like battery-free devices for personal healthcare-a review. *Nanomaterials* (Basel, Switzerland), 2022; 12(3), 334. https://doi.org/10.3390/nano12030334

6 Robust Non-Invasive Support System for Blood Cell Image Classification Using Generative Adversarial Networks

Mohammad Shabaz, Mukesh Soni and Mohammed Wasim Bhatt

6.1 INTRODUCTION

Human blood cell classification detection is an important test in clinical examination. The detection and counting of red blood cells and five types of white blood cells in human peripheral blood can provide important help for disease diagnosis [1]. Traditional blood cell image detection and classification mainly rely on artificial microscopic examination, this method is not only inefficient, but also requires experienced morphological professionals to complete [2]. Recently, deep learning-based object detection methods are mainly used in image processing in the medical field [3]. The application of deep learning relies on large-scale labeling the support of datasets; the rarity of leukocyte samples in blood cells and the complexity of the collection and calibration process may limit deep learning methods in the classification and detection of cell images. Therefore, research on the generation methods of high-quality cell images to expand the training of cell detection networks is particularly important to improve the accuracy of blood cell classification and detection.

Deep learning-based target identification techniques are now mostly separated into two groups. One approach is the candidate frame target identification method, which includes YOLOV1-V3, SSD (Single Shot Detector), Faster RCNN (Region-based Convolutional Neural Networks), and so on [4–6]. This type of method is suitable for large target detection, but the detection accuracy of small targets in blood cell images is poor in the case of adhesion. In this literature [7] YOLO candidate frame is used to classify and detect cells, and in this work [8] Faster RCNN candidate frame is used to detect red blood cells. These detections are all carried out in the case of red blood cell adhesion and occlusion, and the accuracy is low. Second one is the target detection method based on density map, such as FCRN (Fully Convolutional Regression

 DOI: 10.1201/9781003602729-6

Networks) [9] and SDBN [10]. This kind of method regresses the small target to an independent Gaussian kernel; for small targets, the detection effect is better in complex scenes. These two types of methods generally have few cell samples, and the collection and calibration work are difficult, thereby resulting in the accuracy that cannot meet the actual detection needs.

With the emergence of generative adversarial network (GAN), the lack of large-scale labeled datasets has been solved. At the same time, the original GAN generated images without label information by inputting random noise, which cannot solve medical cell images [11]. Reference [12] proposed a conditional generative adversarial network (CGAN) to generate images with controllable results by simultaneously inputting noise and conditional information. Reference [13] proposed pix2pix, which uses the segmentation mask of the scene to achieve image-to-image generation. The conditional information input by the generator in the existing conditional adversarial network is limited, and the discriminator structure that is not suitable for the detailed information of the image at different scales is ignored when generating an image for true and false identification, resulting in a lack of realism in the detailed information (such as brightness sharpness, edge sharpness, etc.) of the cell image generated compared with the original cell image.

To cope with problems with respect to the above-mentioned methods, this paper proposes a multi-scale conditional generative adversarial network (MCGAN) on the basis of a multi-scale discriminator (MD). The structure generator adopts the U-Net [14] encoder–decoder structure, using skip connections. The network extracts deeper image features, fuses shallow and deep features, introduces a MD into the existing CGAN discriminator structure, and undergoes a multi-scale convolution operation (M-Conv), and multi-scale pooling structure (MPS-block) extract the details of real images and generated images at different scales to distinguish between true and false. This improves the performance of the discriminator and promotes the generator to generate the detailed information of the cell image to improve the realism of the image. At the same time, the gradient similarity (GS) loss term is presented to the loss function of pix2pix generator, which improves the generation by minimizing the comparison among the original image and the generated image in terms of brightness, contrast, and gradient structure. Brightness and edge clarity of cell images a detector is added after the CGAN, and its structure is consistent with that of the generator. The cell image generated are used in target classification and detection network training phase for increasing the diversity of cell samples to this augmented training set.

6.2 RELATED WORK

Two networks make up the unsupervised deep learning model known as GAN: discriminator D (discriminator) and generator G (generator). The general process of GAN: G takes noise z as input, generates image $G(z)$, and then the real image x and generated image $G(z)$ are fed as input to D together, and D performs binary classification on x and $G(z)$ to detect if the image is true or false. The output of D is 0 or 1, 0 represents a false image, and 1 represents a real image. The discriminator's goal is to distinguish between true and false samples as much as possible and the

generator's objective is to produce fictitious samples that are indistinguishable by the discriminator.

$$\min G \max DV(G,D) = E_{x\sim P_{\text{data}}} \log D(x) + E_{z\sim P_z}\left(1 - D\left(G(z)\right)\right) \tag{1}$$

In the formula, z refers to the random noise, x refers to the real image, P_{data} refers to the real data distribution, P_z is the uniform noise distribution, $G(z)$ is the generated image, $D(x)$ is the discriminator's identification of the real image, $D\left(G(z)\right)$ is the discrimination of the generated image by the discriminator, and E is the expected value.

On the basis of the original GAN, pix2pix replaces the noise with the conditional information y input generator to realize the process of image-to-image translation. This process is a game problem of inputting binary minimax values with image position masks, and pix2pix generates condition variables that are added to generator G and discriminator D directs the generation of data. The objective function of the pix2pix network is

$$\min G \max DV(G,D) = L_{\text{CGAN}}(G,D) + \lambda L_{L1}(G) \tag{2}$$

$$L_{\text{CGAN}}(G,D) = E_{x\sim P_{\text{data}}} \log D(x) + E_{x\sim P_{\text{data}}, y\sim P_{\text{data}},} \text{loglog}\left(1 - D\left(y(x), G\left(y(x)\right)\right)\right) \tag{3}$$

$$L_{L1}\left(G\right) = E_{x,y}\left(\| x - G\left(y\left(x\right)\right)\|\right) \tag{4}$$

In the formula, λ is a constant term, the input of the pix2pix generator is the condition vector y, and the output is the generated fake sample $G\left(y(x)\right)$. $D(G\left(y(x)\right)$ is the discriminator to the generator to generate fake samples, $D\left(x, y(x)\right)$ is the discriminator's discrimination on the real sample x & the condition variable y.

On the basis of the CGAN loss function, the distance loss is added, the difference is compared pixel by pixel, and the absolute value is taken to reduce the comparison between the generated image and the real image, thereby improving the quality of the generated picture.

6.3 BLOOD CELL DETECTION METHOD BASED ON MCGAN

The structure of MCGAN is shown in Figure 6.1. The network comprises a cell image generator, MD, and a cell classification detector. The cell image generator inputs the cell's position mask and gradient mask, and outputs the generated cell map in the following two forms: (1) take the random number as the center coordinate, specify the radius and color, the randomly generated cell position and gradient mask; and (2) the position and gradient mask extracted from the original cell image. MD input the original cell image and the cell image generated position mask. With the generation of cell image, two-tuples are formed, first through multi-scale convolution operation and second through multi-scale pooling module to obtain global multi-scale features, and lastly the activation function uses the

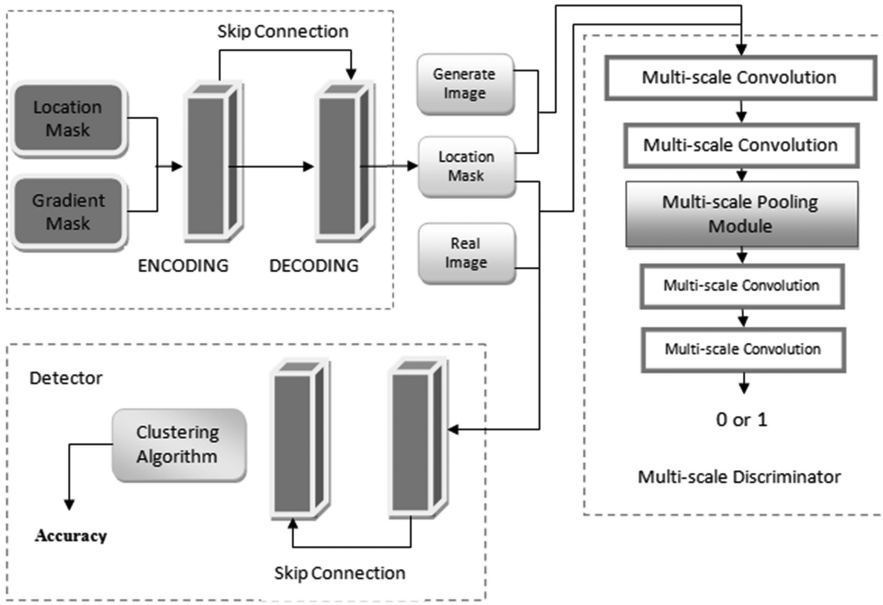

FIGURE 6.1 MCGAN network structure diagram.

Sigmoid function to output the identification result 0 or 1, so as to realize generating true and false identification and position matching identification of cell images; the detector inputs the generated cell image and real cell images, outputs the detected color density map, and then obtains the accuracy of each type of cells through a clustering algorithm, so as to realize the detection of cell images classification detection.

6.3.1 MCGAN Objective Function

For enhancing brightness and edge definition of obtained cell image, a GS loss function is introduced on the basis of the pix2pix objective function. Its output range is $[0, 1.0]$; the closer to 0, the more improved generated image will be. The similarity between the generated image and the real image is evaluated in terms of three aspects: over-brightness, contrast, and gradient structure for ensuring quality image generation. Sobel operator is utilized to acquire actual image gradient and obtained image, including the vertical edge operator and the horizontal edge operator; the gradient magnitude calculation formula is

$$G_x(i,j) = \frac{\partial x(i,j)}{\partial i} + \frac{\partial x(i,j)}{\partial j} \tag{5}$$

The gradient components generated by the horizontal and vertical edge operators are represented by the formula: $\partial x(i,j)/\partial i$, $\partial x(i,j)/\partial j$; here, i, j represent the image's horizontal and vertical directions' pixels, respectively. It is calculated that the GS equals

$$V(x,g)=\left[l(x,g)\right]^{\alpha}\left[c(x,g)\right]^{\beta}\left[e(x,g)\right]^{\gamma} \tag{6}$$

$$l(x,g)=\frac{2u_x+u_g+c_1}{u_x^2+u_g^2+c_1} \tag{7}$$

$$c(x,g)=\frac{2\sigma_x+\sigma_g+c_2}{\sigma_x^2+\sigma_g^2+c_2} \tag{8}$$

$$e(x,g)=\frac{2\sum_j\sum_i G_x(i,j)G_g(i,j)+c_3}{\sum_j\sum_i\left[G_x(i,j)\right]^2+\sum_j\sum_i\left[G_g(i,j)\right]^2+c_3} \tag{9}$$

where u_x, u_g are the average pixel values of the image; σ_x, σ_g are the standard deviation of image pixel values; c_1, c_2, c_3 are constants to avoid a denominator of 0; α, β, γ are constants used to adjust the importance of each component; and $l(x,g)$ is the luminance function of the real image x and the generated image g number; $c(x,g)$ is the contrast function; and $e(x,g)$ is the gradient structure function. The GS loss function is produced by using Eqs. (5)–(9)

$$L_{\mathrm{GS}}(H)=1-\frac{1}{N}\sum_{H=1}^{H}V(H) \tag{10}$$

In the formula, N defines total pixels of an image, and H is the intermediate pixel value. In the cell detection stage, the cross-entropy loss function is utilized as

$$L_{\mathrm{class}}=\frac{1}{W}\sum_i L_i-\sum_{c=1}^{K}y_{ic}\mathrm{loglog}\left(p_{ic}\right) \tag{11}$$

In the formula, W is the minimum training batch; K is the number of categories, value can be either 0 or 1, it is 1 if the category matches the sample category, else, it is 0; and P_{ic} is the probability of the sample which belongs to c category.

In summary, the objective function of the MCGAN network is:

$$\min G\max DV(G,D)=L_{\mathrm{CGAN}}(G,D)+\lambda_1 L_{L1}(G)+\lambda_2 L_{GS}(G)+L_{\mathrm{class}} \tag{12}$$

where λ_1 and λ_2 are constant terms.

6.3.2 MCGAN Generator Structure

The MCGAN generator structure is illustrated in Figure 6.2. It can be observed from Figure 6.2 that the generator comprises of an encoder and a decoder. The generator first inputs the cell position mask and gradient mask, and goes through eight layers of convolution and eight layers of deconvolution. For rectification function (leaky rectified linear units), the gradient is set to 0.2, and batch normalization is

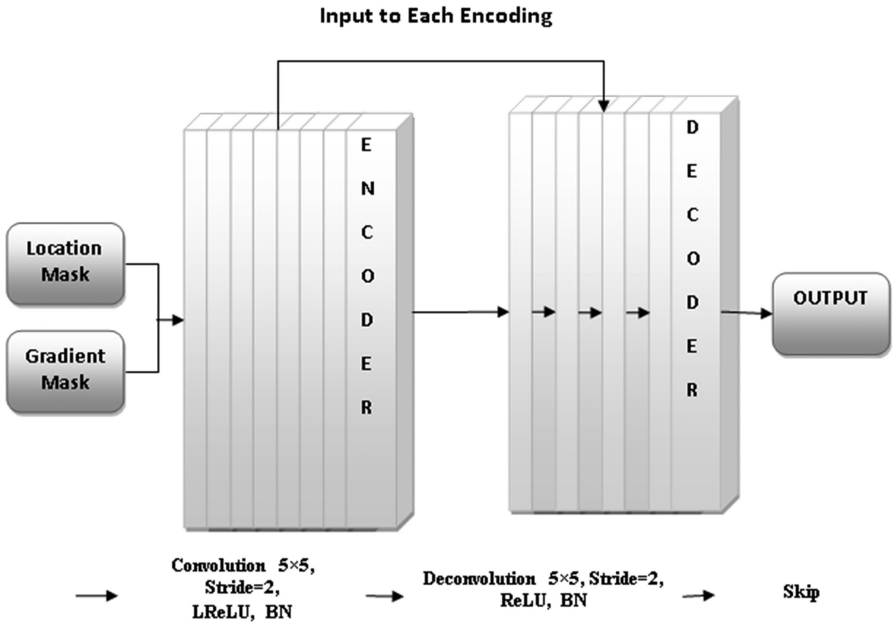

FIGURE 6.2 MCGAN generator block diagram.

used after each layer of convolution to improve the convergence of the network; the activation function of the deconvolution layer adopts linear correction. For rectified linear units, the last layer uses the hyperbolic tangent as the activation function to generate the image, and uses the feature map extracted by the module and the corresponding convolutional layer features in the mirror relationship after each deconvolution. The graph is skip-connected (skip-connect), and the corresponding feature maps are directly superimposed and passed to the next layer, and the features of the deep and shallow layers are fused. The original CGAN inputs two kinds of information: the conditional y and the noise vector z. In this chapter, only conditional information is used in the generator of, so it cannot generate diverse results. During training, this paper randomly drops some parameters (dropout) in the deconvolution output of the first four layers of the generator, which can not only prevent the network from over fitting but also increases the diversity of generated samples to a certain extent.

6.3.3 MCGAN Discriminator Architecture

The MCGAN discriminator is different from the original GAN, which only inputs the generated image and real image. It inputs mask image and cell image generated, and mask image and real cell image together into the discriminator to discriminate between real and fake, so as to ensure the generation of cell images. It is consistent with the information of the input cell location mask. To improve the discriminator's ability to discriminate the detailed information on different scales of the generated

cell samples, this paper makes the following two improvements to the existing CGAN discriminator.

1. The existing convolution operations in the discriminator of the CGAN are all replaced with multi-scale convolution operations (M-conv), as shown in Figure 6.3(a). Convolution kernels (CK) of different scales are utilized to extract features, and these feature maps containing multi-scale information are spliced in a cascaded manner, and then a CK with a size of 1×1 is input for feature mapping to generate a new feature map and input to the next layer.
2. Add a multi-scale pooling structure module (MPS-block) to the discriminator, which is shown in Figure 6.3(b). The specific operation is to pass the feature map of the previous multi-scale convolution operation through four types of pooling operations with different kernel sizes; to maintain the weight of global features, 1×1 convolution is used after each pooling operation to reduce the number of channels at the corresponding level to the original 1/N; splicing the features of different levels in the penultimate dimension and inputting them to the next layer as the global features of the final multi-scale pooling; direct bilinear interpolation upsampling through the low-dimensional feature map to gain a feature map of similar features of actual map.

Most existing discriminators only use smaller or larger receptive fields and learn in one dimension when extracting the original image and generating image features for identification, but in fact, the structural information of the image is often at different scales. However, the feature extraction of a single scale is not enough to completely identify the high-frequency texture regions of the image. To improve the role of the discriminator through convolution and pooling operations at different scales, the features of different scales are fused to improve the discriminator's ability to generate micro image and macroscopic texture. The discriminative ability of geometric features promotes the generator to generate cell samples with more realistic details to improve the accuracy of cell classification detection. The last layer of the discriminator is fully connected, and its output is a true-false binary classification problem, so the activation function adopts the sigmoid function.

6.3.4 MCGAN Classification Detector Architecture

The full convolutional neural network (FCNN) [15] is obtained by switching all the fully connected layers of the convolutional neural network (CNN) [16] with convolutional layers. When the image is classified, it cannot identify the object in a specific part of the picture and can only get the probability that the input image belongs to a certain category, which cannot meet the needs of cell classification detection. In the proposed work, the fully connected layer in CNN is replaced by a convolution layer, and the deconvolution layer is used to perform the feature map extracted by the last convolution layer of the network. Using upsampled feature map sampling, one may do pixel-by-pixel classification while maintaining the spatial information in the original input picture and restore the image to the same scale as the input.

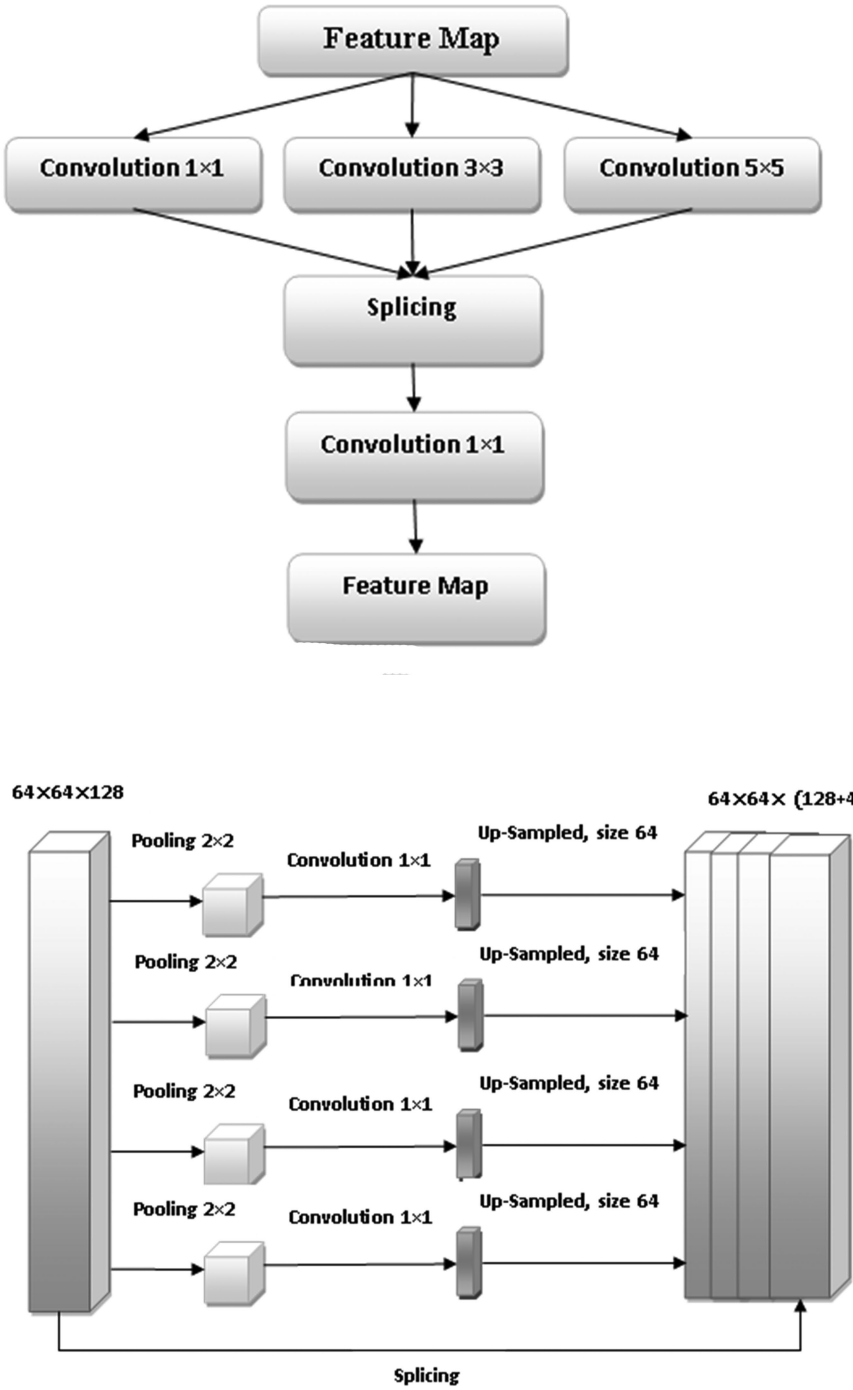

FIGURE 6.3 (a) Multi-scale convolution. (b) Multi-scale pooling module.

For more accurate classification results, a skip FCNN is used after each deconvolution in the fully convolutional network [15] which is obtained by replacing all fully connected layers of CNN [16] with convolutional layers. Since CNN cannot identify objects in specific parts of the image when classifying images, it can only obtain the probability that the input image belongs to a certain class that cannot meet the needs of cell classification and detection.

6.3.5 Clustering Algorithm

The cross-entropy loss is used by the loss function when the detection network trains the cell samples. Preprocessing is done before the calibration map is input into the detection network. The red blood cells and five different types of white blood cells are converted to background values of 0, and the red blood cells are classified as 1, 2, 3, eosinophil, 4 basophil, 5 lymphocyte, and 6 monocytes, for a total of seven different types. The density map obtained from preprocessing is then used to calibrate the network. Once the cell picture is fed into the detection network, the areas containing pixels 1, 2, 3, 4, 5, and 6 are grouped to produce the detection density map. The clustering algorithm is as follows: (1) the principle of proximity: the pixel values are the same and the distance $a = 5$ in this paper; the points within the pixel are classified into the same category; (2) the principle of connectivity: if the pixel value on the connecting line of two points with the same pixel value is higher than 0, then it means that the two pixels are connected, and there is no background in the middle Area. After obtaining the center coordinates of each type of cells in the detection map through the clustering algorithm, find the coordinates in the calibration map, and judge whether the pixel value of the point is consistent with the pixel value of the clustered point in the detection map. If the classification is accurate and inconsistent, then the classification is wrong, so as to obtain the accuracy of each type of cells.

6.4 BLOOD CELL CLASSIFICATION TEST

6.4.1 Experiment Tools

The experiment uses the Linux operating system, TensorFlow 1.13framework, and conducts comparative experiments in a device with a graphics card configured as 4 NVIDIA, 2080Ti-11G, and a memory of DDR4-3000-32G.

6.4.2 Dataset Creation and Preprocessing

The establishment and calibration of the dataset was completed with the Laboratory Department of the Second Affiliated Hospital of Guangxi Medical University. The blood cell analysis samples of 100 patients were randomly selected, and a total of 100 stained glass slides of peripheral blood cells were prepared through operations such as preparation, staining, and pushing, and collected. A total of 4,000 cell images (resolution 256 × 256) were adjusted with an optical microscope under different brightness and angles, and the dataset calibration was completed under the guidance of hospital professionals. Record the position of each cell center in each image

and generate the corresponding position mask; the specific operation process is as follows: mark the red blood cell center position as RGB (255, 255, 255) with a solid circle with a radius of 8 pixels; mark the center positions of the five types of white blood cells with a solid circle with a radius of 15 pixels for neutrophil RGB (0, 255, 255), eosinophil RGB (255, 0, 0), basophil RGB (255, 0, 2 5 5), lymphocyte RGB (0, 2 5 5, 0), and monocyte RGB (255, 255, 0); the position mask is also used as the calibration information of the detection and classification network.

6.4.3 Network Training

Network training is performed in two stages:

1. Cell image generation stage: In this stage, 50% of the 4,000 image samples are used as the dataset, in which the ratio of the training to testing to validating set is 6:2:2, whereas the randomly generated 15,000 position mask and gradient mask images of the experiment are added to the training, validation, and test set, respectively, of the experiment at a ratio of 1:1:1. During training, the generator input cell positions mask and the resolution of gradient mask image is 256×256, and do translation, mirroring, for data enhancement operations such as rotation, every 100 times of training, randomly select batch_ size images from the validation set for validation, save the images generated by validation, and use Adam optimizer for training. The selection strategy for experimental parameter settings is as follows. (1) Randomly discard the coefficient of the parameter which is set to 0.5 by convention. (2) To ensure the diversity of generated cell samples for each validation, the batch size is fixed to 1. (3) The range of the learning rate is generally [0.0001, 0.01]. For smaller batch sizes, to avoid the huge disturbance caused by outliers to the results, a small learning rate should be set, so this paper set it to 0.0001. (4) The setting of the constant term related to the loss function; when extracting the gradient of the original and generated images, it is considered that the importance of each components—brightness, contrast, and gradient—is the same, so α, β, and γ are all fixed as $1, c_1, c_2, c_3$ and $c_1 = 0.01, c_2 = 0.03, c_3 = 0.01$. If the network converges too slowly or if it is too large, the variety of the generated images will be insufficient. For this reason, we take $\lambda_2 = 1, 5, 10, 15$ for comparative experiments. The number of iterations when the generator converges and the generated images are added to the detection network U-Net. Cell images classification detection accuracy is shown in Table 6.1. In this table, I is the number of iterations when the generator converges, P is the classification and detection accuracy of the cell image after the generated image is added to the detection network UNet, and the accuracy may be calculated by dividing the total number of cells by the number of correctly identified cells.

   It can be observed from Table 6.1 that when $\lambda_2 = 10$, the generated image has the greatest improvement in accuracy after adding the detection network, and the convergence speed is faster than $\lambda_2 = 1, 5$ so take $\lambda_2 = 10$; the importance of other loss functions in the experiment is the same, so the coefficients of the remaining loss items are set to $\lambda_2 = 1$, that is, the

TABLE 6.1
Experimental results with respect to λ_2

λ_2	I	P / %
1	100,000	92.4
5	70,000	93.7
10	50,000	94.7
15	40,000	94.1

generator and the discriminator realize the generation of photorealistic cell images in confrontational learning.

2. Cell image detection stage: In this stage, the cell image generated in stage 1 and 50% of the real image are used as training set. The experimental parameter setting selection strategy: the cross-entropy loss function is used as the loss function, and the learning rate is fixed at 0.0001. $K = 7$, which stands for six different cell types and the backdrop; set $W = 5$ to expedite the network training. The images generated by the verification and testing of the cell image generation stage are sent to the detector together with the real images for training, and the remaining real cells are used after the training. The image is tested; the number and center coordinates of various cells are obtained by clustering algorithm; and the accuracy of various cells is obtained by comparing with the calibration map.

6.5 RESULTS AND ANALYSIS

6.5.1 Cell Image Generation Experiment

Visualization of cell image generation results in the network structures of CGAN, pix2pix, pix2pix+MD, and MCGAN were used for comparative experiments. When I = 5,000, 10,000, and 50,000, the images generated by each network are shown in Figure 6.4. From the figure, it is clear that MCGAN can control the type and position of the generated cells by inputting the position mask and gradient mask of the peripheral blood cells, and the shape of the cells is different from the original image, which ensures the authenticity and diversity of the generated cell samples. Compared with CGAN and pix2pix, the loss of the generator and discriminator of pix2pix+MD and MCGAN converge faster, the red blood cells generated by the same number of iterations have more obvious edges in the case of overlapping, and the details of white blood cells are richer. Figure 6.5 displays the loss function curves for the generator and discriminator for each network generation. The loss functions of the generator and discriminator are denoted in the figure by the letters L_G and L_D, respectively. The figure shows that, when CGAN and pix2pix are compared, the generator loss curve of CGAN converges more quickly and has the lowest loss value after convergence, but the discriminator loss value of MCGAN is the highest. In the GAN, the smaller the loss value with respect to generator and the larger the loss value of the

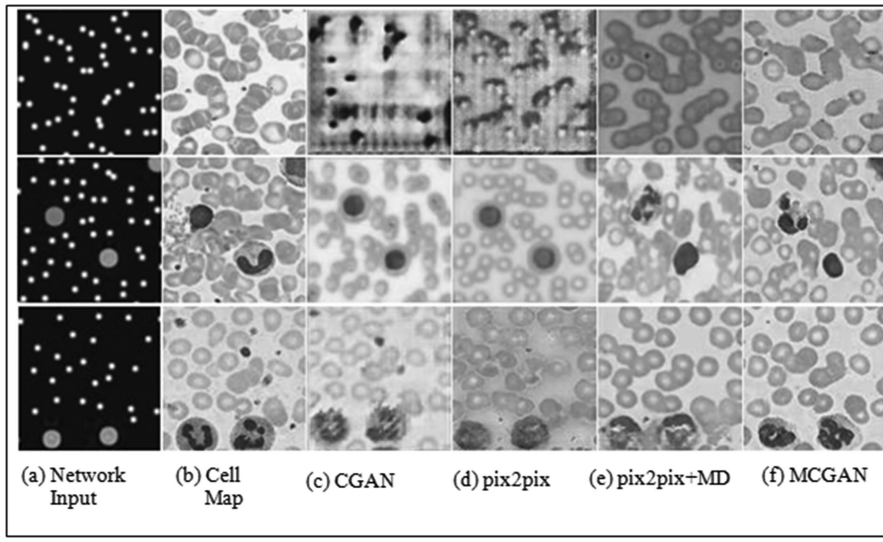

FIGURE 6.4 Cell image generation experiment comparison chart.

discriminator, the better the performance of the network, which proves that MCGAN network has higher performance than that of CGAN and pix2pix.

Create a quantitative evaluation of the image's quality. The feature distance between the real picture and the feature vector of the generated image is measured using the Peak signal-to-noise ratio PSNR [17], Structural Similarity Index (SSIM) [18], and Fréchet inception distance (FID) [19]. The larger the value of PSNR, the higher the authenticity of the generated image, and the calculation formula is

$$R(i,j) = 10\log_{10}\left(\frac{\left(2^n-2\right)^2(HW)}{\sum_{i=1}^{H}\sum_{j=1}^{W}\left(x(i,j)-g(i,j)\right)^2}\right) \tag{13}$$

where n is the number of bits per pixel, and H and W are the height and width of the cell image, respectively.

SSIM can effectively and objectively evaluate the similarity between the real image and the generated image. The evaluation is carried out in terms of three main aspects: brightness, contrast, and structure. The larger the SSIM value, the more similar the two images are; the formula is

$$S(x,g) = \frac{\left(2u_x u_g + c_1\right)\left(2\sigma_{xg} + c_2\right)}{\left(u_x^2 + u_g^2 + c_1\right)\left(\sigma_x^2 + \sigma_g^2 + c_2\right)} \tag{14}$$

In the formula: σ_x^2, σ_g^2 are the variances of x and g, respectively; σ_{xg} refers to the covariance of x and g; and $c_1 = (k_1 L)^2$, $c_2 = (k_2 L)^2$ where L refers to the dynamic range of image pixels $k_1 = 0.01$, $k_2 = 0.03$.

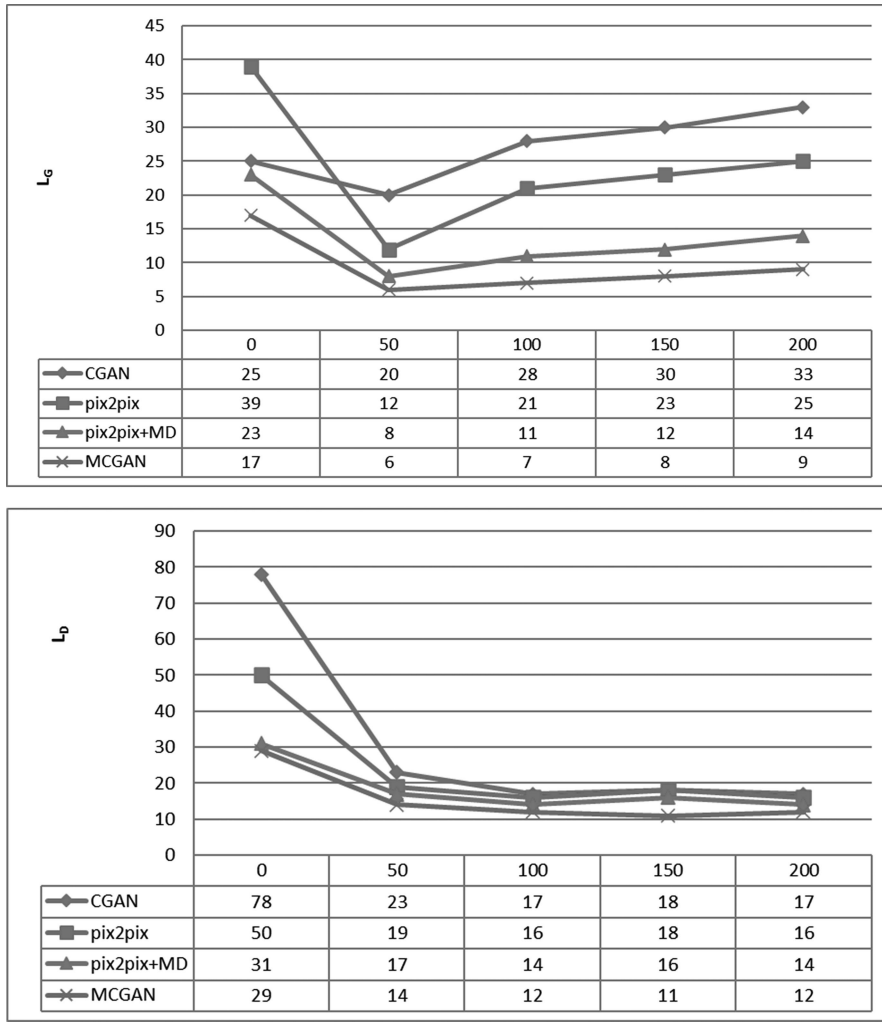

FIGURE 6.5 (a) Builder. (b) Discriminator.

When the generated sample is more similar to the real sample, the smaller the FID is; the formula for calculating the FID is:

$$F(x,g) = \| Z_x - Z_g \|^2 + tr\left(B + O - 2(BO)\right) \tag{15}$$

In this formula, Z_x and Z_g are the mean of the feature vectors of the image x and g, respectively; B and O are the covariance matrix of the real and generated image respectively.

The same learning rate, number of iterations, number of channels, and so on are set in the experiment. When I = 50,000, the PNSR, SSIM, and FID indicators of cell images generated by different network structure models are calculated. The results

TABLE 6.2
PNSR, SSIM, and FID comparison

Model	*R* / *dB*	*S*	*F*
CGAN	13.65	0.58	84.15
Pix2pix	18.43	0.71	54.39
Pix2pix+MD	22.85	0.85	37.36
MCGAN	23.7	0.89	34.47

are depicted in Table 6.2. From the table it is clear that the PNSR value of MCGAN is increased by 5.27 dB, the SSIM value is increased by 0.18, and the FID value is decreased by 19.88 (adding a multi-scale discriminator increases PNSR by 4.42 dB, SSIM by 0.14, and FID by 19.88). It is reduced by 17.03; after adding the GS loss function on this basis, PNSR is increased by 0.85 dB, SSIM is increased by 0.04, and FID is decreased by 2.85. It can be seen that compared with the other three models, the details of the generated images by MCGAN are more realistic, which is more similar to the real image.

6.5.2 Cell Image Classification Detection Experiment

6.5.2.1 Visual Classification and Detection Results

The different network structure models SSD, FCRN, YOLOV3, Res-Net, U-Net, UNet+pix2pix, U-Net+pix2pix+MD (the discriminator structure is added to multi-scale convolution and pooling structure), and MCGAN are compared, the test set is selected from 50% of real peripheral blood cell samples and tested with different models after training. The test results are depicted in Figure 6.6. In (b) and (c), the radius is five pixels. The dots mark the missed cells on the output rectangular box detection result graph; in (e), (f), (g), (h), (i), and (j), the missed cells are marked with oval boxes. Mark on the output density map; mark the falsely detected cells on the output density map with a rectangular box.

It can be seen from Figure 6.6 that without adding the generated image training, 15 SSDs detected by the candidate frame method are missed, 11 are missed by YOLOV3, 8 are missed by the FCRN detected by the density map method, 1 is falsely detected, and Res-Net misses 7 and 1, UNET misses 6 and 1. In the case of adding generated image training, U-Net+pix2pix misses 5, the generator and detector use U-Net, and after adding the multi-scale convolution and pooling structure to the discriminator, 2 missed detections are added. On this basis, the GS loss function is added, and MCGAN has no missed detection. It can be obtained that multi-scale is added to the CGAN. The discriminator and gradient loss function can efficiently enhance the detection accuracy of cell images.

6.5.2.2 Comparison of Different Network Detection Accuracy

The cell classification detection results are shown in Table 6.3. In the table, T is the total number of cells. The authors study the count of each type of cells in blood cells, so two new evaluation indicators are introduced: the number of missed detections

TABLE 6.3
Detection results comparison

Model	*P* / %	*T*	*M*	*e*
SSD	82.7	84,202	11,883	1,254
YOLOV3	86.5	84,202	10,367	824
FCRN	89.3	84,202	8,910	314
Res-Net	89.7	84,202	8,573	291
U-Net	90.4	84,202	7,903	236
U-Net + pix2pix	92.7	84,202	6,138	172
U-Net + pix2pix + MD	94.1	84,202	5,115	121
MCGAN	94.7	84,202	4,624	76

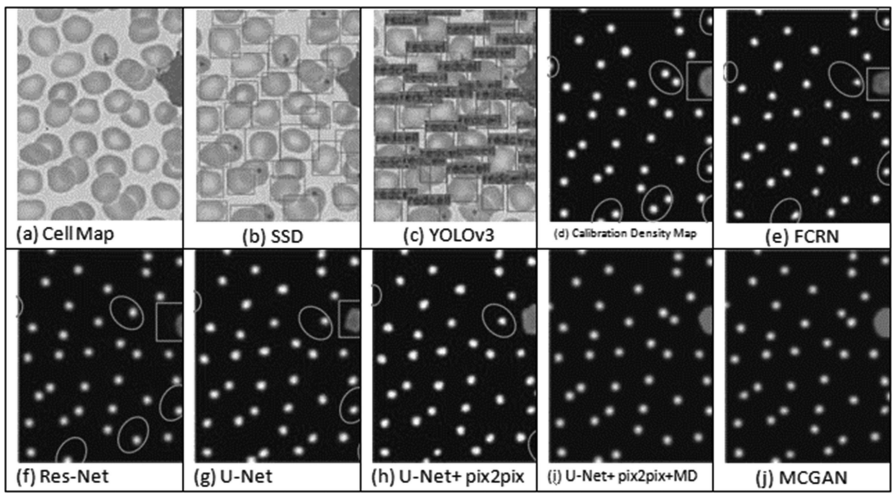

FIGURE 6.6 Comparison chart of cell classification test results.

M and the number of falsely detected; the calibration method is used to train cell images, and the detection accuracy obtained is generally lower than that of using the density map [20]. Combined with the network detection output maps in Figure 6.6, it can be seen that using the density map may effectively enhance the detection in the case of cell adhesion and occlusion and at the image boundary [21].

At the same time, in the case of using the density map to determine, the U-Net network has the best effect in cell detection compared with FCRN and Res-Net, because the skip connection is used after each deconvolution in U-Net, which combines deep and shallow features of images [22]. When adding MCGAN to U-Net to generate cell image database training, the accuracy of cells is significantly improved. Compared with only real database (RD) training, the accuracy rate is increased from 90.3% to 94.7% (among which after adding the multi-scale discriminator, the accuracy is increased to 94.1%, and on this basis, the GS loss function is added to enhance the accuracy to 94.7%).

TABLE 6.4
Comparison of test results of various types of cells in U-Net network under different database training

Training set	P_1	P_2	P_3	P_4	P_5	P_6
RD	90.48	91.28	88.58	87.58	90.88	90.48
RD + CGAN	90.98	91.68	90.68	88.68	91.88	90.98
RD + pix2pix	92.18	93.08	91.68	89.88	93.48	92.18
RD + pix2pix + MD	94.08	96.88	95.48	95.48	96.68	94.08
RD + MCGAN	94.68	99.08	98.88	98.88	98.88	94.68

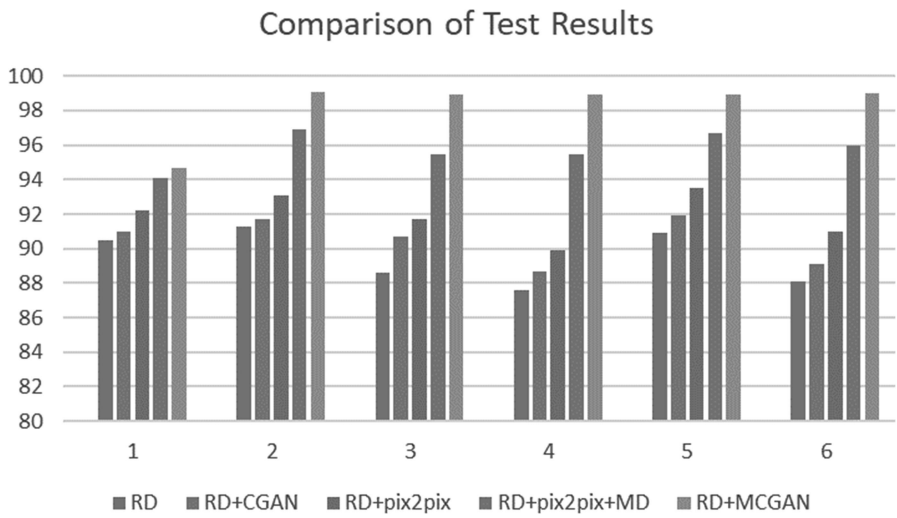

FIGURE 6.7 Comparison of test results of various types of cells in U-Net network under different database training.

Since there are few leukocyte samples in the real data, to highlight the change in accuracy after adding leukocyte samples during training in the U-Net network, red blood cells and other five types of leukocytes are added to different GAN-generated cell samples for training. The accuracy of each type of cell is compared. RD is a real cell image dataset; RD+pix2pix, RD+pix2pix+MD, RD+CGAN, and RD+MCGAN are the cell images and the real image combination dataset, and the results are shown in Table 6.4 and Figure 6.7. In the table, P1, P2, P3, P4, P5, and P6 are red blood cells, neutrophils, eosinophils, basophils, and lymphocytes, respectively, and their accuracy of classification and detection of monocytes is shown. It can be observed from the table that adding images generated by different GAN networks to U-Net improves the detection accuracy, which proves that the use of GANs to increase the detection network training set and to improve the accuracy of cell classification and detection method is feasible [23]. The samples generated by the MCGAN network

have the best effect on improving the accuracy of cell detection, because the lack of loss items in the loss function of the CGAN network and the lack of the discriminator structure in the pix2pix network are solved in the MCGAN network structure to discriminate the multi-scale information of the image.

In the MCGAN experiment, the most significant improvement in accuracy is eosinophils, basophils, and monocytes. In the case of only real image database RD training, the test accuracy is 88.6%, 87.6%, and 88.1%; after adding MCGAN during training to generate cell images, the accuracy increased to 98.9%, 98.9, and 99.0%, respectively (among which the accuracy increased by 8.3, 7.9, and 7.9 units after adding the multi-scale discriminator, respectively, and the accuracy of the GS loss function is increased by 2.0, 3.4, and 3.0 units, respectively), which proves that MCGAN is effective in generating cell samples.

6.6 CONCLUSION

By studying the influence of the generated blood cell image quality on the blood cell detection accuracy, a blood cell classification detection method based on MCGAN is proposed. The proposed method is applied to the blood cell image generation experiment, and the generated blood cell image is included in the categorization detection network's training set. Compared with the image generation and detection methods, the major merits of applied model are: (1) in the blood cell image generation stage, the blood cell images generated by the proposed algorithm are superior to the existing CGAN algorithms in terms of vision and evaluation indicators; (2) in the blood cell image generation stage in terms of classification detection model, it is obtained through the comparison experiment with the current mainstream SSD, YOLOV3, FCRN, Res-Net, and U-Net detection network models, which increases the details and diversity of the generated cell samples, and the classification and detection accuracy of cells is significantly improved. In the future research work, the following two aspects can be improved to reduce the rate of missed detection and false detection of cells: (1) since the missed and falsely detected cells are mainly concentrated in the case of severe cell adhesion, consider increasing the adhesion. (2) Optimize the structure of the cell detection network, enhance the depth and refine the detection accuracy of the detection network in the case of cell adhesion.

REFERENCES

1. Zhang, Y., Lu, Y., Chen, W., Chang, Y., Gu, H., & Yu, B. (2021). MSMANet: A multi-scale mesh aggregation network for brain tumor segmentation. In *Applied Soft Computing* (Vol. 110, p. 107733). Elsevier BV. https://doi.org/10.1016/j.asoc.2021.107733
2. Bhavani, T., VamseeKrishna, P., Chakraborty, C., & Dwivedi, P. (2022). Stress classification and vital signs forecasting for IoT-health monitoring. In *IEEE/ACM Transactions on Computational Biology and Bioinformatics* (pp. 1–8). Institute of Electrical and Electronics Engineers (IEEE). IEEE/ACM. https://doi.org/10.1109/tcbb.2022.3196151
3. Praveen, N., Punn, N. S., Sonbhadra, S. K., Agarwal, S., Syafrullah, M., & Adiyarta, K. (2021). White blood cell subtype detection and classification. In *2021 8th International Conference on Electrical Engineering, Computer Science and Informatics (EECSI)*, pp. 203–207. https://doi.org/10.23919/EECSI53397.2021.9624268

4. Acharya, V., Ravi, V., Pham, T. D., & Chakraborty, C. (2023). Peripheral blood smear analysis using automated computer-aided diagnosis system to identify acute myeloid Leukemia. *IEEE Transactions on Engineering Management*, vol. 70, issue 8, pp. 2760–2773. IEEE. https://doi.org/10.1109/tem.2021.3103549
5. Elhassan, T. A. M., Rahim, M. S. M., Swee, T. T., Hashim, S. Z. M., & Aljurf, M. (2022). Feature extraction of white blood cells using CMYK-Moment localization and deep learning in acute Myeloid Leukemia blood smear microscopic images. *IEEE Access*, vol. 10, pp. 16577–16591. https://doi.org/110.1109/ACCESS.2022.3149637
6. P. K. Maduri, Shalu, S. Agrawal, A. Rai and S. Chaubey. (2021). Malaria detection using image processing and machine learning. In *2021 3rd International Conference on Advances in Computing, Communication Control and Networking (ICAC3N)*, pp. 1789–1792. https://doi.org/10.1109/ICAC3N53548.2021.9725557
7. Xu, X., Wang, C., Guo, J., Gan, Y., Wang, J., Bai, H., Zhang, L., Li, W., & Yi, Z. (2020). MSCS-DeepLN: Evaluating lung nodule malignancy using multi-scale cost-sensitive neural networks. In *Medical Image Analysis* (Vol. 65, p. 101772). Elsevier BV. https://doi.org/10.1016/j.media.2020.101772
8. Dwivedi, P., Sarkar, A. K., Chakraborty, C., Singha, M., & Rojwal, V. (2021). Application of artificial intelligence on post pandemic situation and lesson learn for future prospects. *Journal of Experimental & Theoretical Artificial Intelligence,* vol. 35, issue 3, pp. 327–344. https://doi.org/10.1080/0952813x.2021.1958063
9. Yasmin, S., Pathan, R. K., Biswas, M., Khandaker, M. U., & Faruque, M. R. I. (2020). Development of a robust multi-scale featured local binary pattern for improved facial expression recognition. *Sensors,* vol. 20, issue 18, p. 5391. https://doi.org/10.3390/s20185391
10. Soto-Ayala, L. C., & Cantoral-Ceballos, J. A. (December 2021) Automatic blood-cell classification via convolutional neural networks and transfer learning. *IEEE Latin America Transactions*, vol. 19, issue 12, pp. 2028–2036. https://doi.org/10.1109/TLA.2021.9480144
11. Tran, S.-T., Cheng, C.-H., Nguyen, T.-T., Le, M.-H., & Liu, D.-G. (2021). TMD-Unet: Triple-Unet with multi-scale input features and dense skip connection for medical image segmentation. *Healthcare,* vol. 9, issue 1, p. 54. https://doi.org/10.3390/healthcare9010054
12. Chakraborty, C., Nagarajan, S. M., Devarajan, G. G., Ramana, T. V., & Mohanty, R. (2023). Intelligent AI-based healthcare cyber security system using multi-source transfer learning method. *ACM Transactions on Sensor Networks.* https://doi.org/10.1145/3597210
13. Ma, L., Shuai, R., Ran, X., Liu, W., & Ye, C. (2020). Combining DC-GAN with ResNet for blood cell image classification. *Medical & Biological Engineering & Computing,* vol. 58, Issue 6, pp. 1251–1264. https://doi.org/10.1007/s11517-020-02163-3
14. Yang, F. et al. (May 2020). Deep learning for smartphone-based malaria parasite detection in thick blood smears. *IEEE Journal of Biomedical and Health Informatics*, vol. 24, issue 5, pp. 1427–1438. https://doi.org/10.1109/JBHI.2019.2939121
15. Liu, J., Guo, F., Gao, H., Huang, Z., Zhang, Y., & Zhou, H. (2021). Image classification method on class imbalance datasets using multi-scale CNN and two-stage transfer learning. *Neural Computing and Applications,* vol. 33, issue 21, pp. 14179–14197. https://doi.org/10.1007/s00521-021-06066-8
16. Chaudhury, S., Sau, K., Khan, M. A., & Shabaz, M. (2023). Deep transfer learning for IDC breast cancer detection using fast AI technique and sqeezenet architecture. *Mathematical Biosciences and Engineering*, vol. 20, issue 6, pp. 10404–10427. https://doi.org/10.3934/mbe.2023457
17. Gräbel, P., et al. (2021). Surrounding cell suppression for unsupervised representation Learning in hematological cell classification. In *2021 IEEE 18th International Symposium on Biomedical Imaging (ISBI)*, pp. 526–530. https://doi.org/10.1109/ISBI48211.2021.9433913.

18. Kishor, A., Chakraborty, C., & Jeberson, W. (2021). Reinforcement learning for medical information processing over heterogeneous networks. In *Multimedia Tools and Applications*. *Springer Science and Business Media LLC*. pp. 23983–24004. https://doi.org/10.1007/s11042-021-10840-0
19. Aziz, S., Bilal, M., Khan, M. U., & Amjad, F. (2020). Deep learning-based automatic morphological classification of leukocytes using blood smears. In *2020 International Conference on Electrical, Communication, and Computer Engineering (ICECCE)*, pp. 1–5. https://doi.org/10.1109/ICECCE49384.2020.9179246.
20. Gupta, S., Gupta, M. K., Shabaz, M., & Sharma, A. (2022). Deep learning techniques for cancer classification using microarray gene expression data. *Frontiers in Physiology,* vol. 13. https://doi.org/10.3389/fphys.2022.952709
21. Akil, H., Gordon, J., Hen, R., Javitch, J., Mayberg, H., McEwen, B., Meaney, M. J., & Nestler, E. J. (2018). Treatment resistant depression: A multi-scale, systems biology approach. *Neuroscience & Biobehavioral Reviews,* vol. 84, pp. 272–288. https://doi.org/10.1016/j.neubiorev.2017.08.019
22. Kumar, D., et al. (2020). Automatic detection of white blood cancer from bone Marrow microscopic images using convolutional neural networks. *IEEE Access*, vol. 8, pp. 142521–142531. https://doi.org/10.1109/ACCESS.2020.3012292.
23. Shabaz, M., & Soni, M. (2023). Cognitive digital modelling for hyperspectral image classification using transfer learning model. *Turkish Journal of Electrical Engineering and Computer Sciences*, vol. 31, issue 6, pp. 1039–1060. https://doi.org/10.55730/1300-0632.4033

7 Impact of Channel Thickness on the MoS_2 FET Performance Metrics and Their Application in Biosensing

Sharmila B, Agraj Khare, Monoj Kumar Singha and Priyanka Dwivedi

7.1 INTRODUCTION

The extensive research on two-dimensional (2D) materials is a clear marker of their increased significance and popularity. These 2D materials are found to be the potential candidates for next-generation complementary metal oxide semiconductor (CMOS)-based electronic devices. The introduction of 2D materials in various paradigms has opened doors to exploring a variety of applications, one of which is the design of field-effect transistors (FETs). The FET devices themselves have lucrative properties, such as greater sensitivity, detection capabilities, and batch processing, upon pairing them with materials like MoS_2, WSe_2, WS_2, WO_3, MoO_3, and so on. The FETs tend to possess even more attractive properties (such as high mobility, thermal stability, etc.) which make them ideal for high-sensitivity usage and sensing applications [1–5]. The existing literature suggests that the FET-based sensors are an ideal choice considering the improved dynamic range of operation and much more idealistic electrical properties. FET-based sensors do not follow the same design metrics and methods as a conventional FET device. Structural changes can be observed along with the inclusion of different 2D materials (MoS_2). One of the most significant structural changes is the gate position on these devices; back-gated FET devices prove to be more efficient in terms of space management and sensing area exposure [6,7]. The structural changes along with the inclusion of 2D materials such as MoS_2 have displayed positive changes in terms of scaling, making it possible to scale these devices to submicron range. Considering the material of interest in presented research work—MoS_2, it offers a unique Young's modulus of 0.33 ± 0.07 TPa [8] along with properties like tunable bandgap [9], ambipolar nature [10], and sub-nano range scalability [11], thereby making it an ideal choice for numerous nano-electronic applications [12].

DOI: 10.1201/9781003602729-7

The publicly available literature on the numerous studies of MoS_2-based FETs is a cornerstone for further investigation. The available literature emphasizes the attractive electrical properties of the MoS_2 devices but does not provide substantial evidence on the thickness dependencies even though few studies are available on multilayer MoS_2-based devices [13]. A more in-depth comparative study of monolayer MoS_2-based FET has not been presented. Few references furnish evidence on thickness dependencies and design considerations for these special FETs which in turn help in establishing numerical procedures for deducing electrical properties [14]. The results furnished in the previous studies offer a comparative study between the different thicknesses of MoS_2 in the FETs and how this change in thickness influences the electrical properties of the devices. These research findings will highlight the major differences in the operational tendencies of FET devices with monolayer MoS_2 models with varied thicknesses even though the MoS_2 FETs present to be a good candidate for sensing applications and their functionalities can be further optimized by deducing the ideal thicknesses of the active sensing layer.

The primary purpose of this chapter is to identify the viability of monolayer MoS_2 FET devices based on their MoS_2-layer thickness (0.3 nm, 0.5 nm, 0.7 nm, 1 nm, and 1.5 nm). This research work will be targeting the simulation of these devices to extract their electrical response trends and operational characteristics. These trends will in turn be a basis to comment upon the dynamic range of operation. Conclusions in regard to the sensitivity of these devices will also be drawn through the simulation results. The simulation will not only highlight the conventional transfer characteristics but also help in identifying the optimum potentials of operation like voltages at which the devices perform with utmost efficiency. The focus would be on understanding the changes in response to the changing thickness and doping concentrations, and the effect it has on the transfer characteristics of the devices. This chapter would in turn comment upon which device variant is best suited for various sensing applications. All simulations are performed using the COMSOL Multiphysics 5.6 environment at standard conditions.

7.2 THICKNESS-DEPENDENT FET DEVICES AND SIMULATION MODEL

This section presents the details related to the geometry, material, and mesh used during the simulation. The simulation was carried out using COMSOL Multiphysics 5.6 software at ambient room temperature. Geometry allocation, material definition, and meshing process are the initial steps in the device simulation. Figure 7.1 represents the dimension of MoS_2-based FET devices. The simulation was performed by varying the MoS_2-layer thickness. The details related to the MoS_2-layer thickness with respect to their device ID and study performed through simulation are presented in Table 7.1. Material selection is done by assigning the particular material for their respective blocks. Silicon is used as the substrate material, SiO_2 acts as the oxide layer, MoS_2 material as the channel layer, and gold used as a contact material. The next step is related to the meshing of the geometry. Meshing is an essential task to fine-tune the structure and reduction of memory needs for the simulation.

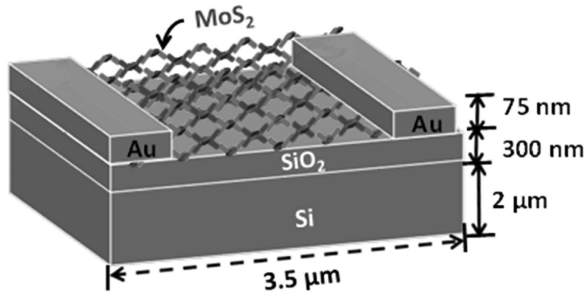

FIGURE 7.1 Schematic of FET device simulated in COMSOL platform.

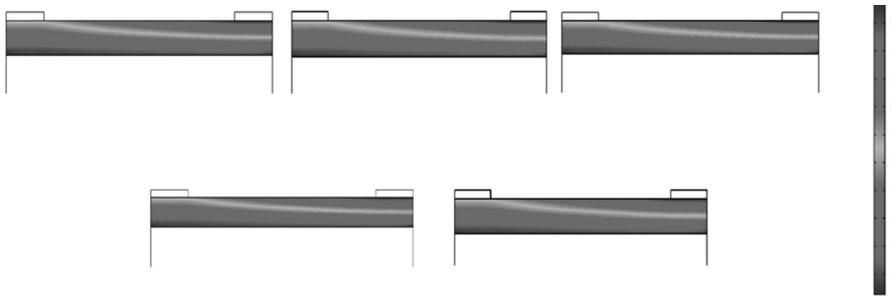

FIGURE 7.2 2D representation of electric potential on different FETs.

TABLE 7.1
Model devices and parameters

S/No	Device labels	MoS_2 thickness	Input–output characteristics		Transfer characteristics
			N_d ($10^{18} \times cm^{-3}$) = 0.5, 1, 2, 3, 4	V_g (V) = 0.1, 0.5, 1, 1.5, 3, 5	V_d (V) = 0.1, 1, 5, 10
1	FET 1	0.3 nm	✓	✓	✓
2	FET 2	0.5 nm	✓	✓	✓
3	FET 3	0.7 nm	✓	✓	✓
4	FET 4	1.0 nm	✓	✓	✓
5	FET 5	1.5 nm	✓	✓	✓

Free triangular meshing is used to mesh the very thin layer. For designing FET in COMSOL semiconductor physics is used. After the successful design the FET, the electrical characteristics were tested by stationary study. The electrical characterization of each FET model was obtained by the application of back-gate voltage. The drift-diffusion model, trap-assisted recombination model, and Poisson equation are used to characterize the electrical property in the simulations. Figure 7.2 depicts electric potential profiles for different FETs. This profile was obtained by varying

the gate voltage at a fixed drain voltage. The aforementioned profile gives information about the potential distribution in the FETs. The dark blue color indicates a low-potential region, whereas the maroon color represents a high-potential region.

7.3 EFFECT OF THICKNESS ON DEVICE PERFORMANCE

This study furnishes results for five different variants of MoS_2-based FET, with thicknesses of 0.3 nm, 0.5 nm, 0.7 nm, 1 nm, and 1.5 nm. Three aspects of electrical operation have been covered in the results for all variants, with input and output characteristics (I_d versus V_d), transfer characteristics (I_d versus V_g), and I_d versus V_d curve for different donor concentrations. Each resultant graph has been presented with varied sweeps to give a comprehensive comparison on the operational abilities of each variant with respect to device performance. Figure 7.3 shows the transfer characteristics of all simulated devices. The I_d–V_g characteristic plots were obtained by varying the gate voltage with the fixed drain voltages (0.1 V, 1 V, 5 V, and 10 V). Focusing on the I_d–V_g characteristic plots for the FET 1 (Figure 7.3(a)), FET 2 (Figure 7.3(b)), and FET 3 (Figure 7.3(c)) variants, we can see a linear region of operation for voltages up to 10 V, with the order of the drain current increasing subsequently with the increasing thickness and hence, the increasing mobility (thickness-dependent mobility). The unconventional operation is evident in the variants with thickness FET 4 (Figure 7.3(d)) and FET 5 (Figure 7.3(e)) where the current experiences an exponential change when the gate voltage reaches 10 V. Such drastic variation in the current order makes the variants favorable for use in wider dynamic range applications (e.g., sensors, detectors, etc.).

Figure 7.4 shows the input and output characteristics (I_d–V_d) of all simulated devices (FET 1–FET 5). The I_d–V_d characteristic plots were obtained by varying the drain voltage for fixed drain voltages. The I_d–V_d curves offer insights into the saturation operation regions of these devices; each variant appears to have marginal order changes in current due to an increase of thickness in small steps (Figures 7.4(a)–7.4(e). Although the saturation region of operation begins at very high voltages, it enables the devices to display current magnitude change for a wider range of voltages. Detection of potential change in small steps is vital for sensing applications, and the devices not only have optimum performance with positive gate potentials but also offer a broad dynamic range with high-order current at negative gate potentials, thus offering high sensitivity to potential changes. The change in the order of current with variations in the doping concentrations is in complete agreement with the FET's general physics. Doping is one of the important strategies to tune the electronic state of the device. It improves the device's performance [15]. To analyze the effect of doping on different FETs, the donor concentration of the channel layer is varied and presented in Figures 7.5(a)–7.5(e). It was elucidated that the FET 5 with 1.5 nm thickness shows the improved response for all N_d values as compared to the other simulated FET devices.

Furthermore, the On/Off ratios and threshold voltage were calculated for all the variants presented in Table 7.2. Figures 7.6(a) and 7.6(b) represent the I_d–V_g characteristics comparison of all the tested devices for threshold voltage and On/Off ratio calculation. It is well known from the literature, the thickness plays a vital role

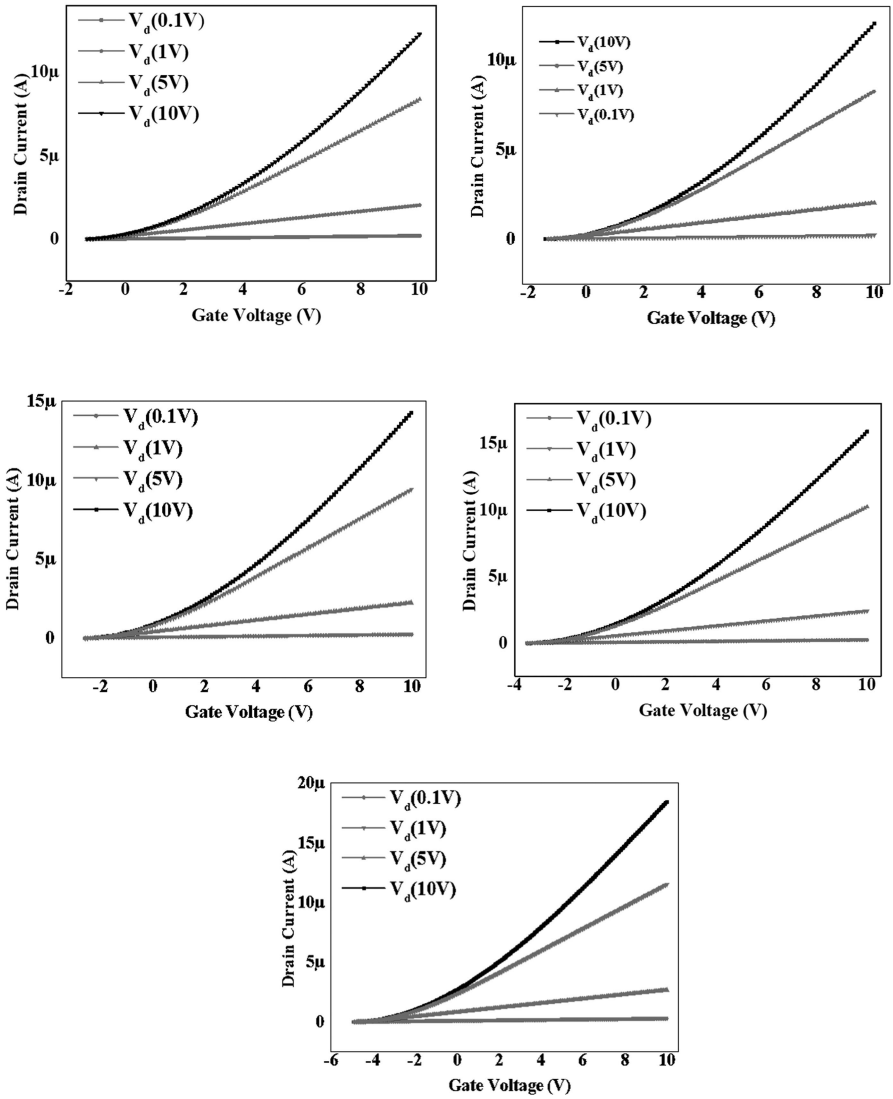

FIGURE 7.3 Transfer characteristics: (a) FET 1, (b) FET 2, (c) FET 3, (d) FET 4, and (e) FET 5.

for the overall device performance. As the thickness increases, the bandgap of the MoS_2 tends to decrease and saturates to the bulk MoS_2 bandgap. With this reducing bandgap, the tendency of thermally generated electrons jumping to the conduction band increases drastically, thereby contributing to a higher magnitude of leakage current. The thickness of the devices implicates the threshold voltage. FET 5 gives the lowest threshold voltage of the other nanometer devices. From the above analysis it can be concluded that FET 5 is preferable for low-power applications owing to its

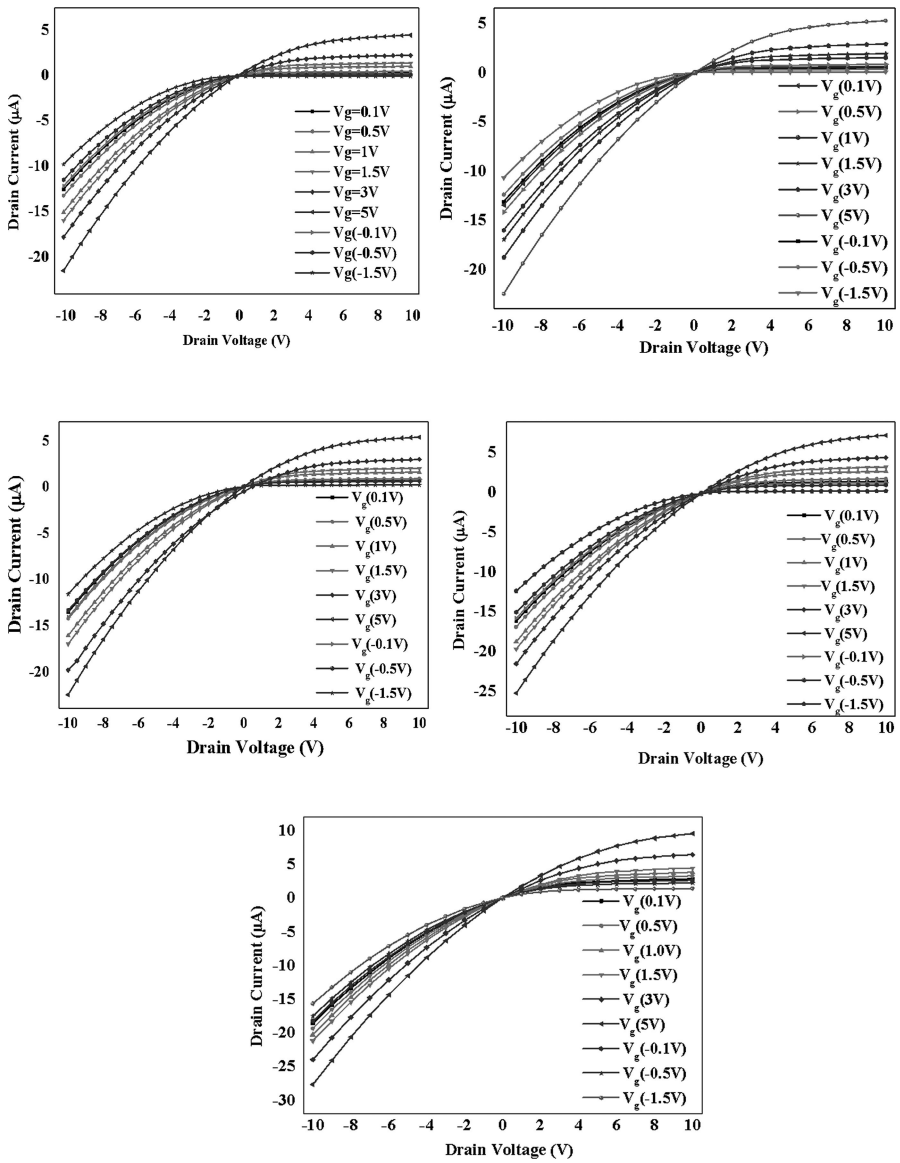

FIGURE 7.4 I_d–V_d characteristics: (a) FET 1, (b) FET 2, (c) FET 3, (d) FET 4, and (e) FET 5.

low threshold voltage. For switching applications, a high On/Off ratio is the predominant characteristic. Here FET 5 offers On/Off ratio in the order of 10^5 which is shown in Figure 7.6(b) (Table 7.2). This chapter elucidates that 1.5 nm is the optimum thickness for the FET. Figure 7.7 depicts the variation threshold voltage and On/Off ratio with respect to the thickness. Both parameters were obtained from the transfer

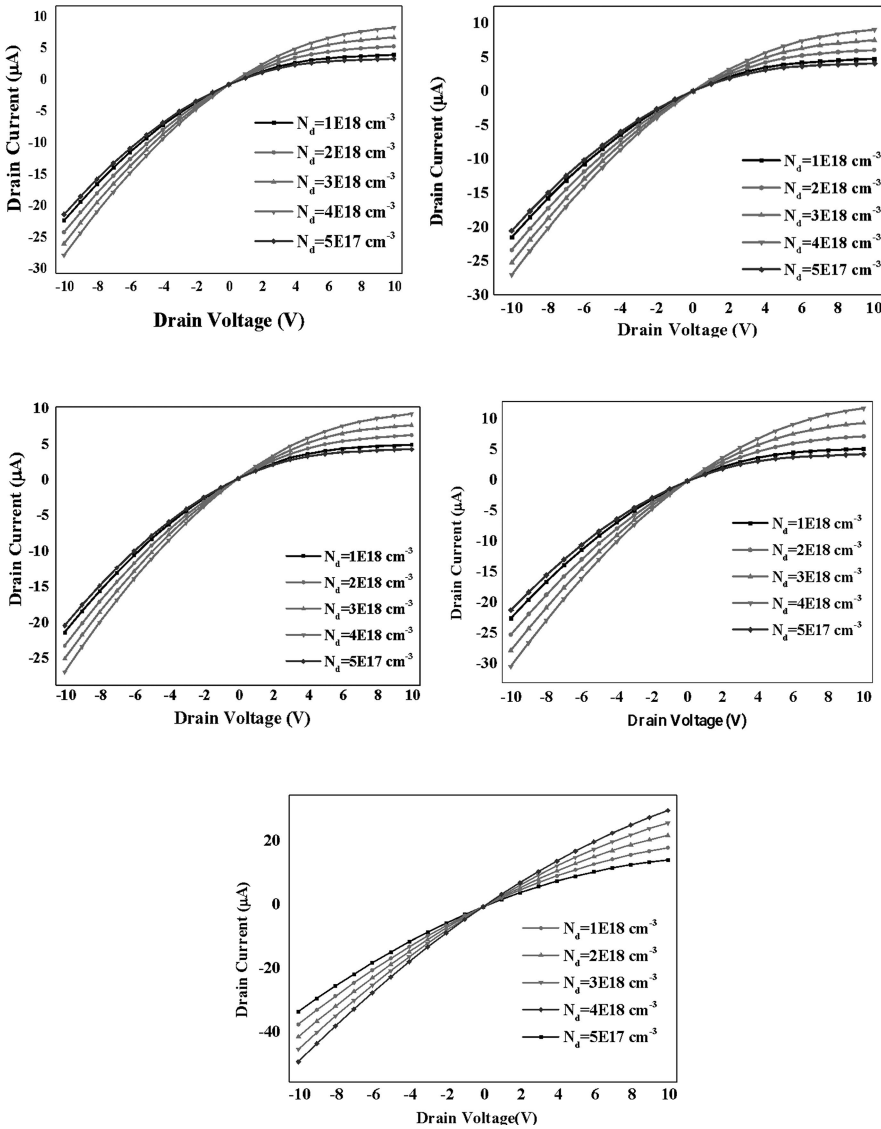

FIGURE 7.5 I_d–V_d characteristics for different N_d: (a) FET 1, (b) FET 2, (c) FET 3, (d) FET 4, and (e) FET 5.

characteristics of the FETs. These parameters (threshold voltage and On/Off ratio) are functions of gate voltage. Figure 7.7 concludes the fact that a lower-gate-voltage device offers a higher On/Off ratio. From the simulation result, it was observed that the FET 5 offers a low threshold and high On/Off ratio. This type of device opens endeavors to different applications such as biomedical switching, low-power devices, switches, and so on.

TABLE 7.2
On/Off ratio calculation

	On/Off ratio			
Thickness	**Drain voltage**			
	0.1 V	1 V	5 V	10 V
0.3 nm	0.46×10^2	0.20×10^3	0.68×10^3	1.00×10^3
0.5 nm	1.00×10^2	0.54×10^3	0.86×10^3	1.92×10^3
0.7 nm	1.53×10^2	0.88×10^3	2.61×10^3	0.42×10^4
1 nm	0.27×10^3	1.8×10^3	0.66×10^4	0.93×10^4
1.5 nm	0.29×10^3	1.85×10^3	0.67×10^4	0.22×10^5

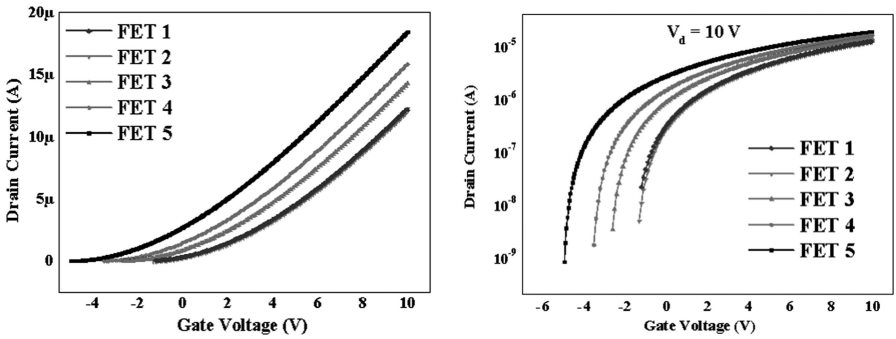

FIGURE 7.6 (a) Threshold voltage for FET 1–FET 5 and (b) On/Off ratio for FET 1–FET 5.

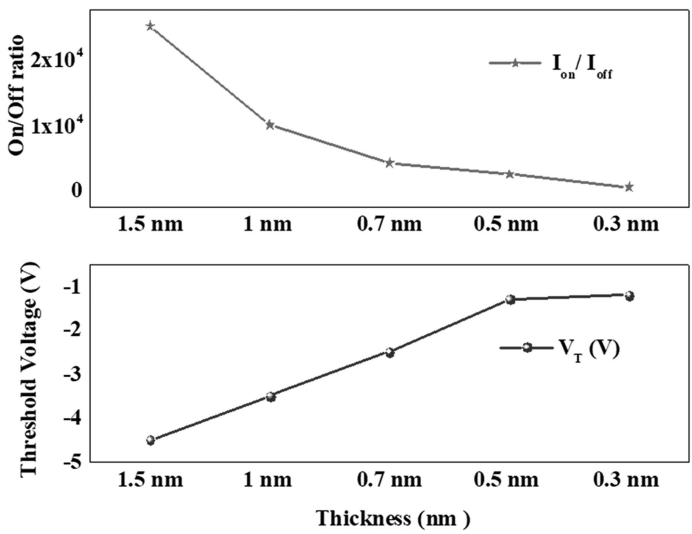

FIGURE 7.7 Relation between thickness versus threshold voltage and On/Off ratio.

7.4 BIOSENSING TEST FOR THE FET-BASED SENSOR

Diabetes is a chronic metabolic disease that occurs due to changes in the blood glucose level. After glucose consumption, a healthy patient's blood glucose level is usually in the range of 4.9–6.9 mM, whereas it rises up to 40 mM in patients with diabetes. It leads to significant damage to the heart, eyes, kidneys, and brain system. According to a report by the World Health Organization, globally 422 million people are affected and 1.6 million deaths occur every year [16–19]. Therefore, the early detection of diabetes is important. The optimized 1.5 nm FET is used to detect the glucose biomarker. The MoS_2 layer of the FET acts as a sensing layer used to detect glucose. To perform this biosensor simulation in COMSOL Multiphysics, electrolysis physics was used. It was observed that, the variation glucose concentration make the changes in the conductivity of the sensing layer. These changes result in a variation in electric current, as depicted in Figures 7.8(a) and 7.8(b). The input–output characteristics (Figure 7.8(a)) and transfer characteristics (Figure 7.8(b)) were observed for the fixed gate ($V_g = 5$ V) and drain ($V_d = 5$ V) voltage, respectively. The concentration of glucose varied from 1 mM to 30 mM for each gate and drain potential, and the corresponding

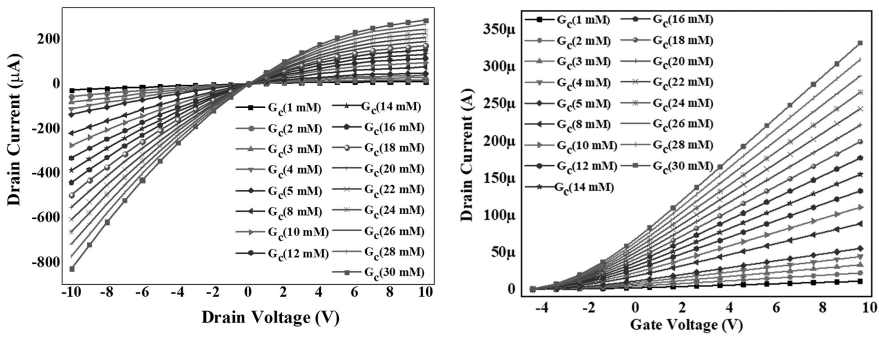

FIGURE 7.8 Concentration of glucose variation plot: (a) input–output characteristics and (b) transfer characteristics.

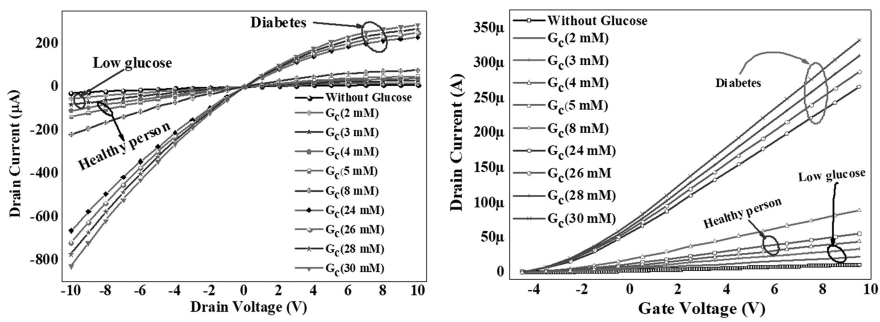

FIGURE 7.9 Comparison plot: (a) input–output characteristics and (b) transfer characteristics.

response was obtained. The drain current was increased with respect to the glucose concentration. In the channel region, concentration of electrons was increased due to the enzymatic reaction. Figures 7.9(a) and 7.9(b) depict the comparison plot of with and without glucose. The limit of detection and sensitivity of the designed sensor are 2.43 mM and 1.9 mA mM^{-1} μm^{-2}, respectively. The optimized device is helpful in the field of biomedical and patient glucose monitoring applications.

7.5 CONCLUSION

With reference to the results obtained through simulation, we can conclude that each variant suits a different application. We cannot disregard the fact that each variant with its unique characteristics definitely has scope to fit into a set of applications. In this chapter, the comprehension of the results suggests that the variant with the thickness of 1.5 nm displays bulk MoS_2 properties, and the change in the order of bandgap and mobility appears to be favorable for a higher On/Off ratio. A higher On/Off ratio is a marker of excellent efficiency and performance. The leakage current tends to be minimal for devices with high magnitudes of On/Off ratios. With all the above stated facts, the 1.5 nm variant appears to be the ideal choice for sensing applications. Furthermore, the investigation of the different TMD materials can be carried out in the future.

REFERENCES

1. Li, H., Shi, B., Pan, Y., Li, J., Xu, Lin, Xu, L., Zhang, Z., Pan, F., & Lu, J. (2018). Sub-5 nm monolayer black phosphorene tunneling transistors. *Nanotechnology,* 29, 485202.
2. Yao, J. D., & Yang, G. W. (2021). All-2D architectures toward advanced electronic and optoelectronic devices. *Nano Today,* 36, 101026.
3. Sharmila, B., Divyashree, P., & Dwivedi, P. (2023). MoS2- based optical device as artificial synapse for neuromorphic computing. *IEEE Transactions on Electron Devices,* 70, 1386–1392.
4. Sharmila, B., & Dwivedi, P. (2022). Ultrasensitive, highly repeatable, ultrafast moo3/p-si heterostructure-based photodetector. *IEEE Sensors Journal*, 23, 2047–2054.
5. Sharmila, B., Divyashree, P., Dhanekar, S., & Dwivedi, P. (2022). Sensing demonstration and scalable production of nanostructured WO3 FET. *Optical Materials*, 134, 113027.
6. Soneja, S., Dwivedi, P., Dhanekar, S., Das, S., & Kumar, V. (2018). Temperature dependent electrical characteristics of nanostructured WO3 based ambipolar bottom gate fet. *IEEE Transactions on Nanotechnology,* 17, 1288– 1294.
7. Dwivedi, P., Soneja, S., & Dhanekar, S. (2018). Highly responsive behavior towards acetone by WO3 based bottom gate field effect transistor. *IEEE Sensors*, 1–4.
8. Li, X., & Zhu, H. (2015). Two-dimensional MoS2: Properties, preparation, and applications. *Journal of Materials*, 1, 33–44.
9. Chu, T., Ilatikhameneh, H., Klimeck, G., Rahman, R., & Chen, Z. (2015). Electrically tunable bandgaps in bilayer MoS2. *Nano Letters,* 15, 8000–8007.
10. Yazyev, O. V., & Kis, A. (2015). MoS2 and semiconductors in the flatland. *Materials Today,* 18, 20–30.
11. Xue, Y., Zhang, Y., Liu, Y., Liu, H., Song, J., Sophia, J., Liu, J., Xu, Z., Xu, Q., Wang, Z., Zheng, J., Liu, Y., Li, S., & Bao, Q. (2016). Scalable production of a few-layer MoS2/WS2 vertical heterojunction array and its application for photodetectors. *ACS Nano,* 10, 573–580.

12. Pierantoni, L., Coccetti, F., & Russer, P. (2010). Radio-frequency nanoelectronics: A new paradigm in electronic systems design. *IEEE Microwave Magazine,* 11, 8–10.
13. Khare, A., & Dwivedi, P. (2021). Design, simulation and optimization of multilayered MoS2 based FET devices. *Engineering Research Express*. https://doi.org/10.1088/2631-8695/ac3d11.
14. Zhang, M., Chien, P-Y., & Woo, J. C. S. (2015). Comparative simulation study on MoS2 FET and FinFET. *IEEE* SOI-3D-Subthreshold Microelectronics Technology Unified Conference (S3S), 1–2.
15. Wu, M., Liu, P., Xin, B., Li, L., Dong, H., Cheng, Y., Wang, W., Lu, F., Cho, K., Wang, W.-H., & Liu, H. (2019). Improved carrier doping strategy of monolayer MoS2 through two-dimensional solid electrolyte of YBr3. *Applied Physics Letters*, 114, 171601.
16. Mostufa, S., Paul, A. K., & Chakrabarti, K. (2021). Detection of hemoglobin in blood and urine glucose level samples using a graphene-coated SPR based biosensor. *OSA Continuum*, 4, 2164.
17. Bruen, D., Delaney, C., Florea, L., & Diamond, D. (2017). Glucose sensing for diabetes monitoring: recent developments. *Sensors,* 17, 1866.
18. Dhanekar, S., Dwivedi, P., Chauhan, N., Vivekanandan, P., Kumar, S., & Singh, P. (2017). Capturing bacteria through a bio-sensitive heterostructure surface: Photoluminescence studies. *IEEE Sensors*, 1–3, doi: 10.1109/ICSENS.2017.8234042. UK: Glasgow.
19. Wang, C., He, T., Zhou, H., Zhang, Z., & Lee, C. (2023). Artificial intelligence enhanced sensors-enabling technologies to next-generation healthcare and biomedical platform. *Bioelectronic Medicine*, 9(1), 17. doi: 10.1186/s42234-023-00118-1. PMID: 37528436; PMCID: PMC10394931.

8 Nanodiagnostics for Precision Breast Cancer Classification in Remote Health—A Comprehensive Study Employing Various Machine Learning Models

Kanik Makhija, Swayam Mahindroo, Mehul Batra and Dr. Safina Shokeen

8.1 INTRODUCTION

Millions of lives are still impacted by breast cancer, a serious worldwide health concern that calls for constant research into new detection and diagnostic methods using different machine learning techniques [1]. Given that it is the second most common cancer globally, the need for improved diagnosis techniques is highlighted by the sheer number of cases. There are few researchers who have explored the different nanomaterials for real-time sensing application [2–4]. In addition, in this setting, a ray of hope for improving accuracy and efficiency has emerged at the junction of medical diagnostics and artificial intelligence, more especially machine learning. Figure 8.1 depicts a data-processing pipeline, which is a series of steps used to prepare raw data for machine learning. The specific pipeline in the diagram is designed to process data for breast cancer diagnosis. The dataset being evaluated is taken from the Breast Cancer Wisconsin dataset and includes important features including mean radius, fractal dimension, smoothness, compact size, concavity, and concave regions. These characteristics are essential to the diagnostic process because they allow a thorough comprehension of the data and provide the framework for an extended analysis.

 DOI: 10.1201/9781003602729-8

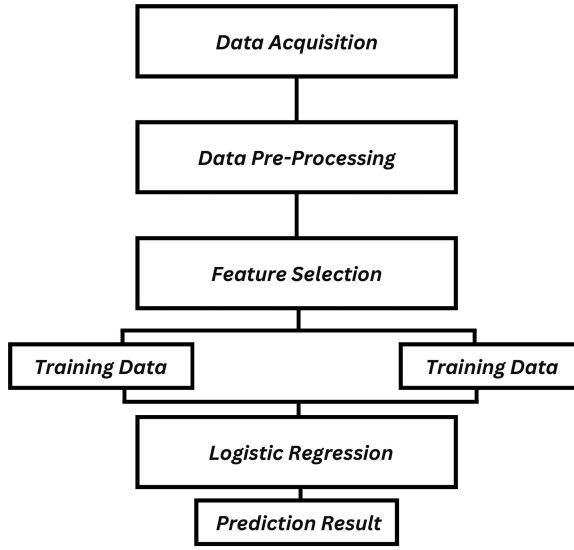

FIGURE 8.1 Data flow diagram of logistic regression.

Through its objectives, the study attempts to evaluate the practicality of using statistical regression as a predictive model in breast cancer identification in addition to applying cutting-edge computational methods to a real-world health issue.

This study is conducted in multiple sections, starting with the collection and preparation of data. A robust foundation for learning is offered by the Breast Cancer Dataset, which is taken from the reliable scikit-learn the deal. Using technologies like pandas and NumPy, the dataset is meticulously digested to provide a clear and comprehensive exploration. Statistical measures, a distribution analysis of the objective variable, and exploratory examination of data are all part of the very first stages of the research.

The main goal of this research is to improve breast cancer classification accuracy by exploring the field of machine learning by utilizing a variety of methods [5]. The complexity of breast cancer, its several subtypes, and the crucial role that an early and precise diagnosis plays in determining treatment outcomes mean that the stakes are quite high.

In conclusion, our work contributes significantly to ongoing efforts aimed at refining breast cancer diagnosis techniques through the application of diverse machine learning models. This study delves into the effectiveness of decision trees, random forest, support vector machine (SVM), k-nearest neighbors (KNN), and logistic regression, thereby leveraging a substantial dataset. The ensuing sections meticulously detail how these algorithms enhance healthcare diagnostics. From the nuanced exploration of datasets to the intricate steps of model creation and subsequent practical predictions, each machine learning approach plays a crucial role in advancing the accuracy and efficacy of breast cancer diagnosis. By using a range of algorithms, we

not only provide a thorough understanding of their individual contributions but also underscore the collective impact of machine learning in transforming and improving the landscape of breast cancer detection methodologies.

8.2 BACKGROUND

8.2.1 Description

A prevalent and potentially fatal worldwide health issue, breast cancer claimed 685,000 lives in 2020. The startling finding that women without any particular risk factors other than age or gender account for almost 50% of the cases highlight the difficulty and urgency of diagnosing breast cancer. This illness affects women of all ages after puberty and is not limited by geography. While men make up a lesser proportion of occurrences (0.5–1%), their vulnerability to breast cancer means that treatment plans ought to be based on those created for women.

8.2.2 Scope of the Problem

The year 2020 witnessed a staggering 2.3 million female diagnoses and 685,000 fatalities attributed to breast cancer. Projections indicated that breast cancer was poised to become the most prevalent cancer globally by the end of 2020, marking it a pervasive and enduring health challenge. The introduction of comprehensive therapies and early detection programs in the 1990s marked a turning point, as mortality rates, stagnant until then, began to witness positive changes. Understanding the risk factors is pivotal, with female gender, age, family history, lifestyle, and specific genetic abnormalities being identified as contributors.

8.2.3 Who Is at Risk?

Gender continues to be the key risk factor for breast cancer; males are afflicted in 0.5–1% of circumstances, debunking the myth that it only affects women. Risk is complex and involves several factors, including reproductive history, radiation exposure, consumption of alcohol, age, obesity, and family history. Inheritable mutations in genes including BRCA1, BRCA2, and PALB-2 are linked to a notable increase in breast cancer risk, even though age and gender are significant contributors to risk for half of all instances of the disease [6].

8.2.4 Signs and Symptoms

Unfortunately, early-stage breast cancer frequently develops silently and shows no symptoms. Palpable breast lumps, changes in the shape or size of the breasts, skin changes, anomalies in the nipples, and abnormal discharge from the nipples are detectable indications. It is imperative that you get medical assistance for any suspicious breast lump. Even though most breast lumps turn out to be benign, early detection is crucial to the effectiveness of treatment since it stops the cancer from spreading to nearby lymph nodes and prevents metastases later on.

8.2.5 Types of Tumor

Benign and malignant tumors are two different forms of aberrant cell development that fall under the umbrella of breast cancer [7]. Benign tumors resemble normal cells but do not invade nearby organs. They are typically confined and noncancerous. These tumors are characterized by sluggish growth and encapsulation, which makes them less dangerous for general health. Malignant tumors, on the other hand, can spread to different areas of the body by metastasis after infiltrating adjacent tissues due to carcinogenic mechanisms. Rapid, uncontrollably growing malignant cells are one of their traits, and their aggressiveness calls for prompt, targeted medical intervention, such as surgery, radiation therapy, and chemotherapy.

It is essential to comprehend these small differences in tumor types to develop efficient diagnostic and therapeutic approaches. The complex interactions between benign and malignant tumors highlight how urgent it is to create sophisticated diagnostic tools, including machine learning models like logistic regression, to improve outcomes and improve early detection in the complicated field of breast cancer.

8.3 MACHINE LEARNING ALGORITHM FOR BREAST CANCER PREDICTION

8.3.1 Logistic Regression

Because breast cancer can be classed as either benign or malignant, as shown in Figure 8.2, logistic regression is a statistical technique that is frequently used for binary categorization problems. This makes it particularly useful for making predictions about breast cancer. Real numbers are mapped into the interval between 0 and 1 by the logistic function, which indicates the likelihood that an instance falls into a particular category.

When there is a nearly linear relationship between the chosen features and the binary outcome, logistic regression performs well in the context of breast cancer prediction. These elements could comprise different clinical information or diagnostic imaging-related attributes. A simple yet accurate method of predicting breast cancer is provided by logistic regression, which models the chance of malignancy.

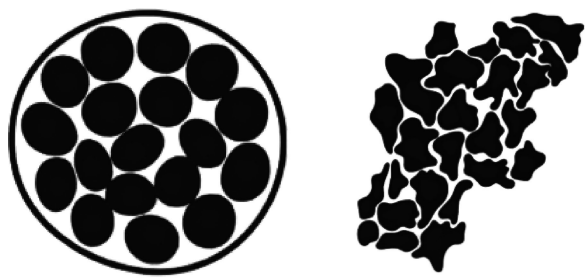

FIGURE 8.2 Types of tumor.

8.3.2 Support Vector Machine

Strong supervised learning instruments that may be used for both regression and classification issues are SVMs. The goal of SVM is to identify the hyperplane that divides the data into the most distinct classes [8]. Because of its exceptional efficacy in high-dimensional spaces, this method can be applied to applications involving several aspects in data, such as breast cancer prediction.

Using characteristics from diagnostic imaging or pertinent data, SVMs can determine the best hyperplane to classify instances as malignant or benign in the context of breast cancer prediction [9]. SVM is a useful method for precise breast cancer prediction because of its capacity to manage complex relationships in high-dimensional domains.

8.3.3 Decision Trees

Decision trees work by splitting the dataset recursively according to the most significant attribute at each node to create a tree structure that produces accurate predictions. To create well-informed decisions regarding breast cancer prediction, decision trees take into account several characteristics, including tumor size, texture, and shape.

Through the identification of patterns that suggest cancerousness, these trees can be utilized to predict breast cancer. Decision trees offer interpretable models that help with understanding the factors impacting the prediction of breast cancer by iteratively assessing the relevance of various features.

8.3.4 Random Forest

During training, the random forest ensemble learning technique generates a vast number of decision trees. The class mode that the ensemble predicts determines the random forest's output. This methodology improves generalization and precision by identifying complex relationships between heterogeneous data.

Random forest is an excellent method for enhancing prediction performance when it comes to breast cancer prediction. It improves accuracy and resilience by utilizing the collective experience of several models to build an ensemble of decision trees. This is very helpful in the breast cancer prediction assignment when handling intricate relationships and interactions.

8.3.5 K-Nearest Neighbors

KNN stands as a prominent instance-based and nonparametric learning algorithm, classifying a data point based on the majority class among its KNN [10]. When applied to the realm of breast cancer prediction, KNN proves its mettle by unraveling patterns and identifying similarities between instances.

The versatility of KNN comes to the forefront in breast cancer prediction, offering a flexible approach that capitalizes on the local structure of the data. This algorithm shines when instances with similar features are likely to exhibit similar outcomes. Its simplicity, coupled with effectiveness, positions KNN as a valuable asset among the array of machine learning algorithms dedicated to breast cancer prediction.

8.4 PROPOSED ALGORITHM

8.4.1 Data Collection and Processing

The initial step in our proposed algorithm involves importing the necessary libraries and loading the breast cancer dataset from the scikit-learn library. Transform the dataset into a Pandas DataFrame, allowing for a comprehensive examination of its structure. As part of the preprocessing stage depicted in Figure 8.3, add the target label, typically denoting the binary classification of benign or malignant. Conduct a thorough exploration of the dataset's statistical measures, ensuring that all necessary information is available and that there are no missing values.

8.4.2 Feature Selection

Feature selection is crucial for building an effective breast cancer prediction model [11]. Extract relevant features from the dataset, such as perimeter, mean radius, and texture, which are known to be significant in breast cancer diagnosis. Utilize scikit-learn to split the dataset into training and testing sets, thereby enabling the model to be trained on one subset and evaluated on another. Figure 8.4 outlines a key aspect of building effective machine learning models: selecting relevant features and

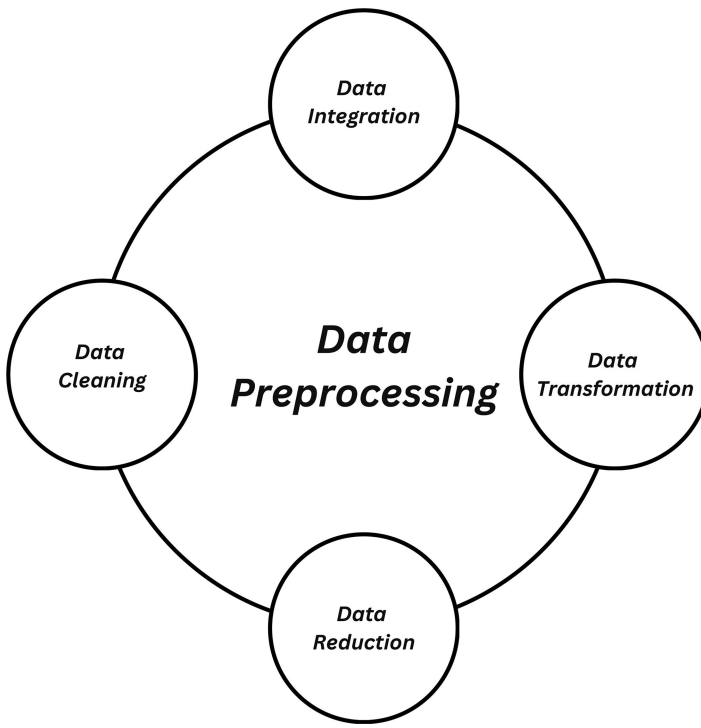

FIGURE 8.3 Data processing units.

training on well-prepared data. This helps ensure the model's generalizability and ability to make accurate predictions on unseen data.

8.4.3 Logistic Regression Model

To predict breast cancer, use the machine learning model of logistic regression. Figure 8.5 is a flowchart depicting how to use logistic regression to predict breast

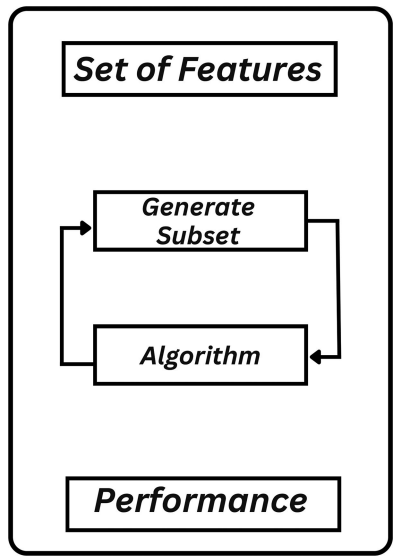

FIGURE 8.4 Feature selection units.

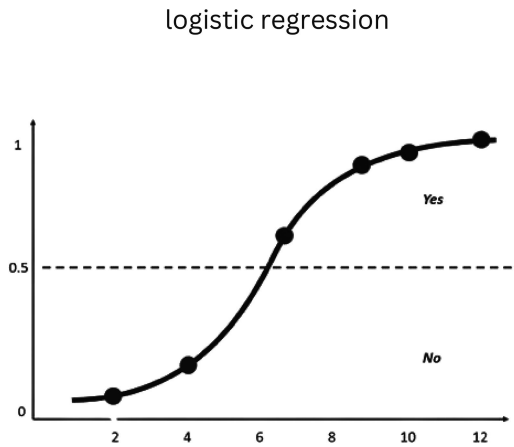

FIGURE 8.5 Logistic regression model.

cancer. Fit the model to the features and associated target labels using the training data. Examine the model's predictions on the test and training datasets to gauge its performance after training. Assess accuracy scores and other pertinent metrics to see how well the logistic regression model differentiates between benign and malignant breast cancer cases.

8.4.4 Decision Tree Model

A decision tree model is a predictive modeling tool that uses a tree-like structure to make judgments. It is utilized for the classification of breast cancer. When it comes to classifying breast cancer, decision trees examine input features associated with the disease's characteristics and apply a set of rules to determine whether a particular occurrence suggests a benign or malignant tumor. The decision tree model to identify brain tumors is shown in Figure 8.6.

> "Is there a brain tumor?" is the starting point. If "Yes," is the response, proceed to the "Symptoms Present?" node. If symptoms manifest, the diagnosis is "Likely tumor. Upon receiving a "No" response at the "Symptoms Present?" node, the diagnosis is "Unlikely tumor."

8.4.5 Random Forest Model

Random forest is an ensemble method that aggregates forecasts from several decision trees.

Decision Trees: Trained on a subset of data, random forest's base learners are decision trees.

Bootstrapping: In bootstrapping, subsets of training data are constructed using replacement.

Feature Randomization: When building a tree, only a random subset of features is taken into account at each split.

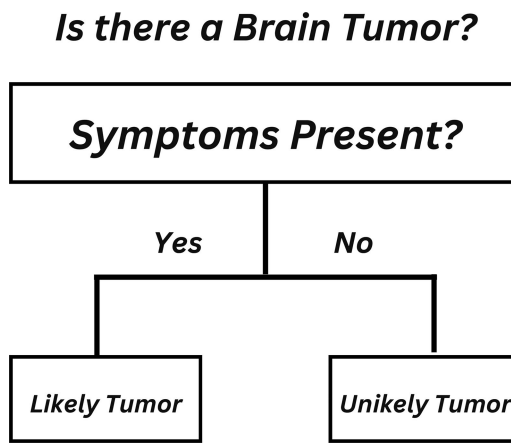

FIGURE 8.6 Decision tree model.

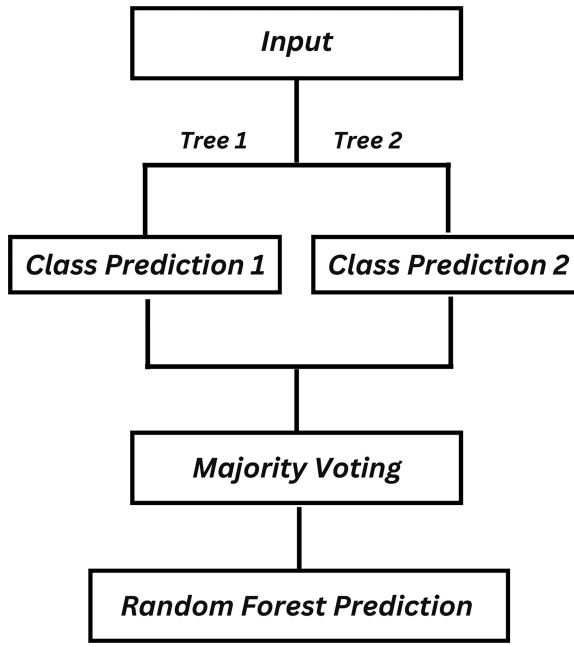

FIGURE 8.7 Random forest model.

Voting Mechanism: In the classification process, each tree "votes" for a class, and the majority class is projected. Regression involves taking the average.

Diminished Overfitting: By reducing overfitting, randomness improves generalization to fresh data.

Extremely Parallelizable: Training separate trees is possible in parallel, which makes it effective for big datasets.

Robust to Outliers: Because of ensemble averaging, random forest is resistant to outliers and noisy data.

Figure 8.7 depicts a random forest algorithm, which uses multiple decision trees with randomness to improve accuracy and reduce overfitting for classification tasks. It leverages bootstrapping, feature randomization, and voting to achieve this.

8.4.6 k-Nearest Neighbor

For the purpose of classifying breast cancer, KNN is used. It makes predictions based on parameters such as tumor size, shape, and texture by using the proximity of data points. The approach uses the class labels of a data point's KNN in the feature space to classify it; the value of k affects the data point's susceptibility to noise. KNNs are useful tools because of their nonparametric nature and simplicity, but they require thorough preprocessing, data normalization, and outlier handling. Even though KNN doesn't naturally contain feature importance information, its interpretability, simplicity of understanding, and adaptability to complicated data distributions make it

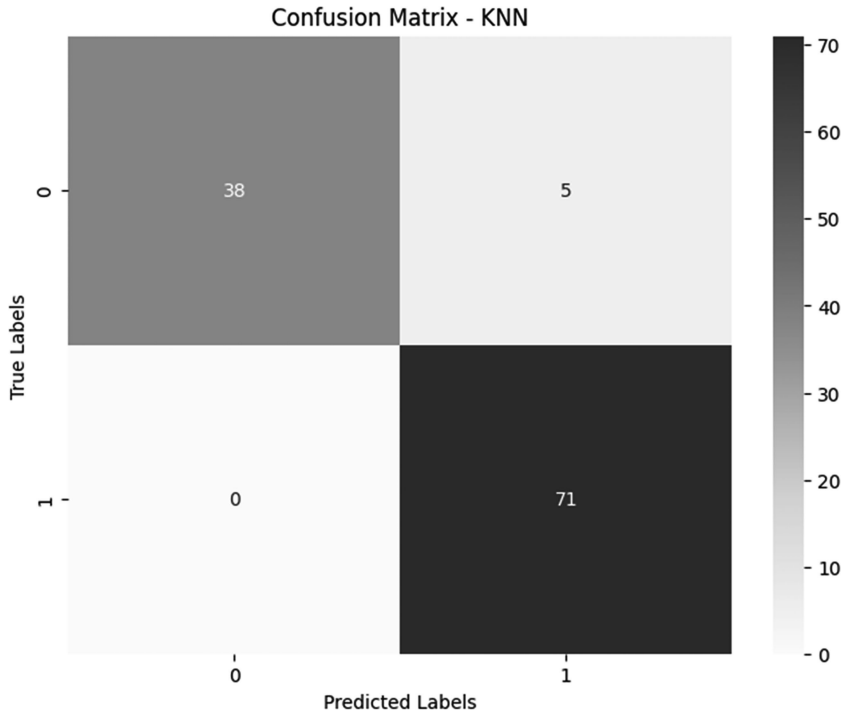

FIGURE 8.8 Confusion matrix of KNN model.

useful in the medical setting for making transparent and accurate predictions about breast cancer diagnosis.

Figure 8.8 visualizes the KNN algorithm, where data points represent patients and their features (such as tumor size, shape, texture) define their position in a multidimensional space.

8.4.7 Support Vector Machine

One potent supervised learning technique that is frequently used for classification tasks, such as the classification of breast cancer, is SVM. It functions by locating the best hyperplane inside the feature space to maximally divide various classes. SVM can handle complex datasets and is especially useful in high-dimensional domains. Strong SVMs exhibit robust generalization to new, unseen data by identifying support vectors, or data points essential for selecting the best hyperplane. In addition, SVM facilitates the modeling of nonlinear interactions by allowing the use of other kernel functions, such as radial basis function. SVM is an important tool in the field of breast cancer diagnosis and classification because of its robust theoretical background and the capacity to handle both linear and nonlinear classification problems and other attributes. Figure 8.9 visualizes the SVM algorithm, where data points represent patients and their features such as tumor size, shape, and texture define their position in a multidimensional space.

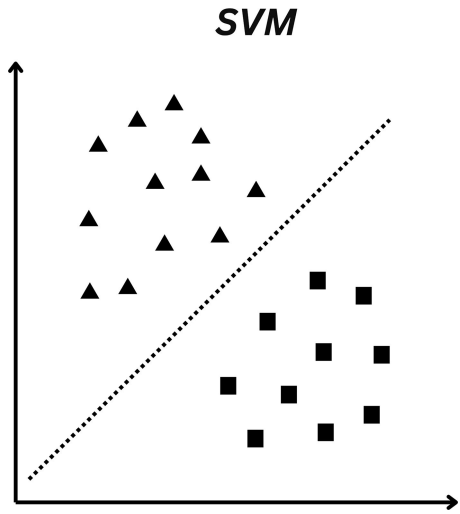

FIGURE 8.9 SVM model.

8.4.8 Input Prediction

To validate the practicality of the model, introduce fresh input data representing features obtained through fine-needle aspiration (FNA). Apply the trained logistic regression model to predict whether the input corresponds to benign or malignant breast cancer. This step serves as a practical test of the model's ability to generalize and accurately classify new, unseen instances.

8.4.9 Model Evaluation and Interpretation

Evaluate the logistic regression model's performance through a comprehensive analysis of metrics such as accuracy, precision, recall, and the receiver operating characteristic curve. Interpret the results to gain insights into the model's strengths and limitations, thereby providing a basis for potential improvements.

8.4.10 Comparison with Other Algorithms

Consider comparing the performance of the logistic regression model with other machine learning algorithms discussed earlier, such as SVM, decision trees, random forest, and KNN [12,13]. This comparative analysis can help determine which algorithm is most suitable for the specific task of breast cancer prediction in the given dataset.

8.4.11 Hyperparameter Tuning

Fine-tune the hyperparameters of the logistic regression model to optimize its performance [14,15]. Experiment with different parameter values and configurations to

find the most effective combination. This step aims to enhance the model's predictive accuracy and generalization capabilities.

8.4.12 Deployment and Integration

Once satisfied with the model's performance, consider deploying it in a real-world setting. Integrate the model into a system or application that can assist healthcare professionals in the early detection and diagnosis of breast cancer. This step involves creating a user-friendly interface and ensuring seamless integration into existing medical workflows.

8.4.13 Continuous Monitoring and Updating

Implement a system for continuous monitoring and updating of the model to adapt to changes in data distribution and evolving patterns in breast cancer cases. Regularly update the model with new data to maintain its relevance and effectiveness over time. By following these steps, the proposed algorithm aims to leverage logistic regression for breast cancer prediction while incorporating best practices in data processing, feature selection, model training, and evaluation. The emphasis on practical input prediction and continuous improvement ensures the algorithm's utility and relevance in real-world healthcare applications.

8.5 RESULT

8.5.1 Test Dataset Generalization

We evaluated the models' ability to generalize to new contexts with an impartial test dataset. With a 92% accuracy rate, logistic regression demonstrated its versatility in a range of scenarios. Decision tree demonstrated a strong generalization with 94.7% accuracy. Random forest produced an accuracy of 96.4%, exhibiting remarkable generalization. SVM maintained high generalization performance, hitting 95.6% accuracy. With an impressive accuracy of 94.7%, KNN demonstrated its flexibility in dealing with unknown cases.

8.5.2 Practical Application

Certain characteristics associated with a breast cancer case were entered into a forecast in a real-world application scenario. As shown in Figure 8.10, 92% of the cases were correctly classified by logistic regression, demonstrating its usefulness. Decision tree's accuracy of 94.7% showed its usefulness in real-world scenarios. With an astounding 96.4% accuracy rate in real-world applications, random forest performed exceptionally well. SVM with its practical accuracy of 95.6% demonstrates its clinical significance. With 94.7% accuracy, KNN proved its usefulness in real-world scenarios, confirming its status as an important tool for medical professionals. The aforementioned findings highlight the various uses of machine learning models in practical healthcare environments and their capacity to support well-informed decision-making.

S no.	Machine Learning Model	Accuracy Score(%)
1	Logistic Regression	92
2	Decision Tree	94.7
3	Random Forest	96.4
4	Support Vector Machine	95.6
5	K - Nearest Neighbour	94.7

FIGURE 8.10 Comparison of accuracy score of various.

The model's successful implementation in a real-world setting validates its clinical applicability and shows its potential as a help tool for medical practitioners. The model's capacity to provide precise forecasts from real-world data further substantiates its contribution to improving diagnosis procedures and fostering well-informed decision-making in healthcare environments.

The relative accuracy of different machine learning algorithms in classifying breast cancer is depicted in Figure 8.11. The accuracy scores of every method are displayed, offering valuable information on how well each algorithm performed on the provided dataset.

A respectable 92% accuracy rate is shown using logistic regression, highlighting its dependability in the categorization of breast cancer.

With an impressive accuracy of 94.7%, decision tree demonstrates how well it can identify intricate patterns in the data.

With an astounding 96.4% accuracy rate, random forest is a strong algorithm for accurate breast cancer detection.

With a 95.6% accuracy rate, SVM demonstrates its ability to identify patterns and correlations in the dataset.

With an accuracy rate of 94.7%, KNN demonstrates its proficiency in categorizing cases of breast cancer.

The classification report presents precision, recall, and F1-score for each class (0 and 1) in addition to overall accuracy, giving comprehensive insights into the machine learning model's performance [16,17]. The model's predictions are compared to the dataset's actual values to compute the metrics.

	Precision	Recall	F1-Score	Support
0	0.98	0.93	0.95	43
1	0.96	0.99	0.97	71
Accuracy	0.96			
Macro Avg	0.97			
Weighted Avg	0.96			

FIGURE 8.11 Representation of the classification report.

Precision: Precision is a measure of how well the model predicts favorable outcomes. The ratio of actual positive predictions to all expected positives is used to compute it.

Recall: The model's capacity to recognize all pertinent occurrences is gauged by the recall, which is also referred to as sensitivity or true positive rate. The ratio of actual positives to genuine positive predictions is used to compute it.

F1-Score: The F1-score is the harmonic mean of precision and recall. It provides a balanced measure that considers both false positives and false negatives. A higher F1-score indicates a better balance between precision and recall.

Support: Support represents the number of instances of each class in the actual dataset.

8.6 CONCLUSION

This study concludes by highlighting the critical impact that certain machine learning algorithms—such as decision tree, random forest, SVM, KNN, and logistic regression—have in improving the diagnosis of breast cancer. Although logistic regression shows remarkable accuracy in identifying breast cancer using data taken from FNA pictures, a thorough comparison shows subtle differences in the performance of several methods.

With an accuracy of 94.7%, our results highlight decision tree's adaptability and show how well it can handle complex patterns in breast cancer data. With a remarkable accuracy of 96.4%, random forest really shines and demonstrates how well it can capture the intricate relationships present in the information. With a 95.6% accuracy rate, SVM shows strong performance and is a useful technique for high-dimensional datasets. KNN shows competitive accuracy of 94.7%, highlighting its flexibility to local data features.

This study supports the larger goal of helping healthcare providers diagnose breast cancer by using a machine learning perspective. The suggested models, which are based on logistic regression and enhanced by additional algorithms, aid in the improvement of diagnostic methods. These developments offer practical consequences for real-world circumstances, holding the potential to become key components in the diagnostic arsenal. The many uses of machine learning, each with its own advantages and insights, highlight the continuous attempts to improve patient outcomes even further. The ultimate goal of this cooperative strategy is to increase

diagnostic accuracy by utilizing the advantages of several algorithms. This will allow for earlier interventions, individualized treatment regimens, and better prognoses for those with breast cancer.

8.7 FUTURE SCOPE

The results of this study provide a foundation for future research by outlining multiple avenues for more investigation and improvement in the diagnosis of breast cancer through the use of machine learning techniques, specifically decision tree, random forest, SVM, KNN, and logistic regression. Prospective areas of future research include the following:

8.7.1 Supplementary Machine Learning Methods

Subsequent investigations may explore other machine learning methods, including decision tree, random forest, SVM, KNN, and logistic regression, to evaluate and improve their prediction ability for the detection of breast cancer [18,19]. Every algorithm has its own merits, and a multi-method ensemble approach could lead to more accurate predictions. Comparing and contrasting these various machine learning models may help determine which approaches are the most effective for the complexities of breast cancer diagnosis.

To broaden the scope of the proposed method, additional extensive and diverse datasets should be incorporated into the analysis. Data from many geographic regions, demographic groups, and medical facilities may be included in this extension. In addition to improving the model's validity, a more comprehensive dataset would enable a more detailed understanding of the variables influencing breast cancer diagnosis. The model's predictive skills could be further improved by adding more characteristics and imaging modalities, thereby offering a more comprehensive picture of diagnostic patterns.

8.7.2 Integration of Diverse Dataset

Future studies should think about adding more large and varied datasets, such as those used in decision tree, random forest, SVM, KNN, and logistic regression analyses, to the suggested method to expand its use. The validity of the model can be strengthened and a more thorough understanding of the factors impacting breast cancer diagnosis made possible by the inclusion of data from diverse geographic locations, demographic groupings, and healthcare facilities. By adding new traits and imaging modalities, the model's predictive abilities could be further improved and provide a more complete view of diagnostic patterns.

8.7.3 Collaboration between Machine Learning and Medicine

Improved breast cancer identification and treatment may result from the combination of other machine learning approaches with decision tree, random forest, SVM, KNN, and logistic regression. Prospective investigations could concentrate on fortifying this interdisciplinary alliance, cultivating cooperation between scholars, data

scientists, and medical professionals. This partnership may lead to the development of more personalized and context-aware machine learning models, enhancing interpretability and utility in real healthcare settings by fusing domain-specific knowledge with clinical expertise.

8.7.4 Explainability and Interpretability

The subsequent research endeavors ought to concentrate on the essential elements of interpretability and explainability in machine learning models, such as decision tree, random forest, SVM, KNN, and logistic regression, utilized in the prediction of breast cancer. Understanding the characteristics and factors influencing model projections is necessary to win over medical experts and ensure responsible adoption. The use of these models in the healthcare sector can be considerably aided by the development of techniques that provide comprehensible and transparent insights into the decision-making process of these models.

8.7.5 Longitudinal Studies and Continuous Monitoring

Using decision tree, random forest, SVM, KNN, and logistic regression analyses in longitudinal research could shed light on how well these models function in dynamic environments over time. To guarantee the usability and effectiveness of these models in real healthcare settings, regular updates with new data and modifications to account for changes in data distribution are crucial.

8.7.6 Patient-Centric Applications

Subsequent investigations might concentrate on creating patient-centered programs that use decision tree, random forest, SVM, KNN, and logistic regression for breast cancer education, awareness, and early detection. By incorporating these technologies into patient care and instruction, people may be inspired to actively participate in their health, which could lead to early identification and better results.

In conclusion, there is a lot of promise for the use of machine learning in breast cancer prediction in the future. Scientists investigating novel algorithms, expanding datasets, collaborating across disciplines, guaranteeing the interpretability of models, and developing patient-focused applications are well-positioned to provide a holistic impact on the identification and management of breast cancer. It is anticipated that the further development of machine learning methods in therapeutic contexts, such as decision tree, random forest, SVM, KNN, and logistic regression, will revolutionize the treatment of breast cancer and improve outcomes for people impacted by this common disease.

8.8 MAJOR CONTRIBUTION

8.8.1 Significant Advancement in Breast Cancer Diagnostics

Through the wide application of machine learning techniques, notably logistic regression, decision tree, random forest, SVM, and KNN, this chapter represents a

significant advancement in the diagnosis of breast cancer. By using a multi-algorithmic method, diagnostic efficacy and precision are increased to unprecedented levels in line with contemporary tactics.

8.8.2 Utilization of Extensive Dataset

A large dataset obtained from FNA pictures is used in the investigation. This dataset is essential since it contains a variety of attributes that are important for diagnosing breast cancer. These characteristics include mean radius, symmetry, concavity, smoothness, compactness, and fractal dimension. The variety of these features improves the model's capacity to identify trends and produce precise forecasts.

8.8.3 Detailed Dataset Understanding

Several preprocessing procedures are carried out by the researchers to guarantee the dataset's validity and applicability. This covers rigorous statistical measures, exploratory data analysis, and data preparation. By taking these stages together, you can ensure that the machine learning model is constructed on a strong basis by developing a comprehensive grasp of the dataset.

8.8.4 Application of Various Machine Learning Techniques

The various machine learning techniques such as decision tree, random forest, SVM, logistic regression, and KNN are explored and applied. By offering a nuanced view of their relative efficacy, this inclusive methodology expands the scientific understanding of machine learning in medical diagnostics, particularly in the context of breast cancer.

8.9 REAL-WORLD RELEVANCE

This study goes beyond theoretical talks by offering a concrete example of how machine learning models are used in the real world. The creation of prediction systems highlights the possible relevance and application of the created models in real-world scenarios by illustrating their translational impact in clinical settings.

8.10 IMPROVEMENT IN DIAGNOSTIC TECHNIQUES

This work makes a substantial contribution to continuing attempts to improve diagnostic tools by demonstrating the capabilities of different machine learning algorithms, with a focus on the combined efficacy of decision tree, random forest, SVM, KNN, and logistic regression. Enhancing productivity and accuracy could lead to earlier and more effective detection of breast cancer, which would eventually improve patient outcomes.

8.11 ADVANCEMENT IN THE DIALOGUE ON MACHINE LEARNING IN MEDICINE

This study adds to the current discussion on the application of machine learning in medical diagnosis by concentrating on breast cancer. Through showcasing the efficacy of an array of algorithms, such as random forest, SVM, KNN, decision tree, and logistic regression, the research considerably advances the wider discourse about the revolutionary possibilities of machine learning in enhancing healthcare procedures.

To sum up, this research's main contribution is its thorough methodology, which embraces a varied dataset and examines several machine learning approaches without giving any one approach undue weight. The work constitutes a significant breakthrough in the field because of its potential to transform current diagnostic tools as well as its practical value.

REFERENCES

1. A. Nevada, A. N. Ansari, S. Patil and B. A. Sonkamble, "Overview of the Use of Decision Tree Algorithms in Machine Learning," In *2011 IEEE Control and System Graduate Research Colloquium*, Shah Alam, Malaysia, 2011.
2. B. Sharmila and P. Dwivedi, "Wafer-Scale, Efficient In_2S_3 Based Optical Memory Devices for Neuromorphic Computing," *IEEE Transactions on Electron Devices, Accepted,* February 2024 (Early access).
3. B. Sharmila and P. Dwivedi, "Optical Sensing and Computing Memory Devices Using Nanostructured WO_3," *Materials Science in Semiconductor Processing*, vol. 173, p. 108106, April 2024, doi: 10.1016/j.mssp.2024.108106.
4. S. B. and P. Dwivedi, "Realization of Optically Stimulated Synaptic Memristor Devices Using MoO_3," *IEEE Photonics Technology Letters*, vol. 36, no. 4, pp. 211–214, February 2024, doi: 10.1109/lpt.2023.3332605.
5. A. Q. Al-Aidaroos and R. Zainuddin, "A Hybrid Approach for Breast Cancer Classification Using Fuzzy Means and Neural Network," *Indonesian Journal of Electrical Engineering and Computer Science*, vol. 9, no. 3, p. 639, 2018.
6. M. 0. Sousa, A. R. Carvalho and M. A. Marques, "Logistic Regression Applied to Breast Cancer Risk Prediction," *Journal of Biomedical Informatics*, vol. 92, p. 103144, 2019.
7. S. Ara, A. Das and A. Dey, "Malignant and Benign Breast Cancer Classification Using Machine Learning Algorithms," In *2021 International Conference on Artificial Intelligence (ICAI)*, Islamabad, Pakistan, 2021.
8. M. A. Hearst, S. T. Dumais, E. Osuna, J. Platt and B. Scholkopf, "Support Vector Machines," *IEEE Intelligent Systems and their Applications*, vol. 13, no. 4, pp. 18–28, July-August 1998.
9. R. Nagarajan and P. Selvaraj, "Automated Breast Cancer Detection in Mammograms Using Fuzzy C-Means Clustering and Fuzzy Support Vector Machines," *Computers in Biology and Medicine*, vol. 87, pp. 250–258, 2017.
10. K. Taunk, S. De, S. Verma and A. Swetapadma, "A Brief Review of Nearest Neighbor Algorithm for Learning and Classification," In *2019 International Conference on Intelligent Computing and Control Systems (ICCS)*, Madurai, India, 2019.
11. N. Mishra, O. Prakash and A. Sinha, "Feature Selection and Classification of Breast Cancer Data Using Logistic Regression," *Journal of King Saud University Computer and Information Sciences*, vol. 32, no. 6, pp. 731–736, 2020.

12. E. Baser and I. Morgül, "A Novel Ensemble Model for Breast Cancer Diagnosis," *Neural Computing and Applications*, vol. 31, no. 12, 8%, pp. 1–8571, 2019.
13. D. Yoo, J. Kang, S. Kim and D. Shin, "Performance Comparison of Machine Learning Algorithms for Breast Cancer Prediction," *Journal of Digital Imaging*, vol. 33, no. 5, pp. 1250–1258, 2020.
14. M. Saeed, A. Zulfiqar and S. Shafique, "Deep Neural Networks-Based Breast Cancer Detection and Classification Using Transfer Learning," *IEEE Access*, vol. 8, pp. 54388–54397, 2020.
15. N. Mishra, O. Prakash and A. Sinha, "Feature Selection and Classification of Breast Cancer Data Using Logistic Regression," *Journal of King Saud University Computer and Information Sciences*, vol. 32, no. 6, pp. 731–736, 2020.
16. P. Divyashree and P. Dwivedi, "AI Computing as Ubiquitous Healthcare Solution: Predict Parkinson's for Large Masses in Society," *IEEE Transactions on Computational Social Systems*, pp. 1–6, 2022, doi: 10.1109/TCSS.2022.3224046.
17. T. Bhavani, P. VamseeKrishna, C. Chakraborty and P. Dwivedi, "Stress Classification and Vital Signs Forecasting for IoT-Health Monitoring," *IEEE/ACM Transactions on Computational Biology and Bioinformatics*, pp. 1–8, 2022, doi: 10.1109/TCBB.2022.3196151.
18. L. Chen, M. Wu, Z. Zhang and Y. Wang, "Comparative Study of Breast Cancer Classification Based on Machine Learning Algorithms," *International Journal of Hybrid Information Technology*, vol. 11, no. 4, pp. 333–340, 2018.
19. M. 0. Sousa, A. R. Carvalho and M. A. Marques, "Logistic Regression Applied to Breast Cancer Risk Prediction," *Journal of Biomedical Informatics*, vol. 92, pp. 103144, 2019.

Index

Note: **Bold** page numbers refer to tables and *italic* page numbers refer to figures.

accelerometers 29, 53–55, 58, 62–63, *66–67*
accessibility 105
accuracy 124
  advantage of SVM 49
  comparison of 149–150, *150*
  of cell classification detection 114
acetone 84, 96
aerospace, strain sensing in 102–103
air quality 78, 86, 103
air–fuel (A/F) ratio 87
alarm 29, 44, 86
alert sensors 29
Alzheimer Estimate system 50
amyotrophic lateral sclerosis (ALS) 1–2, 8, 10, 17
analog-to-digital converter 3, 10, 85
architecture design 55
artificial intelligence (AI) 20, 82–83, 89–90, 138
  algorithms 90
  enabled insulin delivery 35–36, *36*
  techniques 77
artificial neural networks (ANNs) 58–60
  confusion matrix for *70*
  evaluation and testing 59
  international classification for standards data 59
  model 58
  validation loss and accuracy for *69*
asthma 83
automated decision-making 89

bar plot 63, *64*
basophils 116–117, 123–124
battery life 29
benign tumors 141, *141*
bidirectional long short-term memory 48
biological
  nanosensors 98–99
  processes 96–99
biomedical applications 77, 96–97
biomedicine 83, 102
biosensing
  description of 127–128
  effect of thickness on device performance 130–134
  test for FET-based sensor 135–136
  thickness-dependent FET devices and simulation model 128–130
blockchain 48, 90
blood cell image classification
  dataset creation and preprocessing 116–117
  description of 108–109
  detection method based on MCGAN 110–116
  experiment tools 116
  generation experiment 118–121
  network detection accuracy 121–124, **122**
  network training 117–118
  related work 109–110
  visual classification and detection results 121, *122*
blood glucose levels 26–27, 29, 32–35, 98, 135
Bluetooth 28, 29, 31, 44, 83
bootstrapping 145–146
box plot 63, *64–67*
breast cancer
  accuracy and efficacy of 139–140
  classification of 145
  complexity of 139
  detection of 152
  diagnosis 138, 140, 153–154
  prediction of 142
  representation of classification report 150, *151*
  statistical regression 139
  vulnerability to 140
Breast Cancer Wisconsin dataset 138
breath analyzer 84–85
builder 118, *120*

cancer 97
  biomarkers 102
  diagnosis and treatment 102
capacitive sensors 29
carcinogenic mechanisms 141
cardiovascular disease (CVD) risk 52
cell
  classification 114
  position mask 112–113
cell detection
  accuracy of 123–124
  stage 118
cell image
  classification and detection of 108
  generation experiment 110, 118–121, *119*
  generation stage 117–118, **118**
central processing unit (CPU) 85
chemical nanosensors 99–101, *100*
chronic

disease 42, 83, 90
health problems 85
cloud
computing 48–49, 82–83, 89
infrastructure 52
services 28, 83
clustering algorithm 111, 116, 118
communication
networks 43–44
technologies 44
CompactRIO-9035 controller 5
controller 2
embedded hardware design 9–10, **9**
EMG processing module 12, *13*, **14**, *15*
hardware *6*, 8–9, *9*
k-NN-based classification 16, *17*
national instrument 8
software and hardware implementation *8*
solution 20
SVM classification 10–12, *10–12*, 13–16, *15*, **15**
system architecture 5–8
comparison plot *135*, 136
complementary metal oxide semiconductor (CMOS) 127
COMSOL Multiphysics 5.6 software 128, *129*, 135
conditional generative adversarial network (CGAN) 109, 113, 118
discriminator 114
loss function 110
network 118, 124
connected insulin delivery devices 29–31, 35
connectivity
features of 26–27, *27*
need for 24–27, *25–27*
principle of 116
contemporary medicine 95
continuous glucose monitors (CGMs) 26, 29, 34
continuous monitoring 72, 86, 89–90, 104–105, 149
and updating 149
longitudinal studies and 153
of VOCs 86
continuous structural integrity 102
convolution kernels (CK) 114
convolution layer 114
convolutional neural networks (CNNs) 50, 54–58, 114
algorithm 69, *70*, 71, *71*
confusion matrix for *71*
model's performance 56
cost 105
COVID-19 23, 25, 51, 96

data acquisition (DAQ) device 10, 17
data/dataset
analytics 44
collection and processing 143
distribution 110
fusion 50, 89, *90*
normalization 146
overload 105
preparation 58
processing 50, 143, *143*
real-time 52–53
representation 55, 58
security 31, 49, 104
sharing 25
database training 122, *123*, **123**
decision tree (DT) 49, 139, 142, 145, *145*, 152–154
decision-making 50, 95–96
decomposition 2–5, 11–12, 20, 22
deconvolution, convolution and layers of 112–114
deep learning (DL) 44, 54, 109
algorithms 71
based target identification techniques 108
convolutional neural networks 55–58
methods 51
principles 52
techniques 54
Deep Q-Network 49
Deep Sparse Auto Encoder 48
degree of precision 96
deployment 16, 37–38, 89, 149
detection limit 81–82, 88–89
DeTrAs 50
diabetes
individuals with 35
management of 24, 35
digital-to-analog converter 85
direct memory access (DMA) 5
discrete wavelet transforms (DWT) 2–5
architectural design of 12
decomposition 4
features 12, 20
method 18
discriminator 118, *120*
architecture 113–114
multi-scale 124
diseases
identification of 97
prevention 104
related genetic markers 96
diverse dataset 49–50, 152
DMA-FIFO 6, *6*
doping 130
dosing optimization 35
drug delivery 24–25, 97, 104
optimization 104
systems 97
dynamic range 82, 119, 127–128, 130

e-healthcare framework 50
early cancer detection 102
electrical gas sensor 80
electromyography (EMG)
  classification algorithms 1
  processing 11–12, *13*, **14**, *15*
  signals 2–3, *3*, 17–18, 20
electronic health records (EHR) 37, 73, 105
electronic nose (E-Nose) 84–85
electronic-Proof of Work (ePoW) 48
electronics 101–102
encryption 27, 31
environment
  control 78
  monitoring 103
  sensors 31
eosinophils 123–124
ethanol sensing 87–88, 96
Event Process Healthcare (EPH) method 52
explainability 153

F1-score 151
fatality rate 51
feature randomization 145–146
field programmable gate array (FPGA) 5
  block diagram of 6, *7*
  configuration parameters 6, **7**
  performance 9
field-effect transistors (FETs) 127, *131–133*
  characteristics of 132–133
  effect of doping on 130
  electric potential profiles 129–130, *129*
  optimum thickness for 132
  potential distribution in 130
  threshold voltage for *134*
fine-needle aspiration (FNA) 148, 151, 154
firmwares 29, 33, *34*
first-in, first-out (FIFO) buffer 5, 8
fixed drain voltages 130
fluorescence microscopy 96
food safety 103
Frechet inception distance (FID) 119–121, **121**
fuel efficiency 87
full convolutional neural network (FCNN) 114, 116
Fully Convolutional Regression Networks (FCRN) 108–109, 121–122
function generator (FGEN) 5, 10

gas sensors/sensing 79
  and sensing mechanism 79–83
  characteristics of 89
  description of 77–79, *78*
  designing 82
  electrical method of 81, *81*
  electrodes 79
  for agriculture 87
  for industrial processes 86–87
  for pollution monitoring 85–86
  for smart home 86
  future directions and recommendations 88–90
  gas chamber 79
  in real-life applications *78*
  insulating layer 79
  layer 79
  measurement techniques 81
  micro-heater 79
  optical method of *81*
  overview of *80*
  parameters for 81
  smart healthcare 83–85
  substrate 79
  techniques in 79, *80*, 87–88
Gaussian kernel 109
gender 1, 140
General Data Protection Regulation 37, 45
generative adversarial network (GAN) 109–110, 113, 123
generator structure 112–113
geometry
  allocation 128
  meshing of 128–129
global healthcare system 42
glucose variation plot 135, *135*
gold nanoparticle-based nanosensors 102
gradient mask 112–113
gradient similarity (GS) 109
graphene-based nanostructures 82

health data 35–36, 44, 52, 72, 105
Health Insurance Portability and Accountability Act 37, 45
health monitoring framework 46–47, *47*
healthcare
  administration 45
  ecosystem 105
  industry 41
  monitoring and management 44
  noninvasive diagnosis in 84
  noninvasive smart implants in *98*
  personal 103
  proactive 98
  professionals 46
  providers 35
  settings 24
heavy metals 102
human activity recognition (HAR) 42, 47–48, 54
  application of 56, 72
  architecture *63*
  classification of *43*
  CNN architectures for 55
  dataset 71
  deep learning approaches *see* deep learning
  in IoHT 46

integration 71
machine learning approaches *see* machine learning (ML)
promotion of independent living 46
sensor-based approaches 54
systems 46, 73
human behavior 46, 48
hysteresis 82, 87

infectious disorders 97
infusion pump mechanisms 31
inheritable mutations 140
input prediction 148
insulin
delivery devices 28
management applications 26
pens 25
pumps *25*, 26, 29, 34
sensors 32–33
therapy management 28
insulin delivery devices 25, *25–26*, 28–29
actuators used in 31
artificial intelligence in 35, *36*
connectivity feature in 26–27, *27*
IOT-based 28–29, *30*
machine learning-based algorithms for 33–35
nanotechnology in 32–33, *32*
regulatory compliances 35, *37*
intelligent medical equipment 42
Inter Planetary File System 48
interconnected devices 41, 43–44
interdigitated electrodes (IDEs) 86–87
International Diabetes Federation 24
Internet of Healthcare Things (IoHT) 41, 72
communication technology in 44
components and infrastructure of 43
data analytics in 44
data collection for personal health 45
ecosystem 44–45
elements and traits of 43–45
HAR in 46
human activity 45–47
implementation of 45
in healthcare industry 45
in illness management 44
integration in healthcare 43
standardization and interoperability in 44
systems 45–46
Internet of Medical Things (IoMT) 89–90
Internet of Things (IoT) 43–49, 72, 77–78, 82–83, 96
analysis of results 64–71
attribute description 62
background and motivation 42–43
based insulin delivery 29, *30*
cross-validation 61
dataset description 62
description of 41
devices 48–49, 72
evaluation metrics 61–62
experiment analysis 62
exploratory analysis 63–64
framework 52
health monitoring framework using 46–47, *47*
human activity recognition *see* human activity recognition (HAR)
infrastructure 42, 48–49
insulin delivery devices 28–29
integration 71
proposed framework 53
related work 47–53
strategy 51
systems 51
train-test split 61
interoperability 37, 44–45, 105
interpretability 146, 153
intrusion detection system (IDS) 48

k-nearest neighbor (KNN) 2, 49, 51, 139, 142, 146–147, *147*, 152–154
classification 16, *18*
classifiers 17
confusion matrix of 146–147, *147*
versatility of 142

LabVIEW 16
GUI *18*
operations 14
RBF kernel implemented on *15*
real-time application 16
real-time design *10*, 10–12, *12–13*, *17*
real-time module 8
software 8, 20
leukocyte 123
life cycle, gas sensor 82
linearity 82
logistic regression 48, 139, 141, 149, 152–154
data flow diagram of *139*
model 144–145, *144*, 148
long short-term memory (LSTM) 49–50, 54
machine learning (ML) 44, 58, 139
application of 139, 155
artificial neural networks 58–60
feature selection units *144*
in medicine 155
performance evaluation 60
perspectives 151
rate of error 60
recall 61
supplementary methods 152
techniques 52, 138, 153–154
uses of 151

machine learning (ML) algorithm 34–35, 42, 52, 71, 148
  decision trees 142
  k-nearest neighbors 142
  logistic regression 141
  random forest 142
  support vector machine 142
magnetic resonance imaging (MRI) 96
malignant tumors 141, *141*
Mallat algorithm 3–4
MATLAB
  based CAD 20
  function 12, **14**
  KNNpredict 17–18
  SVMpredict 17–18
meal tracking apps 34
mechanical button actuators 31
medical
  assistance 140
  devices 43–44
  diagnostics 138
  equipment 44
medications 24–25, 45, 95, 104
medicine
  contemporary 95
  machine learning in 152–153, 155
  personalized 103
  precision 95
memory
  and storage 28
  needs 128–129
metal oxide (MO) nanostructures 77
micro-level sensors 82
microcontroller 28
microfluidic systems 31
miniaturized sensors 77
model architecture 58
monocytes 123–124
MoS_2 127–128
  bandgap of 131
  electrical properties of 128
  FET 128
  layer thickness 128
  model devices and parameters 128, **129**
motion sensors 29
motor-driven piston actuators 31
multi-scale conditional generative adversarial network (MCGAN) 109–111, 122, 124
  classification detector architecture 114–116
  clustering algorithm 116
  discriminator architecture 113–114
  discriminator loss value of 118
  experiment 124
  generator block diagram *113*
  generator structure 112–113
  network *111*, 112, 123–124
  objective function 111–112
  PNSR value of 121
  structure of 110
multi-scale convolution 109–110, 114, *115*, 121
multi-scale discriminator (MD) 109
multi-scale pooling structure module 114, *115*
multilayer perception (MLP) 48
multimodal
  data fusion 90
  sensing capability 96
  sensor fusion 72–73
multiple single classification (MUSIC) 20
multisensor data 90

nanocomposites 32, 77, 85, 87, 89, 101
nanomaterials 32–33
  advancement in 82
  for real-time sensing application 138
nanometers
  devices 131–132
  scales of 97
nanoparticles 32–33, 85, 99, 101–103
nanoscale 95–99, 101, 105
nanosensors in noninvasive monitoring 95–97, 102
  acceptance and adoption of 105
  adaptability 97, 103
  biological nanosensors 98–99
  challenges 104–105
  chemical nanosensors 99–101, *100*
  data 105
  early cancer detection 102
  future prospects 103–104
  in telemedicine 104
  long-term effects of 105
  nanoscale advantage 97–98
  noninvasive 103
  pathogen detection 103
  physical characteristics of 99
  physical nanosensors 101
  rapid response time of 97
  strain sensing in aerospace 102–103
  water quality 102
  wearable devices using 103, *104*
nanostructured materials 32–33
nanotechnology 32–33, *32*, 95
natural language processing (NLP) scheme 50
Near-Field Communication (NFC) 28
network
  detection accuracy 121–124, **122**
  structure models 120–121
  training 117–118
neural network 50, 55–56, 84–85, 114
neuromuscular disorders (NMDs) 1
  automatic detection of 16
  classification **19**, 20

CompactRIO-9035 controller *see* CompactRIO-9035 controller
computer-aided diagnosis tool of *18*
dataset 2–3
description of 1–2
detection of 1, 10, 16, 20
framework to detect 18
implementation results and real-time evaluation-9035 16–18, *18*
MG signal decomposition based on discrete wavelet transform 3–5
NI-9474 8, *9*
NI-CompactRIO (cRIO) chassis *6*, 8–9
NI-LabVIEW 10
noise distribution 110
noninvasive
diagnosis 83
monitoring 77, 96
nanosensors 103, 105
NumPy 139

on/off ratio calculation 133, *134*, **134**
One-vs-One (OVO) strategy 11
online health monitoring systems 41
organic pollutants 102
outliers, robust to 146
overfitting, diminished 146

palpable breast lumps 140
Pandas DataFrame 143
patch insulin delivery *25*, 26
pathogen detection 103
patients
autonomy 45
care 45
centric applications 153
relations systems 52
pattern recognition 77, 85, 89
peak signal-to-noise ratio (PSNR) 119
performance evaluation 60
peripheral blood cells 116
Peripheral Component Interconnect (PCI) bus 5
personalized healthcare 96, 103, 105
description of 95
imperative for 95–96
nanoscale advantage 97–98
nanosensors 96–97
significance of 95
personalized medicine 95–97, 103, 105
physical nanosensors 101
piezoelectric actuators 31
pix2pix
classification 114–115
generator 109
network 110
objective function 111
PNSR 120–121, **121**
point-of-care diagnostics 96, 104
Poisson equation 129
pollution/pollutants 85
control 78
monitoring, gas sensors for 85–86
power
indication 29
management 28
source 28
precision breast cancer classification 151
collaboration between machine learning and medicine 152–153
dataset 154
description of 138–140
diagnostic techniques 154
explainability and interpretability 153
integration of diverse dataset 152
longitudinal studies and continuous monitoring 153
machine learning algorithm *see* machine learning (ML) algorithm
patient-centric applications 153
practical application 149–151
proposed algorithm *see* proposed algorithm
real-world relevance 154
risk factor 140
scope of problem 140
machine learning algorithm 154–155
signs and symptoms 140
supplementary machine learning methods 152
test dataset generalization 149
types of tumor 141
utilization of extensive dataset 154
precision medicine 95
pressure sensors 29
pressure-based actuators 31
principal component analysis (PCA) 84
principle
of connectivity 116
of proximity 116
privacy, considerations 72
proposed algorithm
comparison with 148
continuous monitoring and updating 149
data collection and processing 143
decision tree model 145
deployment and integration 149
feature selection 143–144
hyperparameter tuning 148–149
input prediction 148
k-nearest neighbor 146–147, *147*
logistic regression model 144–145, *144*
model evaluation and interpretation 148
random forest model 145–146
support vector machine 147, *148*

random forest (RF) 49, 139, 142, 145–146, *146*, 152–154
rate of error 60
RBF kernel 14, *15*, 16
real database (RD) training 122
real-time
  activity recognition 72
  application 16
  data 53
  design *10*, 10–12, *12–13*, *17*
  host 6, *7*
  module 8
  monitoring 103
  sensing application 138
recurrent neural network (RNN) 50, 54
reduced graphene oxide (rGO) 77
rehabilitation process 45
remote drug delivery devices 24
remote insulin therapy; *see also* insulin delivery devices
  actuators used in insulin delivery devices 31
  artificial intelligence in insulin delivery 35, *36*
  description of 24
  firmwares 33
  IOT-based insulin delivery systems 28–29, *30*
  machine learning-based algorithms for insulin delivery 33–35
  nanotechnology in insulin delivery 32–33, *32*
  need for connectivity 24–27, *25–27*
  regulatory compliances 35–37, *37*
  sensors in connected insulin devices 29–31
remote monitoring 24–25, 28, 37, 42
Res-Net 122

scatter plot 63–64, *68*
security 31
  components 28
  considerations 72
selectivity 32, 77, 81–82, 84–85, 88
self-supervised learning 51
sensitivity 13, 27, 32–33, 50–51, 77, 81, 84–85, 87–88, 99–100, 151
sensors/sensing 28, 82; *see also* gas sensors/sensing
  area exposure 127
  fusion 89–90
  in connected insulin devices 29–31
  physical characteristics for 101
  related to wireless communication 29
  signal capturing 77
  technologies 47–48
  types of 77
signal processing 1, 17, 20
single photon emission computed tomography (SPECT) 49
smart contract-based system 48
smart gas sensor technology 77
smart healthcare 77–78, 83, 90–91, 94
  breath analyzer 84–85
  system 90, *90*
  wearable sensors in medical diagnosis 83
smart home
  applications 78
  gas sensors for 86
  intelligent 86
smart life applications 88, **88**, 91
smart sensors 44, 89
smart systems 82
  dissemination of 89
  schematic of *83*
smart visualization 89
smartphones 26, 31, 47–48, 82
SnO_2/rGO sensor 85
Sobel operator 111
software 20, 29
Solenoid actuators 31
SOS warning 47
space management 127
SSDs (Single Shot Detector) 121–122, 124
stability 81
state-of-the-art technologies 89
structural health monitoring process 102
Structural Similarity Index (SSIM) 119–121, **121**
support vector machine (SVM) 2, 48–49, 139, 142, 147, *148*, 152–154
  accuracy advantage of 49
  classification module 13–16, *15*, **15**, *18*
  classifiers 51
  learner and offline training 11, *11*
  models 11, **15**
surface-to-volume ratio 100
Symlet wavelet 4

target gas 84–85
  adsorption of 84
  concentration of 80–81
target/targeted
  biological molecules 98–99
  chemical analytes 100–101
  identification method 108
  therapies 95, 98
technology/technological 44, 89
  advancement 42–43
  in internet, IoT and sensing devices 42
telemedicine 51, 104
temperature
  sensors 29
  working 82
TensorFlow 1.13 framework 116
touch sensors 29
toxic gases 78, 83, 85–86
traditional healthcare monitoring methods 96

training 55–56, 59
  accuracy 69, *69–70*
  loss 68–69, *69–70*
transduction
  mechanism 101
  process 99
treatment plans 24–25, 46, 72, 95, 140
tumor, types of 141, *145*
tunable Q-factor wavelet transform (TQWT) 2

U-Net network 122, *123*, **123**
UCL repository dataset 48, 52
user adoption 105
UV irradiation 88

validation
  accuracy curve 69
  loss curve 68–69, *70*
variation mode decomposition (VMD) 20
virtual instrument (VI) 5
visual classification and detection 121, *122*
volatile organic compounds (VOCs) 79, 84, 86
voting mechanism 146

water quality 102
wearables
  health tech 104
  sensors 77, 83
  technology 44, 48
Wi-Fi 28, 44
wireless technologies 28, 44
World Health Organization 135

Zigbee 44
ZnO sensing layer 84